

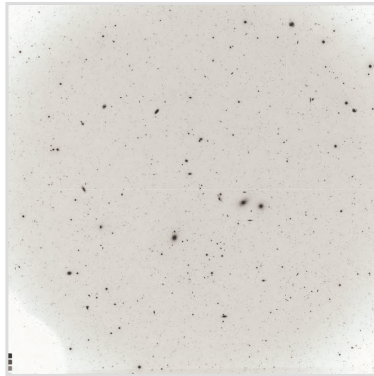
# An Ultra-Deep Survey of Low Surface Brightness Galaxies in Virgo

Elizabeth Helen (Lesa) Moore, BSc(Hons)

Department of Physics

Macquarie University

May 2008



This thesis is presented for the degree of  
Master of Philosophy in Physics



*Dedicated to all the sentient beings living in galaxies  
in the Virgo Cluster*



## CONTENTS

<i>Synopsis</i> . . . . .	xvii
<i>Statement by Candidate</i> . . . . .	xviii
<i>Acknowledgements</i> . . . . .	xix
1. <i>Introduction</i> . . . . .	1
2. <i>Low Surface Brightness (LSB) Galaxies</i> . . . . .	5
2.1 Surface Brightness and LSB Galaxies Defined . . . . .	6
2.2 Physical Properties and Morphology . . . . .	8
2.3 Cluster and Field Distribution of LSB Dwarfs . . . . .	14
2.4 Galaxies, Cosmology and Clustering . . . . .	16
3. <i>Galaxies and the Virgo Cluster</i> . . . . .	19
3.1 Importance of the Virgo Cluster . . . . .	19
3.2 Galaxy Classification . . . . .	20
3.3 Virgo Galaxy Surveys and Catalogues . . . . .	24
3.4 Properties of the Virgo Cluster . . . . .	37
3.4.1 Velocity Distribution in the Direction of the Virgo Cluster . . . . .	37
3.4.2 Distance and 3D Structure . . . . .	38

---

3.4.3	Galaxy Population . . . . .	42
3.4.4	The Intra-Cluster Medium . . . . .	45
3.4.5	Effects of the Cluster Environment . . . . .	47
4.	<i>Virgo Cluster Membership and the Luminosity Function</i> . . . . .	53
4.1	The Schechter Luminosity Function . . . . .	54
4.2	The Dwarf-to-Giant Ratio (DGR) . . . . .	58
4.3	Galaxy Detection . . . . .	59
4.4	Survey Completeness . . . . .	62
4.5	Virgo Cluster Membership . . . . .	63
4.5.1	Radial Velocities . . . . .	64
4.5.2	Morphology . . . . .	65
4.5.3	Concentration Parameters . . . . .	66
4.5.4	Scale Length Limits . . . . .	68
4.5.5	The Rines-Geller Threshold . . . . .	73
4.5.6	Background Galaxy Counts . . . . .	76
4.6	Cosmological Models and the Luminosity Function . . . . .	78
4.7	Applications and Limitations of the Schechter Function . . . . .	82
4.8	Summary: The Virgo Cluster Luminosity Function . . . . .	84
5.	<i>Project Data and Analysis</i> . . . . .	89
5.1	Digital Scanning & Stacking . . . . .	91
5.2	The Virgo Deep Stack . . . . .	95
5.3	Astrometric Calibration . . . . .	100
5.4	Photometric Calibration . . . . .	102

---

5.5	Object Detection . . . . .	107
5.6	Surface Photometry . . . . .	107
5.6.1	Overview of Photometry Techniques . . . . .	107
5.6.2	The IRAF ELLIPSE task . . . . .	109
5.6.3	ELLIPSE Parameter Subsets . . . . .	111
5.6.4	Output Data Files . . . . .	113
5.7	Calculations used in Plotting and Final Measurements . . . . .	114
5.8	Uncertainties in Measurement of Galaxy Properties . . . . .	116
6.	<i>Data Quality and Comparative Results</i> . . . . .	121
6.1	Comparison Profiles . . . . .	121
6.2	Comparisons of the Virgo Deep Stack with Other Surveys . . . . .	124
6.2.1	The Survey by Trentham and Tully (2002) . . . . .	126
6.2.2	The Survey by Caldwell (2005) . . . . .	131
6.2.3	The Survey by Sabatini et al. (2005) . . . . .	134
6.2.4	Dwarf Spheroidal Galaxy Analysis by Durrell et al. (2007) . . . . .	136
6.2.5	Comparisons Summary . . . . .	136
6.3	Bryn's Mystery Object . . . . .	138
6.4	Faint Galaxy Haloes . . . . .	140
6.5	Intra-Cluster Light . . . . .	142
7.	<i>Malin 1</i> . . . . .	151
7.1	New Measurements . . . . .	151
7.2	Malin 1: A Deeper Look (Moore and Parker 2006) . . . . .	154

---

8. <i>The Virgo Deep Stack Catalogue</i> . . . . .	161
8.1 Surface Brightness Classification . . . . .	162
8.2 Morphological Classification . . . . .	163
8.3 Cluster-Membership Classification . . . . .	164
8.4 Galaxy Positions and Measured Properties . . . . .	165
8.5 Galaxy Images and Radial Profiles . . . . .	169
9. <i>Discussion, Conclusions and Future Work</i> . . . . .	197
9.1 Cluster Membership of the New Galaxies . . . . .	197
9.2 Impact on the Luminosity Function . . . . .	200
9.3 Conclusions . . . . .	204
9.4 Future Work . . . . .	205
<i>Appendices</i> . . . . .	209
<i>A. Scale Length and Slope of the Fitting Function</i> . . . . .	211
<i>B. Luminosity-to-Magnitude Conversion of the Schechter Function</i> . . . . .	213
<i>C. Absolute Magnitude and the Hubble Parameter</i> . . . . .	215
<i>D. Image and Data Files Supplied by Royal Observatory, Edinburgh</i> . . . . .	217
<i>E. Virgo Deep Stack Calibration Stars</i> . . . . .	219
<i>F. Gemini Observing Proposals</i> . . . . .	221
F.1 Observing Procedure . . . . .	221
F.2 Observing Proposals . . . . .	224



---

<i>G. Glossary</i> . . . . .	237
G.1 Abbreviations . . . . .	237
G.2 Symbols . . . . .	241
G.3 Definitions . . . . .	244
 <i>Bibliography</i> . . . . .	 246



## LIST OF FIGURES

1.1	The Virgo Deep Stack . . . . .	3
2.1	Three Galaxies . . . . .	9
2.2	Newly-Discovered Virgo VLSB Galaxy 22-1: Image and Radial Profile	13
3.1	The Hubble Tuning Fork Diagram . . . . .	21
3.2	Ultra-Compact Dwarfs in the Virgo Cluster . . . . .	25
3.3	MAP 1: Combined Survey Map . . . . .	33
3.4	Histograms of Galaxy Velocities in the Direction of the Virgo Cluster	38
3.5	Plan Diagram of the Virgo Cluster . . . . .	41
3.6	MAP 2: 3D Structure of the Virgo Cluster . . . . .	43
3.7	NGC 4438: A Tidally Disturbed Galaxy . . . . .	45
4.1	Schechter's Luminosity Function . . . . .	55
4.2	Histogram, N-Magnitude and Log(N)-Magnitude Plots . . . . .	57
4.3	Improper Deblending and the Sabatini et al. (2003) Solution . . . . .	61
4.4	Luminosity Functions and the Trentham and Hodgkin (2002) Data .	67
4.5	A Steep Luminosity Function . . . . .	71
4.6	The Rines-Geller Threshold . . . . .	75
4.7	Loci of Fixed Scale Length . . . . .	75

5.1	Comparisons of Tech Pan and IIIa-F Exposures . . . . .	91
5.2	Characteristic Curves of Tech Pan and IIIa-F Exposures . . . . .	93
5.3	Passband of the OG590-Tech Pan Combination . . . . .	97
5.4	Artefacts in the Virgo Deep Stack . . . . .	98
5.5	The Virgo Deep Stack at High Contrast in False Colour . . . . .	99
5.6	Sub-Frame 22 . . . . .	101
5.7	MAP 3: Dwarf LSB Studies and Sub-Frames of the Virgo Deep Stack	103
5.8	Calibration of the Virgo Deep Stack . . . . .	106
5.9	Isophotes and Masked Pixels in the IRAF ELLIPSE Display . . . . .	111
5.10	Effects of Masking . . . . .	119
6.1	Comparison Profiles . . . . .	123
6.2	MAP 4: Overlap of the Virgo Deep Stack with Other Surveys . . . . .	125
6.3	Galaxies Common to Trentham & Tully and Sub-Frame 16 . . . . .	127
6.4	Two New VLSB Galaxies from Sub-Frame 16 . . . . .	128
6.5	Images and Profiles: Five Trentham & Tully Galaxies . . . . .	129
6.6	Images and Profiles: Two Independently-Verified VLSB Galaxies . . . . .	133
6.7	Image and Profile: SDV 144 . . . . .	135
6.8	A Dwarf Spheroidal Cluster Member . . . . .	137
6.9	Bryn's Mystery Object . . . . .	139
6.10	M89 Shells . . . . .	141
6.11	Intra-Cluster Light in the Heart of the Virgo Cluster . . . . .	143
6.12	Diffuse Intra-Cluster Features . . . . .	143
6.13	IC 3349 - No Tidal Tail . . . . .	144

---

6.14	Intra-Cluster Light - NW Quadrant . . . . .	145
6.15	NGC 4302 - Disk Broadening in the Deep Image . . . . .	147
6.16	IC 3392 - Stars Masquerade as Tidal Tails . . . . .	148
6.17	NGC 4425 and VCC 989 - An Interacting Pair? . . . . .	149
7.1	Fitting Ellipses to Contours of Malin 1 . . . . .	153
7.2	The Inner Disk of Malin 1 . . . . .	154
8.1	MAP 5: Galaxies in the Virgo Deep Stack . . . . .	165
8.2	Presumed Foreground Object: Bryn's Mystery Object . . . . .	169
8.3	Presumed Background Galaxies I . . . . .	171
8.4	Presumed Background Galaxies II . . . . .	173
8.5	Possible Cluster Members I . . . . .	175
8.6	Possible Cluster Members II . . . . .	177
8.7	Possible Cluster Members III . . . . .	179
8.8	Probable Cluster Members I . . . . .	181
8.9	Probable Cluster Members II . . . . .	183
8.10	Probable Cluster Members III . . . . .	185
8.11	Presumed Cluster Members I . . . . .	187
8.12	Presumed Cluster Members II . . . . .	189
8.13	Presumed Cluster Members III . . . . .	191
8.14	Presumed Cluster Members IV . . . . .	193
8.15	Verified Cluster Members . . . . .	195
9.1	Cluster Membership of Newly-Identified Galaxies . . . . .	201
F.1	Sample Display: Gemini Observing Tool . . . . .	223



## LIST OF TABLES

3.1	VCC Cluster Membership . . . . .	29
3.2	Selected Virgo Cluster Surveys and Catalogues . . . . .	36
3.3	Selected Virgo Cluster Distance Estimates . . . . .	39
3.4	Cepheid Distance Moduli to Virgo Galaxies . . . . .	40
3.5	Sub-Structure of the Virgo Cluster . . . . .	42
4.1	Definitions of the Dwarf-to-Giant Ratio . . . . .	59
4.2	Comparing Dwarf-to-Giant Ratio with Faint-End Slope . . . . .	60
4.3	Dwarf Galaxy Properties and Scale Length at Virgo Cluster Distances	69
4.4	Dwarf-to-Giant Ratios for Virgo Strips . . . . .	72
4.5	Luminosity Functions . . . . .	87
5.1	Positional Statistics of the Virgo Deep Stack . . . . .	95
5.2	Base Images for the Virgo Deep Stack . . . . .	96
5.3	Sub-Frame Coordinates . . . . .	102
5.4	Variations Contributing to Uncertainty . . . . .	120
6.1	Comparison Magnitudes: Five Trentham & Tully Galaxies . . . . .	130
6.2	Data: Two Independently-Verified VLSB Galaxies . . . . .	132
6.3	Data: SDV 144 . . . . .	134

8.1	Cluster Membership Classifications . . . . .	164
8.2	Measured Galaxy Data . . . . .	166
9.1	Concentration Parameters for Catalogue Galaxies . . . . .	198
E.1	Calibration Stars . . . . .	220



## SYNOPSIS AND STATEMENT BY CANDIDATE

### *Synopsis:*

Originally planned as a PhD project, but curtailed to a Master of Philosophy due to time constraints and numerous other commitments, the principal objective of this project was to undertake a survey of low surface brightness (LSB) galaxies in the Virgo Cluster. This thesis presents background material and the results of that survey. As considerable research has already been conducted on galaxies in the Virgo Cluster, the early chapters cover: LSB galaxies; current knowledge of the Virgo Cluster; and the luminosity function that describes a galaxy population.

The base data for this project is a unique resource - the Virgo Deep Stack - made from 63 digitally-scanned photographic films centred on the core of the Virgo Cluster. Subsequent chapters describe the data and analysis techniques and compare these new data with previously published work.

On the specific question of the characteristics of the faint end of the luminosity function in the Virgo Cluster, where the low surface brightness dwarf galaxies predominate, most survey results disagree. This project addresses the reasons for the disagreement and explores the quality of the published data sets by comparison with data from the Virgo Deep Stack. Finally, the catalogue of newly-identified galaxies is presented and discussed. The new galaxies and their properties will contribute to the body of scientific knowledge about the cluster and its low surface brightness population.

*Statement by Candidate:*

This thesis has not been submitted for a higher degree to any other university or institution. The work contained in this thesis was carried out while the author was a research student at Macquarie University, Sydney, from February 2005 to May 2008, under the supervision of A/Prof. Quentin Parker.

This thesis is the result of the author's own investigations. All material from external sources is fully referenced.

Signed:

Date:

## Acknowledgements

Many people have contributed to this project in different ways. Several astronomers have given me good advice and helpful support at critical times, particularly in the early stages of the project. My thanks go especially to Stuart Ryder for teaching me the ‘black art’ of surface photometry, Bryn Jones for sending me the detailed notes on performing photometric calibration, Warren Reid for guiding me through the Gemini PIT the first time around and Steve Phillipps and Simon Driver for offering helpful advice and collaborating on our Gemini observing proposals.

I also wish to thank Kristin Chiboucas and Simon Chan for their very good company at the Gemini North Telescope. The fabulous behind-the-scenes tour was certainly an enjoyable consolation when the dome was frozen shut and we were unable to observe.

Closer to home, there are my friends at Macquarie University (staff and students), without whom I doubt I could have stayed sane through the difficult times. Staff members who always managed to be there with support and encouragement include Alan Vaughan, Peter Browne, Mark Wardle, Judith Dawes and Agnieszka Baginska. To Catherine, Korinne, Sarah, Andrew, Brent, Anna and all the rest also go my thanks for sharing the work, the stories, the plans, the frustration, the lollies, the \*hugs\*, the knitting patterns and the recipes. I hope all these good friends manage to finish that which they undertook to achieve. I’m planning to stick around for a while for purposes other than study, so I hope I may continue to give them the same support they’ve given me. And I’ll apologise now for always being so noisy every time I come into the office!

My family have been wonderful throughout my 10-year-long mid-life crisis, of which this project has been just one component. I thank Husband, my dad and ‘Mrs Moore’

for their moral support and pride in my achievements, Jim for all the dinners, Tom for all the smiles and Carol and Harley for finally getting married. Once again, Elaine has done a stupendous job of proof reading for me and I can't thank her enough.

Special thanks, of course, go to Quentin Parker, my supervisor. Quentin has done so much for me, not just in the context of this project, but in offering me so many other opportunities along the way. I also thank Quentin and his lovely family, Carolyn and Sebastian, for their hospitality at the barbecues. Somehow Quentin manages to find a balance between work, which at times must seem overwhelming, and the lighter side of life. I relied on him to be understanding and sympathetic when I hit my 'lows' (I'm sure every PhD student has these) and he responded by pulling me through to the point where I've managed to salvage this Masters thesis from the project. I suppose I am a little sad that it didn't quite turn out to be the PhD, and there are many people, I know, who looked forward to seeing the 'best ever' luminosity function of the Virgo Cluster. To those people, I apologise for not being a better student. Nevertheless, I have no regrets about doing the work, enjoying the distractions and realising the dream of getting to the top of Mauna Kea. None of this would have happened without Quentin's unquenchable enthusiasm and undying support. Thanks Q!



Quentin, Lesa and the Gemini North Telescope

March 2006

## 1. INTRODUCTION

Low surface brightness (LSB)<sup>a</sup> galaxies are difficult to detect. These galaxies do not stand out in the night sky like the shining band of the Milky Way or the familiar naked-eye wonders of the Magellanic Clouds and the Andromeda Galaxy. Even with large telescopes and long-exposure imaging, detection has been, and remains, challenging compared with observations of the well-studied brighter galaxies. LSB galaxies are the faintest galaxies observed. Faint, however, does not mean insignificant, as LSB galaxy sizes range from dwarfs to giants.

The study of LSB galaxies is prompted by their importance in the processes of the formation and evolution of galaxies and clusters. Dwarf galaxies, including LSB dwarfs, are believed to be the building blocks of giant galaxies in a hierarchical model that leads from the simple elements produced in the Big Bang to the giant galaxies, clusters and superclusters that now exist. LSB giants are much rarer beasts, the evolution of which must be markedly different from that of the more typical bright elliptical and spiral galaxies. These evolutionary processes are not well understood because current theoretical modelling is neither able to reproduce the structures and galaxy populations seen today, nor to match the evolution of these structures on timescales that correspond with observations.

To study the evolution of galaxies and clusters, research focuses on observations of all types of galaxies in different environments, both in clusters and in the field. The evolution of cluster galaxies may then be compared with evolution of isolated galaxies in the field to derive an understanding of the interactions and the dynamics

---

<sup>a</sup> Abbreviations, symbols and selected terms are defined in the Glossary (Appendix G).

at work in each case. In keeping with the scientific method, these observations are essential to constrain cosmological models. The Virgo Cluster is an ideal target for cluster studies as it is a rich cluster containing all galaxy types and, at 17 megaparsecs, it is close enough that its faint LSB galaxies may be detected with modern techniques.

The objective of this project is to exploit a unique set of 63 separate high-quality UK Schmidt Telescope (UKST) *OR*<sup>b</sup>-band Tech Pan films taken on the central field of the Virgo Cluster between January 1999 and June 2001. These high-resolution films have been digitally scanned and stacked using the SuperCOSMOS measuring machine at the Royal Observatory Edinburgh (ROE) to produce an ultra-deep image, hereafter referred to as the ‘Virgo Deep Stack’ (refer Figure 1.1). This image has arcsecond resolution over a 25-square-degree field centred at  $12^h27^m+13^\circ30'$  in B1950 coordinates ( $12^h29^m31^s.83+13^\circ09'43''.5$ , J2000).

It has been shown that stacking of digitised astronomical exposures of equal quality can achieve the full canonical Poissonian depth gains (e.g. Bland-Hawthorn et al. (1993)). Hence, this stack of 63 films provides a  $\sim 2.25$ -magnitude gain over the depth of a single Tech Pan film, which is already one magnitude deeper than standard glass-based IIIa-F emulsion (Parker and Malin 1999). The limiting surface brightness is approximately 29 magnitudes per square arcsecond in the *OR*-band in the central 25 square degrees of the 6-degree square Virgo Deep Stack. Deep CCD imaging may reach a similar depth but has the disadvantages of small field size, typically less than one square degree, and the accumulation of cosmic ray defects during long exposures. The Virgo Deep Stack provides a unique opportunity to detect previously unseen LSB galaxies with uniform and unprecedented image quality over a large area. These new data will contribute to the understanding of the Virgo Cluster, the evolution of its galaxies and the cluster luminosity function that is used

---

<sup>b</sup> *OR* is a specific red passband. Throughout this document, passbands are italicised; an upper-case *M* represents absolute magnitude with the subscript denoting the passband; italicised lettering *B*, *V*, *R*, *i'*, etc. is used to represent apparent magnitude in that passband; the subscript *T* denotes ‘total’; in the absence of a specific passband apparent magnitude may be represented by *m* or, for photographic magnitude, *m<sub>p</sub>*.

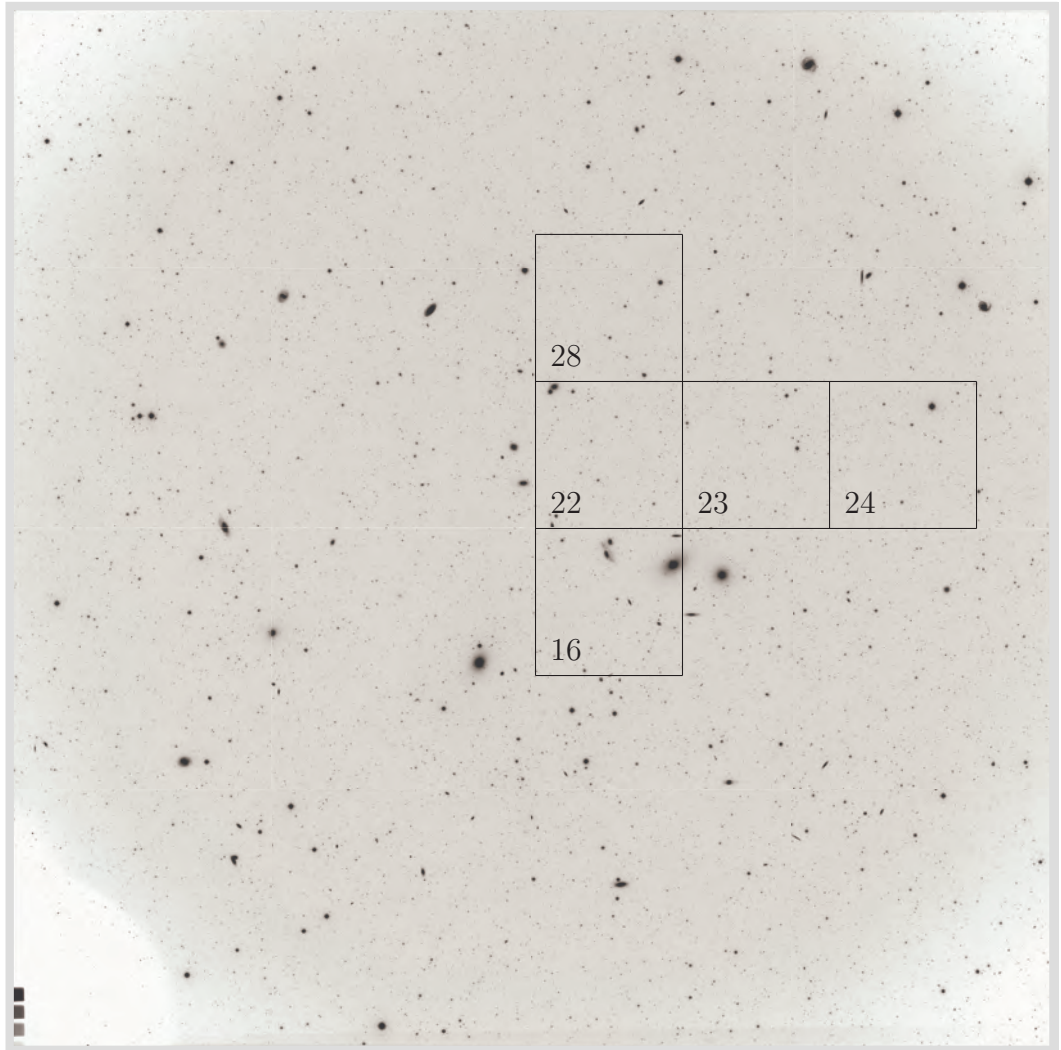


Fig. 1.1: The Virgo Deep Stack

*Pictured is the Virgo Deep Stack image compiled from 63 UKST films. Due to limitations and speed of display software, the field was subdivided into 36 sub-frames for easier study. The sub-frames have been reassembled to produce this composite image and the five that have been studied in detail are numbered. Vignetting (reduced light transmission off the optical axis) is evident around the edges of the field. Part of the sensitometer step-wedge used for photometric calibration of the individual photographic films is visible at lower left. The entire image is six degrees square. The unvignetted portion is uniform over the central 25 square degrees.*

as a measure of the overall galaxy population.

Chapter 2 sets the scene by describing the properties, distribution and importance of LSB galaxies. A summary of the many galaxy surveys within the Virgo Cluster and the resultant wealth of knowledge obtained are condensed into Chapter 3. Chapter 4 addresses the luminosity function, how it describes the galaxy population and how its key parameters vary in different environments. A complete description of the Virgo Deep Stack, how it was obtained and how its LSB galaxies have been analysed for this project is provided in Chapter 5. Comparisons of the Virgo Deep Stack data with published data and studies of some individual objects of interest are presented in Chapter 6. These include details of a large ‘mystery’ object, the nature of which is still unknown, and discussion of the phenomenon of intra-cluster light. One object deserving of special attention is the enigmatic giant LSB galaxy, Malin 1. Chapter 7 is devoted to a review and presentation of newly-measured properties of this galaxy and includes a paper published during the progress of this project: *Malin 1: A Deeper Look* (Moore and Parker 2006).

Due to time constraints, the survey component of this project covers a little less than 5 square degrees of the entire 36 square degrees available in the Virgo Deep Stack. However, within this area, 100 previously uncatalogued galaxies have been detected. Chapter 8 contains the catalogue of newly-identified LSB galaxies (the Virgo Deep Stack Catalogue), including thumbnail images, observational data and derived galaxy parameters. In Chapter 9, the newly-identified galaxies are discussed with particular attention to the issue of cluster membership and the impact of the new identifications on the luminosity function. An overview of potential future work is included.

Observing time was requested for follow-up observations of selected targets, and time was awarded in two semesters on the Gemini North Telescope. Unfortunately, due to poor weather on both occasions, no observations were obtained. Appendix F contains a description of the observing preparations and reproduces the observing proposals. Other Appendices include a glossary of terms, mathematical details and technical data.



## 2. LOW SURFACE BRIGHTNESS (LSB) GALAXIES

Low surface brightness galaxies represent a significant mass fraction of the universe: between 50% and 90% of the general galaxy population is in the form of LSB galaxies. As noted by Bothun et al. (1997) more than a decade ago:

*“In 20 years, low-surface-brightness (LSB) galaxies have evolved from being an idiosyncratic notion to being one of the major baryonic repositories in the Universe.”*

Nevertheless, LSB galaxies are the most difficult to detect because of their very low contrast with the sky background. It is important to be able to measure and to understand the properties of this significant galaxy population, not only because of their domination of the galaxy number density and potentially significant mass contribution, but also because many LSB galaxies are dwarfs. Dwarf galaxies are intrinsic to the formation and evolution of larger galaxies and clusters in hierarchical cosmology models. LSB galaxies, both large and small, also appear to have undergone different evolutionary processes from their higher surface brightness counterparts. By studying LSB galaxies in all environments, and comparing them with other galaxy types, researchers may develop evolutionary histories that feed into, and constrain, modern cosmological models and theories of galaxy evolution.

Detecting these galaxies requires deep surveys using long-exposure imaging techniques. The most recent surveys have been conducted using CCD detectors covering small areas of sky, usually less than one square degree. CCD detectors are far more sensitive to light than traditional photographic emulsions, so equal depth may be

reached with shorter exposures. The disadvantages are that CCDs are affected by cosmic rays, which cause bright spikes in the images, and that no single detector is yet able to match the combination of large area (6-degree-square coverage) and high resolution achieved with the photographic plates and films previously used with the UKST. Furthermore, the significant CCD sensitivity advantage may be offset by multi-exposure stacks of wide-field photographic images.

This project utilises 63 traditional high-resolution UKST Tech Pan photographic films, centred on the heart of the Virgo Cluster, that have been digitally combined to increase depth and minimise the appearance of single-film defects (e.g. satellite trails) whilst still covering a large area on the sky. This unique resource, described in detail in Chapter 5, forms the basis of this new survey of LSB galaxies.

## 2.1 *Surface Brightness and LSB Galaxies Defined*

Surface brightness is a measure of ‘magnitudes per square arcsecond’, usually abbreviated to  $\mu$ . For a given galaxy, surface brightness would have different values at different points in the galaxy and would also depend on the passband of the observation (e.g.  $B$ ,  $R$  or  $I$ ). A curious property of surface brightness is that, in theory, it does not change with distance in the absence of any intervening absorbing medium. For a point source, the intensity of light from an object of given luminosity falls off as the square of its distance. Placing it twice as far away would yield one-fourth the intensity. This applies to stars, for which comparison between apparent magnitude (observed) and absolute magnitude (derived from its properties) can yield a distance. Surface brightness, on the other hand, applies to extended objects. As a luminous extended object is placed further away, a square arcsecond covers a larger area of the object’s surface. Placing it at twice the distance means that an arcsecond includes four times the physical area. The effects of diminishing intensity and larger area coverage with increasing distance cancel each other out meaning that, for an object of uniform surface brightness, the measurement should not change with distance.

In practice, corrections may need to be applied including corrections for Galactic extinction due to the Milky Way (the amount of correction is dependent on the direction to the target galaxy) and general intergalactic extinction, the  $K$ -correction (for the broad-band photometric shifts in wavelength due to recession) and, at high redshifts, a correction for Tolman cosmological surface brightness dimming (dependent on  $(1+z)^4$ , where  $z$  is redshift, and due to the non-Euclidean nature of the expanding universe).

LSB galaxies are classified as those having central surface brightness  $\mu_0$  fainter than  $22\ B\mu$  (Jarrett 1998) or  $23\ B\mu$  (e.g. de Blok (1997), Bothun et al. (1997)). The latter definition is adopted for this project, and is correlated with  $R$ -band magnitudes based on the  $B-R$  colour function of Trentham and Tully (2002) where  $B-R \approx 1.5$  for redder galaxies, including ellipticals. Assuming this holds for LSB galaxies, the threshold by the above definition is  $21.5\ R\mu$ . LSB galaxies range from giants to dwarfs and include spirals, ellipticals, dwarf ellipticals and dwarf irregulars (Jarrett 1998). However, classification of LSB galaxies is strongly influenced by selection effects. For example, a gas-rich galaxy with low surface brightness at a large distance would be classified as an LSB galaxy, but nearby gas-rich late types are usually classified as dwarf irregular (de Blok 1997).

The faintest galaxies are classed ‘VLSB’ for very low surface brightness. VLSB galaxies are defined by Trentham and Hodgkin (2002) as having average surface brightness within a 12-arcsecond radius fainter than  $26.5\ B\mu$  (or  $25\ R\mu$  by the above colour function). At the faint limit would be the ‘extreme LSB’ galaxies with central surface brightness fainter than  $28\ R\mu$ . However, Trentham and Tully (2002) state that no such galaxies are known in the Local Group or elsewhere.

Chapter 8 catalogues and classifies newly-identified LSB galaxies with  $\mu_0 \geq 21.5\ OR\mu$  and VLSB galaxies in accordance with the Trentham and Hodgkin (2002) definition.

## 2.2 Physical Properties and Morphology

LSB galaxies are described by de Blok (1997) as having large gas disks with weak or no spiral structure. Compared with their high surface brightness (HSB) counterparts, LSB galaxies are strongly dark-matter dominated. This is known from their rotation curves which remain flat at large radii indicating the presence of dark matter haloes that stabilise the disk. In fact, dark matter dominates the galaxy potential at virtually all radii right into the core (Bothun et al. 1997).

To compare the gas content of LSB dwarfs in clusters and in the field, Davies et al. (2004) used optical *B*- and *I*-band data taken with the Wide Field Camera on the Isaac Newton Telescope to select samples of galaxies from both environments. Selection of LSB dwarfs in both the Virgo Cluster and, for the field sample, along the Millennium Galaxy Strip (MGS)<sup>a</sup> was based on criteria of central surface brightness in the range  $23 \leq \mu_0 \leq 26$   $B\mu$  and suitable size limits to restrict galaxy distance to a 21 Mpc radius, or 25% farther than the Virgo Cluster core. Of the 257 LSB dwarfs detected in the Virgo Cluster, Davies et al. (2004) observed 107 at 21cm (to detect HI) using the Arecibo Telescope and made only three detections, compared with 18 detections from a sample of 56 galaxies in the MGS.

These results demonstrate two points: (i) the gas surface density (i.e. the amount of gas that would be measured in the disk if viewed face-on)<sup>b</sup> is typically quite low; and (ii) galaxies with comparable size and surface brightness outside the Virgo Cluster are generally more gas-rich than those within it, indicating that environmental factors play a key role in the appearance and physical characteristics of these galaxies. The authors also note a distinction in morphology: in the field LSB dwarfs tend to be clumpy, whilst in the Virgo Cluster they are mainly smooth and diffuse.

A typical LSB galaxy appears featureless and faint compared with nearby objects.

---

<sup>a</sup> This region, covering  $37.5 \text{ deg}^2$ , runs along the celestial equator. It is variously known as the Millennium Galaxy Catalogue (MGC) (Liske et al. 2003), the Millennium Galaxy Survey or, as Davies et al. (2004) refer to it, the Millennium Galaxy Strip.

<sup>b</sup> A formal definition of gas surface density is provided in the Glossary, Appendix G.

It presents a generally smooth disk that is somewhat brighter in the centre, though without a concentrated nucleus, gradually diminishing into the background at the edges. An image comparing a relatively bright galaxy (VCC 674), a typical LSB galaxy ([TH2002] 285) and a newly-discovered VLSB in Virgo is shown in Figure 2.1.

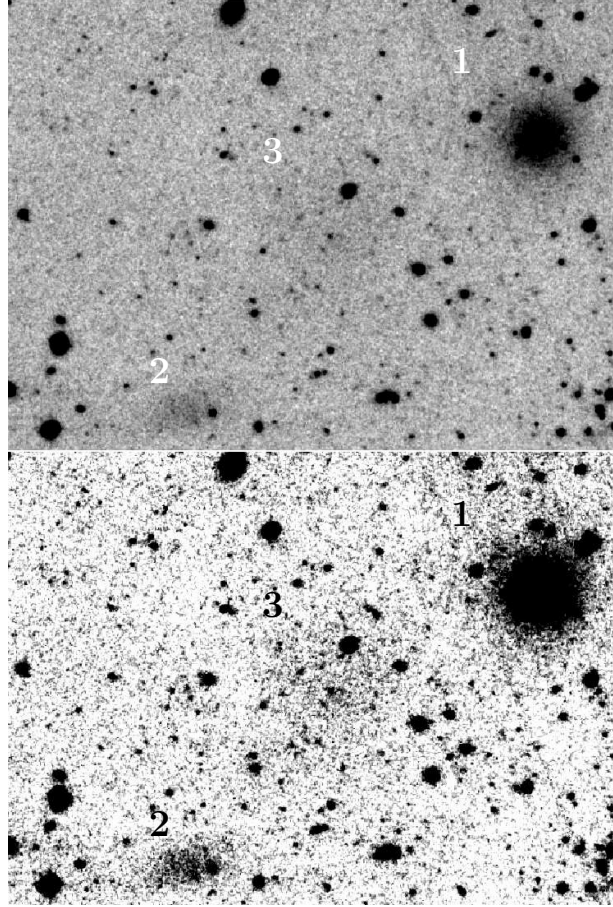


Fig. 2.1: Three Galaxies

*These images, both of the same field but displayed at different contrast levels, show three galaxies (numbered) of different magnitude and surface brightness. At upper right (1) is VCC 674, a bright galaxy listed in the Virgo Cluster Catalogue of Binggeli et al. (1985). The fainter smudge at bottom left (2) is an LSB galaxy identified by Trentham and Hodgkin (2002) and is number 285 in their catalogue. At the centre of the image (3) is a very low surface brightness (VLSB) galaxy, discovered as part of this project, and identified as galaxy 23-22. It has a central surface brightness of  $\sim 26.3$   $R_{\mu}$ . The lower image is displayed at higher contrast to make the galaxies more visible. Image size is approximately 7 arcmin wide by 5 arcmin high. North is at the top and east is to the left.*

Because the gas surface densities are typically below the critical threshold for star formation (refer Kennicutt (1989) and Auld et al. (2006)), these galaxies have very low star formation rates and evolve slowly (de Blok 1997). Their metallicity is low, on average  $\sim 1/3$  solar values (Bothun et al. 1997). The low metallicity makes cooling difficult (de Blok 1997), thereby inhibiting formation of molecular gas. The small molecular component is verified by observations that show that LSB spirals have far less molecular gas than HSB spirals of the same mass (Bothun et al. 1997). The low molecular content further inhibits star formation. Although they have low gas surface densities, LSB galaxies have high mass-to-light ( $M_{HI}/L$ ) ratios due to their faint luminosities and extended HI gas disks. LSB galaxy rotation curves show that the gas and dark-matter components are usually dynamically more important than the stellar component (de Blok 1997).

Whilst LSB galaxies are typically more than 1.5 magnitudes brighter in the red than in the blue (refer, for example, to the  $U-B-R$  comparison profiles of NGC 4551 in Young and Currie (1998) or to the  $B-I$  comparisons of Gavazzi et al. (2005b)), these galaxies are bluer than normal late-type galaxies (de Blok 1997). Davies et al. (2004) find that the colour distribution of cluster LSB dwarfs in  $(B - I)$  is approximately 1.5, i.e. bluer than metal-poor Galactic globular clusters. The blue colour suggests a predominantly young (recently formed) population of stars, which does not appear consistent with the concept of a low star-formation rate in LSB galaxies, where an aging population of progressively reddening stars would be expected.

This paradox may be explained by a reduced contribution to the total light in these galaxies from stellar giants resulting from later or more gradual collapse, compared with HSB galaxies, and delayed formation of their first stars (Bothun et al. 1997). An alternative explanation is that LSB galaxies only form stars sporadically with the slow evolution producing an under-developed old (red) population and the overall colour being dominated by the young (blue) population (de Blok 1997). Schombert et al. (2001) suggest, based on comparison with star formation models, that this dominant stellar population is less than 5 Gyr in mean age.

Star formation may be triggered by large-scale gravitational instabilities in the gas disk (Kennicutt 1989) or by galaxy interactions. Thus, it is often assumed that LSB galaxies must not be experiencing these influences. Nevertheless, LSB galaxies are found in large numbers in rich clusters, such as the Virgo Cluster, where gravitational interactions are likely and the dynamic environment should be hostile to the formation and survival of such diffuse objects (Bothun et al. 1997). A study by de Blok et al. (1999) of the nearby LSB galaxy, NGC 6822, showed that it has low surface brightness, an extended HI disk, low gas and stellar metallicity, a low star-formation rate and high dark matter content. In other words, it fulfills all the criteria for an LSB galaxy. However, high-resolution HI observations reveal that the galaxy may have suffered a recent interaction with another galaxy. Therefore, it should not be assumed that LSB galaxies are non-interacting or dormant systems.

The surface brightness profile of an LSB galaxy is well approximated by an exponential, which is also applicable in describing the disk components of spiral and lenticular galaxies (Freeman 1970). The profile has the form:

$$I(r) = I_0 \exp\left(-\frac{r}{a}\right) \quad (2.1)$$

where  $I$  is the surface brightness of the disk in linear units (intensity) as a function of radius  $r$ ,  $I_0$  is central surface brightness and  $a$  is the exponential scale length of the disk. In logarithmic units, this becomes:

$$\mu(r) = \mu_0 + 1.0857 \left(\frac{r}{a}\right) \quad (2.2)$$

where  $\mu_0$  is the central surface brightness of the disk in magnitudes per square arcsecond. The factor derives from the property that at one scale length, i.e. the radius at which the intensity drops by a factor of  $1/e$  below the maximum value, the surface brightness is 1.0857 magnitudes greater (i.e. fainter) than the central surface brightness (refer Appendix A for derivation).

This relationship means that the radial profile is linear when plotted on a magnitude-radius diagram, allowing for easy extrapolation to determine central surface brightness  $\mu_0$  and scale length  $a$  based on a linear fit to the profile. This is a preferred method for obtaining central surface brightness as it is not subject to small irregular

departures from a smooth profile (refer Figure 2.2). In cases where there is a central bulge present, the profile may be decomposed into bulge and disk components. Most of the LSB galaxies of interest in this project do not have central bulges, but one particularly interesting LSB giant with a prominent central bulge, Malin 1, is studied in detail (refer Chapter 7).

The underlying reason why galaxy disks exhibit exponential intensity profiles has long puzzled astronomers (Freeman 1970). More recently, Bell (2002) modelled galaxy evolution with viscosity caused by non-circular gas motions and turbulence and found that this may transport angular momentum outwards as mass flows inwards which, in conjunction with a suitable star formation rate, may freeze in a nearly exponential stellar surface brightness profile over many scale lengths. In a galaxy with a true solid-body rotation curve, there would be no shear, so viscous evolution would not occur. LSB galaxies more typically have slowly rising rotation curves and this, balanced with low gas surface density, means that viscous evolution from gravitational instability would be nearly as effective in LSB galaxies as in large spirals (Bell (2002) and references therein).

The combination of scale length and central surface brightness derived from radial profiles may be used as a means of estimating distances to LSB galaxies. In concept, if looking at a galaxy of a given physical scale length measured in kiloparsecs, then its angular scale length in arcseconds would decrease with distance while its central surface brightness would remain the same.

Based on assumptions about the range of intrinsic sizes of LSB galaxies, a minimum scale length may be used as a criterion for a likely cut-off of galaxies within a specific distance. This method has been applied to filter for likely cluster members in many surveys where very small angular-scale-length galaxies are considered to be background objects. For example, Dalcanton et al. (1997) surveyed LSB galaxies with central surface brightness in the range  $23 < \mu_0 < 25 \text{ } V\mu$ . This survey covered a large area ( $17.5 \text{ deg}^2$  at around  $+47$  degrees Dec.) and selected objects with scale length  $a > 2.5$  arcseconds. These criteria were intended to select for nearby LSB galaxies and follow-up spectroscopy did, indeed, show that all of the candidates in



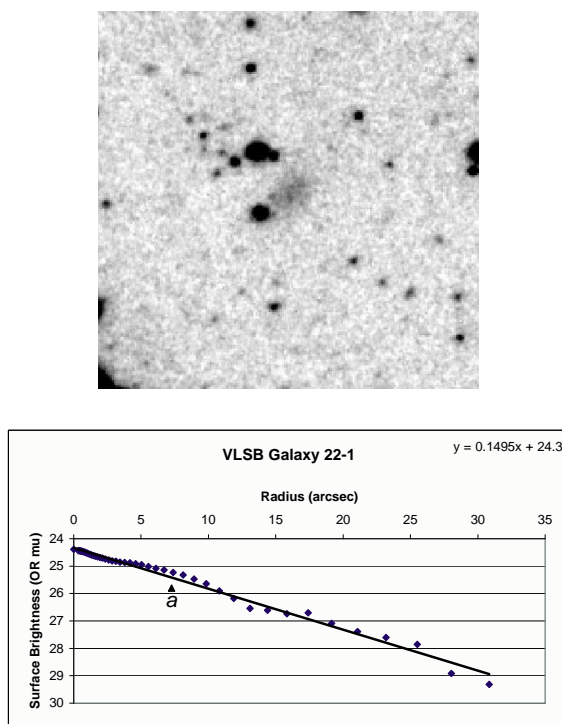


Fig. 2.2: Newly-Discovered Virgo VLSB Galaxy 22-1: Image and Radial Profile

*Top: The smudge at the centre of the image is a previously uncatalogued LSB galaxy, 22-1 of this project. This image is 134 arcsec on a side.*

*Bottom: Galaxy 22-1 has a characteristic exponential profile that appears linear on a magnitude-radius plot. A linear trendline is fitted to the data and the central surface brightness, in this case 24.3 OR $\mu$ , is extrapolated from the fit and read from the trendline equation displayed on the plot. OR refers to the passband of the observation. The slope is used to calculate scale length ( $a$ ) which, in this case, is 7.3 arcseconds and is indicated on the plot. Refer Section 5.6 for the method of generating this plot.*

the final sample have low recession velocities ( $4000 \text{ km s}^{-1} < cz < 9000 \text{ km s}^{-1}$ ). LSB galaxies detected in that survey have intrinsic scale lengths of 1.7 to  $3.6 H_{50}^{-1} \text{ kpc}^c$ , comparable to those of normal galaxies.

---

<sup>c</sup> Physical dimensions of a galaxy must be inferred from angular measurements and distance estimates. Cosmological distances rely on some assumption about the value of the Hubble constant, so values thus derived sometimes show notation that indicates what value has been assumed for  $H_0$ . In the Dalcanton paper,  $H_0 = 50 \text{ km s}^{-1} \text{ Mpc}^{-1}$  was used. Alternatively, the Hubble parameter  $h$  may be left as a variable where  $H_0 = 100 h \text{ km s}^{-1} \text{ Mpc}^{-1}$ .

### 2.3 *Cluster and Field Distribution of LSB Dwarfs*

LSB galaxies are found in both field and cluster environments. Number densities vary between these environments and from cluster to cluster, but dwarf galaxies are the most common stellar systems in the universe (Impey et al. 1988). LSB galaxies constitute 30% of the local galaxy number density (Trachternach et al. 2006) and form the dominant population in rich clusters (Morshidi et al. 1997). Trentham and Hodgkin (2002) explain that evidence is accumulating that low-luminosity galaxies are much more numerous per luminous galaxy in dense environments than in diffuse ones, and that dwarf ellipticals are the dominant types at the faintest magnitudes.

Trentham and Tully (2002) state that, based on their study of the Virgo Cluster, the relationship between giant galaxies and dwarfs is not well established and suggest, for example, the possibility that low-mass galaxies may be clumped around the few galaxies with large bulges. However, more recently, Davies et al. (2004) investigated the association between LSB dwarfs and giant galaxies and found that, while the dwarf-to-giant ratio is higher in the Virgo Cluster than in the field, there is no indication that dwarf galaxies are directly associated with giant galaxies within the cluster. Furthermore, in the Davies et al. (2004) field sample, which includes 110 dwarf galaxies, at most one galaxy with two dwarf companions was found. This paucity of dwarf companions cannot be solely due to the difficulty of detecting LSB dwarfs because, the authors state, if the Milky Way were placed at the same distance as the cut-off of the selection basis, i.e. 21 Mpc, the method should detect five companions. This implies a deficit of dwarf companions to giant galaxies in the field compared with the region around the Milky Way. De Blok (1997) also found that LSB dwarfs are generally more isolated from their nearest neighbours than HSB galaxies.

However, isolated dwarfs and LSB galaxies may be found in large numbers in all environments from rich clusters to sparse field regions. It will be demonstrated in the following chapters that, both in clusters and in the field, galaxy populations are numerically dominated by dwarfs and that the numbers rise with fainter magnitudes. The results from two field studies are compared below and, despite their apparent

differences, both illustrate the richness of the field LSB dwarf population.

Schwartzzenberg et al. (1995) conducted a deep CCD survey of LSB galaxies in 20 fields near the South Galactic Pole using a very broad-band ‘ $VR$ ’ filter and used selection criteria of central surface brightness  $\mu_o \geq 22.5 V\mu$  and exponential scale length greater than 2 arcseconds to filter out stars, HSB galaxies and artefacts and leave only the LSB galaxies. 520 objects meeting these criteria in a total of  $1.2 \text{ deg}^2$  (a surface density of around 430 per  $\text{deg}^2$ ) were detected. The authors also found that a cumulative number density of objects up to scale length of  $5 h^{-1} \text{ kpc}$  infers a volume density of 0.06 per  $(h^{-1} \text{ Mpc})^3$  and concluded that LSB galaxies outnumber normal bright galaxies by factors ranging from 5 to 25.

In contrast, Dalcanton et al. (1997) looked at an area of  $17.5 \text{ deg}^2$  using time-delay-and-integrate observations to achieve extremely accurate flat-fielding. These authors filtered for similar parameters as Schwartzzenberg et al. (1995), using  $23 < \mu_o < 25 V\mu$  and exponential scale length greater than 2.5 arcseconds, and found only around 4 galaxies per  $\text{deg}^2$  or 0.001 galaxies per  $(h^{-1} \text{ Mpc})^3$  that met these criteria.

The results of Schwartzzenberg et al. (1995) and Dalcanton et al. (1997) may appear markedly different. However, differences of 0.5 arcseconds in scale length and 0.5 in magnitude are significant. Inspection of the Schwartzzenberg et al. (1995) histograms reveals that almost 70% of the objects detected would be too faint or too small to fall within the Dalcanton et al. (1997) criteria. The selection criteria and different observation and analysis methods all point out the difficulty of comparing distributions in this way. The preferred means of comparing distributions is the luminosity distribution or the corresponding luminosity function. The luminosity distribution is simply a histogram of galaxy counts binned according to luminosity. A Schechter function (refer Equation 4.1 p.54) matching the distribution is used to parameterise the distribution, with one of the key measures being the slope of the faint end of the luminosity function. A fuller description of the luminosity function is included in Chapter 4.

Distributions of LSB dwarfs remain controversial as each survey appears to produce different results, but two phenomena are universal. One is that clusters are richer

repositories of LSB dwarfs than the field. The other is that, as surveys reach to fainter limiting magnitudes, LSB dwarfs are found in ever-increasing numbers.

## 2.4 *Galaxies, Cosmology and Clustering*

Galaxies are believed to form from the gravitational collapse of primordial overdensities in the distribution of gas and cold dark matter (CDM). One such model is described by Cole et al. (2000) in which, as a dark matter halo collapses, gas is carried with it into a cooling disk where stars begin to form. This ‘semi-analytic’ model uses a combination of simple analytic models for the baryon (gas) component and a Monte Carlo technique to follow the formation of dark matter haloes by hierarchical merging. The model begins with cosmological initial conditions of mean mass density,  $\Omega_0$ , mean baryon density,  $\Omega_b$ , the Hubble constant,  $H_0$ , and the cosmological constant,  $\Lambda_0$  (hence, such models are referred to as  $\Lambda$ CDM models). Values adopted for the reference model are  $\Omega_0 = 0.3$ ,  $\Omega_b = 0.02$ ,  $\Lambda_0 = 0.7$  and  $H_0 = 100 h \text{ km s}^{-1} \text{ Mpc}^{-1}$  with  $h = 0.7$ .

The model proceeds with gravitational collapse, dynamical friction and merging of dark matter haloes. In this scenario, galaxies form within the dark matter haloes. Thus, the model includes astrophysical processes such as gas cooling, star formation, feedback effects of star formation, stellar evolution, mergers, heavy-element production and effects of dust. In the model, disks (producing disk or spiral galaxies) form directly from gravitational collapse whilst spheroids (elliptical galaxies) are produced primarily by galaxy mergers. The model produces observable consequences that may be compared with observational data, thereby helping to test the validity of both the model and  $\Lambda$ CDM theory.

Cole et al. (2000) explain that models using direct simulation are disadvantaged by insufficient resolution to replicate the formation and internal structure of individual galaxies. For the semi-analytic model, resolution may be made arbitrarily high for a small computational cost, but the model suffers from the need to make simplifying assumptions about gas properties. Thus, either type of model has some shortcomings

that should be considered when comparisons with observations are made.

The Cole et al. (2000) model uses, as one of its main constraints, the galaxy luminosity function in the local volume. Any realistic model of galaxy formation should be able to reproduce the observed galaxy luminosity distribution. The bright end of the local luminosity distribution is well known, but there is a great deal of variation in results for the faint end, i.e. where dwarf and low surface brightness galaxies dominate. Cole et al. (2000) attribute variations to differences in either the volume surveyed or the selection characteristics of the surveys on which the luminosity functions are based. This model fits the bright end of the luminosity function well, but the faint end is only crudely constrained because of observational limitations. It is the faint-end slope that is extremely sensitive to feedback processes, so improved agreement in observational data is necessary to help refine the model.

The issue is further complicated when considering dwarf galaxies in different environments, as discussed by Davies et al. (2004). There are far fewer dwarf galaxies in low density environments than are predicted by theory, yet the population of dwarfs is high within rich, high-density environments such as the Virgo Cluster. Davies et al. (2004) argue that this cannot simply be due to infall of dwarfs into the clusters because the dwarf-to-giant ratio found in the Virgo Cluster is too high. These authors suggest that the high density of dwarfs in the Virgo Cluster may be due to environment-dependent formation processes, although it has been shown that tidal stripping may also produce LSB dwarfs (Duc et al. 2007).

The full complexities of cluster evolution remain poorly understood and are beyond the scope of this project. However, theories and models must be matched to observational data. Extant surveys are all limited in various ways, including area coverage and limiting magnitude. Data from the Virgo Deep Stack, sampled in this project, have the potential to cover a large area to very faint magnitude limits, around 28  $R\mu$ . These data, which overlap with many existing and ongoing surveys and catalogues, may prove invaluable in constraining the faint-end slope of the Virgo Cluster luminosity function.



### 3. GALAXIES AND THE VIRGO CLUSTER

The region of the Virgo Cluster is a very well-studied patch of sky. The cluster has been the subject of many surveys using photography, CCD imaging and spectroscopy to obtain information about properties of its individual galaxies and the galaxy cluster as a whole. Section 3.1 explains why the Virgo Cluster is such a useful case study and why it has been the subject of so many surveys. Section 3.2 provides some general background on the broad range of galaxy types that are known to exist in all environments. Section 3.3 details the many surveys of the Virgo Cluster. Some surveys are specific to particular classes of galaxies or particular regions of the Virgo Cluster. Each is made in one or more specific passbands and is limited by surface-brightness depth at some level. In the remainder of this chapter, discussion of properties of the Virgo Cluster and its member galaxies will illustrate that disagreement remains on certain basic cluster properties, such as distance. Hence, further large-scale surveys to ever-deeper surface-brightness limits are necessary to fully understand this complex and important cluster.

#### *3.1 Importance of the Virgo Cluster*

Being a large, relatively nearby cluster at a distance of some 16 to 18 Mpc (e.g. Jacoby et al. (1992)), the Virgo Cluster contains thousands of galaxies and has the observational advantage that it is accessible by telescopes in both the northern and southern hemispheres. It is the closest cluster that contains examples of all major galaxy types including elliptical, spiral and irregular galaxies. Young and Currie (1998) explain that this means a wider variety of the most commonly used distance indicators (e.g. the Fundamental Plane (FP) for elliptical galaxies (Djorgovski and

Davis 1986) and the Tully-Fisher (TF) relation for spirals (Tully and Fisher 1977)) may be used for Virgo galaxies than for other clusters at similar distances, such as the Fornax Cluster and the Leo I group. Virgo galaxies also cover a complete range of galaxy sizes from the largest and most massive giants to the smallest and most compact dwarfs. By surveying the galaxy population in the Virgo Cluster it is possible to develop an overall understanding of the workings of the cluster, its sub-structure, and how its observed physical properties fit in with current theories of the formation and evolution of galaxies and galaxy clusters, within a wider cosmological context. It is the closest true galaxy cluster, much richer than the environment of the Local Group to which the Milky Way belongs, and close enough that its faintest galaxies are within reach of current technology.

The Virgo Cluster covers a huge area on the sky, larger than the entire constellation of the Southern Cross. Its members are distributed across almost 10 degrees in right ascension and 14 degrees in declination, requiring 4 UKST standard survey fields to cover it completely. Physically, it is separated from background galaxies by a deep void, making it relatively easy to distinguish cluster members from background non-members by determining radial velocities from redshift measurements (this technique is described in Section 4.5.1). The maps and survey descriptions provided in Sections 3.3 and 3.4 describe its depth and 3D structure, illustrate the areal extent of the cluster on the sky and reveal the difficulty of trying to cover the entire cluster with a single deep survey. The Virgo Deep Stack, centred on the core of the cluster and covering a large fraction (approximately 25%) of the cluster's area, provides a fresh opportunity to survey its faintest, and most elusive, galaxy population.

### 3.2 *Galaxy Classification*

In both the general field and in cluster environments, there exists an array of galaxy types ranging from the luminous galaxies known in the 1930s to LSB galaxies requiring long integration times on large modern telescopes to be detectable. The former group includes elliptical (E), lenticular (S0), spiral (Sa, Sb and Sc), barred spiral



(SBa, SBb, SBc) and irregular (Irr) galaxies that formed the ‘tuning fork diagram’ originated by Hubble (1936) (refer Figure 3.1).

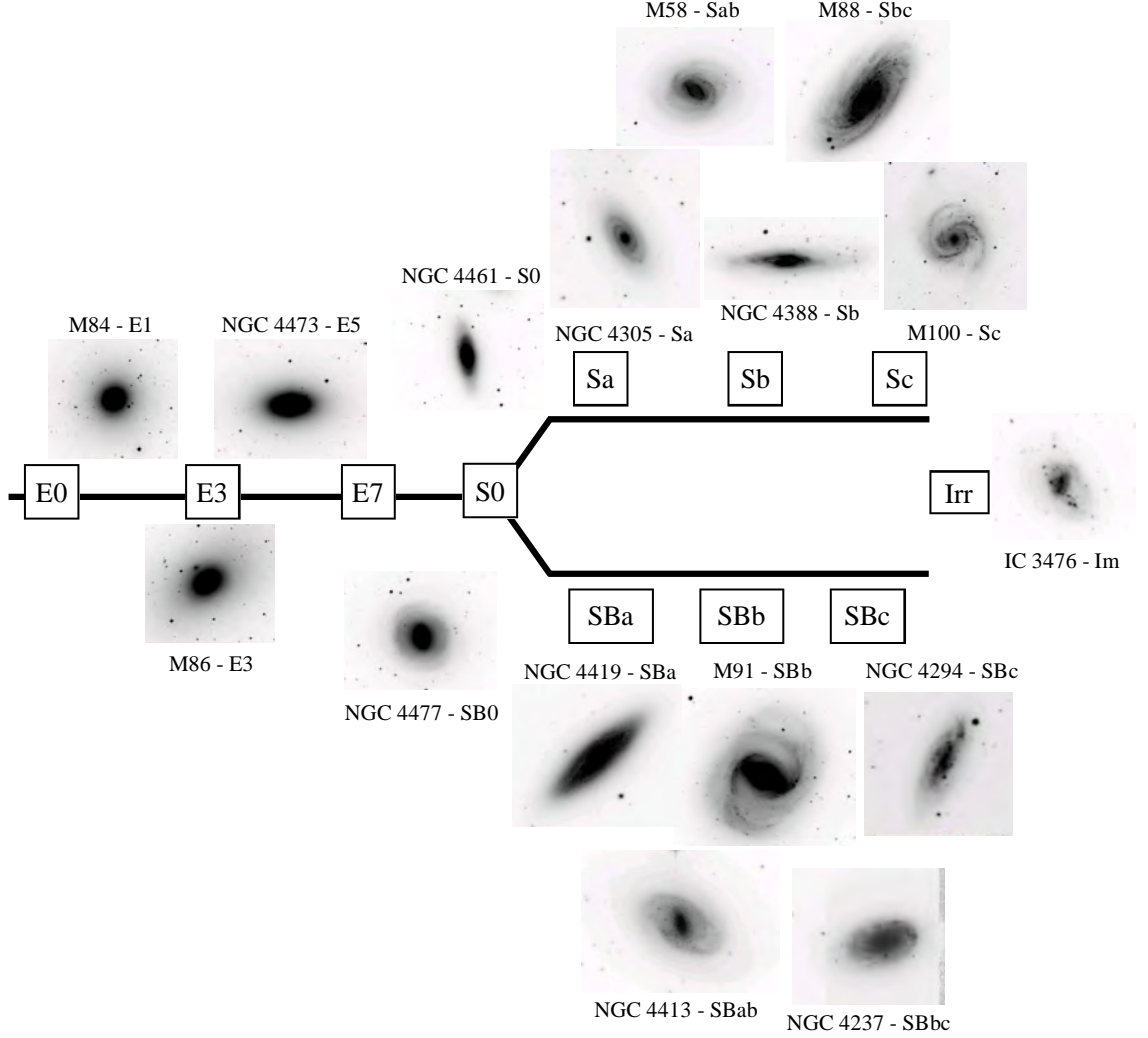


Fig. 3.1: The Hubble Tuning Fork Diagram

*The galaxy classifications of the original Hubble (1936) diagram are shown in the boxed labels along the tuning fork, but subsequent revisions have refined some labels and added intermediate and additional classifications. Galaxy images, extracted from the Virgo Deep Stack, are shown as examples and are labelled with their current classifications. The image of NGC 4237, at bottom right, falls onto the very edge of the stack.*

Based on their morphology, Hubble (1936) arranged galaxies into a sequence of ellipticals and two sequences of spirals - those with and without central bars. Ellipticals

are typified by having smooth, symmetrical, spheroidal structure that can be traced by elliptical contours. Spirals have central bulges and spiral arms, whilst in a barred spiral the arms spring from the ends of a linear ‘bar’ (of variable extent) centred on the nucleus. From left to right, the Hubble tuning fork diagram depicts:

- elliptical galaxies in order of increased flattening (sub-types E0 to E7 defined by  $E_n$ , for  $n = 10(a - b)/a$ , where  $a$  and  $b$  are projected major and minor axes);
- S0 (lenticular, or lens-shaped) galaxies with bulges similar to ellipticals surrounded by disks with no spiral structure;
- an upper branch of spiral galaxies ranging from those with tightly-wound arms (Sa) through intermediate (Sb) to very open, loose spiral arms (Sc);
- a lower branch of corresponding barred spirals (SBa, SBb, SBc); and
- irregular galaxies (Irr) with no morphological symmetry.

Galaxies to the left of the diagram are referred to as ‘early’ and those on the right ‘late’ because Hubble (1936) believed that galaxy structure evolved with time from elliptical to spiral. It is now known that this is not the case, but the nomenclature is still in use.

This classification system and subsequent revisions based on integrated spectral type (Morgan 1958), luminosity (van den Bergh 1960) and detailed morphology (de Vaucouleurs and de Vaucouleurs 1964) are all applicable for relatively bright galaxies. Refer to Sandage and Binggeli (1984) for a full description of the history and developments of the classification scheme.

New classifications that have been added to Hubble’s original scheme include the LSB classification, a special class for the dominant galaxy in a cluster and various classes for ‘normal’ dwarf galaxies and the rarer compact dwarfs.

Brightest cluster galaxies (BCGs) are sometimes classified as giant elliptical (gE), D (for ‘diffuse’) or cD for galaxies with an extended envelope of light over and above a standard fit for an elliptical galaxy (Dubinski 1998).

Dwarf galaxies may be thought of as ‘small’, though there is a continuous transition between dwarf elliptical (dE), dwarf lenticular (dS0) and giant elliptical galaxies (Barazza et al. 2003). Dwarf ellipticals may also be nucleated (dE,N) (Trentham and Tully 2002). Distinctions between dE and dS0 galaxies are subtle, especially as many of them also fall into the class of low surface brightness for which it is difficult to obtain kinematic information at the distance of the Virgo Cluster ( $\sim 17$  Mpc). Visually, the radial profile of a dE is well-fitted by an exponential but, unlike disk galaxies that are also fitted by exponentials, dEs are usually round (Impey et al. 1988).

Ryden et al. (1997) explain that dE galaxies are pressure-supported slowly rotating triaxial systems with no significant disk, while dS0 galaxies have rotationally supported disks and may also have central bulges. These authors conclude that, in the case of the Virgo Cluster, it is not possible to distinguish between dE and dS0 galaxies based on surface photometry alone. Dwarf spheroidals (dSph) are a subset of dE galaxies with faint magnitudes, low surface brightness and no nucleus (Gallagher and Wyse 1994). Most of the newly-identified galaxies in this project (refer Chapter 8) may be considered to be VLSB dSph galaxies. Discussions of dEs often subsume dSph and dS0 galaxies into one class, e.g. Barazza et al. (2003), Boselli et al. (2008). Dwarf irregular (dI) galaxies are irregularly shaped and often show clumps (Sabatini et al. 2005). However, they are seldom nucleated, in contrast to dEs, which often are (Trentham and Hodgkin 2002). Dwarf spirals do not exist, with the faintest spiral class having a mean absolute magnitude of  $-18$ , two magnitudes brighter than the brightest dwarfs (Sandage 2005).

Sandage (2005) gives an absolute magnitude range for dEs & dSphs of  $-16 \leq M \leq -7$ . For the purposes of studying the dwarf-to-giant ratio, Davies et al. (2004) use discontinuous definitions that are converted here from their  $B$ -band classifications to  $R$ -band for comparison (once again using  $B - R = 1.5$ ). By these definitions, dwarfs are classified as those galaxies in the Virgo Cluster with  $-15.5 \leq M_R \leq -11.5$  and  $21.5 \leq \mu_0 \leq 24.5$   $R\mu$  and giants as those with  $M_R \leq -20.5$ . However, Phillipps et al. (1999), in a study of environmental effects on the faint-end slope of the luminosity

function, define dwarfs as having  $-19.5 \leq M_R \leq -16.5$  and giants as those galaxies with  $-23.5 \leq M_R \leq -19.5$ , thus designating all brighter galaxies to one or other classification, but omitting the very faint LSB dwarfs that lie almost exclusively within  $M_R > -16.5$ . Refer Table 4.1 (p.59) for a summary of dwarf-to-giant ratio definitions.

Two classes of compact dwarf are now also recognised: blue compact dwarfs (BCDs), first discovered by Arp (1965); and ultra-compact dwarfs (UCDs), first discovered in the Fornax cluster by Drinkwater et al. (1999). The search for BCDs in the Virgo Cluster by Drinkwater et al. (1996) used the following criteria: classification as ‘galaxy’ or ‘merged’ from Automated Plate Measuring (APM) image analysis software<sup>a</sup>; magnitude range of  $15.70 \leq B_J \leq 17.55$ ; peak intensity of  $\mu_0 < 19.8 B_J \mu$ ; along with eccentricity, compactness and area constraints. Membership of the Virgo Cluster, as obtained from radial velocity measurements, was then used to identify nine BCDs amongst the 303 galaxies that met these criteria.

UCDs in the Virgo Cluster were identified by Jones et al. (2006) from colour-selected star-like targets with  $16.0 < b_j < 20.2$ . These objects have early-type galaxy spectra and are generally classified as stars by APM image analysis software due to their point-like appearance on UKST images (refer Figure 3.2), although they have been resolved by the HST (Drinkwater et al. 2004). Their red absorption-line spectra are indicative of an older stellar population. Their radial velocities confirm Virgo Cluster membership and absolute magnitudes range from  $-12.9 \leq M_B \leq -10.7$ .

LSB galaxies are as defined in Section 2.1. The definition is based on central surface brightness or isophotal magnitude. LSB galaxies may be of any size.

### 3.3 *Virgo Galaxy Surveys and Catalogues*

Many of the surveys discussed in this section are discovery surveys that have identified, classified and catalogued galaxies that were previously unseen, uncatalogued

---

<sup>a</sup> Maddox et al. (1990) describes the image analysis used for the APM Survey.

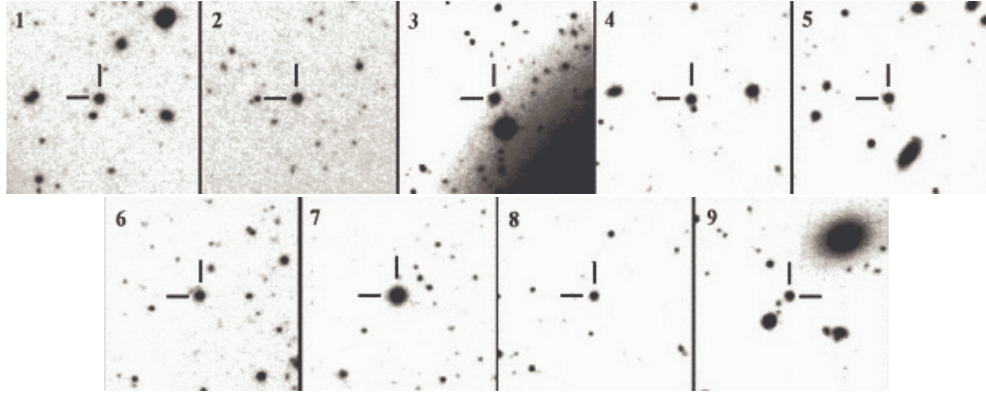


Fig. 3.2: Ultra-Compact Dwarfs in the Virgo Cluster

*Unlike the bright, distinctive galaxies of the Hubble sequence (refer Figure 3.1) or the diffuse, extended LSB galaxies (refer Figure 2.1), ultra-compact dwarfs (UCDs) appear starlike in these images from the Virgo Deep Stack.*

Figure reproduced from Jones et al. (2006).

or misidentified. Also discussed are analyses that have yielded new information about known galaxies, such as photometric data or HI measurements. Information typically appearing in catalogues may include, but is not restricted to:

- position;
- cross-reference to other catalogues;
- cluster membership designation;
- morphological type;
- angular and physical dimensions;
- apparent magnitude in one or more passbands; and
- heliocentric radial velocity (derived from the redshift).

The catalogue data may be used to study galaxy and cluster properties. Galaxy morphology is usually studied using high-resolution images and optical surface photometry. The photometry process results in a radial light profile of the galaxy in

units of magnitudes per square arcsecond ( $\mu$ ). The radial profile is a useful tool in galaxy classification, determination of total apparent magnitude ( $m_T$ ) and studies of galaxy evolution in different environments. The overall population of a cluster may be summarised by its constituent-galaxy luminosity distribution and the matching luminosity function. Analyses based on independent distance measurements, combined with radial velocity information from spectroscopy, are used to study 3D structure within a cluster.

The following list of selected surveys, catalogues and analyses relevant to this project provides a useful background to the large volume of work that has already been conducted in the direction of the Virgo Cluster. The various analysis techniques used and information about the Virgo Cluster gained from these surveys are discussed further in Section 3.4 and Chapter 4. The surveys and catalogues included here are summarised in Table 3.2 (p.36).

**i. The Virgo Cluster Catalogue (VCC), 1985**

One of the landmark surveys in the direction of the Virgo Cluster produced the Virgo Cluster Catalogue (VCC) of Binggeli et al. (1985) which details 2096 galaxies within an area of  $\sim 140 \text{ deg}^2$  to a total apparent  $B$ -band magnitude of  $B_T \approx 18$ , corresponding to absolute magnitude  $M_{B_T} \approx -13.7$ , using a Virgo Cluster distance modulus of  $m - M = 31.7$  (refer Equation 5.16 p.115 for relationship between magnitudes, distance modulus and distance). The catalogue includes galaxies of all major morphological types (spiral, elliptical, dwarf elliptical, and irregular) imaged on 67 photographic plates taken at Las Campanas Observatory between 1979 and 1982.

Identifications of 572 cluster members are based on heliocentric radial velocities in the range  $-1600 \leq v_{helio} \leq 2700 \text{ km s}^{-1}$ , which is generally considered to be the range for true cluster membership. These data are plotted, for reference against other surveys, in all maps (Figures 3.3, 3.6, 5.7, 6.2 and 8.1). However, to date, velocities are not available for all galaxies in the catalogue. Other membership criteria used by Binggeli et al. (1985) are surface brightness (based on correlations between absolute magnitude and surface brightness),

resolution of detailed galaxy structure, and luminosity class. The catalogue includes confirmed and possible cluster members from the Las Campanas survey as well as cluster and background galaxies from the earlier Zwicky et al. (1961-1963) catalogue. The full catalogue contains 1277 certain cluster members, 574 possible cluster members and 245 background galaxies. Foreground galaxies cannot be distinguished from Virgo Cluster members using velocity measurements due to the large range in velocities of genuine Virgo Cluster members, including some with blueshifts (Trentham and Tully 2002). The dynamics and sub-structure of the cluster are further discussed in Section 3.4.

ii. **The Impey, Bothun & Malin (IBM) Survey of LSB Virgo Dwarfs, 1988**

Impey et al. (1988) studied 137 LSB galaxies in the Virgo area using CCD imaging to derive surface photometry. Targets were chosen from two overlapping UKST fields imaged on three IIIa-J photographic plates. Selected areas in the fields, covering  $7.7 \text{ deg}^2$ , were photographically amplified to detect galaxies to a  $B$ -band surface magnitude of approximately  $27 B_\mu$ . The CCD data for these galaxies may be followed out to 29 or 30  $B_\mu$ .

The 27 new galaxies identified in this survey have very low surface brightness and angular diameters  $\gtrsim 30$  arcseconds. They appear, from HI studies, to be gas-poor. Yet, they are unusually blue for ellipticals, implying relatively youthful ages. The authors identified an apparent discontinuity between dwarf and giant ellipticals at  $M_B \approx -16$ . This marks a transition between galaxy radial profiles fitted by an exponential and those with an  $r^{1/4}$  component in the central region, originally believed to indicate that ellipticals and dwarf ellipticals belonged to two distinct families.

However, this distinction was later refuted by Gavazzi et al. (2005b) based on several arguments:  $U - V$  and  $B - H$  colours and metallicity smoothly increase with luminosity; central surface brightness increases monotonically with absolute magnitude; and there is no clear distinction between giants and dwarfs in fundamental plane relations (refer Gavazzi et al. (2005b) for

references). Despite the likelihood of Virgo Cluster membership of the LSB galaxies, one of those discovered by Impey et al. (1988), Malin 1, was found from HI observations to lie well beyond the Virgo Cluster. A fresh analysis of this unusual galaxy using Virgo Deep Stack data is presented in Chapter 7.

### iii. **Spectral Observations of Blue Compact Dwarfs (BCDs), 1996**

Targets were selected by Drinkwater et al. (1996) from UKST plates that were digitised by the APM microdensitometer facility at Cambridge and the equivalent COSMOS<sup>b</sup> measuring machine at ROE. Observations were then made over three observing seasons (1992-1994), using the UK Schmidt FLAIR-II multi-object fibre spectrograph, to obtain spectra of galaxies brighter than  $B_J = 17.6$  in the central  $30 \text{ deg}^2$  of the Virgo Cluster (the same field coverage as that of the Virgo Deep Stack). Targets were selected as candidate BCD and dE galaxies.

The spectra obtained were used to determine cluster membership and to study large-scale structure beyond the Virgo cluster. The authors observed 303 galaxies and obtained reliable velocities for 291 galaxies, nine of which proved to be cluster members. Of the sample, 31 were VCC galaxies. The findings, compared with the original VCC classifications, are shown in Table 3.1. These results support the original VCC membership estimates.

Other results from this survey focus on the two main survey groups: the cluster dE data that are included in the Virgo Photometry Catalogue (VPC, Young and Currie (1998), refer Item iv); and the BCD studies extending to larger distances with  $v_{\text{helio}} < 31,000 \text{ km s}^{-1}$ . This study confirms the completeness of the BCD luminosity function of Binggeli et al. (1988). There is no evidence of red compact dwarfs which suggests either that, if star formation is short-lived, then galaxies must fade beyond the survey's magnitude limit or that star formation is ongoing in these galaxies. The authors also found that the background BCDs serve as a useful probe of large-scale galaxy distribution.

---

<sup>b</sup> COSMOS capabilities are described by MacGillivray and Stobie (1984).



Count	VCC classification	New finding
5	member	member
4	possible member	member
3	possible member	background
10	background	background
3		no reliable redshift
6		redshift from other source
31		

Tab. 3.1: VCC Cluster Membership

*Galaxies from the VCC have their membership of the Virgo Cluster reassessed.*

Data from Drinkwater et al. (1996).

#### iv. The Virgo Photometry Catalogue (VPC), 1998

This catalogue, compiled by Young and Currie (1998) and based primarily on four wide-field UKST plates, presents photographic surface photometry in three passbands:  $U$  using one IIIa-J plate with UGI filter;  $B_J$  using two IIIa-J plates with GG395 filter; and  $R_C$  using one IIIa-F plate with an RG630 filter.<sup>c</sup> The catalogue contains data for 1180 galaxies within a  $23 \text{ deg}^2$  area centred on  $12^h 26^m + 13^\circ 08'$  in B1950 coordinates. The UKST plates were digitised by scanning with the COSMOS measuring machine at ROE. In addition to the photometric data and physical parameters, such as orientation and ellipticity, the catalogue includes heliocentric radial velocities from a number of sources including Drinkwater et al. (1996). Limiting magnitudes are quoted as  $25\mu$  for the  $U$ - and  $B_J$ -band data and  $24\mu$  for the  $R_C$  data. Objects from the catalogue with  $v < 2700 \text{ km s}^{-1}$  are plotted in Figure 3.3.

#### v. Luminosity Function Analysis of Dwarf Spheroidals, 1998

The main purpose of this analysis by Phillipps et al. (1998) was to derive a luminosity function for dwarf spheroidal galaxies. The data were derived from

---

<sup>c</sup> The authors refer to this as Cousins  $R$ , calling it  $R_C$ , although Bessell (1986) notes differences between photoelectric Kron-Cousins  $R_C$  and photographic  $R_{63F}$ .

a set of six UKST exposures of the same field. Each Tech Pan film was digitally scanned by the SuperCOSMOS automatic measuring machine at ROE in nine smaller scan regions. The scans were then median stacked to enhance faint detail to a limiting magnitude of  $25.45 R\mu$ . This study covers two scan regions of  $1.58 \text{ deg}^2$  and  $1.61 \text{ deg}^2$  in the inner and outer parts of the Virgo Cluster field respectively. These regions are shown in Figure 5.7 (p.103). The selection criteria, described in Section 4.5.4, reveal 675 LSB dwarfs in the inner region and 895 in the outer region. These data do not appear to be available as an online catalogue but discussion of the resulting luminosity function is provided in Chapter 4.

vi. **3D Structure of the Virgo Cluster, 1999**

The Virgo Cluster sub-structure was surveyed by Gavazzi et al. (1999). Distances were determined for 134 galaxies in the main A and B sub-clusters, the more distant W and M clouds and the E, S, and N regions. The authors used FP and TF galaxy distance determination methods combined with  $H$ -band photometry of 200 galaxies, known velocity dispersions and some new spectroscopic data to make these distance measurements. Figure 3.5 shows a plan diagram of these regions and 3.6 maps their positions on the sky. This sub-structure is further detailed in Section 3.4.2 and the dynamics of the cluster as a whole are considered in more detail in Section 3.4.

vii. **Faint Galaxies in Different Environments, 2002**

Trentham and Tully (2002) used observations with the 8-m Subaru Telescope to obtain data to derive the faint-end slope of the galaxy luminosity function in five environments of varying galaxy density: the Virgo Cluster, the NGC 1407 Group, the Coma I Group, the Leo Group and the NGC 1023 Group. An area of  $1.2 \text{ deg}^2$  was surveyed in the direction of the core of the Virgo Cluster (refer Figure 3.3).

Concentration parameters were used as selection criteria for cluster membership where no redshifts were available (see further discussion of member identification in Section 4.5). The authors found the density of dwarfs is higher

in the Virgo survey region than in any of the other environments surveyed. The faintest galaxies in the survey have  $R \approx 22.5$  and reach central surface brightnesses of almost  $27 R\mu$ . The survey showed that in more dynamically evolved environments there is a higher ratio of dE to dI galaxies.

viii. **The Luminosity Function of the Virgo Cluster, 2002**

Trentham and Hodgkin (2002) used  $B$ -band CCD imaging of 449 galaxies to study the luminosity function of galaxies in the Virgo Cluster. Data included galaxies from a number of existing catalogues as well as 142 new objects. Images were obtained using the Wide Field Camera on the 2.5-m Isaac Newton Telescope (INT) at La Palma as part of the INT Wide Field Survey. That imaging survey is not specific to the Virgo Cluster, but includes two strips that cross the cluster imaged in the  $i$ - and  $B$ -bands (refer Figure 3.3). The authors followed reduction, galaxy classification and cluster-member identification methods similar to those of Trentham and Tully (2002) to obtain a luminosity function in the range  $-22 \geq M_B \geq -11$ . The survey covers  $24.9 \text{ deg}^2$ . Comparison data, obtained in a  $31 \text{ deg}^2$  region of the INT Wide Field Survey covering the North Galactic Cap, were used to estimate background contamination in the Virgo sample.

ix. **Dwarf LSB Galaxy Survey in the Virgo Cluster, 2003**

Sabatini et al. (2003) presented a study of the faint-end slope of the luminosity function in inner and outer regions of the Virgo Cluster based on  $B$ -band data from a  $\sim 14 \text{ deg}^2$  area of the INT Wide Field Survey east-west strip. The authors followed up with colour and HI line observations (Sabatini et al. 2005) and a similar study of the north-south strip (Roberts et al. 2007). These studies used an automated repeatable procedure for detecting LSB galaxies and an optimum filter to preferentially select cluster members rather than background galaxies. Numerical simulations were used to identify distinguishing properties of member and non-member galaxies (refer Section 4.5). This survey identifies 105 previously uncatalogued galaxies and includes 143 Trentham and Hodgkin (2002) galaxies although, in Davies et al. (2004), the total count is given as

257 LSB dwarf candidates<sup>d</sup>. The 105 newly-identified galaxies are plotted in Figure 5.7 (p.103). The follow-up study of the north-south strip (Roberts et al. 2007) contains 336 objects, 218 of which were previously uncatalogued.

x. **The ACS Virgo Cluster Survey, 2004**

The Advanced Camera for Surveys (ACS) was installed on the Hubble Space Telescope in 2002 and has been used to survey 100 early-type Virgo Cluster galaxies from the VCC in fields 202 x 202 arcseconds in size (refer Figure 3.3). Hence, the survey covers 0.31 deg<sup>2</sup> in total. The goals of the survey include studies of globular clusters associated with the galaxies, isophotal analyses of the galaxies and distance determinations using the surface brightness fluctuation method (Côté et al. 2004).

xi. **HI Observations in the Virgo Cluster, 2005**

Optical surveys may be supplemented by data in other wavelengths, since much of the mass of a galaxy is tied up in its gas (HI) and dark matter components. Using the Arecibo telescope, Gavazzi et al. (2005a) observed 33 Virgo galaxies to complete an HI data set of 355 late types (Sa - spirals with tightly wound arms, Im - irregular ‘magellanic’ types, and BCDs). From this data set the authors derived the Virgo Cluster HI mass function. This survey is complete for cluster members with photographic magnitude  $m_p \leq 18.0$ . The results and comparisons with a field HI mass function and optical luminosity functions indicate that neutral hydrogen is mainly contained in late-type galaxies, with only marginal contributions from early types and isolated HI clouds.

xii. **Analysis of Elliptical Galaxies in the Virgo Cluster, 2005**

Gavazzi et al. (2005b) used *B*- and *I*-band photometry of data from the INT Wide Field Survey to study the properties of 226 elliptical galaxies in the Virgo Cluster. The galaxies cover the full range from giants (E) to dwarfs (dE). The authors studied the relationships between size, surface brightness, luminosity and the Sérsic ( $r^{1/n}$ ) model of light distribution of dE-E galaxies.

---

<sup>d</sup> The other 9 galaxies are presumably listed in the VCC or Impey et al. (1988).

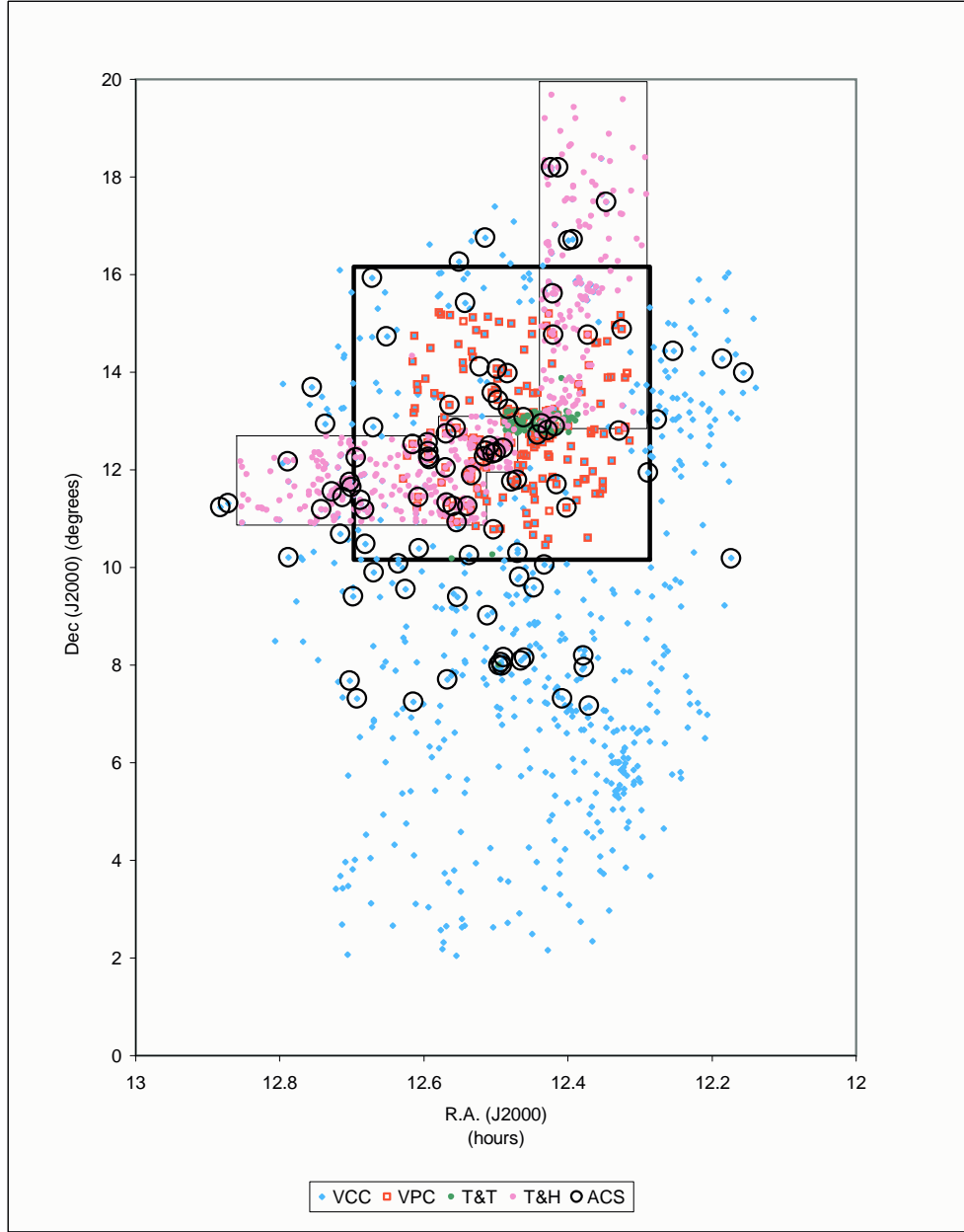


Fig. 3.3: Map 1: Combined Survey Map

*This figure illustrates several survey regions against the backdrop of VCC cluster members ( $v < 2700 \text{ km s}^{-1}$ , blue dots). Red squares are the cluster members examined by Young and Currie (1998) in the Virgo Photometry Catalogue (VPC). Green data points (T&T) are galaxies observed by Trentham and Tully (2002) with the Subaru Telescope. Regions covered by the INT Wide Field Survey (thin boundary lines) are referred to as the N-S strip and the E-W strip. The INT Wide Field Survey data (pink data points, T&H) were used by Trentham and Hodgkin (2002) to derive a luminosity function for the Virgo Cluster. Black circles represent galaxies imaged by the ACS Survey. The heavy square is the region covered by the Virgo Deep Stack.*

The study addresses a distinction between the brightest E galaxies and the rest of the population that is seen in the ‘magnitude - effective surface brightness’ ( $M_B/\mu_{eff}$ ) plane by examining radial profiles and using alternative comparisons. It was found that the observed segregation is due to ‘core’ galaxies in the brighter population ( $M_B < -20.5$ ). These are galaxies for which profiles flatten in the central 100 pc, 1.2 arcsec at the distance of the Virgo Cluster, thus causing a step in the distribution due to the effect of the flattening on effective surface brightness (surface brightness measured at the half-light radius). By instead plotting  $M_B$  vs  $\mu_0$ , the dichotomy disappears and the population shows a smooth distribution. Furthermore, excluding the ‘core’ galaxy population, the Sérsic index ( $n$ ) increases linearly with luminosity.

From the  $B - I$  colour information, Gavazzi et al. (2005b) found that blueness and the amount of spread in colour index both increase with fainter luminosities.

#### xiii. **Ultra-Compact Dwarfs in the Virgo Cluster, 2005**

Prompted by the identification of UCDs in the Fornax cluster by Drinkwater et al. (1999), Jones et al. (2006) used 2dF spectroscopy on the Anglo-Australian Telescope to target 1500 colour-selected star-like objects within one degree of M87 in Virgo. Targets were selected from the APM object catalogue generated from scanning of UKST plates. Nine UCDs were discovered, with properties comparable with those in the Fornax cluster, and with magnitudes in the range  $16.0 < b_j < 20.2$  (refer Figure 3.2). Data from the INT Wide Field Survey were used to measure image sizes and surface brightness profiles and the Virgo Deep Stack was also accessed to search for LSB haloes. No evidence of extended haloes around any of the Virgo UCDs was found. The authors conjecture that these objects of  $\ll 100$  pc in size may have formed through galaxy interactions and be the remnants of nucleated dEs or luminous star clusters.

xiv. **Low Luminosity Galaxies in the Virgo Cluster, 2005**

Caldwell (2005) surveyed seven fields with the Kitt Peak National Observatory (KPNO) Mosaic camera on the Mayall 4-m telescope to search for dwarf elliptical galaxies. The main finding from that survey is that there are galaxies in the Virgo Cluster with central surface brightness down to  $\mu_0 \simeq 27.5 B\mu$ , about two magnitudes fainter than known in the Local Group. By observing three of these newly-found galaxies with the ACS instrument on the Hubble Space Telescope, Caldwell (2006) resolved stars with colour and magnitude that are consistent with them being ‘red giant branch’ (RGB) stars in Virgo Cluster galaxies. Two of these confirmed cluster members are discussed in detail in Section 6.2.2.

xv. **This Project: The Virgo Deep Stack VLSB Galaxy Survey, 2008**

Surveys to date have covered a diverse range of galaxy types, many optical passbands and also HI measurements. The large area and depth covered by the Virgo Deep Stack allow examination of, and comparison with, data from many other surveys. This project explores the VLSB population in the *OR*-band to a depth comparable with the *R*-band data of Trentham and Tully (2002) and *B*-band data of Trentham and Hodgkin (2002). Many VLSB galaxies have been newly identified and catalogued, together with their properties, in Chapter 8.

Although this list of surveys and catalogues appears comprehensive, there is no catalogue of LSB galaxies covering the entire Virgo Cluster that is complete for objects fainter than  $M_B = -14$  and central surface brightness values down to  $26 B\mu$ , values typical of dwarfs in the Local Group (Sabatini et al. 2005). Nor is the above listing fully comprehensive. Many other studies concentrate on certain galaxy types or particular analysis techniques that have limited relevance to this project.

Considerable amounts of data from catalogues based on these surveys and other publications are available through the on-line astronomical databases: *Simbad* and *VizieR*, both maintained by the Centre de Données Astronomiques de Strasbourg at <http://cdsweb.u-strasbg.fr/>; and *NED*, the NASA/IPAC Extragalactic Database at <http://nedwww.ipac.caltech.edu/>, which is operated by Jet Propulsion

Laboratory, California Institute of Technology, under contract with the National Aeronautics and Space Administration.

Description (Reference)	Type <sup>†</sup> $\mu_{lim}$ <sup>‡</sup>	Band Area (deg <sup>2</sup> )	Galaxy Counts and Limiting Magnitudes
i) Virgo Cluster Catalogue <sup>1</sup> (Binggeli et al. 1985)	P $\sim 25.3 B\mu$	$B$ 140	2096 galaxies (all types) to $B_T \sim 18$
ii) Virgo Dwarfs - IBM <sup>2</sup> (Impey et al. 1988)	P & C $\sim 27 B\mu$	$B, V, I$ 7.7	137 LSB galaxies (27 new) to $B_{27} = 20.2$
iii) Blue Compact Dwarfs (Drinkwater et al. 1996)	C	<i>Spec.</i> 30	303 BCDs to $B_J = 17.6$ (291 reliable velocities)
iv) Virgo Photometry Catalogue (Young and Currie 1998)	D 24 $R\mu$	$U, B_J, R_C$ 23	1180 galaxies (all types) to $B_{J25} = 19.0$
v) LF <sup>3</sup> of Dwarf Spheroidals (Phillipps et al. 1998) <sup>4</sup>	D $\sim 25.5 R\mu$	$R$ 3.2	1570 LSB dwarfs to $R \approx 20$
vi) 3D Structure of Cluster (Gavazzi et al. 1999)	N	$H$ per VCC	Photometry of 200 galaxies (distances to 134 galaxies)
vii) Faint Galaxy LF (Trentham and Tully 2002)	C 28 $R\mu$	$R$ 1.2	99 VC galaxies to $R \approx 22.5$ (inc. 51 new dE, dI, LSB)
viii) LF of the Virgo Cluster (Trentham and Hodgkin 2002)	C 27 $B\mu$	$B$ 25	449 various types to $B = 25$ (inc. 142 new dE, dI, LSB)
ix) Dwarf LSB Galaxies (Sabatini et al. 2003) (Roberts et al. 2007)	C 26 $B\mu$ <sup>#</sup>	$B$ 14 15	To $M_B = -9.5$ ( $B \sim 21.5$ ) 231 LSB dwarfs (105 new) 336 LSB dwarfs (218 new)
x) HST ACS Survey (Côté et al. 2004)	C	$g, z$ 0.31	100 VCC galaxies in 202" x 202" fields
xi) HI Observations (Gavazzi et al. 2005a)	R	$21cm$ per VCC	33 Sa, Im, BCD observed (reports on 355 galaxies)
xii) Elliptical Galaxies (Gavazzi et al. 2005b)	C $\sim 27 B\mu$	$B, I, i$ 26	226 VCC ellipticals to $m_p = 20$
xiii) Ultra-Compact Dwarfs (Jones et al. 2006)	C	<i>Spec.</i> 3.14	9 UCDs discovered
xiv) Low Luminosity Galaxies (Caldwell 2005)	C $\sim 28 B\mu$	$B, R$ 3.5	3 verified cluster members
xv) Virgo Deep Stack Catalogue (This project)	D $\sim 28 R\mu$	$OR$ 25 (3.47)*	100 new galaxies in sub-area (82 likely cluster members)

Tab. 3.2: Selected Virgo Cluster Surveys and Catalogues

<sup>†</sup> Type:  $P$  = photographic,  $C$  = CCD,  $D$  = digitised photographs,  $R$  = radio,  $N$  = near infrared.

<sup>‡</sup>  $\mu_{lim}$  is limiting surface brightness, where supplied, and may refer to completeness limit or faint isophote limit (detection threshold) of the data.

1. Referred to as the VCC.

2. Known as IBM after authors Impey, Bothun and Malin.

3. LF = luminosity function.

4. No online catalogue available.

# Limiting central surface brightness.

\* Total image area available (area examined in detail for this project).



### 3.4 Properties of the Virgo Cluster

The Virgo Cluster is the dominant mass concentration in the Local Supercluster and the largest collection of elliptical and lenticular galaxies in the nearby universe (Côté et al. 2004). It is dominated by the bright elliptical galaxies M87, M86 and M49. Its large, complex structure extends from 15 to 29 Mpc in distance (Gavazzi et al. 1999), covers an area of  $\sim 140 \text{ deg}^2$  on the sky (Binggeli et al. 1985) and contains at least 1300 galaxies. It is a dynamic cluster that includes sub-clusters at various distances, each with its own peculiar velocity relative to the dominant sub-cluster (Gavazzi et al. 1999), and contains a high propensity of dwarf galaxies relative to the field population (Roberts et al. 2004). Trentham and Hodgkin (2002) explain that galaxies in the cluster must have undergone many galaxy-galaxy interactions due to its short crossing time ( $\sim 0.1$  of a Hubble time). The galaxies move through a hot intra-cluster medium where strong radio and x-ray emissions are associated with the giant elliptical galaxy, M87 (Young et al. 2002).

The following sections describe some of the cluster's physical parameters and the effects that this environment has on the galactic population.

#### 3.4.1 Velocity Distribution in the Direction of the Virgo Cluster

The Virgo Cluster is a rich dynamic system in which galaxy velocities range between -1600 and +2700  $\text{km s}^{-1}$ . The cluster has an overall velocity dispersion of  $\sim 700 \text{ km s}^{-1}$  (Trentham and Tully 2002). However, it is clearly isolated from background galaxies by a  $\sim 4000 \text{ km s}^{-1}$  void (Young and Currie 1998).

These features are visible in the detailed histogram by Trentham and Tully (2002) (reproduced in Figure 3.4). The data, to  $v = 8000 \text{ km s}^{-1}$ , clearly show the spread of velocities in the Virgo Cluster and the void between the cluster and the Great Wall. It is because of this void that researchers feel confident in assigning galaxies to the Virgo Cluster based on a radial velocity of  $v \lesssim 2700 \text{ km s}^{-1}$ . Unfortunately, velocity measurements cannot be used to distinguish foreground galaxies from Virgo Cluster members as there is no break in these histograms between the Virgo Cluster

and the local environment. In fact, the histogram shows a continuous distribution all the way into the negative (first) velocity bin. According to Sabatini et al. (2003), the huge mass of the Virgo Cluster accelerates member galaxies, giving them high peculiar velocities, with IC 3258 approaching the Milky Way at  $1600 \text{ km s}^{-1}$  (the highest blueshift measured for any galaxy).

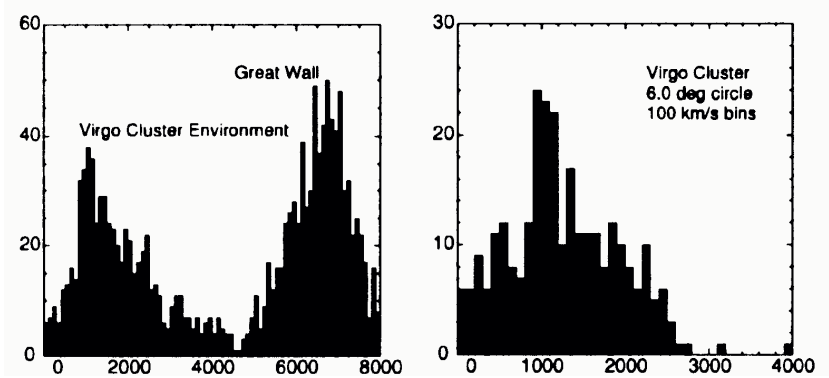


Fig. 3.4: Histograms of Published Galaxy Velocities in the Direction of the Virgo Cluster

*These histograms clearly show the distribution of velocities of Virgo Cluster galaxies. Also visible in the left-hand figure are the void beyond the cluster and the ‘Great Wall’ of more distant galaxies. The left figure covers  $2^\circ$  in RA and  $30^\circ$  in Dec. The right figure is restricted to a circle that minimally encloses the cluster. Note the different velocity ranges of the two figures.*

Figures reproduced from Trentham and Tully (2002).

### 3.4.2 Distance and 3D Structure

Various authors quote an overall distance to the Virgo Cluster as anywhere between 16 and  $\sim 21$  Mpc (refer Table 3.3). The ambiguity is due to different distance measurement techniques, calibration of data, the number of galaxies averaged over, application of corrections and the intrinsic sub-structure of the cluster. The cosmological distance indicator of redshift is not appropriate for accurately determining the distance to the Virgo Cluster because of the range in peculiar velocities and the spread of distances of its member galaxies. Measurements of the distance modulus of

Distance (Mpc)	$m - M$	Method	Reference
$14.4 \pm 1.1$ (M87)	30.79	7	Ciardullo et al. (1998)
15.8 (M87 clump)	31.0	8	Jerjen et al. (2004a)
18.5 (M86 clump)	31.33		
$16.5 \pm 0.1$ (VC)	31.08	8	Mei et al. (2007)
$16.0 \pm 1.7$ (VC)	31.0	1-8, weighted average	Jacoby et al. (1992)
$17.6 \pm 2.2$ (VC)	31.2	1-8, unweighted average	
$20.9 \pm 0.9$ (VC)	$31.6 \pm 0.09$	1-6	Tammann et al. (2000)

Tab. 3.3: Selected Virgo Cluster Distance Estimates

*This table shows distances to M87, regions surrounding M87 and M86 and values indicative of the range of distances obtained for the entire Virgo Cluster.*

*The methods used to derive distances are:*

- 1. Cepheids; 2. Supernovae Ia; 3. 21cm linewidths (Tully-Fisher); 4.  $D_n - \sigma$ ;*
- 5. Globular clusters; 6. Novae; 7. Planetary nebulae; 8. Surface brightness fluctuations.*

*The large value of Tammann et al. (2000) is an ‘outlier’ for the overall cluster distance with the bulk of the literature accepting a value nearer 16 or 17 Mpc.*

galaxy NGC 4548 demonstrate that different results are obtained by different techniques. For this galaxy, Tonry et al. (2001), using the method of surface brightness fluctuations, derived a value of  $31.42 \pm 0.54$ . For the same galaxy, Saha et al. (2006) obtained a value of 30.99 from Cepheid variable measurements after the exhaustive application of corrections. Uncertainties bring these results into agreement. However, in the latter case, the authors also warn that uncertainty in distances may be as high as 10 - 15% due to the intrinsic width of the period-luminosity relation, possible variable absorption and observational errors in magnitude and colour.

Cepheid variable measurements, considered to be the most reliable, have been made for just a handful of Virgo Cluster galaxies (refer Table 3.4). The second column of the table lists those relevant to this discussion, though recently revised measurements and figures for three additional galaxies appear in Saha et al. (2006) and are included

Galaxy	$m - M$	Reference	$m - M$ (Saha et al. 2006)
NGC 4571	$30.87 \pm 0.15$	Pierce et al. (1994)	
NGC 4321 (M100)	$31.04 \pm 0.21$	Ferrarese et al. (1996)	31.18
NGC 4536	$31.10 \pm 0.05$	Saha et al. (1997)	31.24
NGC 4496A	$31.13 \pm 0.10$	Saha et al. (1997)	31.18
NGC 4639	$32.03 \pm 0.22$	Saha et al. (1997)	32.20
NGC 4535			31.25
NGC 4548			30.99
NGC 4527			30.76

Tab. 3.4: Cepheid Distance Moduli to Virgo Galaxies

in the fourth column of the table. Interestingly, Tammann et al. (2000) derived from the five earlier measurements a preliminary Cepheid distance modulus to the Virgo Cluster of  $(m - M)_{Virgo} = 31.45 \pm 0.21$  and claim that this result is ‘well embraced’ by the individual distances shown in Table 3.4. On the other hand, Gavazzi et al. (1999), based on the same five Cepheid measurements, used a value of  $(m - M)_{Virgo} = 31.0$  as the zero-point for their FP and TF analyses, giving greater weight to the galaxies apparently in the main (nearer) parts of the cluster and stating that the more distant galaxy, NGC 4639, should not be used to represent the distance to the Virgo Cluster.

Gavazzi et al. (1999) undertook a detailed study of the 3D structure of the Virgo Cluster. That study obtained distances to 134 galaxies using known velocity dispersions, new spectroscopic and photometric data and FP and TF methods. These distance determinations are not absolute because, as mentioned above, the zero-points of the FP and TF template relations were calibrated using a distance modulus to the cluster of  $m - M = 31.0$ . These authors conclude that the Virgo Cluster is far from virialised and comprises several sub-clusters with various distances and peculiar velocities. The dominant A sub-cluster and the E, S and N clouds lie at  $\sim 15$

Mpc. Sub-cluster B is at 23 Mpc and the W and M clouds are even more distant at  $>30$  Mpc. These regions and their relative distances are as shown in Figures 3.5 and 3.6.

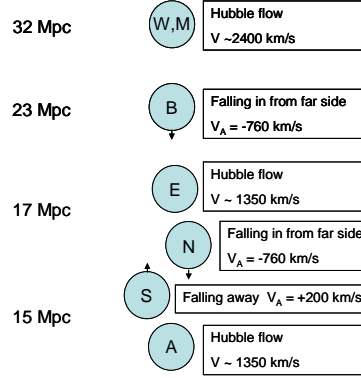


Fig. 3.5: Plan Diagram of the Virgo Cluster

*This plan diagram relates the distances and relative motions of the A and B sub-clusters and the W, M, N, E and S clouds. The A sub-cluster is considered to be the dominant gravitational system. Distances are approximated from those detailed in Table 3.5.*

Distance moduli and peculiar velocities of each of the sub-clusters, as determined by Gavazzi et al. (1999) using  $H_0 = 81.35 \text{ km s}^{-1} \text{ Mpc}^{-1}$ , are detailed in Table 3.5. The authors state that M49, previously believed to belong to the B sub-cluster, is more likely to belong to the S cloud. The distance modulus for this galaxy, used in the study, is also provided in the Table 3.5. Distances shown in Table 3.5 are calculated from the Gavazzi et al. (1999) distance moduli using the distance modulus formula:

$$d = 10^{\frac{m-M+5}{5}} \quad (3.1)$$

One study that helps to distinguish the near-side edge of the cluster from the field or local population is a study of intra-cluster planetary nebulae by Arnaboldi et al. (2002). The sample preferentially traces the nearer edge of the cluster which is found to be approximately 2.1 to 2.8 Mpc closer than M87, the dominant galaxy in sub-cluster A, assuming the distance of M87 to be 14.9 Mpc. This result gives an indication of the approximate depth of the main sub-cluster.

Region	$d(\text{Mpc})$	$m - M$	$V_{pec_A}$
A	14.7	30.84	
N	15.4	30.94	-768
S	15.2	30.91	+202
E	17.6	31.23	-124
B	23.3	31.84	-762
M	35.8	32.77	-736 *
W	29.9	32.38	-151
M49	17.2	31.18	n/a

Tab. 3.5: Sub-Structure of the Virgo Cluster

*The table shows distances and distance moduli of sub-clusters in the Virgo Cluster. Peculiar velocities are relative to sub-cluster A.*

*\* The authors note that the distance for the M cloud may be unreliable as it is based on data for only 4 galaxies.*

Distance moduli and peculiar velocities from Gavazzi et al. (1999).

### 3.4.3 Galaxy Population

The cluster's galaxy population was summarised by Trentham and Tully (2002) in a comparison between the Virgo Cluster, four galaxy groups and the Ursa Major cluster. The Virgo Cluster population includes 107 E/S0/Sab galaxies, 67 Sb/Irr galaxies and has a projected density of dwarfs of 894 per  $\text{Mpc}^2$ . These values make it richer in overall galaxy population and it has a higher projected dwarf density than any of the other regions surveyed. Whilst the Virgo Cluster contains all galaxy types, it is the dwarf and low surface brightness galaxy population that is particularly relevant to this project.

The surface density of dwarfs in the Virgo Cluster was found by Davies et al. (2004) to be on average 20 per  $\text{deg}^2$ , ranging from 40 at the centre to only four at the edge. Those data included LSB dwarfs down to a central surface brightness limit of  $\sim 26 B\mu$ . The variation in surface density of LSB dwarfs was also examined by

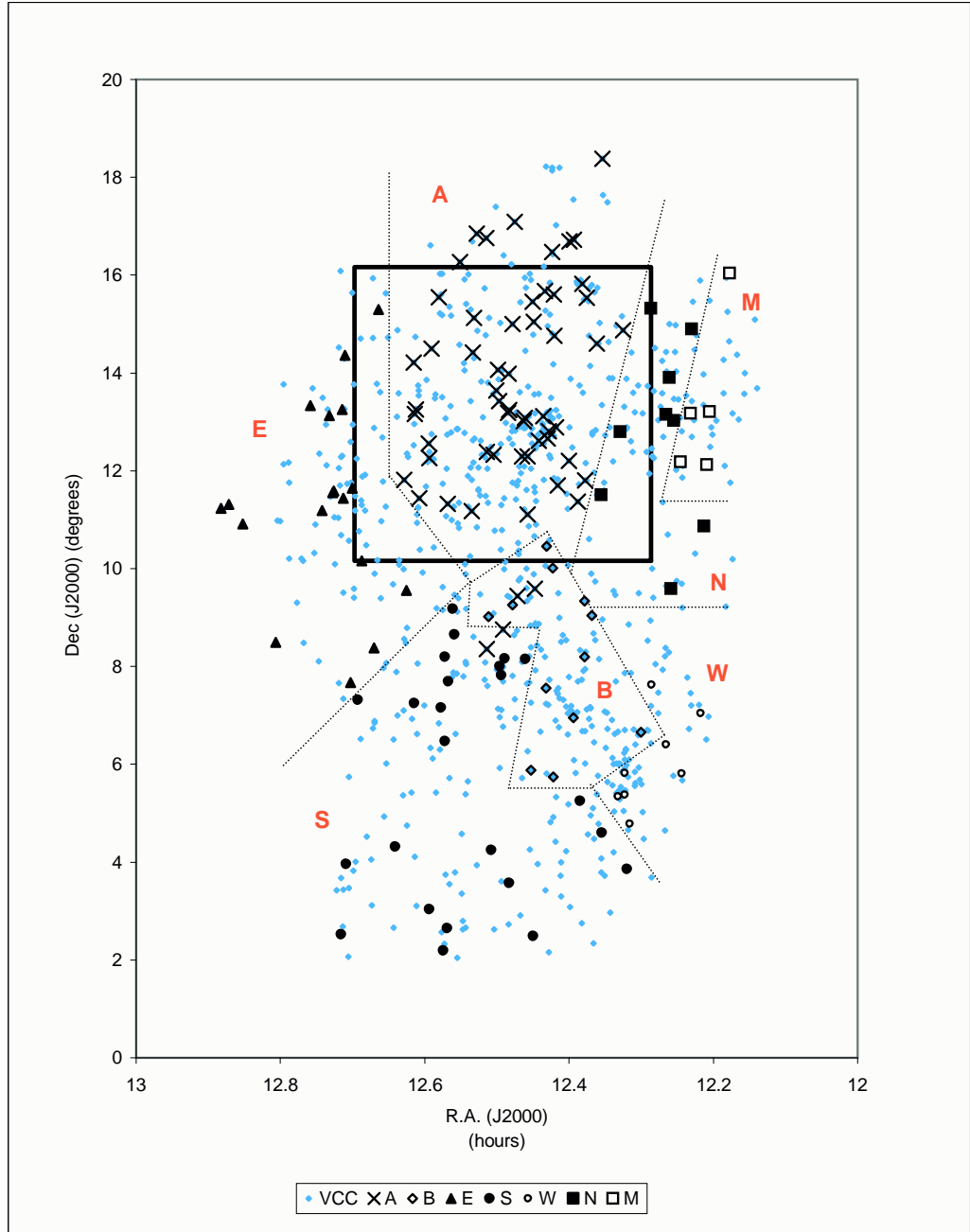


Fig. 3.6: Map 2: 3D Structure of the Virgo Cluster

*Black symbols show 134 galaxies plotted within seven spatial regions (labelled A, B, E, S, W, N and M and shown with dotted lines) based on distance estimates. The small blue points are cluster member galaxies of the VCC. The heavy square is the region covered by the Virgo Deep Stack.*

Figure after Gavazzi et al. (1999).

Phillipps et al. (1998) in a study of two sub-fields within the cluster, each covering around  $1.6 \text{ deg}^2$ . Phillipps et al. (1998) also found that the LSB dwarf density of the cluster core is smaller than that in a region that is 3 degrees from the core. These results suggest that the dense environment of the cluster core either removes the LSB dwarfs or suppresses their formation.

Davies et al. (2004) found a dwarf-to-giant ratio (DGR) of about 20 using a sample of 257 dwarf galaxies in the Virgo Cluster, compared with a ratio of 6 or less in the MGS which covers a region along the celestial equator containing mainly field galaxies. Sabatini et al. (2003) also found that, whilst the surface number density of LSB dwarfs falls off towards the edge of the cluster, the whole cluster has an apparently constant DGR of  $\sim 20$  that does not blend into the field ratio ( $\sim 4$ ) near the cluster's edge. This suggests that the Virgo Cluster is very different from the field environment all the way out to its edge. Binggeli et al. (1988) speculated that dwarf galaxies may be clumped around the few major systems with large bulges. However, Roberts et al. (2007) found that there does not appear to be a prevalence for dwarfs to cluster around giants in the Virgo Cluster.

Sabatini et al. (2005) found that the DGR in the cluster is too high to support formation by infall of units like the Local Group or galaxies from the field, which has a much lower DGR. Although Conselice et al. (2003) found evidence of accretion of field galaxies into the cluster from HI observations of dEs preferentially located near the edges of the cluster, Roberts et al. (2007) suggest that the Virgo Cluster is assembling itself out of sub-clusters that are already rich in dwarf galaxies compared with the population in the field.

The total light due to dwarf LSB galaxies in the Virgo Cluster was estimated by Sabatini et al. (2003) to be only  $1/50$  of the total light due to the brighter, but less numerous, VCC galaxies. However, LSB dwarfs contribute significantly to the mass of the cluster. It was also estimated, based on this survey area (the E-W strip of the INT Wide Field Survey) and the high  $M/L$  ratios found for Local Group galaxies, that the total dwarf mass in the Virgo Cluster is approximately  $1/10$  of the total mass of the VCC galaxies.



### 3.4.4 The Intra-Cluster Medium

Between galaxies in the Virgo Cluster there is evidence of gas (e.g. Minchin et al. (2005), Phookun et al. (1993)), planetary nebulae (Feldmeier et al. 2004), tidal tails from interacting galaxies (refer Figure 3.7), globular clusters (Williams et al. 2007) and individual intra-cluster stars (Caldwell 2006). The hot x-ray-emitting gas is very localised to the region around M87 (Young et al. 2002) so this particular environment is unlikely to have much effect on the dwarf galaxy population as a whole. However, optical light appears to permeate between galaxies at a level of  $\sim 26 V\mu$  and fainter (Mihos et al. 2005). This diffuse light, referred to as intra-cluster light, is defined as luminosity at a surface brightness  $\mu_V > 26.5\mu$  and, in evolved clusters, may contribute 10 to 15% of the cluster's total luminosity (Rudick et al. 2006). Discussion of the intra-cluster light detected in the Virgo Deep Stack is included in Section 6.5. Some phenomena that contribute to intra-cluster light are described below.

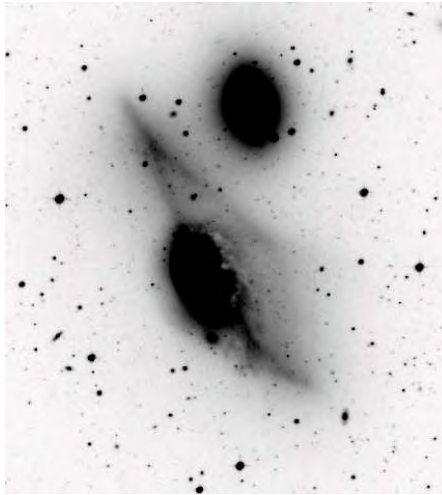


Fig. 3.7: NGC 4438: A Tidally Disturbed Galaxy

*This image from the Virgo Deep Stack shows the effects of tidal disturbance on the large, luminous spiral galaxy NGC 4438 (lower galaxy in image) which is plunging through the centre of the Virgo Cluster at high speed (Vollmer et al. 2005). The upper galaxy, NGC 4435, appears undisturbed but is contributing to the tidal interaction.*

Moore et al. (1999b) modelled galaxy interactions to show that LSB galaxies may be torn apart by gravitational tidal shocks during cluster formation, distributing stars within the cluster. Similarly, modelling by Barai et al. (2007) supports the case for destruction of dwarf galaxies as a source of intra-cluster light. In a variation on this theme, Bekki et al. (2001) suggest that galaxies are not necessarily torn apart but that the process of galaxy ‘threshing’ through tidal interactions may strip outer stars and compress galactic cores, resulting in the formation of UCD galaxies.

These modelling scenarios are supported by observations by Karick et al. (2004), in which a long arc of tidal debris from a dE,N cluster member was detected, and imaging and spectroscopic studies by Mastropietro et al. (2004), which were compared with high-resolution N-body simulations designed to study the evolution of disk galaxies in clusters. Results of these comparisons substantiate the findings that tidal debris contributes to diffuse intra-cluster light and that individual stars may be stripped from galaxies in these interactions.

Some of these individual stars have been directly imaged. Caldwell (2006) used deep HST imaging with the ACS to study tip-red-giant-branch (TRGB) stars in Virgo galaxies and found evidence of ‘free-floating RGB stars’ in the Virgo Cluster. Intra-cluster planetary nebulae have also been detected by Arnaboldi et al. (2002) using the wide-field imager on the European Southern Observatory (ESO) 2.2-m telescope and Feldmeier (2006) suggests that these nebulae may contribute as much as 10 to 20% of the total amount of diffuse light in galaxy clusters.

Extensive faint galaxy haloes are also deemed to contribute to the intra-cluster light even though, strictly speaking, they belong to their parent galaxies. Gonzalez et al. (2000b) observed the brightest cluster galaxy in Abell 1651 and extrapolated its profile to account for all but 5% of that cluster’s intra-cluster light. It is suggested that the remainder may be due to cluster galaxies fainter than the magnitude limit of the data.

Certainly, in the Virgo Cluster, some very extensive galaxy haloes are seen in deep images and, without doubt, there are many individual contributions to intra-cluster light from stars, tidal tails and nebulae. However, making confirmed detections of

large-scale identifiable patches of intra-cluster light has proven challenging. The apparent detection by Katsiyannis et al. (1998), according to the authors, may be due to variations in film sensitivity in the photographic image data. On the other hand, Mihos et al. (2005) produced a striking image of the Virgo Cluster core, made with the 0.6-m Burrell Schmidt Telescope, that clearly shows long streaks and tidal plumes. This image was made by mosaicking together 72 separate 900-s CCD exposures, each with an area of  $1.0 \times 0.75$  degrees. As will be discussed in Section 6.5, many of these features may be corroborated by comparison with the Virgo Deep Stack. The confirmed presence of many diffuse tidal plumes in the Virgo Cluster indicates that tidal stripping is an ongoing process contributing light to the intra-cluster medium and transforming galaxies in this environment.

#### 3.4.5 Effects of the Cluster Environment

The Virgo Cluster has a crossing time of 0.1 of a Hubble time, which means its galaxies have had many opportunities to interact (Trentham and Tully 2002). Sabatini et al. (2003) describe the Virgo Cluster as a very complex, unrelaxed system. Whilst the core is dynamically old, the surrounding region is still infalling. This implies that some galactic evolution must take place as passing galaxies tug on each other over cosmic time and are influenced by the intra-cluster medium. Some evidence of this is found in studies that compare the dwarf population in the Virgo Cluster with that in the field and also in studies that look at noticeable differences between galaxies at different localities within the cluster. These studies, described below, examine morphology, colour and gas content of the galaxies.

A survey by Sabatini et al. (2005) of where dE and dI galaxies are found within the Virgo Cluster showed that the spherically symmetric dE galaxies are found preferentially towards the cluster centre and the more irregular and clumpy dI galaxies are distributed nearer the edges.

In a study of galaxy morphology in different environments (refer Section 3.3 Item vii), Trentham and Tully (2002) found that, in the range  $-17 \leq M_R \leq -11$ , around 70% of dEs in the Virgo Cluster are nucleated. This is a much higher proportion

than in the five other clusters and groups in the study, which have only about 40% in the same magnitude range with nucleations.

For some time, it has been known that nucleated dwarfs have the reddest optical colours (Impey et al. 1988). More recently, Sabatini et al. (2005) compared the colours of dwarf galaxies in the Virgo Cluster with those of galaxies in other environments and concluded that cluster dwarfs are generally gas poor and red compared with field dwarfs, but have an average  $(B - I)$  colour and a velocity dispersion similar to the spiral galaxy population. Sabatini et al. (2005) found that, towards the centre of the cluster, there is a population of gas-poor dE galaxies with a small range of colours, which may indicate an older stellar population. At the same time, there are dI galaxies residing on the outskirts of the cluster that display a wider range of colours and apparent star-forming regions.

HI observations near the cluster core are made difficult by the strong continuum emission from M87. Nevertheless, Sabatini et al. (2005) observed 100 dI and VLSB galaxies farther than one degree from M87 with the Arecibo Telescope. Only three detections of HI in cluster galaxies were made, and two in background galaxies. The cluster galaxies are at projected distances of 2, 5 and 6.5 degrees from the cluster centre. Based on the large number of non-detections, galaxies in the cluster environment were found to be depleted in gas compared with those in the field.

These findings, based on morphology, colour and HI content, suggest that dwarfs nearer the cluster core have evolved differently from those further out in such a way that the inner population is lacking in gas and ongoing star formation. This state leads to their smoother appearance, often with nucleation. Away from the core, dwarfs are more irregular in appearance and are more inclined to have active star formation implying that they have not already consumed or lost all their gas and that there are mechanisms to trigger star formation in this environment despite the typically low gas surface density of LSB dwarfs.

Possible mechanisms for these differing evolutionary histories include: pressure effects due to supernova-driven winds (Mac Low and Ferrara 1999) and ram pressure (Vollmer et al. 2001); and gravitational effects, such as galaxy harassment due to

the total cluster potential (Moore et al. 1998) and galaxy-galaxy tidal interactions (Sabatini et al. 2005). These processes in combination may physically remove gas, lead to the consumption of gas in star formation processes or alter the morphology of dwarf galaxies.

Supernova-driven winds from low-mass galaxies may be effective in modifying the entire galaxy environment. Mac Low and Ferrara (1999) modelled the effects of repeated supernovae from starbursts in dwarf galaxies that contain mass in the forms of gas and stellar mass  $M_g$  in the visible disk and dark matter  $M_h$  in the halo and studied the effects on dwarf galaxies with gas masses (the stellar mass is negligible compared with the gas component) in the range  $M_g = 10^6 - 10^9 M_\odot$ . The models illustrate two types of event: a blow-out where the metal-enriched gas from a supernova escapes from a galaxy leaving the ambient gas more-or-less in place; and a blow-away where the ambient gas is swept up into a shell, ahead of the supernova ejecta, and also escapes the galaxy. It was found that only the smallest galaxies, with gas mass  $M_g \leq 10^6 M_\odot$ , have any interstellar gas blown away and, even then, the mass fraction lost in this way is only a small percentage. In cases of blow-outs, however, it was found that the metal-enriched gas would be accelerated sufficiently to escape the disk in all cases, but that in the more massive galaxies most of this enriched gas would fall back onto the galaxy due to the gravitational potential of the dark matter halo. Only 30% of metals are retained by galaxies with  $M_g = 10^9 M_\odot$ , but in smaller galaxies virtually all the metals escape. Supernova-driven winds may therefore contribute to the observed low metallicity of LSB dwarfs that have undergone starbursts due to the cluster environment.

Ram pressure stripping is the removal of gas from a galaxy, due to the hot intra-cluster medium (ICM), where the pressure due to the ICM exceeds the galaxy's internal gravitational force. The effect was described and modelled by Vollmer et al. (2001). Results indicate that the HI deficiency that is observed in the Virgo spiral galaxy population, compared with field spirals, is consistent with the model. Follow-up HI and H $\alpha$  observations of two spiral galaxies, NGC 4522 (Vollmer et al. 2006) and NGC 4501 (Vollmer et al. 2008), also support the models.

Boselli et al. (2008) made a comprehensive study of dE galaxies, selected from the VCC, using optical, near-infrared and H $\alpha$  imaging along with multi-frequency data from the literature. The comparison between these observations and model predictions favours ram-pressure stripping as the cause of ‘galaxy starvation’. These authors conclude that the entire quiescent dwarf population in the Virgo Cluster may have resulted from infalling, low-luminosity, gas-rich systems in which star formation was halted by ram-pressure stripping over time scales of  $\sim 2$  Gyr.

However, Sabatini et al. (2005) showed that ram-pressure stripping would only be effective in removing gas from the smaller cluster dwarfs if they were located within the inner 0.5 Mpc of the cluster. These authors argue that, at this proximity to the cluster core, a dwarf galaxy ought to be torn apart by tidal forces and should therefore have a disrupted appearance. The galaxies observed that appear to be this close to the core are mainly spherical dEs, i.e. these galaxies do not appear to have been gravitationally disrupted. However, as the galaxies are seen in projection, Sabatini et al. (2005) concede that these galaxies are more likely to lie in front of or behind the cluster core rather than within it.

Ram pressure may not only remove gas, but may also trigger star formation. Vollmer et al. (2001) explain how this may result from re-accretion of stripped gas that has not been accelerated to escape velocity. The other star-forming mechanism at work is gravitational interaction. Whilst this may pull galaxies apart completely, it may also cause mergers, reshape a galaxy or trigger starbursts. Sabatini et al. (2005) explain how continual tidal variation can compress gas and promote enhanced star formation and may be important even at large distances from the cluster core. This may be the cause of the small amounts of star formation seen in the outer cluster dI galaxies. It may also lead to the transformation of dI galaxies into dEs, as they encounter the cluster core, and it may explain the nucleation that is observed in these galaxies.

One potential scenario, where harassment and tidal interactions pull apart large galaxies to leave the gas-poor dwarf population observed today as residuals, is discounted by Sabatini et al. (2005) because only a small number of large galaxies

appear to be currently undergoing such disruptive interactions. A study by Durrell et al. (2007) of the stellar population of one particular dwarf spheroidal galaxy near the cluster core shows that the galaxy is old, at least  $\sim 10$  Gyr, very metal-poor and that there is no obvious evidence of tidal threshing. Durrell et al. (2007) conclude that this galaxy, rather than being the shredded remains of a larger galaxy, is pristine and is falling into the Virgo Cluster for the first time. Thus, it appears that dwarf galaxies fall into the cluster from the field and that their morphologies may be subsequently modified by gravitational interactions and other processes.

The processes discussed in this chapter may all contribute to the observed properties of LSB dwarfs in the Virgo Cluster to varying degrees. These evolutionary processes result in a population that is distinct from the field population in morphology, colour and gas content, and comparisons within the cluster show differing degrees of evolution depending on proximity to the cluster core. This evolution progressively removes (or converts) gas, smooths out clumps in morphology and produces a somewhat redder stellar population than is seen in field LSB dwarfs. Whilst Boselli et al. (2008) favour ram-pressure stripping to account for the gas-loss, Sabatini et al. (2005) and Davies et al. (2004) find that the most efficient mechanism to produce all the observed effects is enhanced star formation due to tidal interactions. Both theories support the infall of relatively gas-rich dwarfs as the source of the currently-observed dwarf population of the Virgo Cluster.





## 4. VIRGO CLUSTER MEMBERSHIP AND THE LUMINOSITY FUNCTION

A means of representing an entire galaxy population, either globally or within a cluster, is a luminosity distribution plot in which counts of galaxies are binned by luminosity or magnitude. The shape of the distribution may be matched by an analytic function. Parameters of this function for a particular cluster may then be compared with those of luminosity functions for other clusters or the global galaxy population to interpret the different evolutionary histories of the various populations. Observed luminosity functions may also be compared with those predicted by cosmological models to test the accuracy of the models. The most commonly applied fitting function is the Schechter function, introduced in Section 4.1. An alternative representation of a population is the DGR, discussed in Section 4.2.

However, to obtain a luminosity function for a cluster, its member galaxies must first be detected and distinguished from foreground and background galaxies. Section 4.3 explains some methods used for detecting galaxies in images and Section 4.4 addresses survey completeness. The crucially important issue of determining cluster membership, several methods that have been applied to this problem and the resulting luminosity functions for the Virgo Cluster are detailed in Section 4.5.

Later sections in this chapter include a brief discussion of luminosity distributions predicted by theory and the limitations of the Schechter fitting function. The various luminosity functions for the Virgo Cluster are reviewed in Section 4.8 and Table 4.5 (p.87) contains a summary of numerous global, cluster (including the Virgo Cluster) and Local Group luminosity functions.

### 4.1 The Schechter Luminosity Function

It is more than 30 years since Schechter (1976) derived an analytic expression for the luminosity function for galaxies. In essence, the luminosity distribution of galaxies may be approximated by the following analytic expression in which  $\phi(L)dL$  is the number of galaxies per unit volume in the luminosity interval  $L$  to  $L + dL$ :

$$\phi(L)dL = \phi_*(L/L_*)^\alpha \exp(-L/L_*)d(L/L_*). \quad (4.1)$$

The function has two parts:

- A power law ( $\phi \propto L^\alpha$ ) that dominates at low luminosities where the luminosity function rises as  $L$  decreases (i.e. faint galaxies are more common than bright ones);
- An exponential cut-off ( $\phi \propto e^{-L}$ ) that dominates at high luminosities (i.e. very luminous galaxies are rare).

$L_*$  is the characteristic luminosity at the break between the two regions,  $\phi_*$  is a volume density parameter and  $\alpha$  gives the faint-end slope of the luminosity function in the  $(\log \phi, \log L)$ -plane when  $L \ll L_*$ . The parameters  $\phi_*$ ,  $L_*$  and  $\alpha$  are determined from the data.

The luminosity distribution is often plotted using  $\log(\text{number})$  vs absolute magnitude (rather than luminosity). Based on the logarithmic relation<sup>a</sup>:

$$M - M_* = -2.5 \log(L/L_*) \quad (4.2)$$

the Schechter function may be written in magnitude form as follows (refer Appendix B for the derivation):

$$\phi(M)dM = 0.4 \ln(10) \phi_* 10^{0.4(\alpha+1)(M_*-M)} \exp(-10^{0.4(M_*-M)}) dM. \quad (4.3)$$

The  $\alpha$  term is the same in both equations 4.1 and 4.3 but the faint-end slope in number-magnitude space is equal to  $-0.4(\alpha + 1)$  (Binggeli et al. 1988). The change

---

<sup>a</sup> In all cases in this document ‘log’ means  $\log_{10}$  and natural logarithms are written ‘ln’.

in sign between the luminosity slope and the magnitude slope occurs because a decrease in luminosity corresponds to a magnitude represented by a larger number. The faint-end slope in terms of magnitude becomes:

$$-0.4(\alpha + 1) = \frac{\log \left( \frac{N_2}{N_1} \right)}{M_2 - M_1} \quad (4.4)$$

where numbers and magnitudes may be measured directly from a plot. In practice, the best fit  $M_*$  and  $\alpha$  are found by minimising  $\chi^2$  in fitting equation 4.3 to the binned magnitude data (Binggeli et al. 1988).

The appearance of the function fitted to a distribution of galaxies from 13 clusters is shown in Figure 4.1 from Schechter (1976).

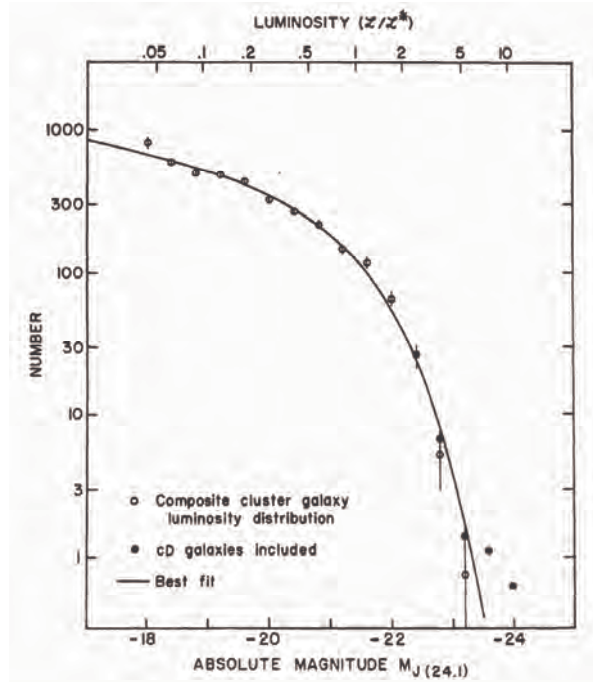


Fig. 4.1: Schechter's Luminosity Function

*The line is the best fit of Schechter's analytic expression to data from 13 clusters. Filled circles show the effect of including the most luminous galaxies. Note the function becomes linear faintwards (to left of)  $M_* = -21.41$  with slope  $\alpha = -1.24$ .*

Figure reproduced from Schechter (1976).

Figure 4.2 shows data for the Virgo Cluster from Sandage et al. (1985) and demonstrates the difference between plotting  $N$  (number of galaxies) and  $\log N$  against magnitude. The linearity of the faint end is clearly evident in both logarithmic plots (i.e. the left-most data of Figure 4.1 and the right-most data of the right-hand plot in Figure 4.2).

The faint-end slope is indicative of the prevalence of faint galaxies in the distribution. A steep slope indicates that as galaxy luminosity decreases galaxy numbers increase. Special cases are where  $\alpha = -2$ , in which case the total luminosity diverges if integrating  $\phi(M)$  to  $M = \infty$  (Sandage et al. 1985), and where  $\alpha = -1$  for a flat luminosity function implying equal numbers of galaxies in all magnitude intervals.

Phillipps (2005) quotes some  $B$ -band estimates for the characteristic parameters of a “representative collection of galaxies”:

$$\phi_* \simeq 0.0055 \text{ Mpc}^{-3};$$

$$L_* \simeq 2 \times 10^{10} L_{\odot} \text{ or } M_* \simeq -20.6 \text{ (close to Milky Way brightness);}$$

$$\text{and } \alpha \simeq -1.2.$$

However, parameters of the luminosity function vary depending on many factors including: galaxy type and environment; detection methods and selection effects; cosmological assumptions and consequent corrections to measured magnitudes; magnitude limits over which the function is fitted; and, in the case of clusters, the selection criteria used to assign a galaxy to a cluster.

Sandage et al. (1985) made the point that, since a global luminosity function is a sum over all galaxy types, the contribution to the faint end is weighted by the number density of dwarf galaxies in the sample compared with the overall population. Observationally, it is important to know if all galaxy types are being seen or if certain classes of galaxies, such as LSB dwarfs, are being omitted due to selection effects. Simply seeing more faint galaxies leads to a steepening of the faint end of the luminosity function. Thus, corrections may be applied for incompleteness based on modelling which galaxy types would be seen and which would be missed in any particular survey.

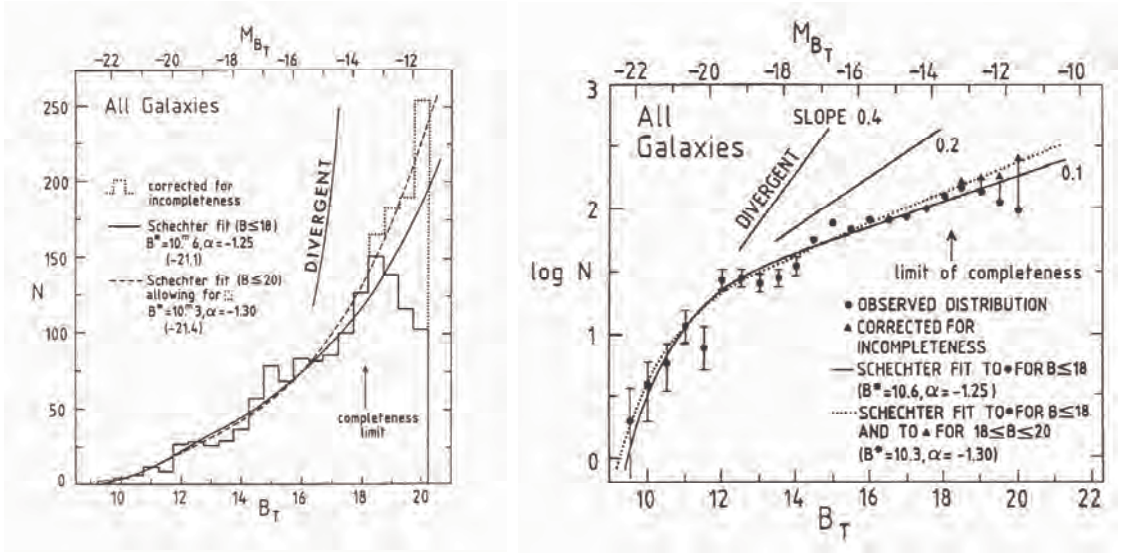


Fig. 4.2: Histogram, N-Magnitude and Log(N)-Magnitude Plots

These two plots show a Schechter function fitted to the distribution of 1647 galaxies in the Virgo Cluster. At left is a histogram showing the galaxy counts ( $N$ ) in half-magnitude bins. At right the same Schechter function is plotted against  $\log N$ . Fitting parameters are shown on the diagrams.

Figures reproduced from Sandage et al. (1985).

For global luminosity functions, cosmological corrections must also be applied. One of these is the  $K$ -correction (Oke and Sandage 1968). This term corrects for the fact that sources observed at different redshifts are compared with standards at rest-frame wavelengths (Hogg et al. 2002). Another correction is for galaxy evolution. As the star formation rate changes, the stellar population evolves leading to a change in spectral type with cosmic time (Norberg et al. 2002).

The effects of variations in survey area, processing of the data, galaxy detection methods, measurements of galaxy parameters and how corrections are applied may all lead to different results for global luminosity functions based on large-area surveys. For example, Driver et al. (2005) found that for the MGS, which samples galaxies along the celestial equator, the luminosity function parameters are:

$$\phi_* = (0.0177 \pm 0.0015) \text{ Mpc}^{-3};$$

$$M_{*B} = -19.6 \pm 0.04;$$

$$\text{and } \alpha = -1.13.$$

The 2dF Galaxy Redshift Survey (2dFGRS) produces a faint-end slope of  $\alpha \simeq -1.21 \pm 0.03$  (Norberg et al. 2002) and the Sloan Digital Sky Survey (SDSS) result is  $\alpha \simeq -1.05 \pm 0.01$  (Blanton et al. 2003). The former targets mainly nearby (i.e. younger) galaxies and the latter focuses on older galaxies with redshift around  $z = 0.1$ , but both are corrected for galaxy evolution.

Distinctions based on galaxy type appear to produce different results. Popesso et al. (2006) analysed 69 cluster luminosity functions and found that the luminosity function specific to late-type galaxies is well fitted by a single Schechter function but that a double Schechter function is a better fit when considering only the early-type galaxies. Further, the authors found that the faint-end upturn of the global cluster luminosity function is due to early-type cluster galaxies.

It has also been shown that the faint-end slope  $\alpha$  is found to be notably steeper in the cluster environment than in field samples (Binggeli et al. 1988). Typically the faint-end slope for a cluster is approximately  $\alpha = -1.5$  as is found, for example, in the Centaurus Cluster (Chiboucas and Mateo 2006). However, quite a range of values of  $\alpha$  may be found, even for the same cluster, as will be demonstrated in the case of the Virgo Cluster.

## 4.2 *The Dwarf-to-Giant Ratio (DGR)*

In recent literature there have been trends towards using methods other than the luminosity function to represent galaxy distributions. These include the DGR (e.g. Sabatini et al. (2003) and Roberts et al. (2004)) and more complex multivariate distributions based on galaxy properties (Driver 2004). Multivariate distributions are useful for analysis of larger galaxies that may be decomposed into bulge and disk components. The DGR may be preferred when there are too few galaxies to

construct a luminosity function (Sabatini et al. 2003). As previously noted, there is no consistent definition of the DGR. Table 4.1 summarises some definitions that have been applied.

Giant	Dwarf	Reference
$M_B \leq -19$	$-14 \leq M_B \leq -10$	Sabatini et al. (2005) Roberts et al. (2004)
$-23.5 \leq M_R < -19.5$	$-19.5 < M_R \leq -16.5$	Phillipps et al. (1999)
$M_R \leq -17$	$-17 < M_R \leq -11$	Trentham and Tully (2002)

Tab. 4.1: Definitions of the Dwarf-to-Giant Ratio

*The dwarf-to-giant ratio is a confusing non-standard relationship due to different definitions being used by different authors.*

Using the first definition from Table 4.1<sup>b</sup>, Roberts et al. (2004) found that the DGR is much higher in the surveyed region of the Virgo Cluster (20:1) than in the Local Group (5:1). The same team found a DGR in the field of somewhere between 4:1 (Sabatini et al. 2003) and 6:1 (Roberts et al. 2004). Galaxies in groups are classified as field galaxies by Binggeli et al. (1988). Thus, similar statistics for groups, including the Local Group, and the field are to be expected. The variation in the DGR in various parts of the Virgo Cluster is further discussed in Section 4.5.4. Roberts et al. (2004) provide a table for comparing the DGR to the faint-end slope of the luminosity function. That table is reproduced below for reference (Table 4.2).

### 4.3 Galaxy Detection

The earliest detection method used was simple visual inspection of photographic images with the aid of an eyepiece (Binggeli et al. 1985). More recently, with the use of CCD images and digital scanning of photographs, computerised methods of object detection have become routine. The obvious advantages are that computer

<sup>b</sup> All further references to the DGR will use this first definition.

$\alpha$	DGR
-0.8	1:1
-1.0	4:1
-1.2	18:1
-1.4	80:1
-1.6	367:1
-1.8	1735:1
-2.0	8371:1

Tab. 4.2: Comparing Dwarf-to-Giant Ratio with Faint-End Slope

*This table shows the value of the DGR, as defined by the first row in Table 4.1, that corresponds with various values of the faint-end slope ( $\alpha$ ) of the luminosity function.*

Table from Roberts et al. (2004).

processing is quicker and that the algorithm should not accidentally miss any objects that fall within its detection parameters. The most common type of algorithm is the connected-pixel type used by the software packages **PISA**, **FOCAS** and **SExtractor**.<sup>c</sup>

Phillipps et al. (1998) used **PISA** to find objects in a six-stack scanned photographic image. Objects were filtered for a minimum area of 25 pixels (11 square arcseconds) to exclude spurious data from the processing. Further filtering was subsequently applied to select LSB dwarfs from the sample. This filtering is discussed in Section 4.5.4. However, connected-pixel algorithms have been found to be problematic for the lowest surface brightness objects that tend to be broken up into multiple components (Chiboucas and Mateo 1999). When Driver et al. (2005) applied **SExtractor** to the MGS, all non-stellar sources were visually inspected to check for incorrect deblending. In such cases, the data set was reprocessed using different extraction parameters until a satisfactory result was achieved.

---

<sup>c</sup> Software packages of this type are based on algorithms that were developed for the analysis of data obtained with the APM, COSMOS and SuperCOSMOS plate-scanning machines. ‘COSMOS’ stands for CoOrdinates, Sizes, Magnitudes, Orientation and Shape.



To overcome the possibility of incorrect deblending prevalent in connected-pixel algorithms, Sabatini et al. (2003) developed an algorithm, optimised for the LSB dwarf population, that uses convolution of the image with matched filters (refer Figure 4.3).

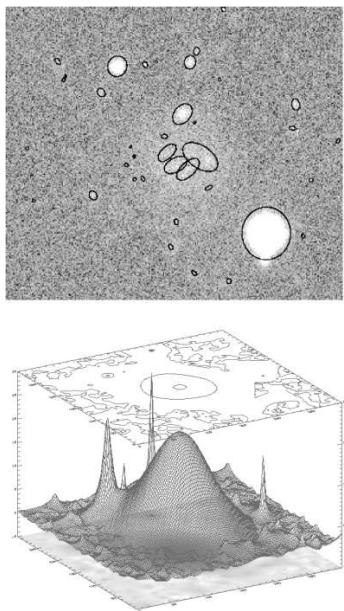


Fig. 4.3: Improper Deblending and the Sabatini et al. (2003) Solution

*Top: The output from SExtractor showing an LSB galaxy detected as a group of small objects.*

*Bottom: The output from the algorithm of Sabatini et al. (2003) reveals the galaxy as a single object far above the noise level.*

Figure reproduced from Sabatini et al. (2003).

The technique was applied to deep CCD images of a strip through the Virgo Cluster to detect LSB dwarfs down to a surface brightness of  $26\ B\mu$ . This technique is demonstrated to be effective at detecting faint, diffuse objects and has the advantage of simultaneously measuring their photometric properties. Tests using artificial galaxies were used to measure the efficiency of the algorithm as a function of scale length and central surface brightness. These tests allow for estimation of completeness and contamination of the detection method for which corrections may be applied.

#### 4.4 *Survey Completeness*

Completeness refers to the missing of faint galaxies beyond the detection limit of a survey, image or observation. It may be thought that the limiting surface brightness of a survey would lead to incorrect measurements of magnitudes of galaxies due to the loss of data to the background at the outer edges. However, this would only apply to aperture magnitudes, where a measurement is made inside an enclosing circle or ellipse, and is not usually a problem for LSB dwarfs, where extrapolated exponential profiles are integrated to infinity. In practice, the faint magnitude bins of the luminosity function may be more strongly affected by completely missing these galaxies where their low surface brightness puts them below the detection threshold of the data.

Completeness corrections may have a large impact on the luminosity distribution. Based on work using photographically amplified UK Schmidt plates, Impey et al. (1988) compared galaxies discovered by their method with the then-known population of galaxies in the Virgo Cluster. The resulting luminosity function used the earlier data of Sandage et al. (1985), added data for 26 new LSB galaxies and made large completeness corrections. It was explained that these corrections were required due to the breakdown of the surface brightness-to-luminosity relation for LSB galaxies. A much steeper slope ( $\alpha = -1.7$ ) than the earlier Sandage et al. (1985) result of  $\alpha = -1.30$  was derived. Interestingly, Impey et al. (1988) noted that many of the newly-discovered galaxies were *not* in the lowest luminosity bin and concluded that the uncertainty in the luminosity function of dwarf galaxies is large. More recent observations to fainter limiting magnitudes attempt to address this uncertainty.

The completeness problem is discussed in depth by Trentham and Hodgkin (2002). These authors note that incompleteness is not only due to non-detection of LSB galaxies but may also be caused by false rejection of high surface brightness cluster members because of their resemblance to luminous background galaxies. This issue feeds into criteria for cluster membership discussed in Section 4.5. Data in the Trentham and Hodgkin (2002) survey are not seriously affected by the non-detection problem because, the authors state, the deep Subaru images do not reveal new

galaxies that were missed in earlier surveys, suggesting that there are not large numbers of galaxies with  $M_B < -11$  and surface brightness below the survey limit of  $\sim 28 R\mu$ . The galaxy types affected by the high surface brightness problem are blue H II galaxies and red compact dwarfs. Only two such galaxies were found in the sample (one of each type), for which velocity measurements confirm that the galaxies are cluster members. The authors conclude that this problem is not detrimental to the data because these types of galaxies are rare.

## 4.5 *Virgo Cluster Membership*

It was originally believed that it would be easier to obtain the luminosity function for a cluster than for a field sample because it would not be necessary to know distances to the individual galaxies (Binggeli et al. 1988). Finding distance is an important step in determining a global luminosity function where luminosity or absolute magnitude must be derived for galaxies that are all at different distances.

However, contamination by foreground and background galaxies is now considered a problem for finding a cluster luminosity function where cluster membership of individual galaxies may be difficult to ascertain. Jerjen et al. (2004b) investigated the problem of cluster-member identification and concluded that ambiguity in attributing membership status to cluster candidates is still the main source of uncertainty in finding the accurate shape and faint-end slope of the luminosity function. The Virgo Cluster has been well studied and this problem shows up in the many values obtained for the parameters of the luminosity function evident in Table 4.5 (p.87).

Contamination may be dealt with in several ways: by finding distances to galaxies; by filtering using criteria to optimise the detection of galaxies within a limited range of distances; or by statistical analysis of probable background contamination that is then subtracted from the data counts of the luminosity distribution. A number of distance-estimation methods are more appropriate for bright objects (the TF and FP relations, Cepheid variable measurements and surface brightness fluctuations) and will not be further discussed. Other methods are appropriate for faint dwarfs

and LSB galaxies, particularly in the context of deriving a luminosity function. These methods include: selection based on morphology, concentration parameters, scale-length limits and magnitude-surface brightness criteria; and corrections based on field galaxy counts. These will be the topics of the following sections, but some discussion of a primary distance measure, radial velocity, is included for reference.

#### 4.5.1 *Radial Velocities*

Whilst redshift alone is not an appropriate indicator of distances in a full analysis of the structure of a cluster, where sub-clustering and peculiar velocities complicate the analysis, it is a direct and useful method for assessing likely cluster membership based on a velocity histogram in the direction of the cluster (e.g. Figure 3.4 p.38). Such a histogram typically shows clumping at the distance to each cluster along the line of sight where, at low redshifts, velocity measurements may be estimated using the simple relation:

$$v = cz \tag{4.5}$$

in which  $z$  is redshift and  $c$  is the speed of light. However, there tends to be blending between clusters and intermediate field regions due to peculiar velocities of the cluster members.

Contamination by local galaxies and galaxies in the Local Supercluster, in studies of the Virgo Cluster, is discussed by Trentham and Tully (2002). The velocity distribution in the direction of the Virgo Cluster is displayed in Figure 3.4 (p.38). These authors state that legitimate Virgo Cluster members in the sample lie in the range  $-500 < v_{GSR}^d < 2800 \text{ km s}^{-1}$ . The cut-off is subjective and Drinkwater et al. (1996) include any galaxies with  $v < 3500 \text{ km s}^{-1}$  as cluster members. Negative velocities indicate that some cluster galaxies show blueshift, increasing the difficulty of distinguishing cluster members from foreground objects (Binggeli et al. 1985) when relying on spectroscopic measurements alone. The broad range of velocities

---

<sup>d</sup> The subscript GSR means velocities are corrected to the Galactic standard-of-rest (GSR) frame.

for the cluster is due to the dynamic nature of member galaxies discussed in Section 3.4.1.

Apart from the issue of distinguishing cluster members from local and background galaxies, where there are no distinct cut-offs, it is extremely difficult to measure redshifts for certain types of objects. Obtaining redshifts of LSB dwarfs in the Virgo Cluster is challenging. Davies et al. (2004) describe them as being “doubly cursed” because of the difficulty in obtaining distances from either optical spectroscopy, due to low surface brightness, or 21-cm redshift, due to low gas surface density. For LSB galaxies, where redshifts simply are not available, other cluster membership criteria must be relied upon.

#### 4.5.2 Morphology

In analysing an early photographic survey of the Virgo Cluster, Binggeli et al. (1985) used galaxy morphology as the main criterion to establish cluster membership of 2096 galaxies. Radial velocity measurements, where available, were used to confirm the morphological assessment. All observed LSB dwarfs were assigned to the cluster based on the correlation between absolute magnitude and surface brightness for dE and Im galaxies. The authors noted that spiral and irregular galaxies in the background appeared poorly resolved so, where knots of star-forming regions were seen, those galaxies were included as cluster members. Luminosity class was also used in conjunction with size and magnitude to infer distance. These criteria were justified by the authors because comparison with velocity measurements yielded a success rate of 98% for identifying members and 95% for identifying background galaxies (refer also Table 3.1 p.29). These methods were applied to all data with  $B_T \leq 18$  (absolute magnitude of  $M_{B_T} = -13.7$  assuming a Virgo distance modulus of  $m - M = 31.7$ ). Fainter than this limit only dE and Im dwarfs with surface brightness down to  $25.5 B_\mu$  were included.

*Morphology result:* The luminosity function derived from these data, shown in Figure 4.2 (p.57), has a faint-end slope of  $\alpha = -1.3$  (Sandage et al. 1985).

### 4.5.3 Concentration Parameters

Trentham and Hodgkin (2002), in a study of the Virgo Cluster, and Trentham and Tully (2002), in follow-up work on the faint end of the global luminosity function, used concentration parameters to identify members of the Virgo Cluster. This approach is based on the principle that dwarf galaxies have low surface brightness and consequently larger sizes and less concentrated light profiles than background galaxies of the same apparent magnitude. Inner and outer concentration parameters are defined respectively, using aperture  $R$  magnitudes (Trentham et al. 2001), as:

$$\text{ICP} = R(4.4 \text{ arcsec}) - R(2.2 \text{ arcsec})$$

$$\text{and OCP} = R(12 \text{ arcsec}) - R(6 \text{ arcsec})$$

for the Trentham and Tully (2002) survey and corresponding parameters in  $B$ -band for the Trentham and Hodgkin (2002) survey. Both inner and outer parameters are negative for LSB galaxies and close to zero for stars.

Trentham and Tully (2002) restricted selection of LSB galaxies to those with:

$$R(6 \text{ arcsec}) < 20, \text{ ICP} < -0.7 \text{ and } \text{OCP} < -0.4$$

$$\text{or } 20 < R(6 \text{ arcsec}) < 23 \text{ and } \text{ICP} < -0.4.$$

The authors state that this method should only miss extreme LSB galaxies with central surface brightness below  $28 R\mu$  and HSB low-luminosity galaxies. Both these galaxy types are considered to be rare. The overall result for the five environments studied by Trentham and Tully (2002) (the Virgo Cluster and four galaxy groups, refer Section 3.3, Item vii), produced a mean faint-end slope of  $\alpha \simeq -1.2$ . For the Virgo Cluster in particular, an unusually shallow faint-end slope of  $\alpha \simeq -1.03$  was derived. The method of determination of galaxy magnitudes in this survey may have contributed to this result and is discussed in detail in Section 6.2.1.

Trentham and Hodgkin (2002) used a more complicated criterion using the OCP in the  $B$ -band, the  $B(6 \text{ arcsec})$  magnitude and background galaxy counts with the

same parameters from the North Galactic Cap (similarly obtained in the INT Wide Field Survey) to derive a probability of Virgo Cluster membership. The luminosity distribution thus derived is shown in Figure 4.4.

*Concentration parameter results:* The Trentham and Tully (2002) luminosity function for the Virgo Cluster has a faint-end slope of  $\alpha = -1.03$ . The Trentham and Hodgkin (2002) luminosity function, shown in Figure 4.4, has a faint-end slope of  $\alpha = -1.35$  overall and  $\alpha = -1.7$  over a limited magnitude range.

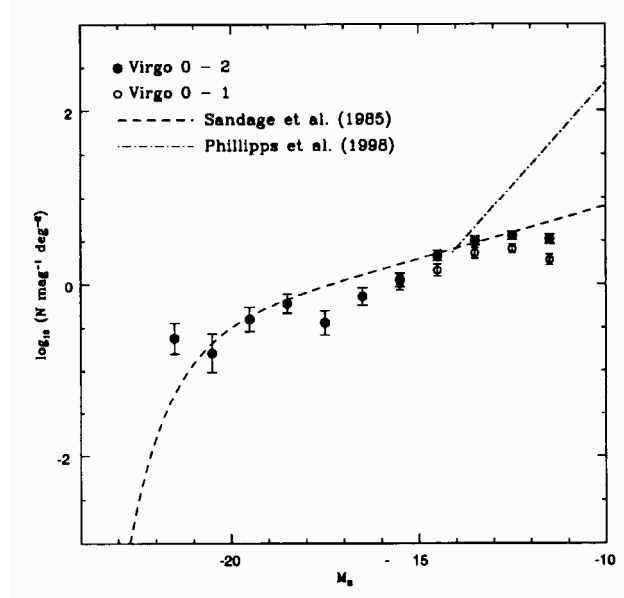


Fig. 4.4: Luminosity Functions and the Trentham and Hodgkin (2002) Distribution

The Virgo Cluster luminosity distribution of Trentham and Hodgkin (2002) with  $\alpha = -1.35$  and a steepening to  $\alpha = -1.7$  in the range  $-17 < M_B < -14$ : filled circles are data for all galaxies including doubtful cluster members; open circles are data for galaxies considered to be more probably cluster members. The dashed line is the luminosity function fit of Sandage et al. (1985) with  $\alpha = -1.30$ . The dotted-dashed line represents the steep power-law fit of Phillipps et al. (1998) to an inner-area sample, scaled for colour differences (refer also Figure 4.5). The two fits are scaled vertically to have the same number of galaxies as the data at  $M_B = -14$ .

Figure reproduced from Trentham and Hodgkin (2002).

#### 4.5.4 Scale Length Limits

Impey et al. (1988) state that to detect LSB galaxies (similar to dwarf spheroidals of the Local Group) at the distance of the Virgo Cluster, a survey would need to be sensitive to a magnitude limit of  $\mu_{lim} = 27 B\mu$  and galaxies with scale length of a couple of arcseconds and limiting angular size of 5 arcsec. However, it is also stated that galaxies meeting these criteria are generally regarded to be background galaxies. Conversely, criteria of this type have been used to select, from survey data, galaxies that are likely to be cluster members (e.g. Phillipps et al. (1998), Sabatini et al. (2003)).

Diameters and distances of four dwarf galaxies in the Local Group from Karachentsev et al. (2004) are used to estimate the scale length that would be measured for similar dwarf galaxies in the Virgo Cluster (refer Table 4.3). The ratio of scale length  $a$  to radius  $r$  varies, but  $a = 0.31(\pm 0.11)r$  is the average (and standard deviation) of all ratios for galaxies studied in this project (refer Section 8.4 for source data). The average value is used to estimate scale diameter from physical diameter for the four Local Group dwarfs. Angular (radial) scale length is then calculated based on distances of 15 and 32 Mpc to correspond with the nearer and more distant parts of the Virgo Cluster.

The data in Table 4.3 show that dwarf galaxies in the more distant parts of the Virgo Cluster may have scale lengths as small as  $a < 1.0$  arcsec. At the distance to sub-cluster A, all but the smallest dwarfs would have  $a \geq 1.5$  arcsec. By comparison, bright background field galaxies typically have  $a \lesssim 1.0$  arcsec and fainter field galaxies measure even smaller with  $a \lesssim 0.5$  arcsec (Windhorst et al. 1994). Thus, it is evident that measurements of  $a \approx 1.0$  arcsec would not clearly distinguish between cluster dwarfs and background galaxies, but galaxies with  $a \geq 2.0$  arcsec are highly likely to be cluster members if they exhibit dwarf morphology. Two sets of results using more conservative scale length criteria, one by Phillipps et al. (1998) and the other by (Sabatini et al. 2003), are presented below.

Phillipps et al. (1998) used a combination of scale length and magnitude criteria to preferentially select LSB dwarfs in the Virgo Cluster. The galaxies included have



Dwarf Galaxy Property	Leo II	Carina	UMi	Draco	Sag
Major angular diam in arcmin (at 25 $\mu$ )	12	24.3	30.2	35.5	450
Distance (Mpc)	0.21	0.1	0.06	0.08	0.02
Major physical diameter (pc)	733	707	527	826	2618
Diameter at 1 scale length (pc)	227	219	163	256	812
Estimated radial scale length at 15 Mpc	1.6	1.5	1.1	1.8	5.6
Estimated radial scale length at 32 Mpc	0.7	0.7	0.5	0.8	2.6

Tab. 4.3: Dwarf Galaxy Properties and Scale Length at Virgo Cluster Distances

*The table lists properties of some Local Group dwarf galaxies and shows calculated values of scale length if these galaxies were placed at the distances of sub-cluster A and the more distant W and M clouds of the Virgo Cluster. Angular diameters and distances are from Karachentsev et al. (2004). The calculation of scale length is based on the average ratio of scale length to total observed radius of galaxies studied for this project.*

scale length  $a \geq 3$  arcsec and  $\mu_0 \geq 22$   $R\mu$  with a completeness limit of  $\mu_0 \leq 24.5$   $R\mu$ . The authors did not obtain individual galaxy profiles but, instead, selected on the basis of isophotal sizes and magnitudes that are consistent with galaxies having exponential profiles. This survey covered a region near M87 containing 675 galaxies and a second region  $\sim 3$  degrees further out containing 895 galaxies meeting the selection criteria.

Background contamination was dealt with statistically by subtracting counts obtained from images of 20 fields near the South Galactic Pole (Schwartzzenberg et al. 1995). The authors state that the correction is small, a few percent, compared with the total number of LSB galaxies detected. The result is a luminosity function with a much steeper faint end than that resulting from any other survey or method (refer Figure 4.5). However, it is likely that these data suffered from photometric or selection errors (S. Phillipps, private communication, 2006) that resulted in contamination by background galaxies. The process of background subtraction is further discussed in Section 4.5.6.

Sabatini et al. (2003) used selection criteria of  $23 \leq \mu_0 \leq 26$   $B\mu$  and  $3 \leq a \leq 9$  arcsec to detect LSB dwarfs in the Virgo Cluster. These criteria put the sample in the range  $-14 \leq M_b \leq -10$ . Using this method 257 galaxies were detected (refer also Davies et al. (2004)), 105 of them previously uncatalogued and 143 listed by Trentham and Hodgkin (2002). The criteria are the result of numerical simulations of a galaxy population at the approximate distance of the Virgo Cluster described by Sabatini et al. (2003). All input data to the simulation had exponential profiles and the selection criteria were optimised for maximising cluster member detection and minimising background contamination. The efficiency of the simulation was tested to estimate the completeness and contamination of the method so corrections could be made for these effects.

Inconsistencies in the method of scale length cut-off may arise from poor seeing conditions at the time of the observations. Trentham and Hodgkin (2002) state that poor seeing makes galaxy images appear larger and have less concentrated light profiles than images taken under more typical conditions or in background fields. In practice, the observations used by Sabatini et al. (2003) had a poor 2-arcsec seeing, so the measured scale length cut-off was effectively increased to 4 arcsec.

This criterion was tested on the data by considering the fall in surface density of detections with increasing distance from the cluster centre and by measuring background galaxies in offset fields. By plotting the number counts as a function of distance from the cluster core, Sabatini et al. (2003) were satisfied that the galaxy density decreased, as expected, falling to the background galaxy density at  $\sim 6.5$  degrees from the centre of the cluster. Were the sample highly contaminated by background galaxies, this plot would appear flat. Selected galaxies, corrected for background contamination (as obtained from the numerical simulation) and incompleteness (based on the efficiency of the algorithm at detecting artificial galaxies) were used to produce a final luminosity function.

In this way, Sabatini et al. (2003) justify the selection criteria of scale length  $a \geq 4$  arcseconds (adjusted from a base value of  $\sim 3$  arcseconds by convolution with a 2-arcsecond seeing disk) and central surface brightness  $\mu_0 \geq 23$   $B\mu$  to maximise

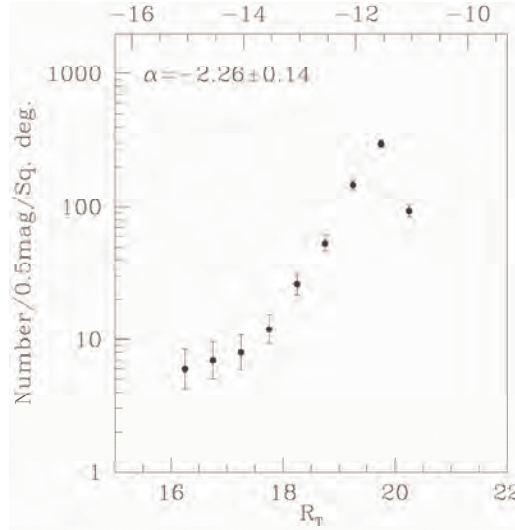


Fig. 4.5: A Steep Luminosity Function

*The luminosity distribution of the outer region of the Phillipps et al. (1998) survey is the steepest found to date for any region in clusters or in the field. The faint-end slope is  $\alpha = -2.26$ . The upper x-axis shows  $M_R$  and may be used to compare this figure with Figure 4.4.*

Figure reproduced from Phillipps et al. (1998).

detection of cluster galaxies. Results show that, in the east-west strip of the INT Wide Field Survey area, the luminosity function appears to be strongly dependent on environment with the slope in the outer region much steeper ( $-1.8$ ) than in the inner region ( $-1.4$ ) of the cluster (Sabatini et al. 2003). The overall stated result after correction for incompleteness is a faint-end slope of  $-1.6 \pm 0.1$ .

Sabatini et al. (2003) also applied the DGR across the east-west region and found it fairly constant at about 20:1 (refer Figure 10 of Sabatini et al. (2003), which plots the DGR from the core out to 7 arcsec from M87). If the DGR is a valid substitute for the luminosity function, it would be expected that the DGR would vary between inner and outer regions of the cluster in the same way that the luminosity function varies. The apparently constant DGR does not seem to support this and the quoted DGR figures also do not appear to correspond with the conversions shown in Table

4.2 (p.60). The DGR plot does show some higher values in the outer regions of the cluster, but the authors attribute the most extreme data point to a dip in the distribution of giants at  $\sim 5$  degrees from the cluster core.

Nevertheless, the variations in the luminosity function between the core and edge of the cluster demonstrate the sensitivity of such studies to the region included. Similarly, when Roberts et al. (2007) investigated the north-south strip of the survey using the same detection algorithm and the same selection criteria as Sabatini et al. (2003), much higher values of the DGR were found. In that paper, DGR statistics are included for both surveys, with some refinement, as shown in Table 4.4.

Region	DGR ( $\leq 4^\circ$ )	DGR ( $4^\circ - 8^\circ$ )	Mean DGR
N-S	$27 \pm 11$	$35 \pm 16$	$31 \pm 9$
E-W	$16 \pm 5$	$15 \pm 9$	$16 \pm 4$

Tab. 4.4: Dwarf-to-Giant Ratios for Virgo Strips

*These data show that the DGR is higher in the N-S strip than in the E-W strip and also that it is significantly higher in the outer region of the N-S strip than in the inner region of the same strip, probably due to coverage of the more distant galaxy clouds of the Virgo Cluster.*

Table from Roberts et al. (2007).

Because the analyses by Sabatini et al. (2003) and Roberts et al. (2007) of both regions are fully self-consistent, the very different findings from the two survey strips must be attributed to differences in the galaxy population. The earlier survey of Sabatini et al. (2003) covers a region that is almost entirely within the dominant A sub-cluster. Roberts et al. (2007) point out that the north-south strip probably overlaps parts of the more distant, infalling, M and N clouds (refer Figure 3.6 p.43) which accounts for the discovery of more faint galaxies in that strip and, in particular, in the outer region of that strip. Unfortunately, in the more recent study, no actual luminosity function values are provided.

*Scale length-limited results:* The luminosity functions derived by Phillipps et al. (1998) have faint-end slopes of  $\alpha = -2.18 \pm 0.14$  for the inner region (shown in Figure 4.5) and  $\alpha = -2.26 \pm 0.12$  for the outer region of the Virgo Cluster.

The luminosity functions derived by Sabatini et al. (2003) have faint-end slopes of  $\alpha = -1.4 \pm 0.2$  for the inner region and  $\alpha = -1.8 \pm 0.2$  for the outer region of the Virgo Cluster, with an overall faint-end slope of  $\alpha = -1.6$  in the range  $-14.5 \leq M_B \leq -10.5$ .

#### 4.5.5 The Rines-Geller Threshold

Rines and Geller (2008) assessed Virgo galaxies within 1 Mpc, or approximately 3.4 degrees, of M87 (an area slightly offset from, but very similar in areal coverage to, the Virgo Deep Stack image). Data were from the SDSS 6th Data Release (DR6) which has almost complete spectroscopic and photometric coverage to  $r = 17.77$  (Rines and Geller (2008), with reference to Strauss et al. (2002)). Within the specified region, galaxies with  $|\Delta cz| \leq 2000 \text{ km s}^{-1}$  were selected to initially distinguish cluster members from background galaxies. After visually checking the data and identifying additional cluster members for which there was no SDSS spectroscopy (by searching NED for literature radial velocities), 487 definite or probable cluster members were identified out of 4215 galaxies within 1 Mpc of M87. These data produce a luminosity function for the Virgo Cluster with a faint-end slope of  $\alpha = -1.28 \pm 0.06$ .

As this result is derived using spectroscopic measurements, it more properly belongs under the heading *Radial Velocities*. However, the authors conducted further analyses comparing surface brightness, apparent magnitude, absolute magnitude and colours of the cluster members and non-members in the sample. It is one of these analyses that presents a potentially useful threshold for assessing cluster membership. The comparison of central surface brightness with apparent magnitude suggests this may be a good indicator of probable cluster membership. Unlike previously discussed selection criteria that use two parameters with fixed cut-offs, i.e. scale length  $a$  and central surface brightness  $\mu_0$ , this linear relation utilises the

dependence of the total apparent magnitude  $m_T$  on both of these terms and may be applied over a continuous range of values. The Impey et al. (1988) method for deriving total apparent magnitude is:

$$m_T = \mu_0 - 2.5 \log(2\pi a^2) \quad (4.6)$$

Figure 3 from Rines and Geller (2008) (reproduced as Figure 4.6) shows a plot of  $\mu_0$  against  $m_T$ . The figure clearly suggests a threshold between cluster members and non-members. The data are in  $r$ -band and the equation of the threshold, measured from the figure, is:

$$\mu_0 = \frac{10}{11} m_T + 6.0909. \quad (4.7)$$

Although there is some scatter across the threshold, galaxies above the threshold (fainter  $\mu_0$  for  $m_T$ ) are mostly Virgo Cluster members and those below the threshold are mostly background galaxies. It is possible to simultaneously solve Equations 4.6 and 4.7 to find the intersection of the Rines-Geller threshold with the locus of a specific value of scale length. It should be noted that the threshold runs almost along, but not exactly parallel to, the 3-arcsec locus (refer Figure 4.7).

Assuming that the relation may be extrapolated to fainter magnitudes, the intersection of the threshold with the 3-arcsec locus occurs at an apparent total magnitude of  $r = 18.8$  and central surface brightness of  $\mu_0 = 23.18 \text{ } r\mu$ . In this project it is proposed that these values may be used as a guide to galaxy parameters for which a 3-arcsec scale-length limit is appropriate. However, at brighter magnitudes and central surface brightnesses, a larger scale length would be a more reliable choice.

Because equation 4.6 is linearly dependent on  $\mu_0$ , the relation should hold for small photometric corrections from  $r$ -band to  $R$ - or  $OR$ -band as the corrections would be similar on both axes and should make little change to the slope or position of the threshold. If this assumption is valid, then the solution above may be compared with other  $R$ -band data. The threshold is applied to the galaxies surveyed for this project in Section 9.1.

*Radial velocity result:* The Virgo Cluster luminosity function derived by Rines and Geller (2008) has a faint-end slope of  $\alpha = -1.28$ .

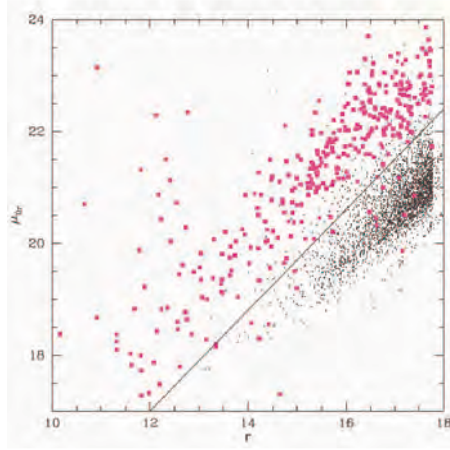


Fig. 4.6: The Rines-Geller Threshold

*This plot compares central surface brightness with apparent magnitude for galaxies within 1 Mpc of M87. Virgo Cluster members are represented by large pink spots and background galaxies by small black dots. Distinctions were made based on radial velocities. The straight line indicates the approximate division between cluster members and background galaxies.*  
Figure reproduced from Rines and Geller (2008).

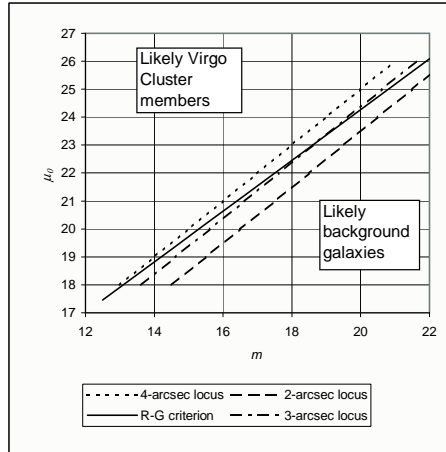


Fig. 4.7: Loci of Fixed Scale Length

*In this plot the loci of galaxies with fixed scale length are shown as broken lines using the relationship between scale length, central surface brightness ( $\mu_0$ ) and apparent magnitude ( $m$ ). The Rines-Geller threshold (refer Figure 4.6) is shown as a solid line intersecting the 3-arcsec locus at  $m = 18.8$  and  $\mu_0 = 23.18$ . The proximity of this threshold to the 3-arcsec locus supports the use of a 3-arcsec cut-off as a criterion for cluster membership.*

#### 4.5.6 *Background Galaxy Counts*

Galaxy counts from field surveys may be used in a number of ways to estimate the background contamination in cluster surveys where direct methods of distance determination cannot be applied. Various methods used in the Virgo Cluster are discussed and comments from other studies are included for comparison.

The most direct method is to use subtraction of a field luminosity function from the overall cluster data to leave a cluster-only luminosity function. This was the method used by Phillipps et al. (1998). For that analysis, cluster data come from a six-deep stack of digitised UKST Tech Pan *OR*-band films. Background data were from CCD images of the South Galactic Pole (Schwartzberg et al. 1995) using a broadband ‘*VR*’ filter. Appropriate colour corrections were applied to the data for comparisons of galaxy properties. By using a similar connected-pixel detection method and similar selection criteria to isolate the LSB galaxies of appropriate sizes from both the field and cluster surveys, Phillipps et al. (1998) state that the background-subtraction correction required was only “a few percent”.

However, this analysis produced a very steep luminosity function that, to date, has not been reproduced in any subsequent studies (and, in fact, could not be reproduced from the same data (B. Jones, private communication, 2006)). A private communication by S. Phillipps (cited by Sabatini et al. (2003)) suggests that the last data point may have been highly background contaminated. Neglecting this data point would change the faint-end slope from steeper than  $-2$  to approximately  $-1.9$  (Sabatini et al. 2003) or  $-1.8$  (S. Phillipps, private communication, 2006) which compares favourably with the Sabatini et al. (2003) value of  $-1.8$  for the outer region of the Virgo Cluster. This discussion points out the sensitivity of the luminosity function fit to the data in the faintest magnitude bins where the errors are likely to be greatest. It also shows that limiting the magnitude range over which the function is fitted can have a significant effect on the result.

The background subtraction method was also applied by Chiboucas and Mateo (1999) to a study of cluster A3526. This study showed that in the magnitude range  $19.5 < V < 21.5$  for that particular sample there is, in fact, an excess of control field



counts over cluster counts. This is attributed to possible variations in field counts, to selection effects or to problems of extracting LSB galaxies from the data. In follow-up studies Chiboucas and Mateo (2006) state that the problem with background subtraction is that it assumes that the control field is representative of the cluster's background population. Unfortunately, this is often not the case, making proper accounting for the background population problematic.

The variation in field counts was examined by Picard (1991). Results show a difference of 30% in the galaxy surface density in two widely-separated regions of sky covered by the Palomar Observatory Sky Survey (POSS-II). It is suggested that this is attributable to large-scale structure with size of the order of  $50 h^{-1}$  Mpc. The result is based on seven fields in the north galactic hemisphere, centred on  $\sim 15^h00^m00^s +30^\circ00'00''$  ( $l = 45^\circ, b = +61^\circ$ ) and nine in the south centred on  $\sim 0^h20^m00^s +5^\circ00'00''$  ( $l \approx 110^\circ, b \approx -55^\circ$ ). The north field is found to be approximately 30% more populous than the south field in the range  $16.5 > r > 19.0$ .

Different results from global surveys listed in Table 4.5 (p.87) highlight the potential variation in field galaxy counts. The range of faint-end slopes between  $\sim -1.00$  and  $\sim -1.30$  suggests considerable variation in the relative population of the fainter galaxies. If this is dependent upon the region covered by the survey, it implies significant non-uniformity in the field galaxy population. This kind of variation could lead to errors in luminosity functions based on background subtraction methods depending on the region chosen for examination.

There are other methods of utilising background counts that may be less sensitive to this problem. The Trentham and Hodgkin (2002) method is to calculate a probability of cluster membership based on concentration parameters for a Virgo sample and for a background sample. However, the authors warn that, without a characterisation of the field-to-field variation of field galaxies as a function of surface brightness, this method must be treated with caution. Therefore, Trentham and Hodgkin (2002) did not rely solely on this probability, but visually inspected every galaxy to make a judgement regarding its cluster membership and rejected from the dwarf selection (which was based on concentration parameters) galaxies

with obvious spiral structure or bulge + disk morphology. These are likely to be background giant galaxies. This cut removed  $\sim 15\%$  of galaxies that would otherwise have been classed as possible cluster members. The resulting overall luminosity function has a faint-end slope of  $\alpha = -1.35$  but over the limited magnitude range of  $-17 < M_B < -14$  it steepens to  $\alpha = -1.7$ . Figure 4.4 (p.67) shows this steepening and also illustrates the very steep Phillipps et al. (1998) result that covers a fainter magnitude range.

In another approach, Sabatini et al. (2003) used modelling based on a luminosity function derived from the 2dFGRS to populate a cone of the universe using set cosmological parameters. This population was input into a numerical simulation to derive the background contamination in a Virgo Cluster sample. Results are different for inner and outer regions of the Virgo Cluster, but the overall result is a moderately steep faint-end slope of  $\alpha = -1.6$ . This approach may be questioned on the basis that the 2dFGRS includes galaxies to large distances, some 25 times the distance to the Virgo Cluster, so is dominated by giant galaxies. Therefore, using this method to correct for contamination, which mainly concerns the dwarf population at the faint end of the luminosity function, may not yield the most accurate results.

The method of dealing with background contamination is not the only contributing factor to these varied results, but would contribute at some level. The relative significance of this problem compared with detection methods and other processing is discussed in Section 4.8.

#### 4.6 *Cosmological Models and the Luminosity Function*

Modelling of galaxy formation and evolution has followed one of two approaches. One approach is referred to as ‘hierarchical clustering’ (e.g. the oft-cited Moore et al. (1999a) and Klypin et al. (1999)) and includes  $\Lambda$ CDM cosmology as one example. In this approach, small-scale fluctuations in the initial density field collapse to form dark-matter haloes. These sub-units merge hierarchically to form, at later epochs,

massive galaxies that exhibit ongoing star formation and sometimes starbursts. The other (more recently popular) approach is to assume that massive galaxies formed early, as a primordial population, and have evolved with declining star formation rates. In this ‘cosmic downsizing’ model (e.g. Nelan et al. (2005)), active star formation and the formation and growth of black holes shift to lower-mass galaxies as the universe evolves.

Kauffmann and Charlot (1998) discount the downsizing model due to the apparent deficiency of massive galaxies at  $z = 1$  and the unlikely possibility that galaxies that may exist are heavily obscured by dust. These authors, based on the  $K$ -band luminosity function at  $z = 1$ , favour the model in which massive galaxies continue to form hierarchically until the present. However, there is recent observational evidence for cosmic downsizing based on studies of stellar populations as a function of galaxy mass (Nelan et al. 2005). This model argues against hierarchical clustering based on the assumption that galaxy mergers should induce new bursts of star formation, or at least support a younger population of stars in ‘old’ galaxies due to recent mergers with star-forming smaller galaxies. The Nelan et al. (2005) study finds only old stars in old galaxies, supporting downsizing, but apparently contrary to hierarchical clustering.

Hierarchical clustering models have other problems too, in that they are generally unable to predict the observed galaxy luminosity function. Whilst the models appear robust, in that both the Moore et al. (1999a) and Klypin et al. (1999) simulations are insensitive to variations in cosmological parameters  $\Omega$  and  $\Lambda$  and to the exact formation epoch, these models predict a large number of dark matter satellites in a random distribution. The Moore et al. (1999a) model implies that the Milky Way should be surrounded by about 500 galaxies larger than dwarf spheroidals. This is about 50 times more than the nine satellites that were known at the time, though recent analyses of SDSS data have brought the tally to 22 (refer, e.g. Belokurov et al. (2007), Zucker et al. (2006a) and Zucker et al. (2006b)). However, the recent discoveries are of dwarf galaxies and, rather than lying in a random distribution, the entire Milky Way satellite population is found to lie in a plane approximately

perpendicular to the disk of the Milky Way (Kroupa et al. 2005).

The model of Klypin et al. (1999) also over-predicts the population of satellite galaxies by an order of magnitude in both the Milky Way environment and the Local Group. Klypin et al. (1999) suggest that the predicted dark matter haloes may exist but that, through some physical mechanism such as supernova-driven winds or gas heating by intergalactic ionising radiation, the haloes failed to form stars.

The higher number of dwarf haloes showing up in these models would steepen the faint-end slope of a corresponding luminosity function. The semi-analytic model of Cole et al. (2000) also leads the authors to favour models that produce luminosity functions with “quite steep faint-end slopes” in order to achieve a good fit to the bright ends of the  $B$ - and  $K$ -band luminosity functions and to match other observed properties including colours, disk sizes and the elliptical-to-spiral ratio. More recent work by Governato et al. (2004) investigates formation of Milky Way-type galaxies in both  $\Lambda$ CDM and warm-dark-matter (WDM) cosmologies. The  $\Lambda$ CDM simulation over-predicts the number of satellites and, whilst the WDM simulation reduces the number of satellites, it fails to reproduce the extended disk and other physical features of the Milky Way’s bulge-disk-halo structure.

The results of a model by Fontanot et al. (2007) are compared with galaxy counts and the redshift evolution of the  $K$ -band luminosity function. This model attempts to reconcile a hierarchical cosmology with the observed downsizing through improved modelling of infall and cooling in dark matter haloes. The model succeeds in reproducing the overall build-up of stellar mass, but predicts too many massive galaxies (with  $M = 10^{10} - 10^{11} M_{\odot}$ ) at  $z \sim 1$  and too many bright galaxies in the local universe.

Differences between the field and cluster environment were considered in the Lemson and Kauffmann (1999) model that used  $N$ -body simulations of hierarchical clustering. Results indicate that the environment only affects the mass distribution and that other properties, such as type, luminosity and colour, are consequences dependent solely on the halo mass function. Further, the model infers that in high-density

environments (local overdensity  $\delta = 1.5$ ) the ratio of high-mass galaxies to low-mass galaxies is higher than in low-density environments ( $\delta = -0.60$ ). However, Roberts et al. (2004), based on the DGR for the Virgo Cluster compared with that for the field, state that this is “completely opposite to what is observed”.

The Boselli et al. (2008) study of dE galaxies in the Virgo Cluster also contradicts the Lemson and Kauffmann (1999) model. The study shows that the mean stellar age in low-luminosity galaxies is far younger than that predicted by hierarchical clustering models and that, although clustering dominated galaxy evolution at early epochs, “secular evolution” and the effects of the environment have become important since then.

There is still no single model that is able to reproduce galaxies with the observed characteristics and the observed distribution. The solution may turn out to be a combination of influences, and advances should be made with better-refined simulations. For example, Neistein et al. (2006) find, in a simulation of galaxy evolution, that downsizing is compatible with hierarchical clustering when gas processes and baryonic feedback mechanisms are included.

Unfortunately, there are few cases in which theoretical predictions may be directly compared with observed galaxy luminosity functions because theorists rely heavily on mass functions (e.g. Lemson and Kauffmann (1999)) or velocity functions (e.g. Moore et al. (1999a)) rather than luminosity functions. Comparison relies on the inferences that higher velocities imply larger masses and that larger masses exhibit higher luminosities. However, discussion by Gonzalez et al. (2000a) and White and Frenk (1991) relating circular velocity to luminosity show that there is no simple direct correspondence between the faint-end slope of the luminosity function and the slope of the velocity function.

One model that does make a direct comparison is presented by Bullock et al. (2000). This model includes suppression of gas accretion in low-mass haloes after the epoch of reionisation. This allows for the formation of dwarf galaxies, at  $z \approx 5 - 12$ , from small amounts of gas available before reionisation, after which photoionisation prevents further gas accretion. The model predicts that bright galaxy haloes should also

contain multiple dark matter haloes that may be detectable through gravitational effects. The velocity function for the predicted observable haloes, i.e. those that successfully produce galaxies, accurately matches the observed velocity function of satellite galaxies around the Milky Way and M31. This success demonstrates that, if the suppression process works according to the model, there is no hidden population of dwarf galaxies in the local volume that has yet to be discovered. Nevertheless, Sabatini et al. (2005) counter this scenario based on results from the Wilkinson Microwave Anisotropy Probe (WMAP) project that show that reionisation occurred earlier, at  $z \approx 20$ , which would not have allowed sufficient time for dwarf galaxies to form if the process was effective under the conditions described.

By using comparisons across velocity, luminosity and the DGR, it is possible make inferences about the success or otherwise of theories of galaxy formation but, while observers look for more faint galaxies to satisfy the faint-end inferences of some theories (i.e. that  $\alpha$  should be ‘steep’), the theorists seek better agreement between observers on the properties of the faint end of the luminosity function to help to refine the models.

#### 4.7 *Applications and Limitations of the Schechter Function*

In its original conception, the Schechter Function was intended to be fitted to data in a complete range of luminosities. Three fitting parameters are specified ( $L_*$ ,  $\phi_*$  and  $\alpha$  of Equation 4.1) and the linear faint-end slope is one component of the fit - but the ‘fit’ is exactly that, and even in its earliest application there are data points that lie above and below the fit (refer Figures 4.1, p.55, and 4.2, p.57). It is therefore noteworthy that some authors consider it appropriate to piecewise fit the Schechter Function to, or read the slope of, individual sections of a distribution.

The Virgo Cluster luminosity function of Trentham and Hodgkin (2002) is analysed in detail, comparing overall faint-end slope  $\alpha$  with the Sandage et al. (1985) and Phillipps et al. (1998) results (refer Figure 4.4, p.67). The Trentham and Hodgkin (2002) distribution is more in keeping with the earlier Sandage et al. (1985) result

than with the steeper Phillipps et al. (1998) luminosity function, which is measured over a restricted magnitude range. Trentham and Hodgkin (2002) also consider separate values of  $\alpha$  based on 3-magnitude ranges throughout the distribution, stating that the “curvature” thus derived is real and statistically significant (i.e. the errors are small). Values of  $\alpha$  in individual components of this analysis range from -0.90 to -1.65.

This issue may be viewed from two perspectives. On the one hand, consistent full-distribution fitting makes it straightforward to compare the faint-end slopes of distributions from different surveys. On the other hand, the Schechter function, with its linear faint end, may not represent the optimum fit to real data. Whilst it appears consistent with many earlier results (with shallower surveys and larger uncertainties) it is still only a mathematical construct with no physical basis. Other recent results also point to this problem where the luminosity function yields different faint-end slopes if including all the data or if only considering data points within a set magnitude range. This is evident in Table 4.5 (p.87) in cases where two different values are quoted (with the second value and criteria given in brackets).

In some cases, fitting is best achieved using a Gaussian for the bright end in combination with a Schechter function at the faint end (e.g. as used by Trentham and Tully (2002) for the Virgo Cluster) or a double Schechter function (e.g. as suggested by Trentham et al. (2005) for a combined cluster luminosity function or as used by Popesso et al. (2006) for early-type galaxies). Nevertheless, with the amount of literature quoting single values of  $\alpha$  over a complete distribution, it would appear that such a comparison will continue to be implemented.

### 4.8 *Summary: The Virgo Cluster Luminosity Function*

A number of luminosity functions for the Virgo Cluster have been described and are summarised in Table 4.5. Variations in faint-end slope  $\alpha$  are attributable to many factors: regions of the cluster surveyed; galaxy detection methods; cluster membership criteria; corrections for completeness; and the methods and magnitude ranges of the fitting of the Schechter function to the distribution. It is hardly surprising that there is considerable disagreement between the results. However, two consistent trends may be noted.

The first is that cluster luminosity functions typically have steeper faint ends than those of the field, meaning that there are proportionately more dwarf galaxies in denser environments. This trend may be observed by comparing Virgo Cluster and other cluster data with the sample Global data in Table 4.5.

The second is that within the Virgo Cluster there are variations in the luminosity function that are region-dependent. For example, results from Sabatini et al. (2003) and Phillipps et al. (1998), whilst in disagreement on values for  $\alpha$ , both show that the slope in the outer region is steeper than in the inner region of the cluster ( $-1.8$  outer and  $-1.4$  inner in the former case,  $-2.26$  outer and  $-2.18$  inner in the latter case). The clear discrepancy between these results is accounted for by Sabatini et al. (2003) whose data are corrected for incompleteness, whereas the Phillipps et al. (1998) data are not and, if the last point in the Phillipps et al. (1998) luminosity function is omitted, the two sets of results are consistent (within uncertainties) once completeness corrections are taken into account. These results demonstrate that the luminosity function is shallower near the core of the cluster than near the edge.

The same effect is observed in Abell 496, where the luminosity function steepens from  $-1.4 \pm 0.1$  in the central region to  $-1.8 \pm 0.1$  in the southern envelope of that cluster (Boué et al. 2008). This suggests that, in very dense environments, dwarf galaxies may not survive gravitational encounters. However, other factors that may contribute to these results include the difficulty of detecting LSB galaxies within luminous haloes of giant galaxies and, in the Virgo Cluster, possible effects of the



underlying sub-structure of the cluster (refer Figure 3.6, p.43).

This variation between the core and edge of the Virgo Cluster is also seen by Roberts et al. (2007), but in this case it is the other way round with a DGR of 27 in the outer 4 degrees compared with 35 in the inner 4 degrees along the north-south strip of the INT Wide Field Survey (refer Table 4.4 p.72). This may be accounted for by the probable detection of many faint galaxies belonging to the more distant M and N clouds in the outer part of the strip.

Sabatini et al. (2003) also note that the DGR does not blend into the background value, even near the edge of the cluster, suggesting that the Virgo Cluster environment is very different from that of the field right out to its outermost regions. Roberts et al. (2007) observe that the infalling clouds also appear to have high DGRs, similar to that of the main sub-cluster, but that the origin of this dwarf population is still not fully explained.

Sources of error when comparing luminosity functions are mainly attributable to issues of contamination and cluster member identification. It is difficult to reconcile these issues whilst different groups continue to use different detection methods and different membership criteria.

In a study of the luminosity functions of galaxy groups Trentham and Tully (2002) suggest that a preferred method is to have a survey that blankets an entire region as a homogeneous data set. In the case of the Virgo Cluster, because of its large extent ( $\sim 140 \text{ deg}^2$ ), this seems unlikely. Deep surveys that seek the elusive faint end of the luminosity function have tended to focus on smaller sub-sections of the cluster than the original all-inclusive VCC of Binggeli et al. (1985). However, the Virgo Deep Stack does encompass approximately 25% of the Virgo Cluster covering  $25 \text{ deg}^2$ , centred on the main (A) sub-cluster, to a limiting surface brightness of  $\approx 28 \text{ OR}\mu$ . Its uniformity, depth and large area coverage make this unique resource an invaluable tool for visually inspecting and analysing parameters of galaxies included in numerous other surveys. In this way, data from the other surveys, where the individual galaxies (and their properties) are catalogued, may be compared. Some such comparisons are included in Chapter 6.

However, the prospect that there will ever be universal agreement on the parameters of a full-cluster Virgo Cluster luminosity function still appears remote.

---

#### Footnotes to Table 4.5

---

<sup>a</sup> Faint magnitude bins include completeness correction and the number of galaxies is extrapolated.

<sup>b</sup> The authors use a composite of a Gaussian and a Schechter function to match the sample.

<sup>c</sup> Total galaxy count is from Davies et al. (2004); *B*-band DGR figures are from Roberts et al. (2007).

<sup>d</sup> No  $\alpha$  figures supplied, only the DGRs.

<sup>e</sup> This  $\alpha$  is fitted to data excluding cD (giant elliptical) galaxies.

<sup>f</sup> The authors' Figure 1 shows a polynomial fit to the data, not the Schechter function described in the figure caption.

<sup>g</sup> RC1: The first *Reference Catalogue of Bright Galaxies* (de Vaucouleurs and de Vaucouleurs 1964).

<sup>h</sup> ESP: ESO Slice Project redshift survey.

<sup>i</sup> 2dFGRS: 2dF Galaxy Redshift Survey.

<sup>j</sup> SDSS: Sloan Digital Sky Survey.

<sup>k</sup> MGS: Millennium Galaxy Survey.

<sup>m</sup> Refer Appendix C for explanation of log  $h$  notation.

Reference	Region	$\alpha$	Magnitudes / DGR	Number of galaxies
Sandage et al. (1985) <sup>a</sup>	Virgo Cluster (VC) VC dwarf ellipticals	-1.30 -1.35	-22 < $M_B$ < -12 -18 < $M_B$ < -12	1647 1131
Impey et al. (1988)	VC completeness-corrected	-1.7	-22 < $M_B$ < -12	26 new + Sandage (above)
Phillipps et al. (1998)	VC outer region VC inner region	-2.26 ± 0.14 -2.18 ± 0.12	-16 ≤ $M_R$ ≤ -11	895 675
Trentham and Tully (2002) <sup>b</sup>	VC	-1.03	-18 < $M_R$ < -10	99 new + Sandage (above)
Trentham and Hodgkin (2002)	VC INT both strips	-1.35; (-1.7)	-18 < $M_B$ ; (-17 < $M_B$ < -14)	449
Sabatini et al. (2003) <sup>c</sup>	VC INT E-W strip	-1.6	-14 < $M_B$ < -10	257
	outer region	-1.8 ± 0.2	DGR <sub>B</sub> = 15 ± 9	
	inner region	-1.4 ± 0.2	DGR <sub>B</sub> = 16 ± 5	
Roberts et al. (2007) <sup>d</sup>	VC INT N-S strip		DGR <sub>B</sub> = 31 ± 9	336
	outer region		DGR <sub>B</sub> = 35 ± 16	
	inner region		DGR <sub>B</sub> = 27 ± 11	
Rines and Geller (2008)	VC < 1Mpc from M87	-1.28 ± 0.06	-21.5 < $M_r$ < -14	487
Chiboucas and Mateo (2006)	Centaurus Cluster	-1.4 ± 0.2	-23 < $M_V$ < -11	78
Boué et al. (2008)	Abell 496	-1.55 ± 0.06	-23 < $M_{r'}$ < -13	487
Schechter (1976) <sup>e</sup>	Cluster	-1.24 ± 0.05	-23 < $M_B$ < -16	13 clusters
Trentham et al. (2005)	Cluster	-1.6; (-1.24)	-17 < $M_R$ < -14; (-19 < $M_R$ )	~5670
van den Bergh (1992) <sup>f</sup>	Local Group	-1.1	-21.1 ≤ $M_V$ ≤ -7.6	27
Trentham et al. (2005)	Local Group	-1.1 ± 0.1	-22 < $M_R$ < -8.5	43
Schechter (1976)	Global(RC1) <sup>g</sup>	-1.24 ± 0.19	-23 < $M_B$ < -16	184
Zucca et al. (1997)	Global (ESP) <sup>h</sup>	-1.22; (-1.6)	-22 < $M_{b_i}$ < -12; (-17 ≤ $M_{b_i}$ )	3342
Norberg et al. (2002)	Global (2dFGRS) <sup>i</sup>	-1.21 ± 0.03	-22 < $M_{b_j}$ - 5 log $h^m$ < -16.5	110500 ( $z \approx 0.0$ )
Blanton et al. (2003)	Global (SDSS) <sup>j</sup>	-1.05 ± 0.01	-24.26 < $M_r$ - 5 log $h$ < -16.11	147986 ( $z \approx 0.1$ )
Roberts et al. (2004)	Global (MGS) <sup>k</sup>	-0.8 to -1.0	Based on DGR ≤ 6	110
Driver et al. (2005)	Global (MGS)	-1.13 ± 0.02	-21 < $M_B$ - 5 log $h$ < -14	10095
Trentham et al. (2005)	Global	-1.29; (-1.26)	-25 < $M_R$ < -9; (-19 < $M_R$ )	SDSS+LG(43)+Groups(228)

Tab. 4.5: Luminosity Functions

Data for a number of Virgo Cluster luminosity functions are listed in the top part of the table. Those for other regions are listed in the bottom parts for comparison. The parameter  $\alpha$  is the faint-end logarithmic slope of the Schechter luminosity function fitted to each galaxy distribution. DGR is the dwarf-to-giant ratio as defined by Roberts et al. (2004) in Table 4.1 (p.59).



## 5. PROJECT DATA AND ANALYSIS

Traditional photography has played an important role in large-scale surveys covering large fractions of the northern and southern skies, offering high-resolution imaging over large areas when combined with Schmidt telescopes with wide fields of view. The SuperCOSMOS Sky Surveys (SSS) are based on high-quality microdensitometer scans of photographic images obtained during the second half of the twentieth century (e.g. Hambly et al. (2001)) using a wide variety of wide-field telescopes, such as the 1.2-m Palomar Oschin Telescope, the 1.0-m Schmidt telescope of the ESO and the 1.2-m UKST.

To obtain deeper images, and to aid in analysis of those images, various techniques have been used. The high-sensitivity fine-grained film, Kodak Tech Pan, was introduced at the UKST in 1992 in place of traditional glass plates (Phillipps and Parker 1993). Comparisons of images made with an *OR*-band OG590 filter found that this panchromatic film, once suitably hypersensitised, produces images that not only have higher resolution and lower grain noise (refer Figure 5.1), but also reach one stellar magnitude fainter than equivalent IIIa-F glass plates (Parker and Malin 1999).

To increase the information gain from photographic images, photographic amplification techniques have been used, including superimposing multiple exposures to reduce grain noise and using unsharp masking to bring out low-contrast detail (Malin 1979). More recently, with the development of digital scanners, it has been possible to convert plates and films into a computer-readable format that allows the photographic exposures to be more readily analysed and digitally combined. Individual scans from COSMOS (an earlier version of the SuperCOSMOS facility) were used by Phillipps and Parker (1993) to quantify the magnitude gain of Tech Pan film over

standard IIIa-F plates described above.

The stacking of exposures may be used to increase signal to noise and push down the background to reveal much fainter detail than is visible in a single exposure. It has been shown that the magnitude gain from stacking  $N$  exposures of equivalent quality is given by  $2.5 \log \sqrt{N}$  magnitudes (Bland-Hawthorn et al. 1993).

Whilst it may be claimed that there is no substitute for using a linear detector, such as a CCD, to record properties of LSB galaxies (Impey et al. 1988), the photographic exposures from the UKST offer the advantage of covering large fields with high uniformity. Furthermore, the digital stacking of many exposures of the same field allows detection of features to very faint surface-brightness limits.

A total of 63 UKST Tech Pan films, all exposed on the same sky field through an OG590 red filter, were digitally scanned by SuperCOSMOS and stacked to produce a unique, ultra-deep  $R$ -band image covering 36 square degrees of the central portion of the Virgo Cluster. This is the Virgo Deep Stack. The faintest surface brightness reached in the image is approximately  $29 R\mu$ , at least 2 magnitudes deeper than a single Tech Pan film (Phillipps and Parker (1993) quote a limit of  $27 R\mu$  for a single film). The data have been optimised for faint magnitudes in the scanning and stacking processes. Comparisons show that images from the Virgo Deep Stack compare well with the best available CCD images (refer Section 6.2), reaching a similar limiting surface brightness. This depth and large area coverage make the Virgo Deep Stack ideal for the study of LSB galaxies. The focus of this project is on detection of previously unseen galaxies and measurement of faint galaxy extremities in sample regions of this image.

The following sections describe: technical aspects of the scanning and stacking processes; technical details of the Virgo Deep Stack; the subdivision of the large (2 Gb) image file into manageable subsets of data; the astrometry used to apply coordinates to these smaller sub-frames; the photometric calibration of the data; and subsequent analysis processes used to measure the properties of LSB galaxies in the image.

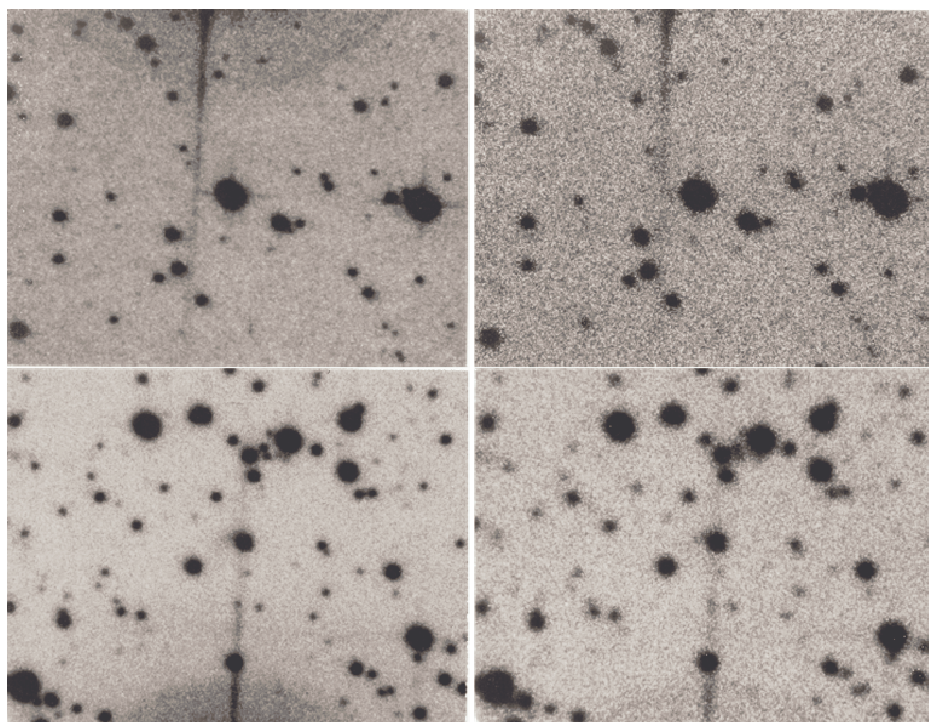


Fig. 5.1: Comparisons of Tech Pan and IIIa-F Exposures

*These images illustrate the higher resolution and lower grain noise of Tech Pan film (left) compared with IIIa-F plates (right). Each image measures  $2.2 \times 1.7$  arcminutes. North is at the top and east is to the left.*

Figure reproduced from Parker and Malin (1999).

## 5.1 Digital Scanning & Stacking

Photographic exposures<sup>a</sup> may be transformed into digital images by scanning with a microdensitometer. Three machines used for this purpose were the COSMOS measuring machine (MacGillivray and Stobie 1984) and the newer SuperCOSMOS machine (Knox et al. 1998), both at ROE, and the APM machine at Cambridge (Kibblewhite et al. 1984). All three machines have now been de-commissioned. The scanning process relies on transmission of light through the film. The derivation of relative intensity values from scanned images is described by Hambly (1998b) as follows.

---

<sup>a</sup> Exposures may be films or plates - in this discussion, the term ‘film’ is used generically.

The relationship between transmission  $T$  of the film and density  $D$  of grains on the emulsion is non-linear, and is given by:

$$D = \log(T_C/T) \quad (5.1)$$

where  $T_C$  is transmission measured through clear air. Intensity  $I$ , used in measuring magnitudes, is related to density by:

$$D = \gamma \log I \quad (5.2)$$

where  $\gamma$  is the contrast, or density difference produced by a specific exposure difference, and represents the slope of the characteristic curve (refer Figure 5.2) of the film. A typical survey-grade Schmidt film has  $\gamma \sim 2.5$ .

The non-linear portions at the extremities of the relation between  $T$  and  $I$  are caused by saturation effects at high intensity, reciprocity failure at low intensity (both of these occurring in the film) and scattered light and diffraction in the imaging system during scanning. In the case of SuperCOSMOS, calibration is of the form:

$$\log I \propto \gamma^{-1} \log(1/T) \quad (5.3)$$

with  $\gamma^{-1} = 0.3$  being suitable for fine-grained emulsion on a survey film.

The data files obtained by scanning result in images of similar format to CCD images, i.e. image areas, or pixels, correspond to the aperture of the scanning instrument and pixel values may represent intensity, transmission or photographic density. Hence, analysis may be performed using computer software designed to work with these digital data files.<sup>b</sup>

Data that have been produced by scanning may be digitally added (stacked) to increase the signal-to-noise (S/N) level. Parker and Phillipps (1999) and Schwartzberg (1996) stacked six exposures in each case for surveys of dSph galaxies in the Virgo cluster. Thirteen films were co-added for the Katsiyannis et al. (1998) deep-imaging study of selected galaxies in the Virgo Cluster. The Virgo Deep Stack is

---

<sup>b</sup> Software originally designed to analyse microdensitometer data from wide-field photographic scans is now commonly utilised for CCD data analysis.



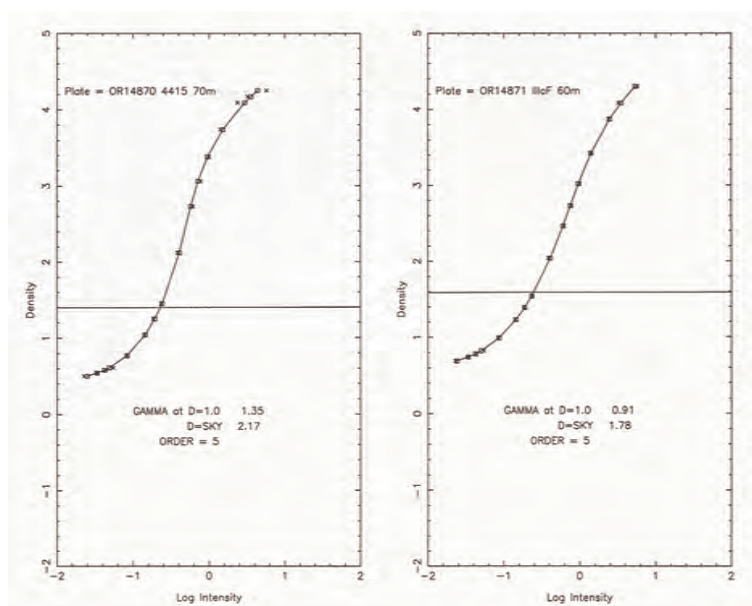


Fig. 5.2: Characteristic Curves of Tech Pan and IIIa-F Exposures

*Characteristic curves of Tech Pan film (left) and IIIa-F plates (right) from UKST exposures. The horizontal lines represent sky background levels.*

Figure reproduced from Parker and Malin (1999).

an ultra-deep stack of 63 films<sup>c</sup>, scanned by SuperCOSMOS, which reaches fainter *R*-band magnitudes than have been possible before photographically. Whilst CCD imaging may go deeper (fainter) with long exposures, few surveys to date have matched the depth of the Virgo Deep Stack (refer Table 3.2, p.36) and, typically, CCD imaging systems have small fields of view. The advantage with this stack over the deepest available CCD data is the full 6-degree-square field available, with an unvignetted radius of 2.7 degrees.

Bland-Hawthorn et al. (1993) calculated the magnitude gain from stacking equivalent photographic data to be  $2.5 \log \sqrt{N}$  where  $N$  is the number of films added together. The magnitude gain from stacking six films is almost one magnitude, and the gain with 63 films is  $\sim 2.25$  magnitudes. The stacking process, described

<sup>c</sup> These films were originally taken as part of a program to search for MACHOs (Tadros et al. 1998).

in detail by Schwartzberg et al. (1996), involves sky subtraction and scaling and alignment of the separate images. Knox et al. (1998) described the effects of various image-combining algorithms on stacks of 4, 8 and 16 IIIa-J UKST plates and assessed the extent to which artefacts, such as satellite trails and dust appearing on single frames, can be removed during stacking. It was found that there is a reduction in S/N in faint images with the use of any pixel-rejection algorithm but that weighting individual films according to their S/N characteristics and using an ‘average sigma clipping’ bad-pixel algorithm optimises both depth and the removal of spurious images.

The SuperCOSMOS scanning and stacking of the films and the preliminary processing of the image for this project were all performed at ROE and the resulting data were supplied in electronic format (a complete file listing appears in Appendix D). A very brief description of the processing is provided here, but references may be consulted for further details.

Each separate film was scanned in lanes as described by Hambly (1998a). Scanning covers  $28 \text{ lanes} \times 1152 \text{ pixels} = 322.56 \text{ mm}$ , or 6 degrees at the plate scale of  $67.14 \text{ arcsec mm}^{-1}$  (corresponding to the 1.2-m Schmidt Telescope plate scale). The final pixel scale of a scanned image is  $0.6714 \text{ arcsec}$  (10 microns) per pixel and the entire image measures  $32256 \times 32256 \text{ pixels}$ . After scanning, the images were digitally stacked after methods described by Knox et al. (1998). With average sigma clipping, statistics are calculated for whole scan-lengths so that clipping may be used to reject bad values. The weighted mean value for each pixel is then calculated from the non-rejected values (N. Hambly, private communication, 2008).

Processing of the stacked image included the same data analysis and object detection methods as those used for the SuperCOSMOS Sky Survey (Hambly et al. 2001). The object detection algorithm used in ‘image analysis mode’ (IAM) is a connected-pixel type that detects data above a specified threshold, fixed as a certain percentage cut (usually  $\sim 7\%$ ) above the estimated local sky background. The algorithm deblends large or extended objects, including some galaxy images and haloes and diffraction spikes around bright stars, into ‘parent’ and ‘child’ objects.

For each parent and child object detected, 32 image parameters are written to the `iam.srtrd` file. These include object position, extent, orientation, ellipticity, magnitude and surface brightness measurements, classification as parent or child, and a quality flag. A complete listing of data outputs and units is supplied by Hambly (1998a). Standard deblending parameters for measuring star and galaxy properties cause spurious deblending of LSB features into multiple objects, as illustrated by Sabatini et al. (2003) (refer Figure 4.3 p.61), and a total of 1210712 objects were detected in the Virgo Deep Stack. Unfortunately, this standard IAM type of image detection is of little use in discerning the LSB galaxies of interest to this project. Instead, mapping mode (`mm`) pixel data were used directly. However, the IAM data may have applications in other studies that could be based on the Virgo Deep Stack. Some details of the files supplied by ROE are provided in Appendix D.

## 5.2 The Virgo Deep Stack

The Virgo Deep Stack is a square image that measures six degrees on a side and is centred near M87, encompassing a large portion of sub-cluster A and parts of the N and E clouds of the Virgo Cluster (refer Figure 3.6, p.43). Positional statistics of the imaged field are provided in Table 5.1.

R.A. range (J2000)	$12^h 17^m 10^s$ to $12^h 41^m 50^s$
Dec. range (J2000)	$+10^\circ 09' 43''.5$ to $+16^\circ 09' 43''.5$
Image centre (J2000)	$12^h 29^m 31^s.81$ $+13^\circ 13' 25''.5$
Image centre (B1950)	$12^h 27^m 00^s$ $+13^\circ 30' 00''$

Tab. 5.1: Positional Statistics of the Virgo Deep Stack

The 63 A-grade Tech Pan films were exposed between January and June in 1999, 2000 and 2001, as dictated by the visibility season for Virgo from the UKST. Exposure times were mostly 60.0 minutes, though 13 were a little shorter, probably due to interference by cloud (refer Table 5.2). The filter used was a Schott glass OG590 *R*-band filter, which transmits longward of 590 nm (UKSTU (1983)). The Tech Pan

emulsion has a cut-off at 699 nm (Parker and Malin 1999). Together, these result in a passband with transmission between 590 and 699 nm (refer Figure 5.3), which is referred to as *OR*-band to distinguish it from the standard Cousins *R*-band and the UKST *SR*-band.<sup>d</sup>

Plate No.	Date Exposed	LST	Exp. time (mins)	Grade	–	Plate No.	Date Exposed	LST	Exp. time (mins)	Grade
OR18261	990213	1216	60.0	a		OR18755	000210	1203	60.0	a
OR18267	990214	1210	60.0	a		OR18757	000216	1244	60.0	a
OR18272	990215	1153	51.1	a		OR18776	000302	1135	60.0	a
OR18279	990216	1215	60.0	a		OR18781	000313	1254	60.0	a
OR18293	990221	1127	55.2	a		OR18794	000329	1145	60.0	a
OR18298	990224	1059	26.6	aUX		OR18797	000330	1151	60.0	a
OR18314	990311	1017	60.0	a		OR18804	000403	1140	55.0	aD
OR18322	990312	1123	60.0	a		OR18822	000428	1216	55.0	a
OR18327	990314	1201	60.0	a		OR18825	000429	1216	60.0	a
OR18331	990315	1108	60.0	a		OR18828	000430	1326	60.0	a
OR18337	990320	1200	60.0	a		OR18850	000522	1100	60.0	aT
OR18348	990326	1457	60.0	aT		OR18856	000604	1115	60.0	aD
OR18362	990412	1218	60.0	a		OR18865	000622	1239	60.0	aD
OR18367	990414	1215	60.0	a		OR18870	000625	1251	50.0	a
OR18369	990415	1220	60.0	a		OR19090	010122	1058	60.0	a
OR18375	990416	1206	60.0	aE		OR19094	010123	1057	60.0	a
OR18377	990418	1203	60.0	aE		OR19101	010125	1100	60.0	a
OR18384	990419	1227	60.0	a		OR19116	010222	1155	50.0	a
OR18390	990420	1138	60.0	a		OR19120	010223	1148	60.0	a
OR18398	990422	1306	60.0	aI		OR19125	010228	1142	60.0	a
OR18414	990505	1027	60.0	a		OR19145	010326	1118	60.0	a
OR18416	990506	1123	36.2	a		OR19153	010331	1241	60.0	aID
OR18418	990507	1126	60.0	a		OR19167	010417	1203	60.0	aD
OR18427	990514	1254	60.0	a		OR19170	010418	1232	60.0	aD
OR18431	990517	1159	60.0	a		OR19172	010419	1238	60.0	a
OR18433	990518	1130	60.0	aE		OR19174	010422	1206	60.0	aD
OR18436	990519	1220	45.0	a		OR19175	010424	1235	60.0	aD
OR18440	990607	1122	60.0	aD		OR19181	010514	1128	60.0	aD
OR18735	000204	1202	60.0	aI		OR19186	010515	1144	45.0	a
OR18739	000205	1235	32.0	aU		OR19187	010516	1143	45.0	aE
OR18743	000207	1220	60.0	a		OR19195	010524	1042	45.0	a
OR18751	000209	1220	60.0	a		OR19196	010524	1149	45.0	a

Tab. 5.2: Base Images for the Virgo Deep Stack

*The table provides details of all the individual films that were scanned and stacked to form the Virgo Deep Stack. This list may be queried from the UKST Plate Catalogue (<http://www.roe.ac.uk/ifa/wfau/ukstu/>) by selecting all images with the unique project identifier (T number) 1129. Only the A-grade images were used.*

Because the SuperCOSMOS scanning system rejects off-axis scattered light, the effective range in optical density is considerably less than in the original films (Miller 1995). The range in data counts was optimised for the faint end of the magnitude

<sup>d</sup> SR, or ‘short red’, is a narrower passband transmitted by an RG630 filter.

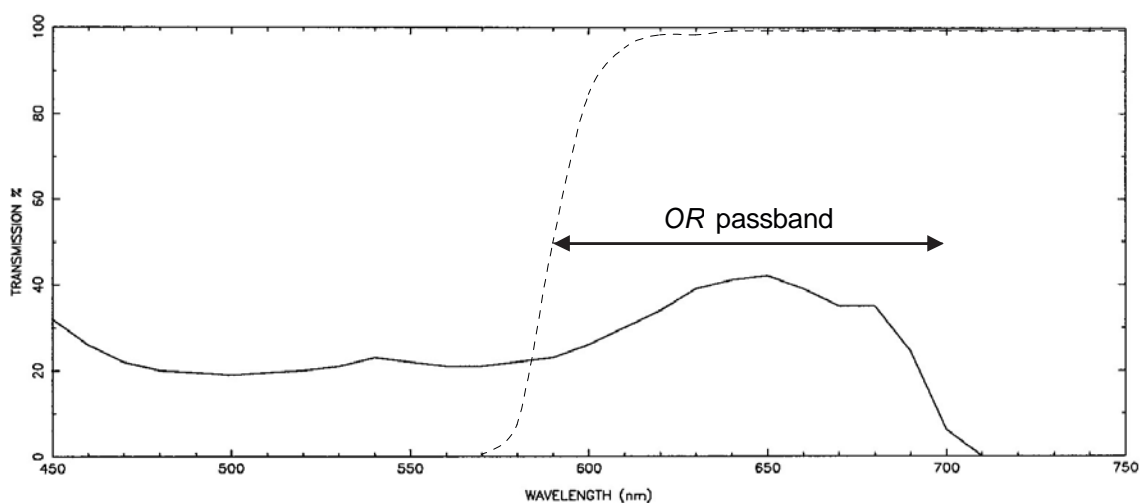


Fig. 5.3: Passband of the OG590-Tech Pan Combination

*The response curve of Tech Pan emulsion (solid) and the OG590 Schott filter transmission curve (dotted) combine to produce the 590 nm to 699 nm ‘OR’ passband (arrowed) of the Virgo Deep Stack.*

Tech Pan transmission curve reproduced from Parker and Malin (1999).

OG590 transmission data from <http://www.optical-filters.com/og590.html>.

distribution in the scanning process, so bright stars and galaxy cores are affected by saturation. Each pixel typically has data counts between  $\sim 6000$ , at the level of the sky background, and  $\sim 32000$  in saturated star or galaxy cores.

Despite the expectation that single-film artefacts would be naturally removed from the Virgo Deep Stack in the stacking process, some minor image defects do remain. Occasional dust haloes, possible reflection artefacts and some residuals of bright satellite trails are visible (refer Figures 5.4, 6.9 p.139 and 6.16 p.148). The dust haloes may have occurred at the same location on several films but satellite trails would only have appeared on a single film of the stack, so residuals of these are rare, patchy and difficult to discern.

There is also a large, very low-contrast set of concentric rings and radial features caused by the system used to hold the film in place during exposure. Photographic glass plates were clamped by their edges to a mandrel that matched the curved focal

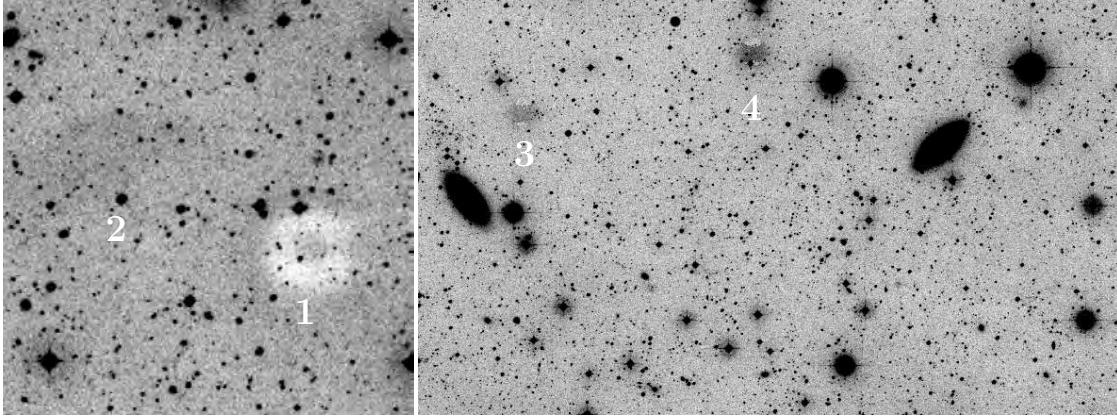


Fig. 5.4: Artefacts in the Virgo Deep Stack

*Left: In this standard UKST negative image a dust halo (1) appears as a bright C-shaped feature below and to the right of a very diffuse LSB galaxy (2) at image left. Image size is approximately 9 arcmin on a side.*

*Right: Two ‘bubble’-shaped LSB artefacts (each dark in the middle and light at top and bottom) appear near the top of this image (3 and 4). They are probably due to internal reflections in the telescope optics. Image size is approximately 38 arcmin wide by 22 arcmin high.*

surface of the UKST. This method could not be used to secure flexible photographic film. Instead, a light vacuum was applied through shallow channels cut into the mandrel. Positions of these channels are discernible when the Virgo Deep Stack is displayed at very high contrast. There is a large  $\times$ -shaped pattern that runs across the diagonals of the image (refer Figure 5.5) and, harder to see, are two concentric rings (one is partly visible in Figure 6.14, p.145). Also, at this contrast level, the circular vignetting pattern, due to the mode of light transmission through the Schmidt telescope, is obvious.

However, localised artefacts have a negligible effect on the evaluation of properties of LSB galaxies. Artefact problems and deblending issues are further described by Hambly et al. (2001).



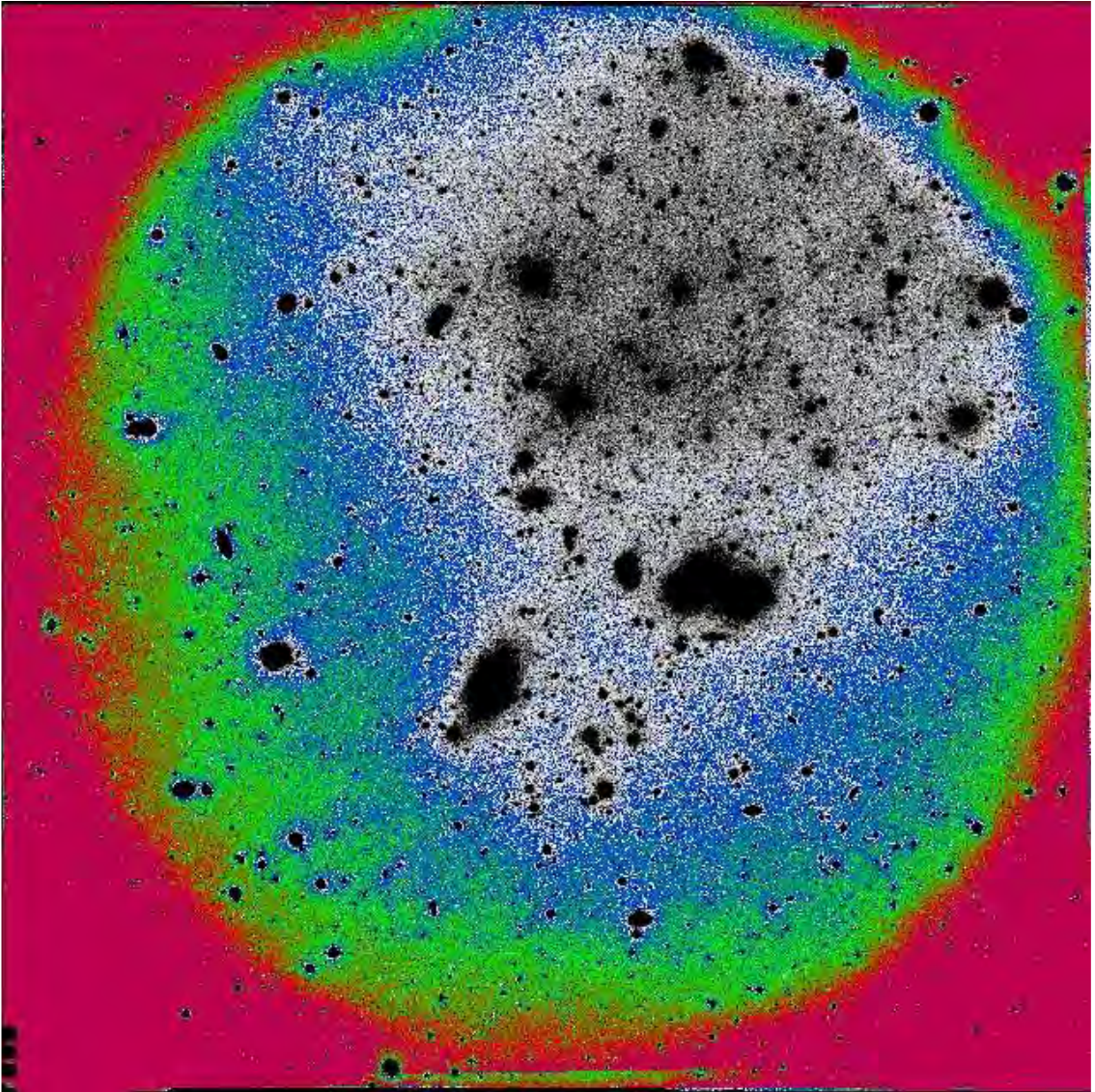


Fig. 5.5: The Virgo Deep Stack at High Contrast in False Colour

*Displayed at high contrast, the extent of massive galaxy haloes is revealed. Also evident is the vignetting that particularly affects the outer boundary of the image. A barely-discernable  $\times$ -shaped feature across the diagonals of the image is due to channels in the mandrel through which a light vacuum was applied to hold the photographic films to the focal surface during the exposures. Shading between the galaxies may be due to intra-cluster light, but this is very difficult to measure. Note that this is the same image as shown in Figure 1.1, but viewed with different display parameters.*

### 5.3 Astrometric Calibration

The SuperCOSMOS Virgo Deep Stack `FITS`<sup>e</sup> file is 2 Gb in size (with  $32256 \times 32256$  pixels) but, unlike most SuperCOSMOS products, this is a specially-stacked ‘one-off’ data set with no RA and Dec coordinates in the `FITS` header. Thus, when viewing the raw image, only pixel position data are displayed and no World Coordinate System (WCS) on-sky position coordinates are available. Preliminary processing of the image included subdivision into smaller files and the necessary and careful application of a WCS as described below.

The `FITS` file is too large to be readily displayed or studied in any available image processing software. The inner 5-degree square of the image, excluding the outermost 0.5-degree border where the vignetting is worst, has been subdivided into 36 sub-frames using `imcopy` in `IRAF`<sup>f</sup>. For the whole image and each sub-frame, north is at the top and east is to the left. Each sub-frame is approximately 50 arcminutes square. The sub-frames are numbered from left to right (i.e. decreasing in right ascension) in rows from bottom to top (i.e. ascending in declination). WCS coordinates were applied to each sub-frame using 30-arcmin-square reference images from the SuperCOSMOS Sky Survey<sup>g</sup> (images obtained using source survey ‘POSSII Red’) and fitting  $\sim 8$  stars for each sub-frame with `Karma Koords`<sup>h</sup>. After applying WCS to these sub-frames, photometric integrity was checked by comparing coordinates at the corresponding corners of adjacent sub-frames. The mean error for 6 matched locations was found to be 0.7 arcseconds. Furthermore, stars listed in the Sloan Digital Sky Survey (SDSS)<sup>i</sup> were readily located to within one pixel.

---

<sup>e</sup> Flexible Image Transport System image file format.

<sup>f</sup> `IRAF` is distributed by the National Optical Astronomy Observatories, which is operated by the Association of Universities for Research in Astronomy, Inc. (AURA) under cooperative agreement with the National Science Foundation.

<sup>g</sup> SSS data available at: <http://www-wfau.roe.ac.uk/ss/pixel.html>

<sup>h</sup> `Karma` is a software toolkit written by Richard Gooch (1996) and available online at: <http://www.atnf.csiro.au/computing/software/karma/>

<sup>i</sup> Funding for the Sloan Digital Sky Survey (SDSS) has been provided by the Alfred P. Sloan



Due to time constraints for this project, just five of the 36 sub-frames were selected for detailed study. One of the five is sub-frame 22, which contains a large, unidentified LSB feature (Bryn’s Mystery Object, refer Figure 5.6).

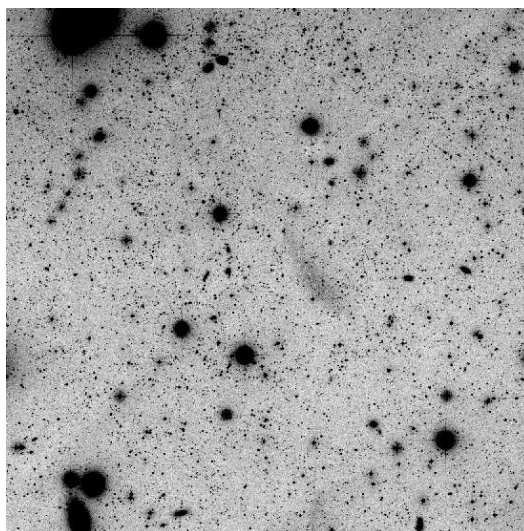


Fig. 5.6: Sub-Frame 22

*Pictured is sub-frame 22, one of four central sub-frames from the Virgo Deep Stack. Each sub-frame measures 50 arcmin on a side. North is at the top and east is to the left. The large galaxy at upper left (overlapped by a bright star) is NGC 4459. The group of three objects at lower left includes a star and the galaxies NGC 4458 and NGC 4461. The elongated diffuse patch just to the right of the image centre is a newly-discovered but, as yet, unidentified object (refer Section 6.3) first noticed by Bryn Jones (private communication, 2005) and, hence, dubbed ‘Bryn’s Mystery Object’.*

These sub-frames sample regions at varying proximity to the Virgo Cluster core. They overlap parts of the areas examined by Young and Currie (1998), Trentham and Hodgkin (2002), Phillipps et al. (1998) and Trentham and Tully (2002) but

---

Foundation, the Participating Institutions, NASA, the National Science Foundation, the U.S. Department of Energy, the Japanese Monbukagakusho, and the Max Planck Society. The SDSS Web site is at <http://www.sdss.org/>.

also include some regions that have not previously been covered by deep surveys. Sub-frame coordinates for the five regions are listed in Table 5.3 and the regions are shown in Figure 1.1 and Maps 3, 4 and 5 (Figures 5.7, 6.2 and 8.1 respectively).

Number	R.A. range (hh mm ss.ss)	Dec. range (dd mm ss.s)
16	12 26 06.79 to 12 29 31.78	12 19 29.2 to 13 09 41.4
22	12 26 06.06 to 12 29 31.63	13 09 34.8 to 13 59 48.0
23	12 22 40.26 to 12 26 05.25	13 09 18.7 to 13 59 40.4
24	12 19 14.58 to 12 22 38.80	13 08 51.5 to 13 59 23.9
28	12 26 05.23 to 12 29 31.51	13 59 40.6 to 14 49 54.2

Tab. 5.3: Sub-Frame Coordinates

*Sub-frames studied in detail and approximate coordinates of SW (bottom right) and NE (top left) extremities of each sub-frame. All declinations are positive. The sub-frames abut perfectly but do not overlap. Apparent mismatches in edge coordinates are due to the representation of portions of the (curved) celestial sphere with 50-arcminute square planar images.*

## 5.4 Photometric Calibration

Accurate photometric calibration of digitally scanned images is necessary so that uniform and reliable integrated stellar magnitudes, or in the case of galaxies, surface brightness per square arcsecond, may be calculated. Calibration may be performed using one of two methods. One method involves separate observations of standard stars using CCD imaging in the same (or similar) passband as the original image and comparing the CCD magnitudes with intensities of the same stars in the scanned photographic image. The other method involves making comparisons between magnitudes of stars in the digital image with magnitudes of the same stars from a reliable database, and applying any necessary colour corrections. The latter method was used for calibrating the Virgo Deep Stack.



Fig. 5.7: Map 3: Dwarf LSB Studies and Sub-Frames of the Virgo Deep Stack

*Sabatini et al. (2005)* surveyed an extended area of the INT Wide Field Survey E-W strip (coded SDV2005 on NED). Previously uncatalogued galaxies discovered in that survey are shown as grey data points. The two green boxes are the regions used by Phillipps et al. (1998) to compare inner and outer cluster environments. The heavy orange boxes (numbered 16, 22, 23, 24 and 28) are sub-frames from the Virgo Deep Stack examined for this project. All these data have been used to study dwarf LSB galaxies that contribute to the faint end of the luminosity distribution. VCC galaxies, the Virgo Deep Stack boundary (heavy black box) and the INT Wide Field Survey N-S strip (vertical rectangle) are shown for reference.

Photometric data for 21 stars in the range  $18.2 \leq R_C \leq 20.1$  (to avoid saturation but still obtain reasonable photometry) were obtained from the SDSS Data Release 4 (DR4). Transformations were applied according to those of Lupton (2005), quoted on the SDSS DR4 web page.  $R$ - and  $I$ -band magnitudes in the Cousins photoelectric system were derived from the SDSS  $r$ - and  $i$ -band data using the following equations:

$$R_C = r - 0.2936(r - i) - 0.1439 \quad (5.4)$$

$$I_C = r - 0.2936(r - i) - 0.1439 \quad (5.5)$$

The need for both  $R_C$  and  $I_C$  magnitudes is due to the small difference between the  $R_C$  passband and that of the  $OR$  passband used for the UKST observations. This transformation is quoted by Morgan and Parker (2005) as

$$OR - OR' = (-0.043 \pm 0.030) \times (R - I) \quad (5.6)$$

in the range  $-0.1 < (R - I) < +1.6$ , where “unprimed values are standard photoelectric magnitudes [and] primed values are calibrated instrumental magnitudes”. This is interpreted as meaning that the correction relates the authors’ instrumental magnitudes  $OR'$  to Cousins  $R$  rather than to a ‘standard’  $OR$  (which does not exist in the Cousins system). Final magnitudes ( $OR'$  from the above equation) for the selected stars were calculated using Equations 5.4, 5.5 and the modified version of 5.6. Note that the uncertainty in Equation 5.6 is large and in this analysis, when measurements from the image were compared with values thus calculated, a very different factor was derived from the least-squares fitting function. That result will be discussed shortly.

Instrumental magnitudes were measured from the Virgo Deep Stack using the aperture photometry tool in the Graphical Astronomy and Image Analysis software, GAIA<sup>j</sup>. The method uses concentric circular regions with the object of interest lying entirely within the innermost circle (the ‘aperture’), and the outer annulus covering sky only.

---

<sup>j</sup> GAIA is part of the Starlink Software Collection.

From measurements of data counts in each pixel of the aperture  $C_i$ , the number of pixels in the aperture  $n$  and the average sky background count in the annulus  $C_{sky}$  the total data value in the aperture  $C_{object}$  is derived from:

$$C_{object} = \sum_{i=1}^n C_i - nC_{sky}. \quad (5.7)$$

In theory, stellar magnitudes  $m_{object}$  in the scanned image may be determined using the following formula:

$$m_{object} = Z_{image} - 2.5 \log(C_{object}). \quad (5.8)$$

In this case,  $Z_{image}$ , which is the zero-point correction or so-called ‘plate constant’ for the scanned image, is unknown. Its value is found by plotting magnitudes from the reference data against measurements of  $2.5 \log(C_{object})$  from the aperture photometry of stars in the scanned image. The plate constant is then the  $y$ -intercept of a linear least-squares fit to the data.

In analysing the 21 selected stars, two were eliminated because they were outliers to the fit, possibly due to them being variable. Three were outside the  $R_C - I_C$  magnitude range of Morgan and Parker (2005) but, of these three, one was already removed as an outlier and one was only marginally fainter ( $R_C - I_C = 1.65$ ) and was retained. This left 18 stars for the fit. Fitting was performed in *Microsoft® Office Excel 2003* (hereafter referred to as *Excel*) using a trendline to the plot of measured data versus  $OR'$ . Initially the fit was poor in the sense that the slope was less than unity. This could be due to small-number sampling statistics or the  $OR$  colour term. Ideally, several hundred stars should be sampled rather than just this number, but time constraints prevented this during conduct of the project. This could be followed up at a later time. Removing the colour transformation (i.e. presuming  $OR = R_C$ ) also left an unsatisfactory result. Therefore the multiplier of Equation 5.6 was adjusted to obtain a one-to-one slope of magnitudes and the plate constant  $Z_{image}$  is the resulting  $y$ -intercept. The final empirical transformation used was:

$$OR' = R_C - 0.0565 \times (R_C - I_C). \quad (5.9)$$

Not only is the multiplier different-valued, but it has the *opposite sign* to that given by Morgan and Parker (2005). As suggested, this transformation could be further investigated by studying a larger sample of stars taken from different regions of the image.

The result from this data set, showing a reasonably tight linear relation over  $\sim 1.5$  magnitudes, is presented in Figure 5.8. Raw data are included in Appendix E. Uncertainty is based on the standard deviation of the data from the fit. The final calibration constant is:

$$Z_{image} = 31.5 \pm 0.1 \quad (5.10)$$

The result will be used later in comparisons of profiles from the Virgo Deep Stack with published  $R$ -band radial profiles but it agrees, within uncertainty, with the value derived independently by Bryn Jones (private communication, 2006) using 20 stars and the same method, but from a different region of the image. That result, quoted in Moore and Parker (2006) (refer Section 7.2), was  $31.54 \pm 0.02$ . The plate constant shown at Equation 5.10 has been applied to all subsequent measurements of image data for this project.

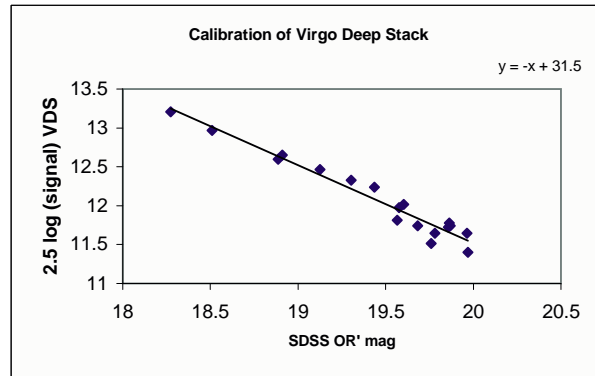


Fig. 5.8: Calibration of the Virgo Deep Stack

*The fitting function to obtain the plate constant  $Z = 31.5 \pm 0.1$  shows a reasonable linear fit to  $\sim 19.5$  on the SDSS axis. The scatter increases at fainter magnitudes.*

## 5.5 Object Detection

Unlike the automated detection methods of Phillipps et al. (1998), or Sabatini et al. (2003), the LSB galaxies discovered in this project were found by visual inspection of sub-frames of the image displayed on a computer monitor. Although this is a slow and partly subjective process, it allows for detection of objects that may otherwise be missed because of proximity to bright galaxy haloes or diffraction rings and spikes from stars. It also allows for the contrast to be varied by setting the high- and low-value pixel counts in the display.

WCS-calibrated sub-frames 16, 22, 23, 24 and 28 were carefully examined using suitable display parameters in the DS9<sup>k</sup> and/or GAIA image display packages. Each detection was compared with the NED database to ascertain whether or not it had been previously catalogued. Over 100 previously uncatalogued galaxies have been identified in these five sub-frames. For each of these detections a smaller image was cut from the sub-frame for the purpose of applying surface photometry. Images of all the newly-identified galaxies are included in Chapter 8.

## 5.6 Surface Photometry

Surface photometry software traces elliptical isophotes on a galaxy image and evaluates the mean intensity of the data associated with each ellipse to obtain a radial intensity profile of the galaxy. This may also be derived as, or converted to, a magnitude profile as shown in Figure 2.2 (p.13).

### 5.6.1 Overview of Photometry Techniques

Impey et al. (1988) explain that surface photometry of LSB galaxies is sometimes difficult due to low S/N and the clumpiness often seen in galaxies of this type. There are often changes to eccentricity and position angle of successive ellipses due

---

<sup>k</sup> SAOImage DS9 was developed by Smithsonian Astrophysical Observatory and is available from <http://hea-www.harvard.edu/RD/ds9/>.

to the chaotic structure of some LSB galaxies. Masking may overcome problems of foreground stars and background galaxies, but genuinely clumpy galaxies will have poor exponential fits to their profiles.

Various parameter sets have been used to characterise galaxy profiles. Integrated magnitudes measured over successively larger ellipses to obtain growth curves allow derivation of effective surface brightness and effective radius where the growth curve reaches half its asymptotic value (Barazza et al. 2003). However, the total magnitude at or within an outer radius or isophote of an LSB galaxy has a large uncertainty due to sensitivity of the measurement to the correct setting of the sky level and the dynamic range of the detector.

One method of utilising the high S/N central data, described by Trentham and Hodgkin (2002), is to use an exponential profile fitted to data within a radius of 12 arcseconds. The equation of this limited profile, from which scale length  $a$  and central intensity  $I_0$  are derived as fitting parameters, is:

$$B(r) = -2.5 \log \int_0^r I_0 \exp(-r/a) 2\pi r dr. \quad (5.11)$$

Total apparent magnitude is then  $B_T = B(\infty)$ . The disadvantage with this method is that derivation of the fitting parameters is based on the profile of the inner 12 arcseconds which, in some cases, may not agree well with the fit at larger radii.

Measurement of extrapolated central surface brightness  $\mu_0$  and scale length  $a$  based on a fit to the entire profile utilises all the available information including the data in the high S/N parts of the image. The  $\mu_0$  and  $a$  terms are considered to be more reliable than effective surface brightness and effective radius where the exponential fit is a good match to the profile (Impey et al. 1988). Total magnitude, calculated from Equation 4.6 (p.74) is integrated to infinity so as to include outer galaxy data below the background threshold.

Uneven backgrounds may adversely affect any measurements of magnitude from radial profiles. Two problem cases are described by Trentham and Tully (2002). One case is where a small galaxy lies in the halo of a very luminous galaxy. In such a case, the Trentham and Tully (2002) method is to make an estimate of



the underlying sky from a profile of the luminous galaxy. The other case is where a galaxy has a very close companion. For these, measurement of the half of the galaxy opposite the companion may be extrapolated to derive total flux.

### 5.6.2 The IRAF ELLIPSE task

For this project, surface photometry of whole galaxies was obtained, based on the Impey et al. (1988) recommendation. Extrapolated central surface brightness  $\mu_0$  and scale length  $a$  were used to derive apparent magnitudes using Equation 4.6, described previously and again listed in Section 5.7. The surface photometry software used was the ELLIPSE task in the IRAF STSDAS.ANALYSIS.ISOPHOTE package. This software was used by Gavazzi et al. (2005b) in an analysis of elliptical galaxies in the Virgo Cluster. The details of how the process works is described in detail by Jedrzejewski (1987).

The task operates by first inscribing an ellipse around the centre of a galaxy and finding a mean intensity (data count per pixel) associated with that ellipse. It then steps outwards delineating isophotal ellipses of increasing semi-major axis until it reaches a user-specified limit or finds that the mean count is no longer decreasing. It then resumes from the first ellipse, working its way inwards. The software may be left to freely trace the isophotes, adjusting itself according to results of iterations around previous values, or the parameters for the task may be set by the user. For a complete description, the reader is referred to the IRAF help files for the task, but a brief description of operation and some of the parameters utilised for this project follows.

In interactive mode, the task works in conjunction with a display panel, so a display window in DS9 is opened before commencing. At the command line, the parameter input list is opened by typing `epar ellipse`. Some parameters are entered directly. The minimum requirement is for the user to specify the input file (`filename.fits`), and the name of the output table (`filename.tab`). The user may also make specifications in four parameter subsets - `geompar`, `controlpar`, `samplepar` and `magpar` (refer Section 5.6.3). Each parameter set may be opened by moving the cursor to

the appropriate entry and typing `:e`. Typing `:q` exits each subset and typing `:q` again exits parameter editing.

An initial first run, without holding any geometric parameters fixed, allows the task to freely follow the isophotes, giving the user an idea of the shape and extent of the galaxy. In interactive mode, once instigated, the software displays the image. In the display window, masking of bright foreground stars or bright background objects may be applied by clicking the mouse on the image and typing `m`. Masked pixels are excluded from the measurements. Mask size may be set as a parameter and the final mask is automatically saved (as a `.fits.pl` file) for subsequent runs on the same galaxy. If the automatic object locator fails (as is often the case with LSB galaxies or in crowded fields containing numerous bright objects) or if the object centre has not been specified, the software awaits user input to approximately locate the object's centre. This involves clicking the mouse at the desired location on the image and typing `x`, then `f`, whilst the cursor is still in the display window. Each ellipse is fitted by typing `n` (next), eventually producing ellipses fully overlying the galaxy in the display window (refer Figure 5.9).

If not held fixed, the initial centroid is automatically updated according to the asymmetry of each isophote measured and the first free run will accurately locate the pixel coordinates of the galaxy's brightest concentration. These  $x, y$  coordinates are then used as inputs in the next run to ensure that radii from a specified point are used to obtain a meaningful radial profile. In the second run, with the centre held fixed, suitable ellipticity and position angle are noted based on the appearance of the ellipses against the display of the galaxy. This choice is subjective, but values used on galaxies profiled for this project are recorded in Chapter 8 for reference. These values are also held fixed for the third and final run used to produce the profile.

In cases where the surface photometry fails altogether, due to very low surface brightness and/or the presence of unrelated bright sources, ellipse parameters may be estimated by eye and held fixed for the entire photometry routine. Two runs may be needed. The first is to verify that the estimated parameters are suitable and

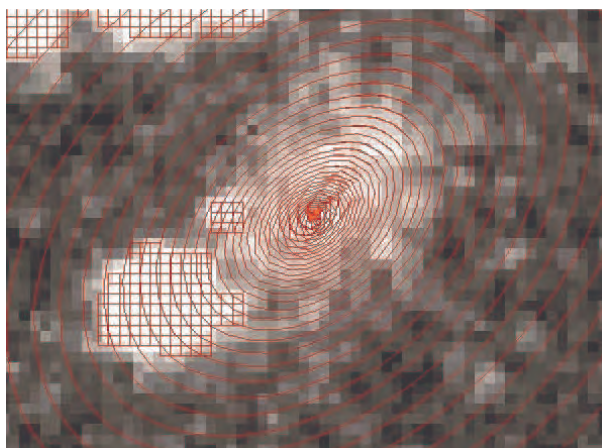


Fig. 5.9: Isophotes and Masked Pixels in the IRAF ELLIPSE Display

*When running the ELLIPSE task in interactive mode the red ellipses overlie the base galaxy image. This is the same galaxy as is shown in Figure 2.2 (p.13). Masking of contaminant objects has been applied in the meshed regions.*

allows masking to be performed. The second is the final run to obtain and save the measurements.

### 5.6.3 ELLIPSE Parameter Subsets

This section outlines the main components of the ELLIPSE parameter subsets and details those that were set to specific values for this project.

In `geompar`, fixed values may be entered for the galaxy centre, `x0` and `y0`, initial ellipticity `e0` (must be non-zero) and position angle `pa0` (in the range  $-90 < pa \leq 90$ ). These values are derived from earlier runs, as described above, with ellipticity and position angle being judged visually from the outer isophotes and the brightest centroid being automatically located by the software. Other parameters available are the minimum and maximum semi-major axes and size of the initial semi-major axis. It is useful to choose an initial semi-major axis about halfway between the centre and the visible edge of the galaxy, so settings for these parameters depend on the specifics of the individual image. For most dwarf galaxies the initial semi-major

axis was set to 10 pixels and the minimum was always zero. The maximum was set to a value larger than the likely limit of the galaxy and the profile was suitably truncated at the plotting stage (refer Sections 5.6.4 and 5.8).

The **linear** option, if set to **yes**, will space the isophotes at equal intervals. For this project **linear** was set to **no**, so that a geometric growing mode was applied in which the semi-major axis length was increased by the factor  $1 + \text{step}$  as the ellipses grew outwards (or similarly decreased on the inward run). The step size chosen was the default 0.1, but this may be specified by the user. If a semi-major axis length is set for the parameter **maxrit** then, from that ellipse outwards, the same centre, ellipticity and position angle are used. This was left as **INDEF**, or ‘undefined’.

If set to **yes**, the **recenter** parameter allows the software to update the centre after successful object detection, and **xylearn** updates the centre with each isophote. Both these parameters must be set to **no** to keep the centre fixed at (**x0**, **y0**) for the final run.

The parameter subset **controlpar** allows the user to set algorithm-control parameters, such as the maximum number of iterations, before accepting each isophotal ellipse. Iterations will cease when either convergence cannot be reached, **maxit** iterations are reached or too many data points have no valid data in them. Convergency criteria and numbers of iterations were left with their default values. To hold the geometric parameters fixed at their initial values throughout the fitting sequence (specified, as above, in the **geompar** parameter set), the **controlpar** parameters **hcenter**, **hellip** and **hpa** were set to **yes** for the final run. Other parameters in this set were left with their default values, though adjustment of **maxgerr**, which allows for a dip or a spike in the magnitude gradient, may be useful in the outer regions of LSB galaxies where the profile may fluctuate.

The parameters in **samplepar** control the way sampling is performed at each iteration of the isophote-fitting algorithm. The **harmonics** parameter is more applicable if studying spiral galaxies where spiral arms show up as features in the Fourier power spectrum. Most parameters in this set were left at default values, but the sigma clipping controls **usclip**, **lsclip** and **nclip** (upper, lower, and number of clipping

iterations, respectively) were each set to 3 to allow the algorithm to skip over unmasked foreground stars and background galaxies in the initial run without halting or causing spurious peaks in the profile. This is also recommended for skipping bad pixels if using CCD images. These settings allow the software to produce reasonable profiles in most cases without the need for masking out small-area features that are a lot brighter (or darker) than the mean intensity on a given isophote, as extreme values will be clipped out by the algorithm.

The `magpar` subset allows for the output intensities to be expressed in a magnitude scale. This feature was not used for this project. Magnitudes were obtained separately using the output intensity tables, background intensity measurements and the zero-point plate constant.

#### 5.6.4 Output Data Files

Outputs may be viewed graphically using the command `isopall filename.tab`, which plots the results, or using `tread filename.tab`<sup>1</sup>, which displays the table of values for each ellipse in order from the innermost to outermost ellipse. The first two columns of the output table are the semi-major axis length (in pixels) and the mean isophotal intensity (in data counts per pixel). Other columns list ellipticity, position angle, ellipse centre, magnitude (if used), gradient, flux, harmonic information, flagging and iteration statistics. Errors for relevant measurements are also written to the table. `Tread` is exited by typing `Ctrl+D`, then `e`. The ellipse centre at the smallest semi-major axis from this read-out on the initial run was used as the object centre (`x0`, `y0`) for subsequent runs.

Further analysis of each profile using `filename.tab` was performed in *Excel*, which does not recognise the `.tab` format. The `.tab` files were written to `.txt` files using the command `tdump filename.tab > filename.txt`. The `.txt` files, unfortunately, do not align the column headers with the data columns. Each file was opened with *Excel* using the ‘delimited’ by ‘space’ options to put the data into spreadsheet

---

<sup>1</sup> This is part of the STSDAS ‘tables’ package, a database management tool.

columns. Macros were written to realign the column headers, calculate the semi-major axis in arcseconds (from semi-major axis in pixels) and surface brightness in magnitudes per square arcsecond (from per-pixel intensity) for each row in the table and produce a preliminary plot of the data.  $C_{sky}$  is the measured sky background intensity. This is unique to each galaxy because background variations, due to intra-cluster light and extended haloes of giant galaxies, are inherent across the photographic image. Intensities in four to six background regions in the near vicinity of each galaxy were measured separately, using **GAIA**, and the mean background intensity  $C_{sky}$  was entered manually into the *Excel* spreadsheet for each galaxy.

### 5.7 Calculations used in Plotting and Final Measurements

The output table for each radial profile produces data in rows, one for each isophote, and columns, beginning with semi-major axis in pixels and mean intensity in data counts per pixel.

Semi-major axis in pixels  $r_x$  was converted to semi-major axis in arcseconds  $r$  for each row of the table using the scale of the image scanning process, i.e.  $x = 0.6714$  arcseconds per pixel, with the formula:

$$r = r_x \times 0.6714. \quad (5.12)$$

The per-pixel isophote intensity at each semi-major axis  $C_r$  was converted to surface brightness in units of magnitudes per square arcsecond  $\mu_r$  for each row of the table, based on Formula 5.8 using:

$$\mu_r = Z - 2.5 \log \left[ \frac{C_r - C_{sky}}{x^2} \right]. \quad (5.13)$$

The value of the plate constant ( $Z=31.5$ ), was written into the macro but entered in a separate cell of the spreadsheet so that it may be modified pending any future refinement of the calibration of the Virgo Deep Stack. The factor  $1/x^2$  is the conversion from pixel dimensions to square arcseconds (with the value of  $x$  as shown above).

The radius (in arcseconds) and surface brightness data for each galaxy were plotted in *Excel* and a trendline was fitted to the data with the trendline equation being displayed on the plot (refer Figure 2.2 p.13). The extrapolated *OR*-band central surface brightness  $\mu_0$  (y-intercept) and slope  $s$  were read from the plot and entered manually on the spreadsheet. The slope was used to calculate the scale length  $a$  of the galaxy by the relation:

$$a = \frac{1/\ln(100^{1/5})}{s}. \quad (5.14)$$

Refer Appendix A for a full derivation of this term.

Total apparent *OR* magnitude for the galaxy was derived using Equation 4.6, repeated here for easy reference:

$$OR = \mu_0 - 2.5 \log(2\pi a^2). \quad (5.15)$$

Absolute magnitude may be determined assuming a suitable distance modulus applicable for the Virgo Cluster and allowing for Galactic extinction. Distance modulus ( $m - M$ ) is defined as:

$$m - M = -5 + 5 \log(d) \quad (5.16)$$

where  $m$  is apparent magnitude,  $M$  is absolute magnitude and  $d$  is distance in parsecs. Considering the distance values in Tables 3.3 (p.39) and 3.4 (p.40), a distance modulus of 31.1 (or mean distance of 16.6 Mpc) has been assumed.

Finally, the absolute magnitude of a galaxy is given by:

$$M_{OR} = OR + 5 - 5 \log(d) - A_R \quad (5.17)$$

or, applying the adopted distance modulus, by:

$$M_{OR} = OR - 31.1 - A_R. \quad (5.18)$$

Galactic extinction  $A_R$  may be found using the NED *Coordinate Transformation & Galactic Extinction Calculator*<sup>m</sup>. *R*-band data are the closest available to the *OR*

---

<sup>m</sup> The calculator uses data sourced from Schlegel et al. (1998) and is available online at <http://nedwww.ipac.caltech.edu/forms/calculator.html>.

passband of the observations.  $A_R$  is checked for each galaxy individually (typically  $\leq 0.15$  mag). The final apparent and absolute magnitudes are in the *OR*-band. No attempt has been made to colour-correct to standard *R* magnitudes as no data in any other passbands are available for these galaxies.

The results from the above calculations are included in the Virgo Deep Stack Catalogue (Chapter 8). Files containing the surface photometry tables (*.tab*, *.txt* and *.xls* files) and radial profile plots are provided separately on a supporting CD.

### 5.8 *Uncertainties in Measurement of Galaxy Properties*

Uncertainties may arise in several contexts along the train of the data processing, from initial calibration of the image, through the surface photometry process and finally to the fitting of the linear function to the  $\mu$ -*r* profile plot.

Uncertainties in magnitude at individual semi-major axes in the profile tend to be smoothed over by the fitting function applied. However, the uncertainty in magnitude of the outer ellipses is large due to sensitivity to the background intensity. At the edge of the galaxy the signal is small relative to a large background count, so small uncertainties in the background measurement lead to large errors in the signal. The background sensitivity often outweighs any other random or systematic errors in the surface photometry. This trend is ubiquitous for radial profile data at galaxy edges so, very often, no uncertainties are shown on radial profiles (e.g. Young and Currie (1998), Jedrzejewski (1987), Phillipps and Parker (1993), Impey et al. (1988), Peletier et al. (1990)).

A method of estimating uncertainty due to the background measurement is to use the standard deviation of intensity counts in the background (i.e. lower and upper intensities) to derive high and low surface brightness values over the whole profile. These will produce slightly altered slope and extrapolated central surface brightness allowing uncertainties in these and all derived parameters to be estimated. The radial profile of the giant LSB galaxy, Malin 1 (refer Figure 4 p.157), shows error



bars on the plot based on this technique. It is clear how large the surface brightness error is at the galaxy's edge.

Contaminant objects (e.g. stars and other galaxies) may overlie the target galaxy and interfere with surface photometry measurements. Whilst the `ELLIPSE` software is able to generate a profile without any masking of contaminants, this does not always produce a satisfactory result. For example, surface photometry of Galaxy 22-4, discovered in this project, shows that differences of around  $0.07 OR_{\mu}$  in the central surface brightness and 0.03 magnitudes per arcsec in the slope arise depending on whether it is performed with or without masking (refer Figure 5.10).

In most cases it is only necessary to mask bright contaminants close to the centre of the target galaxy. At larger semi-major axes stars and background galaxies are usually skipped over naturally by the 3-sigma clipping used in the `samplepar` parameter set.

Another source of uncertainty is in the surface photometry itself and the flexibility to allow the software to vary position angle and ellipticity or to subjectively nominate values for these and hold them fixed. Simply redoing the surface photometry using slightly different position angle and ellipticity will change parameters of the linear fit, resulting in variations to extrapolated central surface brightness, scale length and final apparent magnitude. However, results from this project show that these uncertainties are typically less than  $0.1 \mu$ , 1.0 arcsecond and 0.2 magnitudes, respectively.

Finally, deciding where to terminate the fitting function (another subjective decision) has an effect on the result, as fluctuations in the profile due to clumpiness of the galaxy alter the fit depending on where the fit cuts off. For this project, functions are fitted out to the data point with faintest surface brightness before the profile flattens out to the background. This does not always produce the best fit in cases where portions of the profile may have a slightly different gradient, but it does provide a better summary of the galaxy as a whole than fitting over only linear or central portions.

Changes to the parameters measured from the fitting function flow through to the derived values of magnitude and scale length. To evaluate the size of the masking errors, data for 42 galaxies for which profiles were generated with and without masking were compared. The mean absolute difference in central surface brightness was 0.1 magnitudes and the mean variation in scale length was 16% of the ‘with masking’ result. The difference in the magnitude calculation resulting from variations of this size is 0.22 magnitudes.

Variations due to other factors were estimated by modifying the background level, the plate constant and the length over which the profile was fitted for a typical profile. Effects of all the variations are summarised in Table 5.4. Improper masking contributes the largest error term, so careful masking of contaminants in the inner profiles of galaxies has been performed, where necessary. Hence, the final uncertainties adopted are the values from adding three terms in quadrature: the variation for profile length; one background term; and the uncertainty in the plate constant. Larger allowances should be made in cases where an exponential is a poor fit to the galaxy profile.

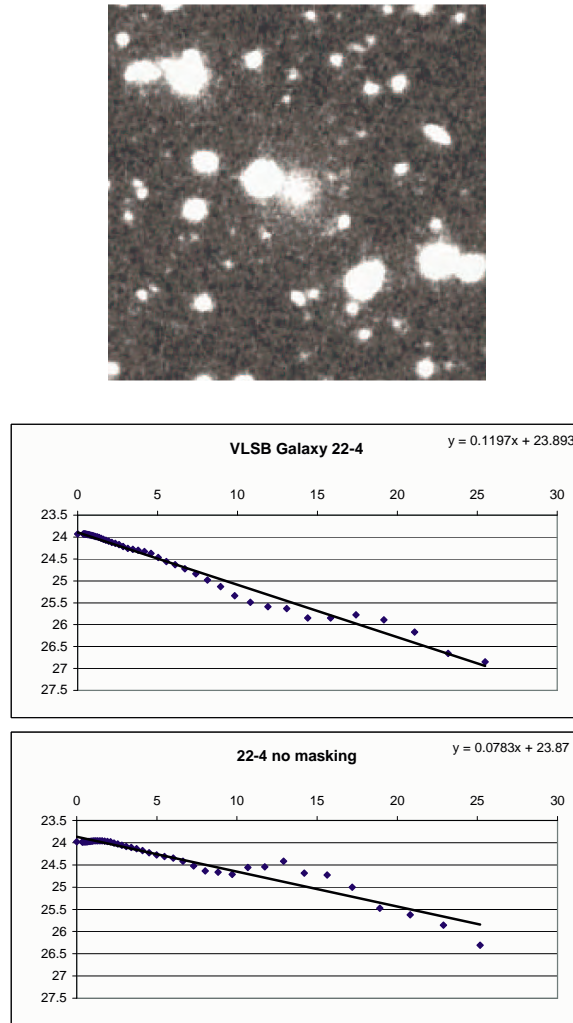


Fig. 5.10: Effects of Masking

*Image:* The image of Galaxy 22-4 has a bright foreground star immediately adjacent to the east (left). Image size is 134 arcsec across.

*Middle:* With masking of the bright star in the ELLIPSE processing, the profile is predominantly smooth. Surface brightness (OR) is on the y-axis. Radius (semi-major axis) in arcsec is on the x-axis in both plots.

*Bottom:* Without masking, the profile is lumpy. The inclusion of the light of the foreground star is evident in the bulge between 10 and 20 arcsec radius. The slope and central surface brightness values (shown before rounding) are affected, as may be seen from the best fit shown at the top right of each plot.

Change affecting measurement	Effect on measurement		
	$\mu_0$	$a$	$OR$
1. Masking variation	0.10	16%	-0.22
2. Shorter profile	0.02	4%	-0.07
3. Background + 3 counts pixel <sup>-1</sup>	-0.06	-12%	0.23
4. Background - 4 counts pixel <sup>-1</sup>	0.03	11%	-0.20
5. $Z + 0.10$	0.10	—	0.10
1, 2, 3 and 5 in quadrature	$\pm 0.15$	$\pm 20\%$	$\pm 0.34$
2, 3 and 5 in quadrature	$\pm 0.12$	$\pm 13\%$	$\pm 0.26$
Final values adopted	$\pm 0.1 \mu$	$\pm 13\%$	$\pm 0.3 \text{ mag}$

Tab. 5.4: Variations Contributing to Uncertainty

Typical values of individual uncertainties due to improper masking, profile truncation, random errors in background measurements and variation to the image calibration constant ( $Z$ ) and their impact on central surface brightness ( $\mu_0$ ), scale length in arcseconds ( $a$ ) and apparent magnitude ( $OR$ ) are compared. Effects of changing position angle and ellipticity are comparable to those of changing the background so are not added in separately. Totals are added in quadrature: the first total line omits the smaller ( $-4 \text{ counts pixel}^{-1}$ ) background data; the second total line is as for the first, but also omitting the masking error. It may be assumed that effective masking has been performed on all profiles displayed in the Virgo Deep Stack Catalogue (Chapter 8). Final uncertainties adopted for this project therefore exclude the masking error.

## 6. DATA QUALITY AND COMPARATIVE RESULTS

In this chapter, the quality and properties of the Virgo Deep Stack data are assessed by comparison with published data. A small region is studied in detail to ascertain that galaxies detected in other surveys are readily seen in these data and that new, additional galaxies that lie below the thresholds of previous surveys are also seen. With regard to the Virgo Cluster luminosity function, these data hint at why other authors find different values for the faint-end slope. New data on some individual galaxies are also presented.

The Virgo Deep Stack, with its depth and wide area coverage, is a useful data set for examination of the phenomenon of intra-cluster light. The Virgo Deep Stack data are, therefore, compared with other images that reveal tidal streamers and broad, diffuse galaxy haloes.

### 6.1 *Comparison Profiles*

As discussed in Section 5.4, calibration of the Virgo Deep Stack was achieved by performing aperture photometry on a limited number of stars in the stack and comparing with accurate reference magnitudes independently determined for the same stars. This method could be made more reliable by considering a much larger number of stars. However, it is also possible to compare whole galaxy profiles directly with published data. In some cases, this has been used as an alternative calibration method, e.g. by Phillipps and Parker (1993) in studying the properties of Kodak Tech Pan film and by Schwartzenberg et al. (1996) in assessing a method of digitally stacking films. This calibration method works well where the measured and comparison data are in the same passband and have equivalent surface-brightness

ranges. With the slight differences between *OR*-band and the standard Cousins *R* and *R<sub>CCD</sub>* passbands (Bessell 1986), comparisons are still useful as they yield insight into the saturation and background levels of the Virgo Deep Stack, compared with those of the published data, and also reveal the effects of the slightly different passbands on galaxy profiles.

Measurements from the Virgo Deep Stack are compared with *R*-band data from Jedrzejewski (1987), which were obtained with the Royal Greenwich Observatory CCD camera at the prime focus of the 3.9-metre Anglo-Australian Telescope in April 1982. Exposures ranged from 60 to 100 seconds. The data were calibrated to a ‘standard’ *R*-band against earlier photographic work. This surface photometry catalogue contains tables of values that are easily plotted against data from other sources. The catalogue only contains data on brighter galaxies and some of the tables truncate (each table is only a single page) before reaching what would have been the observable edge of the galaxy.

Nevertheless, for the purpose of comparison, surface photometry was performed on the eight galaxies common to Jedrzejewski (1987) and the Virgo Deep Stack. Of these, two of the tables contain insufficient data to make a meaningful comparison (NGC 4374 (M84) and NGC 4486) because the Jedrzejewski (1987) data only cover the bright galaxy centres that do not overlap the unsaturated portions of the Virgo Deep Stack data. For four galaxies (NGCs 4476, 4478, 4551 and 4387), the profiles show excellent matches (refer Figure 6.1). One has surface brightness differences of  $\lesssim 0.2 \mu$  (NGC 4458) and one shows a larger difference of  $\sim 0.37\mu$  (NGC 4473). These values refer to segments of the profiles that are not affected by saturation or background, typically spanning around 30 arcseconds of each profile. Overall, the *OR*-band data are marginally fainter than the Jedrzejewski (1987) data.

The comparisons demonstrate that the Virgo Deep Stack data suffer complete saturation by  $20.0 \text{ } OR\mu$ , but that the effect begins to show up at around  $20.9 \text{ } OR\mu$ . The Jedrzejewski (1987) data have a much shallower background, detectable where the profiles extends far enough to reach  $\sim 24.5R\mu$ .

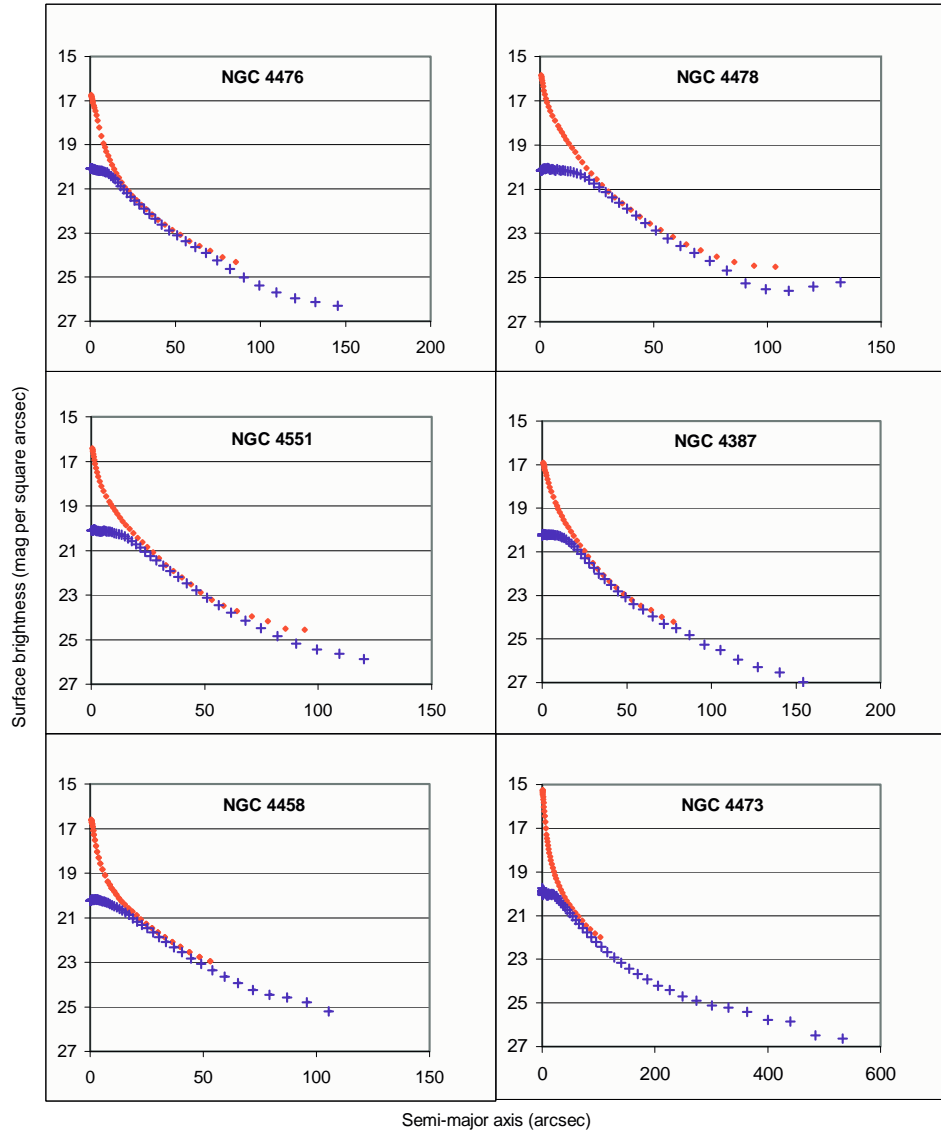


Fig. 6.1: Comparison Profiles

Radial profiles for six bright galaxies (numbered on the plots) are compared. Blue crosses are OR-band data from the Virgo Deep Stack. Red dots are CCD R-band data from Jedrzejewski (1987). The Virgo Deep Stack data begin to be affected by saturation at about 20.9 magnitudes (note the turnovers at the left-hand edges of the plots). The shallower background of the Jedrzejewski (1987) data may be seen in the earlier upturns at the faint end of some profiles.

Top Four Plots: Profiles of NGCs 4476, 4478, 4551 and 4387 are well matched where unaffected by saturation or background.

Bottom Left: NGC 4458 shows small differences of around  $0.2 \mu$ .

Bottom Right: The poorest match is for NGC 4473 with a  $0.37$  surface brightness difference between profiles, with the difference possibly due to the slightly different passbands of the observations and the intrinsic colour of the galaxy.

The small surface brightness differences between the two data sets may be due to variations in the intrinsic colours of the galaxies, as measured in the different passbands, rather than any calibration or random errors. Bessell (1986) compared the standard Cousins  $R$ -band ( $R_C$ ),  $R_{CCD}$  and others.  $R_C$  covers 5500 to 8750 Å, with a width (full-width-half-maximum) of 1450 Å ranging between  $\sim 5650$  and  $\sim 7100$  Å. The  $OR$ -band has a sharp filter cut on at 5900 Å, an emulsion cut-off at 6990 Å and an overall narrower transmission curve (refer Figure 5.3, p.97). It is difficult to discern if such a colour-dependent effect is significant over this small number of comparisons, considering the size of the uncertainty in the measured data. In follow-up work, but beyond the scope of this project, profile data from the Virgo Deep Stack data could be further compared with those from Peletier et al. (1990) and Young and Currie (1998), which are available in the online *VizieR* database.

The comparison profiles above show that the  $R$ -band data of Jedrzejewski (1987) do not reach the surface brightness limit of the Virgo Deep Stack. To find this limit effectively requires measurement of radial profiles of LSB galaxies that are set against particularly dark backgrounds. Surface brightness at extremities of the galaxies measured for this project are listed in Chapter 8. An indicative value for the limiting surface brightness in the deepest parts of the image is  $29.7 \text{ OR}\mu$ . The galaxy profile presented in Figure 2.2 (p.13) goes close to this, reaching  $29.3 \text{ OR}\mu$ .

## 6.2 Comparisons of the Virgo Deep Stack with Other Surveys

Chapter 3 detailed earlier surveys of dE and dSph galaxies. These surveys included LSB galaxies and some of the regions covered by those surveys overlap with the area covered by the Virgo Deep Stack (refer Figure 6.2).

Existing online catalogue data in this area mainly come from Trentham and Hodgkin (2002), Trentham and Tully (2002) and the Virgo Photometry Catalogue (VPC) of Young and Currie (1998). Almost all of the galaxies from these surveys are readily seen in the Virgo Deep Stack. However, many galaxies that do not appear in the catalogues and have no current listings on NED have also been detected as



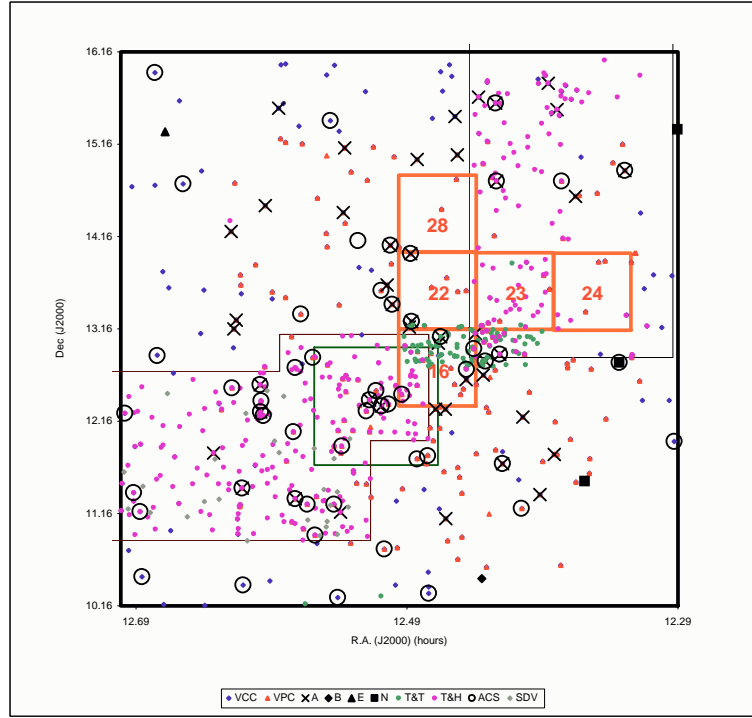


Fig. 6.2: Map 4: Overlap of the Virgo Deep Stack with Other Surveys

*This map shows in detail the surveys that overlap with sub-frames 16, 22, 23, 24 and 28. The region common to sub-frame 16 and the Trentham and Tully (2002) data (green dots) is discussed in detail in the text. The green box is one region studied by Phillipps et al. (1998). The fine red and black lines delineate the E-W and N-S strips of the INT Wide Field Survey, respectively.*

part of this project. This clearly demonstrates the power of the Virgo Deep Stack and its potential to reveal significant numbers of additional LSB galaxies in the Virgo Cluster. Comparisons of observability and properties of galaxies from three very deep surveys and one additional dSph analysis below verify the depth and comprehensive coverage of the Virgo Deep Stack.

### 6.2.1 The Survey by Trentham and Tully (2002)

The deepest comprehensive set of comparison  $R$ -band data is that of Trentham and Tully (2002), which overlaps with the upper portion of sub-frame 16 of the Virgo Deep Stack (refer Figure 6.2).

All but two galaxies of the Trentham and Tully (2002) survey that are contained within sub-frame 16 are clearly visible in the Virgo Deep Stack (refer Figure 6.3). However, close inspection of the common region also reveals five VLSB galaxies in the Virgo Deep Stack that were not catalogued in the Trentham and Tully (2002) survey. Three of these are considered to be background galaxies, based on morphology. Galaxies 16-6 and 16-23 show hints of spiral structure and galaxy 16-9 is a likely E/S0. Refer to Chapter 8 for images and measured properties of these galaxies. The other two VLSB galaxies, catalogued in this project as 16-16 and 16-31 (shown in Figure 6.4), have appearances and properties comparable with those in the Trentham and Tully (2002) survey. Galaxy 16-16 is very diffuse and barely distinguishable from the background. Galaxy 16-31 lies in a complex region with foreground stars.

It is impossible to know whether or not these two new VLSB galaxies were detected in the Trentham and Tully (2002) survey because those authors do not provide a full catalogue of all detections and specific reasons for exclusion of particular candidates from the Virgo Cluster.

Galaxy 16-31 may have been removed from the Trentham and Tully (2002) sample due to the foreground stars (which, the authors state, would produce very negative concentration parameters in the analysis technique, making it appear like a background object). Galaxy 16-16 was almost certainly missed due to its diffuse nature and very low surface brightness. Both galaxies are considered, in this project, to be new detections of VLSB galaxies in the Virgo Cluster. Measured properties of these galaxies are provided in Chapter 8.

This comparison suggests that the surface brightness limits of the Virgo Deep Stack and the Trentham and Tully (2002) survey are approximately the same. Without quoting a limiting surface brightness, Trentham and Tully (2002) state that extreme

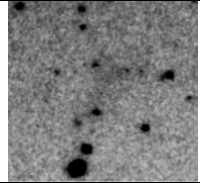
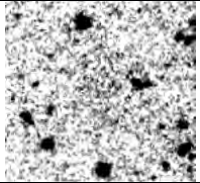
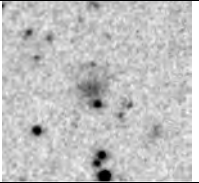
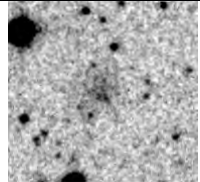
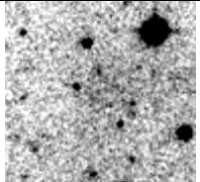
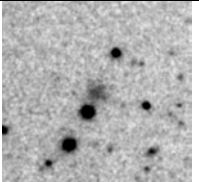
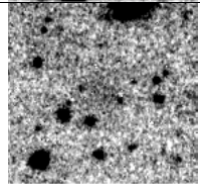
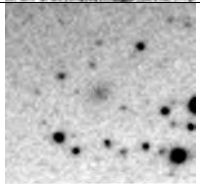
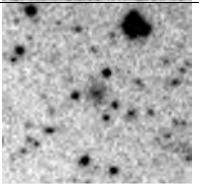
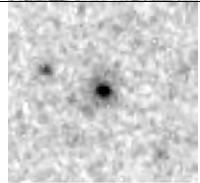
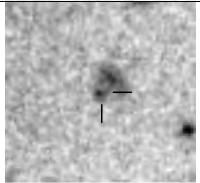
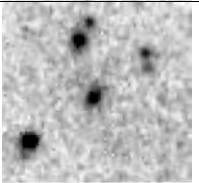
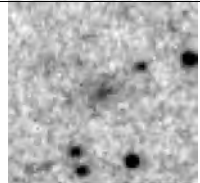
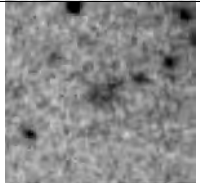
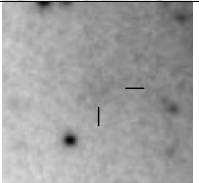
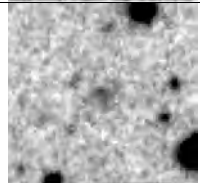
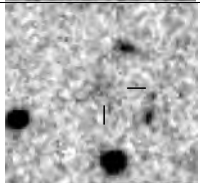
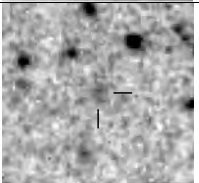
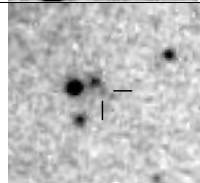


	54 dI/ VLSB		57 dI/ VLSB		59 dE
	61 dE/ VLSB		63 dI/ VLSB		64 dE/I
	66 dI/ VLSB		67 dE		68 dE
	70 dE,N		74 dE		75 dI
	80 dI		82 dE/I		83 dI
	86 dI		93 dE/I		94 dI
	95 dI		97 dI		98 dI

Fig. 6.3: Galaxies Common to Trentham & Tully and Sub-Frame 16

Images are from the Virgo Deep Stack. Galaxy ID numbers (in order of decreasing total magnitude) and classifications are those assigned by Trentham and Tully (2002). Image sizes: 54 - 68 (upper nine images) are 94 arcseconds on a side; 70 - 98 (lower 12 images) are 44 arcseconds on a side. North is at the top and east is to the left. Positions of galaxies are indicated where they are difficult to discern. The faintest galaxies, 97 and 98, are not visually discernable in the Virgo Deep Stack.

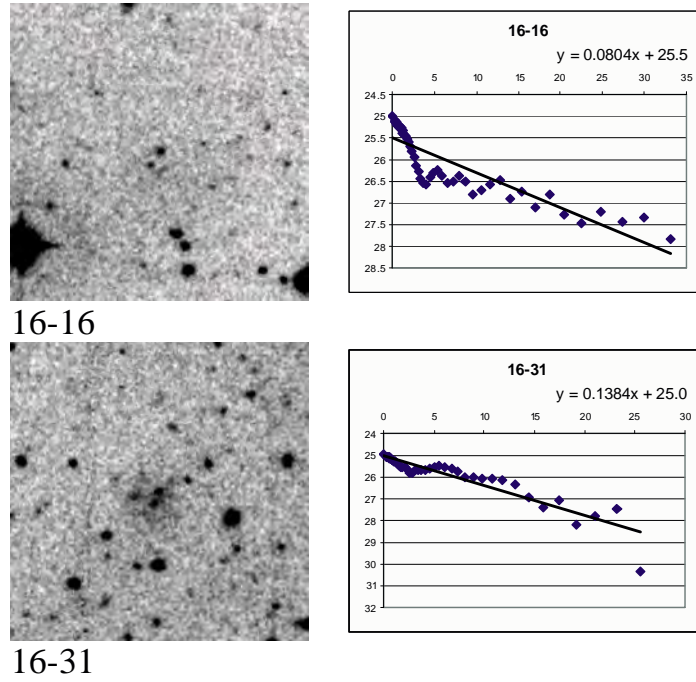


Fig. 6.4: Two New VLSB Galaxies from Sub-Frame 16

*In the region of overlap between sub-frame 16 and the region covered by Trentham and Tully (2002), two new VLSB galaxies have been detected in the Virgo Deep Stack. Galaxy 16-16 is very diffuse and appears just below centre of the top image. Galaxy 16-31 (bottom image) is more obvious but is overlaid by foreground stars. Images measure  $134 \times 134$  arcsec. North is at the top and east is to the left.*

LSB galaxies with central surface brightness below  $28 R\mu$  would not be detected. As part of this comparison, surface photometry was performed on those common galaxies that were classified by Trentham and Tully (2002) as VLSB. Images of these galaxies from the Virgo Deep Stack appear together with their profiles in Figure 6.5. Magnitudes derived from the profiles are compared with data supplied in Trentham and Tully (2002) in Table 6.1 and a complete list of derived properties is provided in Chapter 8.

It may be noted that these Virgo Deep Stack profiles all reach beyond  $28 R\mu$  at the galaxy extremities, suggesting that the completeness limit of both data sets is

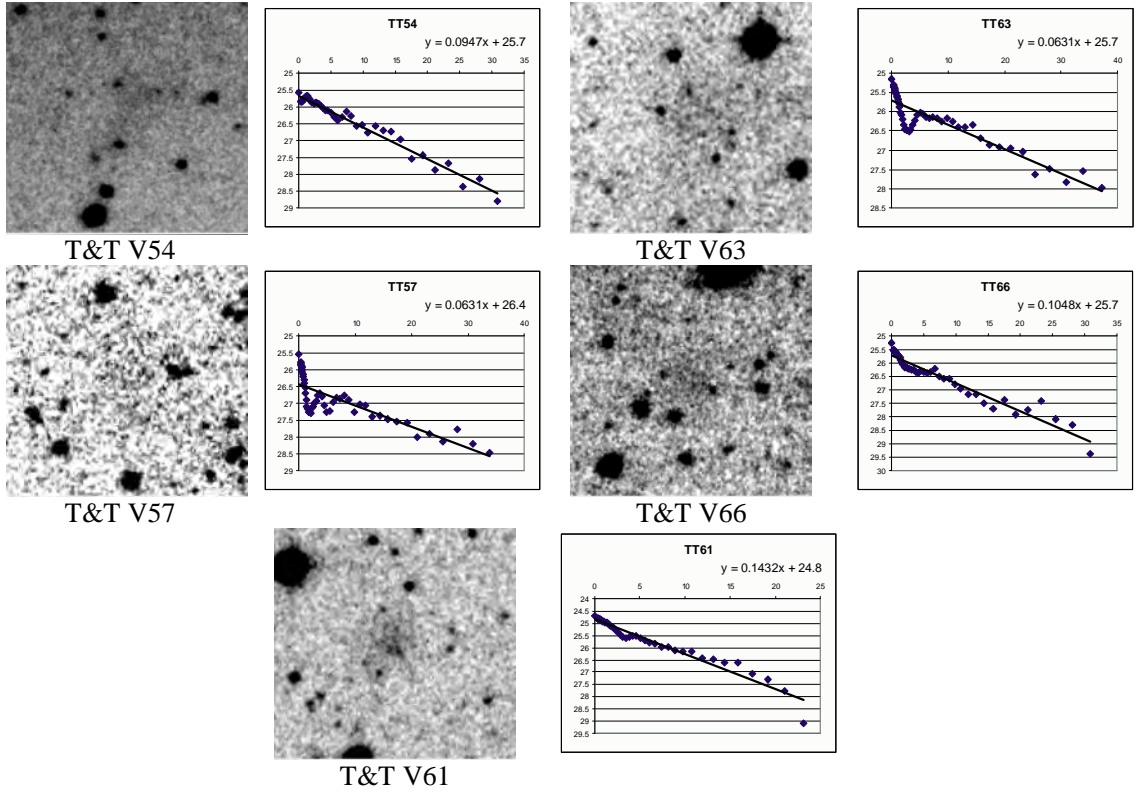


Fig. 6.5: Images and Profiles: Five Trentham & Tully Galaxies

*Images and profiles, obtained from sub-frame 16 of the Virgo Deep Stack, of five galaxies classified by Trentham and Tully (2002) as VLSB galaxies. Images measure  $94 \times 94$  arcsec. North is at the top and east is to the left.*

approximately  $28 R\mu$ . The galaxy total magnitudes are all brighter, according to Virgo Deep Stack full-galaxy profile measurements, compared with the Trentham and Tully (2002) results. The latter data are based on aperture magnitudes that are corrected by subtraction of foreground stars and background galaxies and augmented by extrapolation of the profile to infinity. Uncertainties are not discussed, but the aperture corrections are stated to be rarely more than 0.5 mag. The authors also state that this method does not work well in cases where the exponential fit is poor or where galaxies have very close companions. Similarly, obtaining magnitudes from the full radial profile (the method used for this project) is not ideal when the exponential fit is poor.

ID (T&T)	T&T $R_T$	Virgo Deep Stack $OR_T \pm 0.3$	T&T - VDS Var App
54	18.84	18.37	0.47
57	19.53	18.27	1.26
61	19.71	18.43	1.28
63	19.83	17.53	2.30
66	20.04	18.62	1.42

Tab. 6.1: Comparison Magnitudes: Five Trentham & Tully Galaxies

*Apparent magnitudes of the five galaxies shown in Figure 6.5 as quoted by Trentham and Tully (2002) and as measured from the Virgo Deep Stack. Magnitude differences are listed in the last column. All galaxies measure brighter in the Virgo Deep Stack than in the Trentham and Tully (2002) data.*

It is evident from the profiles and images (Figure 6.5) that an exponential is a very poor fit for galaxies 57 and 63 and all five galaxies in this comparison have superimposed foreground stars. Foreground stars were carefully masked for the Virgo Deep Stack profiles. Nevertheless, magnitude differences shown in Table 6.1 are large. For galaxy 63, with a poorly-fitting profile, the difference is more than two magnitudes. Even where the exponential is an acceptable fit, as for galaxy 61, the difference is more than one magnitude.

One possible source of error in the Trentham and Tully (2002) data is in measuring the initial aperture magnitudes. A method of aperture photometry is described in Section 5.4 and relies on the outer annulus (used to measure the sky background) being placed at a sufficient radius from the galaxy centre that it is actually measuring background, rather than the outer periphery of the galaxy. This is not normally a problem when measuring stellar magnitudes but, for a diffuse LSB galaxy, if the background measurement is ‘high’ (because it is not really background) then the galaxy magnitude will be fainter than if a true measurement were obtained.

A source of error in measurement using radial profiles comes from non-uniformity in galaxy shape. The equations used to calculate scale length from slope of a

magnitude-radius plot (Equation 5.14 p.115) and apparent magnitude from scale length and central surface brightness (Equation 5.15 p.115) do not take into account any ellipticity and assume the galaxy is round. This could result in a magnitude measurement that is brighter than the true magnitude when using the slope of a radial profile plotted against the semi-major axis of an ellipse, rather than the radius of a circle.

This comparison suggests that inherent errors may be large in measurements of properties of diffuse galaxies at these very low surface brightness levels and that different measurement techniques appear to yield conflicting results.

### 6.2.2 The Survey by Caldwell (2005)

A more recent success in detecting objects of very low surface brightness is reported by Caldwell (2005). Seven deep CCD images from the KPNO Mosaic Camera on the Mayall 4-m Telescope were examined with the aim of detecting Virgo Cluster dE galaxies with fainter surface brightness than any galaxies known in the Local Group. The fields were searched using both visual inspection and automated detection methods. A full catalogue of objects found in that survey has not yet been published, but the two VLSB galaxies reported on had already been independently detected in this project, though not announced, at the time of the Caldwell (2005) publication. The designations in this project are 22-8 and 16-45. The corresponding Caldwell (2005) identification numbers are N lsb10 and SW2 lsb31, respectively. Virgo Deep Stack images and radial profiles of these two VLSB galaxies are shown in Figure 6.6.

Caldwell (2006) followed up with observations using the HST ACS instrument to produce colour-magnitude diagrams of resolved stars in both galaxies, plus four other galaxies and some intra-cluster stars. The other galaxies were VCC 941, VCC 871, NGC 4407 and a dwarf spheroidal that is visible in the Virgo Deep Stack, but which lies deep within a diffraction halo of a bright star (and, hence, could not be measured in this project). These new data for TRGB stars verify that both of the VLSB galaxies are Virgo Cluster members. From the study of these six galaxies

Caldwell (2006) derived a mean distance modulus of  $31.0 \pm 0.05$  or a distance of  $16.1 \pm 0.4$  Mpc. Data from these follow-up observations and the Virgo Deep Stack on the two VLSB galaxies are compared in Table 6.2.

Data	Caldwell (2006)	Virgo Deep Stack	Caldwell - VDS
ID	N lsb10	22-8	
$\mu_0$	$26.6 \pm 0.6 R\mu^a$	$25.9 \pm 0.5 OR\mu^b$	$0.7 \mu$
$m$	$R = 18.54 \pm 0.13$	$OR = 18.2 \pm 0.3$	$0.34 \text{ mag}$
$r_{max}$	$30'' (2 \text{ kpc})$	$30''.85$	-
$\mu_{r-max}$	$28.6 R\mu^a$	$27.6 \pm 0.5 OR\mu$	-
$m - M$	$31.0 \pm 0.12$	-	-
ID	SW2 lsb31	16-45	
$\mu_0$	$26.2 \pm 0.2 R\mu^a$	$24.8 \pm 0.5 OR\mu^b$	$1.4 \mu$
$m$	$R = 17.76 \pm 0.05$	$OR = 17.9 \pm 0.3$	$-0.14 \text{ mag}$
$r_{max}$	-	$28''.04$	-
$\mu_{r-max}$	-	$27.9 \pm 0.5 OR\mu$	-
$m - M$	$30.9 \pm 0.1$	-	-

Tab. 6.2: Data: Two Independently-Verified VLSB Galaxies

*Measurements from Virgo Deep Stack radial profiles and those from the surface brightness conversion applied by Caldwell (2006) are compared.*

<sup>a</sup> *Values are calculated from Caldwell (2006)  $B - R$ ,  $B_0$  and  $B\mu$  values.*

<sup>b</sup> *Large uncertainties are quoted due to the poor fit to the profiles.*

It should be noted that Caldwell (2006) was unable to perform surface photometry on the ACS images of these galaxies and, instead, used measurements from a surface-brightness conversion based on photometry measurements of VCC 941. This may contribute to the differences in magnitude and surface brightness measurements provided in Table 6.2 although, in this comparison, differences are much smaller than those detailed in the previous section. Also, although the central sur-



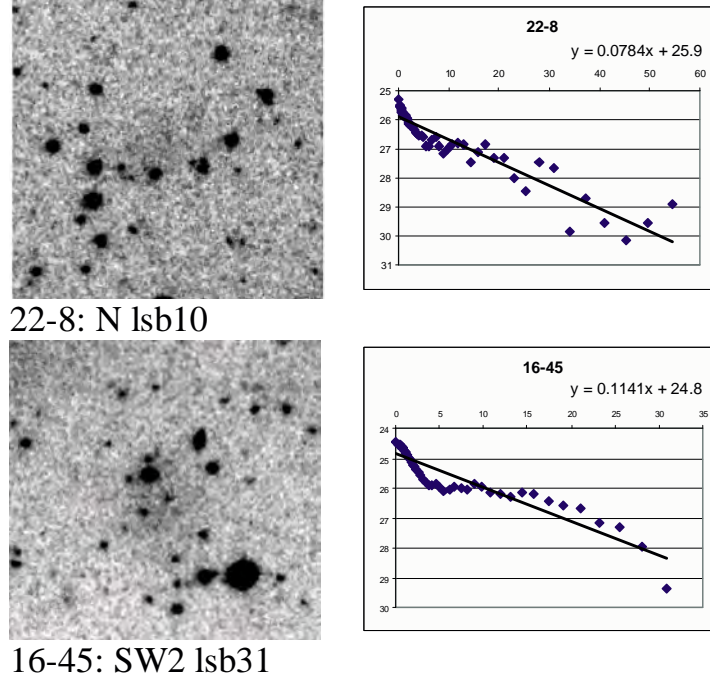


Fig. 6.6: Images and Profiles: Two Independently-Verified VLSB Galaxies

*Virgo Deep Stack images of two VLSB galaxies catalogued during the progress of this project and independently found by Caldwell (2005). Images measure  $134 \times 134$  arcseconds. North is at the top and east is to the left.*

face brightnesses are both brighter in the Virgo Deep Stack measurements, the total apparent magnitude comparisons show that galaxy 16-45 is fainter and galaxy 22-8 is brighter in the Virgo Deep Stack than in the Caldwell (2006) data. These results imply that, although there are errors associated with measuring such diffuse LSB objects, the methods of Caldwell (2006) and this project produce results that are close to agreement within uncertainties.

### 6.2.3 The Survey by Sabatini et al. (2005)

Sabatini et al. (2005) present  $B$ - and  $I$ -band data for galaxies in the E-W strip of the INT Wide Field Survey and one galaxy, that the authors describe as “almost impossible to see on the  $B$ -band image”, is clearly visible in Figure 6.7 from the Virgo Deep Stack data. This is the dI galaxy numbered 144 of that survey (SDV 144) and is located at  $12^h38^m41^s +11^\circ58'43''$ . No  $I$ -band data are presented by the authors for this galaxy due to insufficient S/N in the  $I$ -band image.

The authors included this galaxy in an HI survey. HI velocity measurements from that survey confirm that the galaxy is a cluster member, at a distance of 16 Mpc, and has a high HI mass-to-light ratio of 6.2. Optical measurements of this galaxy’s properties from that study and from the Virgo Deep Stack are compared in Table 6.3. Once again, a different analysis method was used by Sabatini et al. (2005). For that study, properties were derived from the convolution algorithm used for detection and an aperture that included total galaxy flux but excluded nearby objects was used. The comparison shows differences in magnitude and scale length.

The difference in scale length is readily explained by the sensitivity of the measurements to the span of the profile and the background level specified, as demonstrated in the analysis of uncertainties for this project (refer Table 5.4 p.120).

Data	Sabatini et al. (2005)	Virgo Deep Stack	Sabatini - VDS
$\mu_0$	$26.6 \pm 0.5 \text{ } B\mu$	$25.3 \pm 0.1 \text{ } OR\mu$	$1.3 \text{ } \mu$
$m$	$B = 19.8 \pm 0.5$	$OR = 17.7 \pm 0.3$	2.1 mag
$a$	9 arcsec	$13 \pm 2 \text{ arcsec}$	4.1 arcsec

Tab. 6.3: Data: SDV 144

*Comparison measurements for a VLSB galaxy of Sabatini et al. (2005). It should be noted that the data are in different passbands and, if applying a colour term of  $B-R \approx 1.5$ , then the Virgo Deep Stack magnitude would become  $B = 19.2$ .*

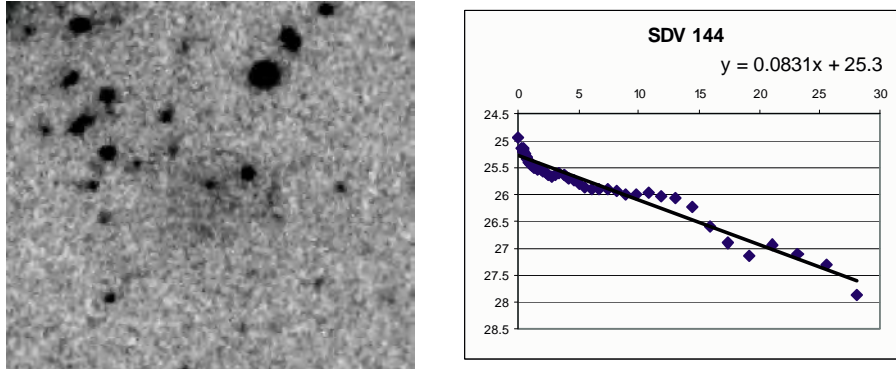


Fig. 6.7: Image and Profile: SDV 144

*Pictured is a Virgo Deep Stack image of galaxy 144 described by Sabatini et al. (2005). The image measures  $134 \times 134$  arcseconds. North is at the top and east is to the left.*

Because the comparison data are in different passbands, magnitude differences of  $\sim 1.5$  magnitudes are expected. Thus, the total apparent magnitude difference of 2.1 is not as much of a concern in this case as with the Trentham and Tully (2002) comparison although, again, the Virgo Deep Stack yields a brighter total magnitude and central surface brightness. Mean magnitude errors in the Sabatini et al. (2005) data are quoted in the earlier Sabatini et al. (2003) paper as  $\pm 0.5$  magnitudes. Therefore, allowing for uncertainties in both sets of measurements and a 1.5-magnitude difference due to passbands, the magnitude data are in broad agreement.

#### 6.2.4 Dwarf Spheroidal Galaxy Analysis by Durrell et al. (2007)

Durrell et al. (2007) report on the analysis of a Virgo Cluster dwarf discovered, using HST images, during a survey of intra-cluster stars. Once again, the object was independently discovered and catalogued during the conduct of this project and is designated Galaxy 16-19. HST and Virgo Deep Stack images of this galaxy are compared in Figure 6.8. Its radial profile appears in Figure 8.15 (p.195).

The colour-magnitude diagram obtained by Durrell et al. (2007) indicates that the galaxy lies at a distance of  $17.6 \pm 1.4$  Mpc ( $m - M = 31.23 \pm 0.17$ ). The authors state that the galaxy is easily resolved and has an absolute magnitude of  $M_V \approx -10.6 \pm 0.2$ . The measurement obtained in this project is  $M_{OR} = -11.9 \pm 0.1$ . The difference of 1.3 magnitudes may be entirely attributable to the difference in passbands, although a conversion value from  $V$ -band to  $OR$ -band has not been investigated.

One particularly useful finding from this comparison relates cluster membership to the size of the galaxy. The measurement of the galaxy's scale length from this project yields a value of  $a \approx 3.7$  arcseconds. Theoretically, scale lengths as small as 3 arcseconds indicate likely cluster membership (refer discussion in Section 4.5.4) but poor seeing may affect the reliability of this limit. In this case, it is clear that galaxies with scale lengths in the range  $3 < a < 4$  may, indeed, be cluster members. Also, it appears that seeing considerations that may have an impact on the cluster-member threshold in a single image have been overcome, either by the use of only A-grade films in the Virgo Deep Stack, or as a by-product of the stacking process.

#### 6.2.5 Comparisons Summary

It is evident from these comparisons that the depth and high quality of the data from the Virgo Deep Stack are equal to those of recent deep CCD surveys. In addition, with the exception of the Virgo Photometry Catalogue of Young and Currie (1998), which focussed on selected brighter VCC galaxies, the Virgo Deep Stack covers

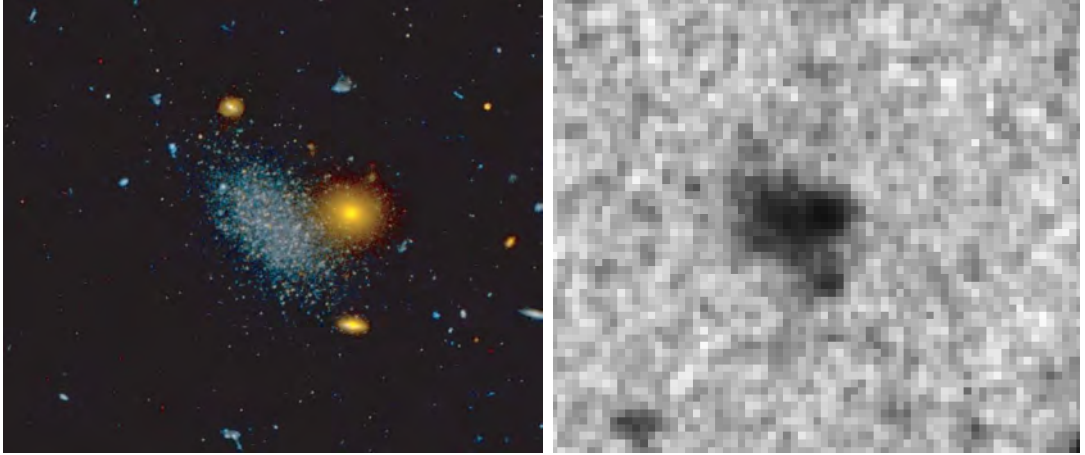


Fig. 6.8: A Dwarf Spheroidal Cluster Member

*Galaxy 16-19 of this project was independently discovered and analysed by Durrell et al. (2007). The HST image (left) measures  $28 \times 24$  arcseconds. The Virgo Deep Stack image (right) measures  $47 \times 40$  arcseconds. North is at the top and east is to the left in both images. The galaxy is a confirmed cluster member (refer text).*

HST image reproduced from Durrell et al. (2007).

substantially more area of the main sub-cluster (A) and its immediate surroundings than any other single survey.

The difficulty of obtaining radial profiles of galaxies of such low surface brightness is evident from the uneven nature of the profiles in some cases. Various methods of analysing the galaxies to obtain magnitudes and surface brightness measurements have been shown to produce some diverse results. According to measured properties of magnitude and surface brightness, galaxies measure equally bright or brighter in the Virgo Deep Stack than in many other data examined. This appears to be mainly due to the different analysis methods used by various authors rather than any systematic error in calibrating or analysing the Virgo Deep Stack data. Automated algorithms (e.g. Sabatini et al. (2005)) and concentration parameter methods (e.g. Trentham and Tully (2002)) may fail to include all the light from a galaxy, making the magnitudes too faint, but calculation of the total magnitude from an extrap-

olated radial profile (as performed in this project) does not take into account the ellipticity of the galaxy, potentially making the magnitudes too bright. The impact of these magnitude discrepancies on the Virgo Cluster luminosity function will be discussed in Section 9.2.

### 6.3 *Bryn's Mystery Object*

An unusual discovery in the Virgo Deep Stack is a very large-scale low surface brightness feature that defies immediate classification. The object and profile are shown in Figure 6.9. This may be a nearby foreground nebula in the Milky Way or a foreground galaxy, perhaps a VLSB Local Group member. It is comparable in angular size to the Leo II dwarf galaxy, although Leo II has the appearance of a dSph, whereas this object is clearly elongated. It is included in Chapter 8 with the object identifier for this project of 22-5, but is also referred to as Bryn's Mystery Object (refer Figure 5.6 p.101).

Its 'central' surface brightness is around  $25.2 R\mu$  and its scale length is approximately 212 arcsec, though the exponential profile is not an ideal fit. It extends some 10 arcminutes from end to end. With its large angular size and lack of structure, this object is unlikely to be a Virgo Cluster galaxy. At the Virgo Cluster distance of  $\sim 17$  Mpc, its length would measure some 50 kpc in physical size - comparable with the size of a large elliptical galaxy.

It may turn out to be an artefact due to an off-axis internal reflection (which would occur at the same location on the 63 films), although comparison with some identified artefacts (refer Figures 5.4 p.98 and 6.16 p.148) clearly illustrates that artefacts do not generally resemble galaxies.

Follow-up study of this object would require deep large-field imaging to verify its existence and spectroscopy or analysis of its stellar population to ascertain the nature of the object. A request has been lodged, in collaboration with George Jacoby, to observe it using the Sparsepak integral field unit (IFU)<sup>a</sup> on the WIYN 3.5-metre

---

<sup>a</sup> An IFU is a unit that utilises multiple optical fibres to deliver light from a two-dimensional

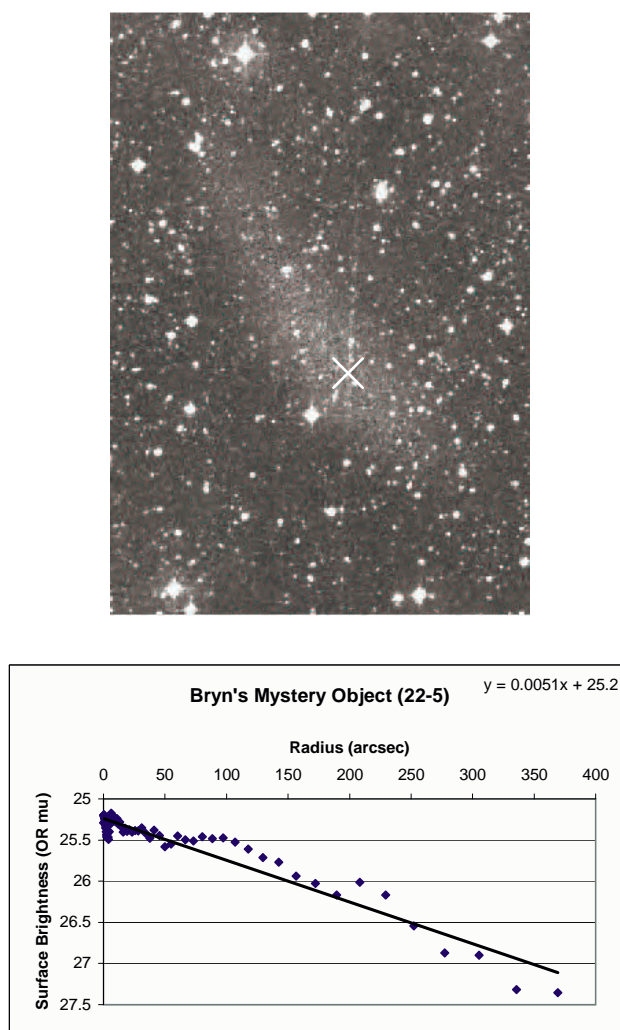


Fig. 6.9: Bryn's Mystery Object

*This unusually large feature could be a foreground galaxy, a tidal tail, a nebulous object or an artefact. The feature extends at least 10 arcmin from end to end. The image measures 19 arcmin high and 16.75 arcmin wide. North is at the top and east is to the left. The white '×' marked on the image is the centroid position at  $12^h27^m28^s.46 + 13^\circ33'04''.3$ . The object sits in sub-frame 22 (project identifier 22-5) and may be compared with Figure 5.6 (p.101), which shows its position in the sub-frame. A satellite trail residual is visible running vertically through the image.*

telescope at Kitt Peak National Observatory. It does not appear to have a massive hydrogen component, as a search at its location in the HI Parkes All-Sky Survey (HIPASS) online catalogue shows only local emission typical of any region of the Milky Way. Follow-up analysis remains as a future project.

### 6.4 *Faint Galaxy Haloes*

Two large galaxies visible in the Virgo Deep Stack were studied by David Malin using photographic amplification techniques. One of these is M89, a prominent member of the Virgo Cluster. The other is Malin 1, a much more distant object, discussed in depth in Chapter 7.

M89 exhibits shells, as seen in a number of elliptical galaxies and reported on by Malin (1979) and Malin and Carter (1983). M89 also exhibits a ‘jet’ of material, most likely the remnant of an earlier interaction with another galaxy. The shells and jet are readily apparent in the Virgo Deep Stack, where the galaxy is well-placed in an unvignetted portion of the image, and may be displayed and studied in new detail at various contrast levels (refer Figure 6.10). These images clearly show the features identified by Malin (1979), i.e. the jet (A), arcs B and C, condensation D, the E feature (a separate galaxy - VCC 1613) and the F arc.

The new data show that starlight extends somewhat further than was revealed in the earlier images. The Virgo Deep Stack images show, for the first time, a virtually complete shell of light at the radius of the F arc identified by Malin (1979).

Starlight extending beyond that measured in previous observations is also observed in the distant galaxy Malin 1, where the optical light is found to correspond well with the HI extent of the galaxy (refer Chapter 7). Following this success, the Virgo Deep Stack was examined for any light corresponding to the location of the reported ‘gas galaxy’, HI21 ( $12^h17^m51^s +14^\circ46'31''$ , J2000). This dark hydrogen cloud in the Virgo Cluster described by Minchin et al. (2005) was shown by Haynes et al. (2007) to be tidally linked to NGC 4254 (M99). Minchin et al. (2005) failed to find any optical counterpart to a surface-brightness level of  $27.5 B_\mu$ . Visual



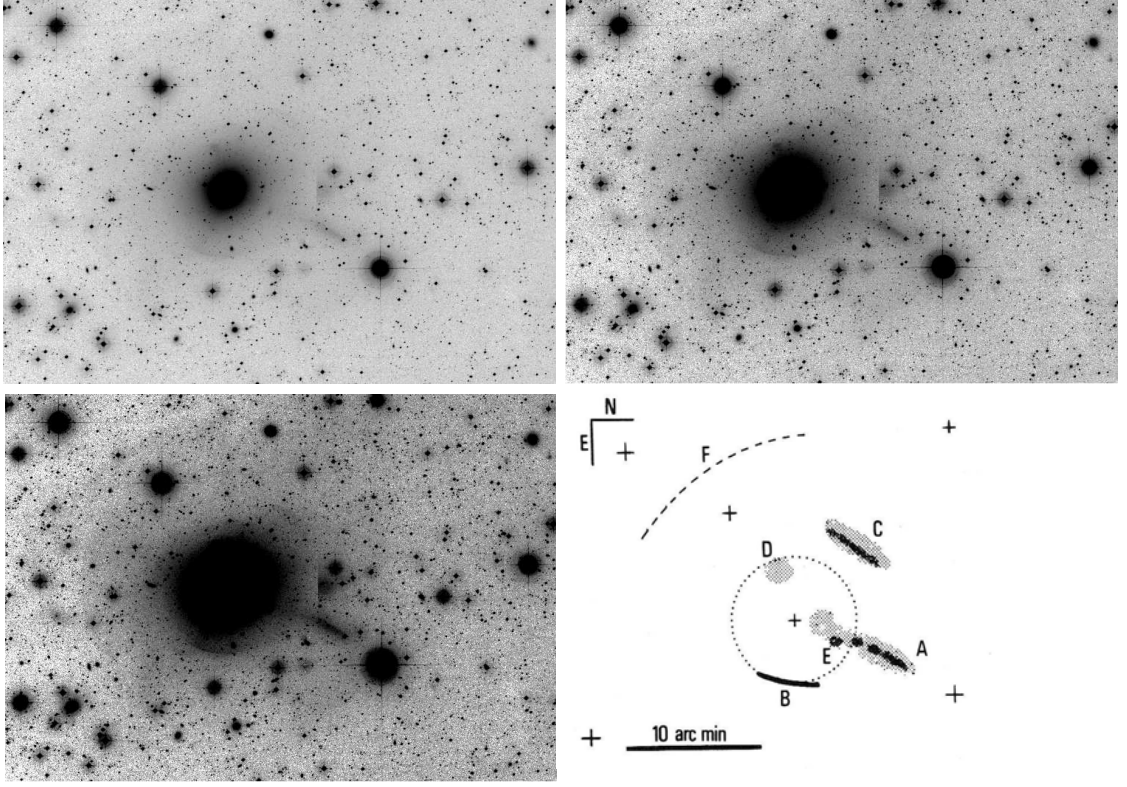


Fig. 6.10: M89 Shells

*Shells around M89 reported on by Malin and Carter (1983) are seen here in new detail. A vertical feature just above the jet in these images is an artefact due to the scanning of the original films in lanes. At this location the intensity scaling is not perfectly matched on both sides of one lane division.*

*Top Left: The image shows the B and C arcs, the D condensation and jet A.*

*Top Right: The outer F shell becomes apparent and is seen to extend around the galaxy to the east.*

*Bottom Left: The F shell continues below the galaxy.*

*Bottom Right: Diagram reproduced from Malin (1979).*

inspection of the Virgo Deep Stack also showed no surface-brightness enhancement at that location. Unfortunately, the region does not lie in the optimum part of the Virgo Deep Stack, but is located in the upper right corner where vignetting cuts in. No surface photometry in this region has been performed so the surface-brightness limit of this part of the image is unknown.

### 6.5 *Intra-Cluster Light*

A deep CCD image by Mihos et al. (2005) of a region covering approximately  $1.5 \times 1.5$  degrees of the Virgo Cluster displays extended galaxy haloes, tidal tails and diffuse intra-cluster light. Many features noted in that image are also discerned in the Virgo Deep Stack. To display these features it is necessary to use appropriate display levels and large-scale features become more obvious using ‘tophat’ smoothing with a 7-pixel kernel radius. Figure 6.11 shows a portion of the Virgo Deep Stack that overlaps with the Mihos et al. (2005) data and displays in detail the central portion of Figure 5.5 (p.99) which covers the entire image. These are negative images so galaxies, stars and intra-cluster light appear dark. Specific features detectable in the Virgo Deep Stack are those labelled by Mihos et al. (2005) (refer Figure 6.12) as the A and B streamers extending to the north-west of M87, the D, E, F, L2 and L3 tidal plumes, and the extensive galaxy haloes I, J and M.

The Virgo Deep Stack does not show the small H feature, probably because of vignetting. The curve marked C by Mihos et al. (2005) is obscured by the impression from the mandrel. The feature marked by Mihos et al. (2005) as the G tidal plume and described as extending from IC 3349 southwards does not connect in the Virgo Deep Stack image (refer Figure 6.13 for detailed image).

The K crown of diffuse light to the north of the M84-M86 (J) region shows up in Figure 6.11 as a complex mottled region. Between the J and K regions this figure also shows two sawtooth-shaped prominences that are not evident in the Mihos et al. (2005) data. However, the L1 feature, described by the author as a filament, does not appear to be detectable in the Virgo Deep Stack.

Some features identified by Mihos et al. (2005) do not appear distinctly in this image but the Virgo Deep Stack does appear to show details missed by Mihos et al. (2005), demonstrating that the difference in limiting magnitudes is marginal. The Mihos et al. (2005) image reaches  $28.5 V\mu$ , which appears consistent over the entire image, whereas vignetting means that some parts go slightly deeper than others in this region of the Virgo Deep Stack.

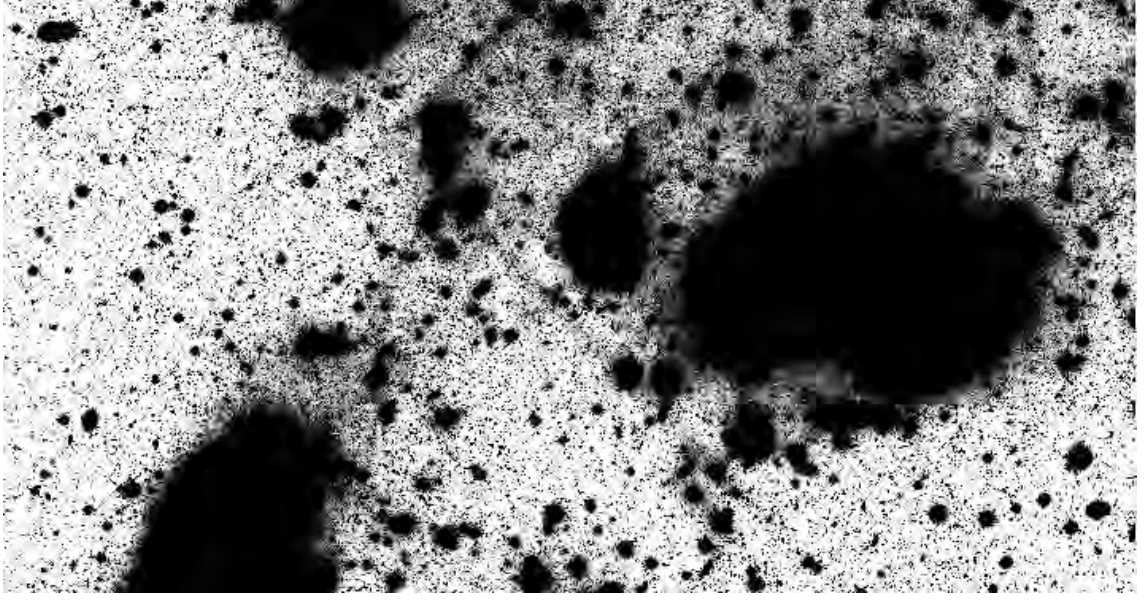


Fig. 6.11: Intra-Cluster Light in the Heart of the Virgo Cluster

*Intra-cluster light in the Virgo Deep Stack (pictured) is comparable with that detected by Mihos et al. (2005). The diagonal features due to the mandrel cross over in the upper left of the image. Refer text for full description.*

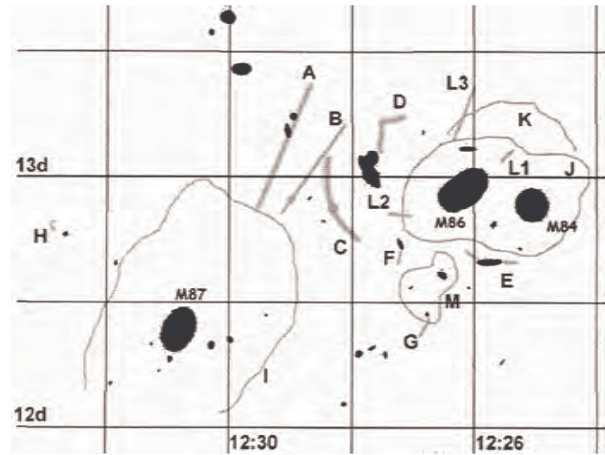


Fig. 6.12: Diffuse Intra-Cluster Features

*This diagram covers the same region as Figure 6.11 and shows features detected by Mihos et al. (2005) that are referred to in the text.*

Figure reproduced from Mihos et al. (2005).



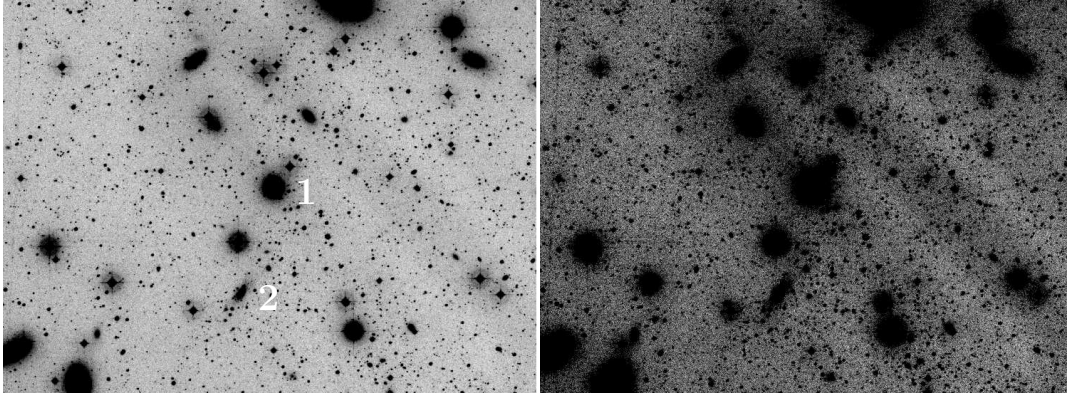


Fig. 6.13: IC 3349 - No Tidal Tail

*The region surrounding IC 3349 at normal contrast (left) and high contrast (right). Just above centre is galaxy IC 3349 (labelled 1). Below it is the galaxy catalogued V8L19 by Impey et al. (1988), labelled 2 in the left-hand image and diagonally elongated in the right-hand image. Mihos et al. (2005) detected a tidal tail extending from IC 3349 southward (the G feature of Figure 6.12), but in the Virgo Deep Stack no tidal tail is evident. Images measure approximately  $26.5 \times 19$  arcminutes. North is at the top and east is to the left. The diagonal features running from top centre to lower right are due to the mandrel.*

In consideration of the vignetting problem demonstrated by this comparison, clearly the most significant portion of the Virgo Deep Stack, with regard to intra-cluster light, is that part least affected by vignetting. From Figure 5.5 (p.99), it may be observed that the north-west quadrant, which appears grey in the false-colour image, deserves special attention.

A detail of this section is shown in Figure 6.14. The upper image is displayed at high contrast, but with green contours overlaid at 6580 data counts to highlight the low surface brightness features. The lower image is the same image at normal contrast and is overlaid with reference information described in the following text.

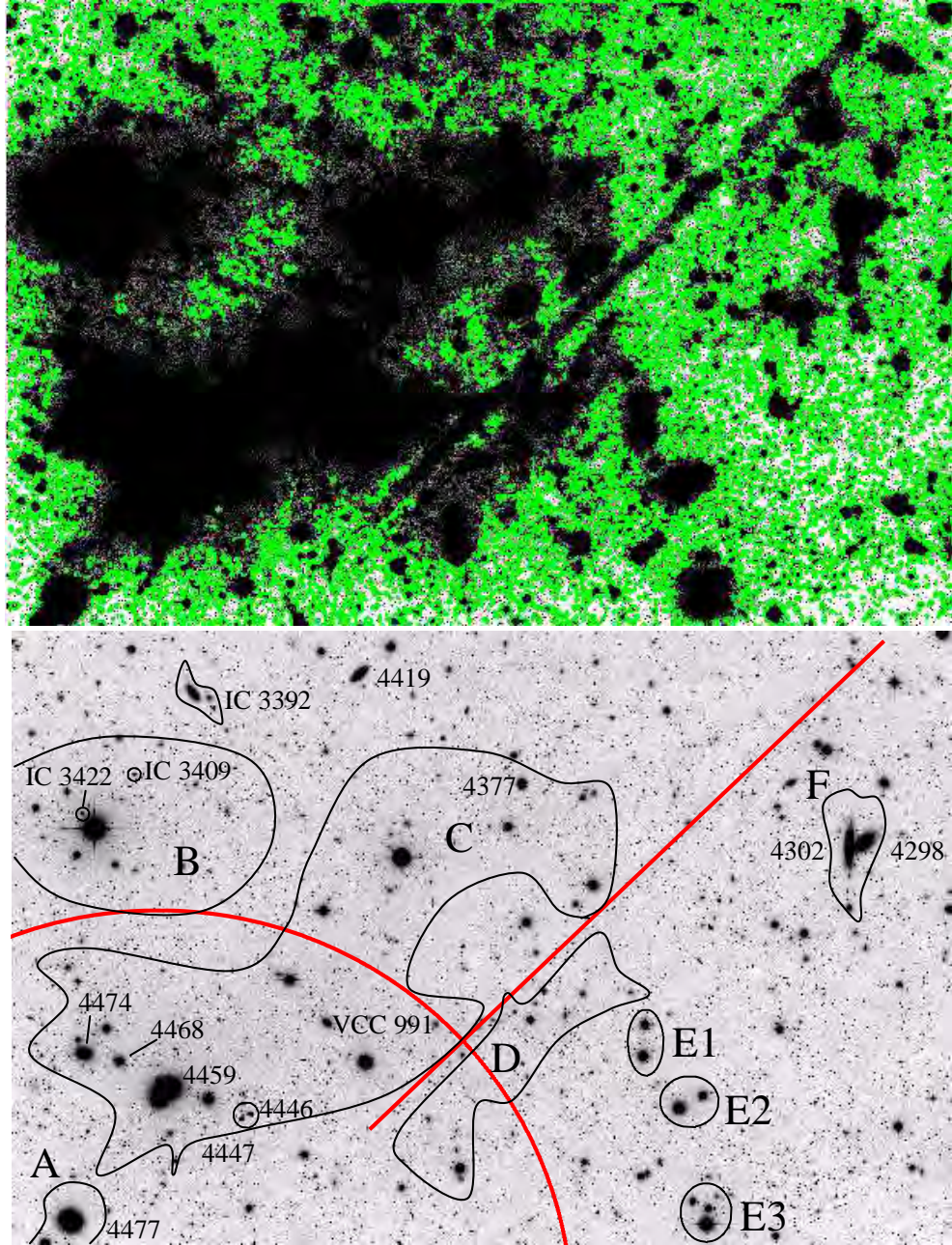


Fig. 6.14: Intra-Cluster Light - NW Quadrant

*Top:* This detail of the north-west quadrant of the Virgo Deep Stack shows dense shrouds of intra-cluster light surrounding numerous galaxies at lower left. Some of the light blooms in the rest of the image are due to bright stars. *Bottom:* Specific features are labelled in this reference image. Images measure approximately  $2.2 \times 1.5$  degrees. North is at the top and east is to the left. Marks due to the mandrel are shown in red. Refer text for a full description.

Unfortunately, in this region, there are many bright stars that bleed light into the photographic image. The positions of the stars are evident from the diffraction spikes in the lower image. This means that it should not be assumed that all the blooms are due to intra-cluster light, as some patches are due to the meeting up of the faint tails of the Gaussian point-spread functions of the stars. However, by comparing features at various contrast levels it is possible to deduce the nature of the light in each region.

The strong diagonal streak is again due to the mandrel, as is the large ring arcing around the lower left corner of the image. These features are drawn in as thick red lines (but not labelled) in the reference image. Region A is the extended halo of galaxy NGC 4477. The left part of region B contains a lot of scattered light from the bright star adjacent to galaxy IC 3422 but the remainder of this region, and the light bridge joining it to region A, appear to be true intra-cluster light. The denser portions of the centre and upper right sections of the complex C region are predominantly starlight with contributions from galaxies NGC 4377 and VCC 991. However, the light in the lower left section is almost all due to the shared halo from galaxies NGC 4474, 4468, 4459, 4446 and 4447, with a contribution from the star adjacent to galaxy NGC 4459.

The light in the less-dense peripheral regions of the C complex appears to be due to diffuse intra-cluster light. The less-dense portions of the D region are also probable intra-cluster light, but the more dense patches and the three ellipses marked E1, E2 and E3 may be seen to correspond with stars.

The F region is a blend from galaxies NGC 4302 and 4298 and stars to the south of the pair. A close-up of NGC 4302 does show some apparent broadening of the northern part of the disk (refer Figure 6.15) comparable with David Malin's deep image ([http://www.aao.gov.au/images/deep\\\_html/n4298\\\_d.html](http://www.aao.gov.au/images/deep\_html/n4298\_d.html)). It is unclear from this image if this broadening is genuinely part of the galaxy, perhaps due to a tidal perturbation or supernova blow-out, or is a separate superimposed LSB galaxy. The remaining dense circular patches of Figure 6.14, particularly across the top of the image, are due to stars. No significant tidal streamers are seen in this



field, but the extensive galaxy haloes are consistent with those seen in Figure 6.11.

It is important to realise how much the presence of light blooms from stars in wide-field photographic images may affect the appearance of low surface brightness features. Resolved stars, themselves, may be misinterpreted. For example, the region surrounding IC 3392 in Figure 6.14 appears at large scale to include tidal extensions off the ends of the galaxy, but a high-resolution close-up view (refer Figure 6.16) reveals a smattering of stars to the north and several more bright stars to the south of the galaxy. When pushed to high contrast with smoothing applied, these features simply join up to masquerade as tidal tails.

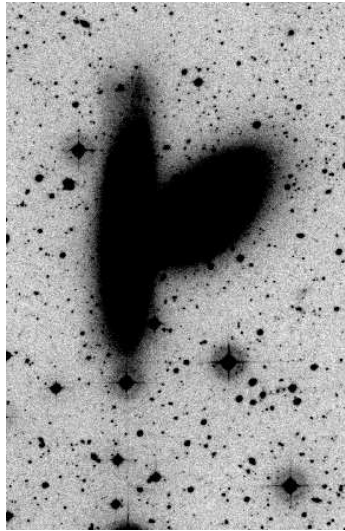


Fig. 6.15: NGC 4302 - Disk Broadening in the Deep Image

*Galaxy NGC 4302 is the edge-on spiral galaxy at left of image. It shows some apparent broadening of the northern part of its disk, perhaps due to tidal perturbation or supernova blow-out. NGC 4298 is the elliptical galaxy on the right. The image measures approximately  $10 \times 16$  arcminutes. North is at the top and east is to the left.*

Figure 6.17 shows a detail of the F feature of Mihos et al. (2005) which, it is suggested, is a tidal tail to the south of the galaxy NGC 4425. In the Virgo Deep Stack, it is seen to be a distinct LSB galaxy that may be interacting with NGC 4425. It has, in fact, already been catalogued as VCC 989. In the same figure, the nearby

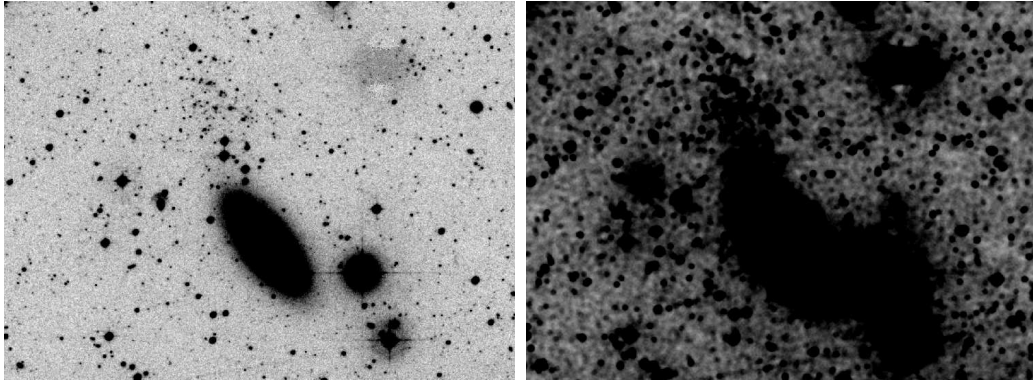


Fig. 6.16: IC 3392 - Stars Masquerade as Tidal Tails

*IC 3392 seen (left) at normal contrast and (right) at high contrast with smoothing applied. In the right-hand image, light blooms from the stars to the north-east and south-west of the galaxy join up to masquerade as tidal tails. The patch at upper right of the image is an artefact. Images measure approximately  $13 \times 10$  arcminutes. North is at the top and east is to the left.*

galaxy IC 3363 at first glance also appears to have a tidal tail to its north (not detected by Mihos et al. (2005)), but in the close-up image it is discerned as the newly-identified LSB galaxy 16-37 (refer also Figure 8.14).

It is evident that much of the intra-cluster light visible in the Virgo Cluster is due to large extended galaxy haloes readily seen in deep images. Whilst not as extreme as the case reported by Gonzalez et al. (2000b), where a single galaxy in Abell 1651 contributes all but 5% of the intra-cluster light, the numerous bright galaxies of the Virgo Cluster do make the major contribution. However, some of the diffuse light is not directly associated with particular galaxies and must be attributable to other sources such as intra-cluster stars and planetary nebulae that have been stripped in galaxy-galaxy encounters and are now free-floating. The appearance of many tidal features is evidence of the dynamic environment of the Virgo Cluster that is continuously reshaping the galaxies that move through it. It is also clear that previously unrecognised LSB galaxies may also be contributing to what may be misinterpreted as tidal filaments or intra-cluster light.



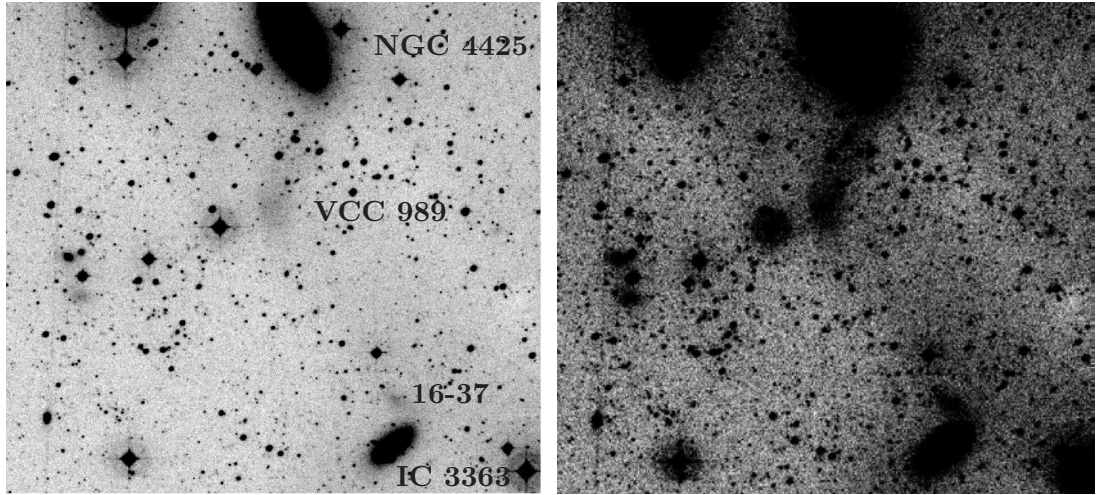


Fig. 6.17: NGC 4425 and VCC 989 - An Interacting Pair?

*Two images of the same region at different contrast. Beneath galaxy NGC 4425 (top centre of images) is the feature labelled *F* by Mihos et al. (2005) and described as a tidal tail but it is, in fact, VCC 989. From the high-contrast image (right) it appears possible that the two galaxies are interacting. Just above the smaller galaxy IC 3363 (bottom right) is a newly-identified LSB galaxy, 16-37 of this project, which may also be mistaken for a tidal tail. Images measure approximately  $14 \times 12.5$  arcminutes. North is at the top and east is to the left. Once more, the diagonal LSB feature from upper left to lower right is due to the mandrel.*



## 7. MALIN 1

Malin 1 is a famous giant LSB disk galaxy that lies at a distance of 330 Mpc  $h_{75}^{-1}$  and falls within the area covered by the Virgo Deep Stack. It has a  $M_{HI}/L_B$  ratio of  $> 3$ . This is high compared with typical values for spiral galaxies which range from 0.1 to  $\sim 1$  (Phillipps 2005). However, accurate measurements of HI mass rely both on HI observations and on a good knowledge of the inclination of the galaxy, usually derived from an optical image. Uncertainty in measurements of the inclination of this galaxy has, in the past, been high due to the very low surface brightness of the disk of the galaxy (e.g. Pickering et al. (1997) quote  $45 \pm 15^\circ$ ). The Virgo Deep Stack image has now provided the opportunity to make new deep measurements of the optical properties of Malin 1.

### 7.1 *New Measurements*

Using the Virgo Deep Stack, it is possible to detect light beyond the extent seen previously and to refine the inclination measurement. An ellipticity measurement was derived by averaging the axis ratios of ellipses fitted by eye to contour plots. This method is illustrated in Figure 7.1 and was necessary because the `ELLIPSE` routine in `IRAF` fails to trace the isophotes automatically due to the faintness of the galaxy's disk. Once derived, the ellipticity and position angle were held fixed to obtain the radial profile.

Inclination  $i$  was derived from the ellipse axis ratio  $b/a$  by assuming the galaxy is an oblate spheroid. The original Holmberg (1958) relation is:

$$\sin^2 i = \frac{(b/a)^2 - p^2}{1 - p^2} \quad (7.1)$$

where  $i$  is the inclination of the principal plane to the line of sight,  $b/a$  is the ratio of apparent minor and major diameters and  $p$  is the ratio of the smallest to largest axis of the spheroid. This last term is known to vary by galaxy type. For the analysis of Malin 1, a value of  $p = 0.2$  was applied. If  $i$  is zero, the galaxy is viewed edge-on. The inclination of Malin 1, calculated from the ellipticity measurements of the Virgo Deep Stack image described above, was found to be  $38 \pm 3^\circ$ .

It was also possible to relate the extent of this optical light to independent HI observations. The main finding from the image data is that the light (i.e. detectable visible emission from stars) corresponds fully with the gaseous extent of the galaxy and hints at spiral structure, both in the denser inner region and in the outermost extremities of the galaxy. The rotation direction discerned from the Virgo Deep Stack image corresponds with that revealed in a recent HST image of the inner disk of Malin 1, reproduced from Barth (2007) in Figure 7.2.

The results gleaned from the Virgo Deep Stack image were published in Moore and Parker (2006) with figures that display the optical extent of the galaxy and a new radial profile. That paper is reproduced in Section 7.2, presented in the format of the final publication in *Publications of the Astronomical Society of Australia*.<sup>a</sup> The figures reveal what appears to be a dusty outer spiral arm and a diffuse lobe to the north of the galaxy which may be evidence of an interaction.

Subsequent to that publication, the galaxy was studied in infrared by Rahman et al. (2007). The non-detection of the diffuse optical disk in mid- and far-infrared indicates that the galaxy contains only very cold dust ( $T < 10$  K) or no dust at all.

Sancisi and Fraternali (2007) compared the radial profile from Moore and Parker (2006) with a re-analysis of the HI data from Pickering et al. (1997) and found a ‘maximum disk’ mass-to-light ratio of  $M_{HI}/L = 5.2$ , which is in the range of values found for luminous early-type galaxies. The authors concluded that the rotation curve shows a close correlation with luminosity, i.e. the gas mass follows the light.

---

<sup>a</sup> This paper was written by me with guidance, encouragement and constructive criticism from my supervisor, Quentin Parker. We also thank the referees for their helpful suggestions.

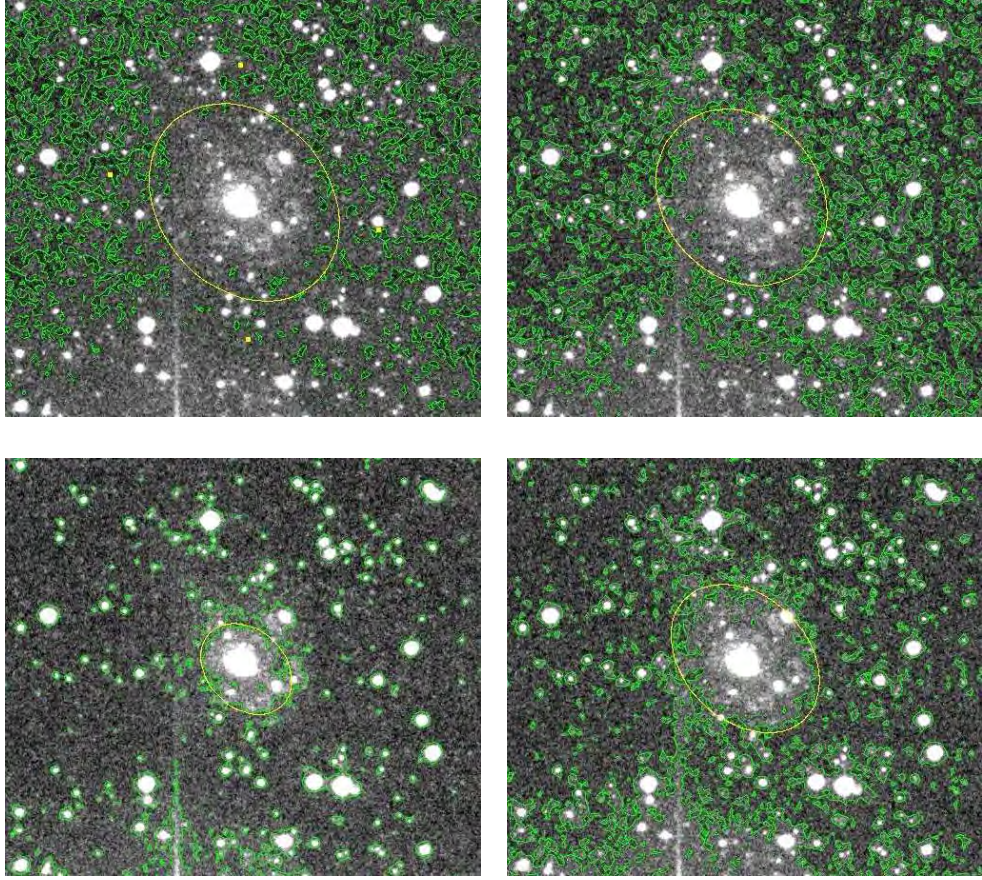


Fig. 7.1: Fitting Ellipses to Contours of Malin 1

*These figures illustrate how ellipses were fitted by eye to contour plots to establish the ellipticity of the giant LSB galaxy, Malin 1. Contours shown in these four frames are at (clockwise from top left) 6360, 6380, 6400 and 6440 data counts. Images measure  $5'36''$  across. North is at the top and east is to the left.*

The new radial profile was also used by Mapelli et al. (2008) to compare with simulations that illustrate that collisions consistent with CDM cosmology may, in the first 100-200 Myr, form ring galaxies (like the Cartwheel Galaxy) that later evolve into giant LSB galaxies over timescales of 1.0 to 1.4 Gyr. Simulations were used to study the effects of the collision of an intruder dark matter halo with a progenitor galaxy containing a stellar bulge, stellar disk, gas disk and dark matter halo. The



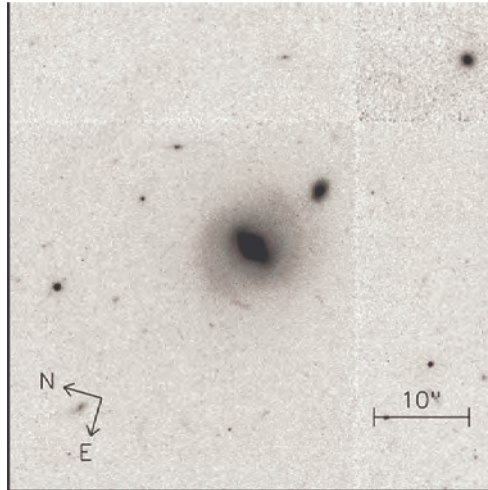


Fig. 7.2: The Inner Disk of Malin 1

*This HST I-band image clearly illustrates the spiral structure of the inner disk of Malin 1.*

Figure reproduced from Barth (2007).

result of the simulation is a match to the radial profile of Malin 1 in overall shape and extent, reaching 150 kpc radius after 1.4 Gyr, but with some fluctuations that are not evident in the observed radial profile. The authors attribute the discrepancies to density fluctuations in the model. Further, no spiral arms are seen in the model, possibly due to lack of numerical resolution. However, the authors suggest that a secondary ring, produced by the simulation, may be deformed by disk rotation and observationally confused with a spiral arm. The success of the model is that it reproduces, for the first time, a galaxy with a disk resembling that of Malin 1 from initial conditions consistent with CDM cosmology.

## 7.2 *Malin 1: A Deeper Look (Moore and Parker 2006)*

Refer following pages.

## Publication

Due to copyright restrictions, the article that appeared on the following pages has been omitted from this thesis. Please refer to the link below for the abstract details and access to the article.

Moore, Lesa & Parker, Quentin A. (2006). Malin 1: a deeper look. *Publications of the Astronomical Society of Australia*, 23(4), 165-169.

<http://dx.doi.org/10.1071/AS06022>













## 8. THE VIRGO DEEP STACK CATALOGUE

This catalogue contains data for all the galaxies that were identified during this project which were, at the time they were detected, new discoveries. Most have not been catalogued elsewhere. Three galaxies (refer Figure 8.15) have since been identified by other authors and established as Virgo Cluster members. Although a few galaxies in the catalogue are brighter, most are VLSB galaxies. Classifications of the galaxies according to surface brightness and cluster-membership assignment, based on morphology and scale length, are discussed in Sections 8.1, 8.2 and 8.3.

Positions of the newly-identified galaxies are plotted in Figure 8.1 and the galaxies are listed in Table 8.2 (refer Section 8.4) along with derived parameters.

Images and radial profiles appear in Section 8.5. All images have north at the top and east to the left. Profiles have *OR* surface brightness in magnitudes per arcsec<sup>2</sup> on the *y*-axis and semi-major axis in arcseconds on the *x*-axis.

Supporting data are provided separately on CD. The files included on CD are those containing the surface photometry tables (**.tab** and **.txt** files), masking data (**.fl** files), radial profile data with plots (**.xls** files) and images (**.fits** and **.jpeg** files). All the data necessary to reproduce the tabulated results (background measurements, galactic extinction terms, ellipticity and position angle settings, *x0* and *y0* positions and pixel values of the profiles) may be found within the CD file set included inside the back cover of this thesis.

### 8.1 Surface Brightness Classification

Classifications of galaxies as LSB or VLSB are based on the definitions at the beginning of Chapter 2. Ignoring any small modification for the *OR* passband and assuming the  $B - R$  correction of  $\sim 1.5$ , this means LSB galaxies are those with  $\mu_0 \geq 21.5 R\mu$  and VLSB galaxies have a mean surface brightness of  $\langle \mu \rangle \geq 25 R\mu$  within a 12-arcsec radius. Since the galaxies of interest have exponential surface brightness profiles (linear on these magnitude-radius plots), the latter criterion may be ascertained based on the following argument. Assuming a galaxy at least fills a 12-arcsec radius then, within that radius  $r_{12}$ , if half the area of the galaxy has surface brightness higher and half has surface brightness lower than the threshold, the average will equal the threshold. Hence, simply checking where the  $25 R\mu$  gridline intersects with a critical radius  $r_c$  (the radius that divides an inner circle and an outer annulus with equal areas) will quickly classify the galaxy. That critical radius is found from the relations:

$$\begin{aligned} \text{Total area } (\pi r_{12}^2) &= \pi \times 12^2 \approx 452 \text{ arcsec}^2 \\ \pi r_c^2 &= \pi(r_{12}^2 - r_c^2) \\ 2r_c^2 &\approx 452/\pi \\ r_c &\approx 8.485 \end{aligned}$$

Thus if the galaxy is brighter than  $25 R\mu$  beyond approximately 8.5 arcsec, it is classified LSB and if it dips below  $25 R\mu$  at a smaller radius, it is classed as VLSB.

## 8.2 *Morphological Classification*

Of the newly-identified galaxies, those that have distinct elliptical, lenticular or spiral shapes (as distinct from the typical round appearance of an LSB dE, dI or dSph galaxy) are classified as E, S0 or S. The morphology criteria are: distinct elongation indicating an elliptical galaxy with small scale length (E or E/S0); symmetrical extensions or concentrations indicating a spiral galaxy with small scale length (S, Sc or Sbc); elongation but with insufficient resolution to discern if the galaxy is an edge-on spiral, E or S0 type (VLSB).

The bulk of the catalogue contains galaxies with dE, dI or dSph morphology. These have not been explicitly categorised as such, but due to their low surface brightness may be considered to be LSB or VLSB dSph galaxies.

### 8.3 Cluster-Membership Classification

The galaxies that have been morphologically classified as elliptical or spiral are deemed to be background galaxies due to small angular size and small scale length which, in the case of spiral or elliptical galaxies, usually implies that they lie at large distances. In the absence of distance information, there is no way of knowing for certain if the apparent LSB and VLSB dwarfs (the majority of the newly-identified galaxies) are cluster members or background galaxies. Absolute magnitudes shown in Table 8.2 presume cluster membership for LSB and VLSB galaxies of any scale length, unless classified morphologically as background objects. In Section 9.1, the use of scale length as a distance indicator is discussed. Because of the relevance of scale length, the image and radial profile figures in Section 8.5 are organised by broad membership probability based on morphological classification and scale length. The high quality of the data supports the use of a small scale-length division (say 1.5 arcsec, based on data in Table 4.3 p.69) between members and non-members. However, a 3-arcsec cut-off is in keeping with the Rines-Geller threshold which is well-supported by spectroscopic distance determinations. Therefore, categories have been assigned as follows:

Membership Classification	Scale length range (arcsec)	Count in Catalogue	Corresponding Figures
Presumed foreground	$a \sim 213$	1	8.2
Background E, S0, S	$a \leq 5.7$	17	8.3, 8.4
<i>dSph galaxies:</i>			
Possible cluster member	$1.5 \leq a \leq 2.9$	27	8.5 - 8.7
Probable cluster member	$3.2 \leq a \leq 4.8$	21	8.8 - 8.10
Presumed cluster member	$4.8 < a \leq 59$	34	8.11 - 8.14
Verified cluster member	$3.7 \leq a \leq 13.8$	3	8.15
Total in catalogue		103	

Tab. 8.1: Cluster Membership Classifications



## 8.4 Galaxy Positions and Measured Properties

All catalogued galaxies are plotted in Figure 8.1. The data table following contains the measured parameters of all these galaxies, as well as those used in the comparisons in Section 6.2.

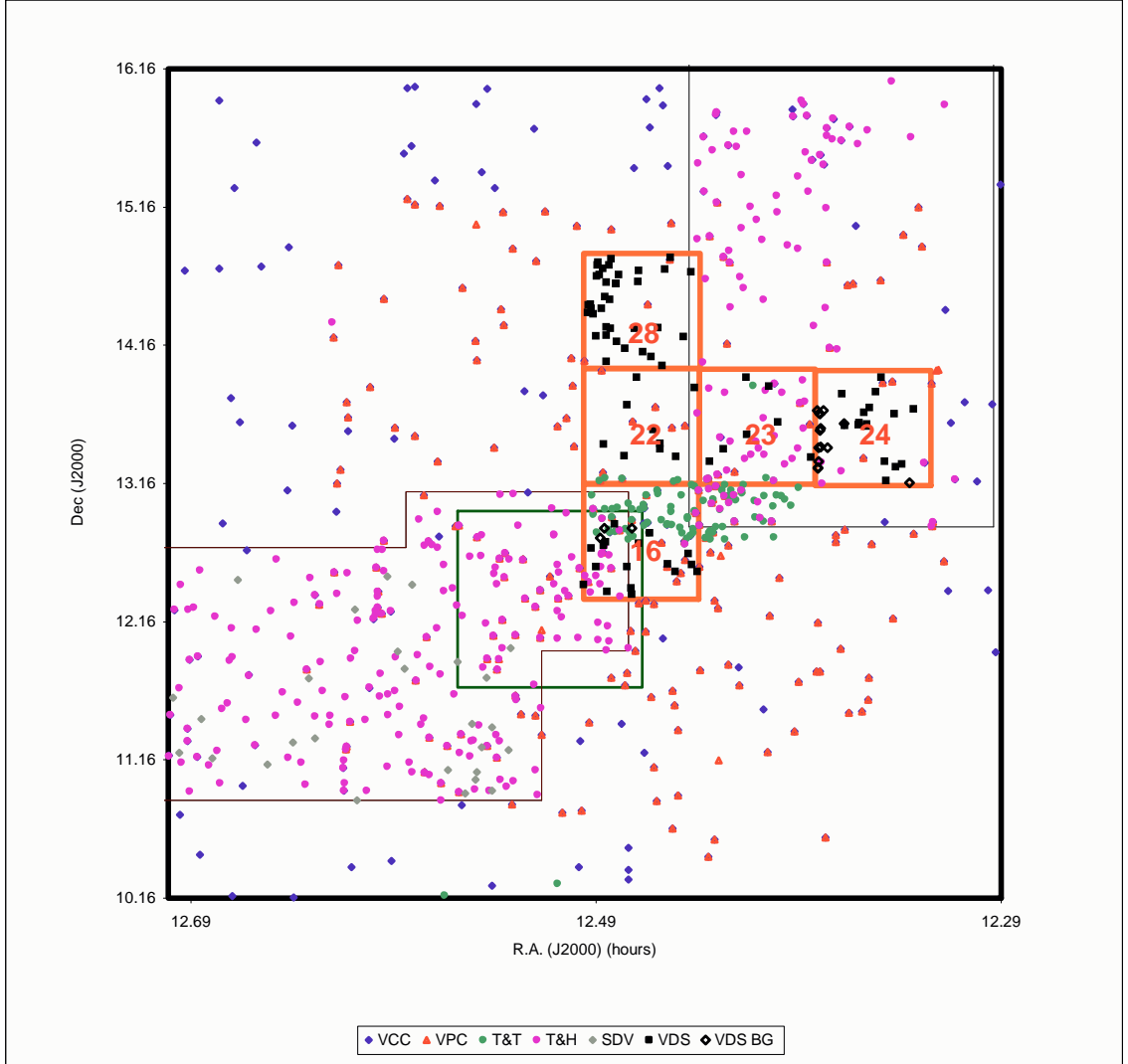


Fig. 8.1: Map 5: Galaxies in the Virgo Deep Stack

*Galaxies catalogued in this project are plotted as black symbols (VDS). Those classified as morphologically-assessed background objects are shown as open diamonds. Possible and probable cluster members are shown as solid squares. Data from other surveys are included, as in Figure 6.2. The region covered by this map is identical to that covered by the Virgo Deep Stack.*

Table columns contain data as follows:

1. ID number in this catalogue or other designation if from a previously-published catalogue. (Cross-reference to Figure with image and radial profile for newly-identified galaxies.)
2. Classifications: Bg = background (based on morphology); brightness classifications are Br (bright), L (LSB), otherwise VLSB; morphologies are E (elliptical), S0 (lenticular), Sbc and Sc (spiral), dI (dwarf irregular), dE (dwarf elliptical), otherwise dSph; N = not classified; Blank = VLSB dSph. Identifiers from Caldwell (2005) and the notation *DWC* for Durrell et al. (2007) are included in three cases where galaxies were independently identified.
3. RA (hh mm ss.ss, J2000.0)
4. Dec (dd mm ss.s, J2000.0)
5. Ellipticity
6. Position angle (degrees)
7. Extrapolated central surface brightness ( $\mu_0$  in *OR*-band,  $\pm 0.1\mu$ ) for LSB and VLSB galaxies where an exponential is a good fit; otherwise peak surface brightness of the radial profile where an exponential fit is not appropriate.
8. Scale length (arcsec,  $\pm 13\%$ ) for LSB and VLSB galaxies where an exponential fit is appropriate; otherwise blank.
9. Maximum semi-major axis of profile-fitting function (arcsec). This value indicates the angular size of the galaxy.
10. Surface brightness at maximum semi-major axis ( $\mu_{max}$  in *OR*-band). This value is indicative of the limiting surface brightness of the detections.
11. Apparent magnitude (*OR*,  $\pm 0.3$  magnitudes) for LSB and VLSB galaxies where an exponential fit is appropriate; otherwise blank.
12. Absolute magnitude ( $M_{OR}$ ,  $\pm 0.3$  magnitudes) based on apparent magnitude, *R*-band Galactic extinction from NED and a distance modulus of 31.1. Blank for galaxies that are classified as background galaxies.

Tab. 8.2: Measured Galaxy Data

(1) ID (Fig.)	(2) Class.	(3) RA	(4) Dec	(5) $e$	(6) $pa$	(7) $\mu_0$	(8) $a$	(9) $r_{max}$	(10) $OR_{max}$	(11) $OR$	(12) $M_{OR}$
TT V54	dI	12 26 17.2	12 48 03	0.3	-48	25.7	11.5	31	28.8	18.4	-12.8
TT V57	dI	12 29 17.0	13 04 46	0.1	10	26.4	17.2	34	28.5	18.3	-12.9
TT V61	dE	12 27 14.1	12 53 55	0.1	10	24.8	7.6	23	29.1	18.4	-12.7
TT V63	dI	12 26 56.6	12 59 40	0.3	45	25.7	17.2	37	28.0	17.5	-13.6
TT V66	dI	12 26 27.8	12 45 50	0.3	80	25.7	10.4	31	29.4	18.6	-12.6
SDV 144	dE/I	12 38 40.6	11 58 40	0.1	80	25.3	13.1	28	27.9	17.7	-13.5

continued on next page

Tab. 8.2: *continued*

(1) ID (Fig.)	(2) Class.	(3) RA	(4) Dec	(5) $e$	(6) $pa$	(7) $\mu_0$	(8) $a$	(9) $r_{max}$	(10) $OR_{max}$	(11) $OR$	(12) $M_{OR}$
16-1 (8.7)	Bg Sbc Bg E/S0/S	12 29 31.46	12 25 40.1	0.42	-16.5	24.0	2.8	4.6	26.9	19.8	-11.4
16-2 (8.5)		12 29 18.36	12 41 45.7	0.4	86	23.9	2.1	8.9	28.6	20.2	-10.9
16-4 (8.13)		12 29 09.65	12 33 30.5	0.55	-69	25.5	9.4	26	28.6	18.6	-12.6
16-6 (8.3)		12 29 02.77	12 46 10.5	0.11	-34	22.7	2.1	6.7	28.2	20.2	—
16-9 (8.4)		12 28 54.96	12 50 24.7	0.67	47.5	24.6	5.4	26	29.8	18.9	—
16-10 (8.8)		12 28 52.78	12 44 12.3	0.15	63	24.1	3.9	13	27.1	19.2	-11.9
16-11 (8.8)		12 28 56.12	12 42 51.5	0.17	34.5	24.7	3.8	11	27.6	19.8	-11.4
16-12 (8.5)		12 28 49.91	12 22 52.1	0.3	6	23.8	2.1	6.7	27.9	20.3	-10.9
16-16 (8.13)		12 28 37.22	12 52 03.3	0.3	-60	25.5	13.5	33	27.8	17.9	-13.3
16-19 (8.15)		12 28 15.15	12 33 37.1	0.3	56	24.1	3.7	11	27.9	19.3	-11.9
16-20 (8.5)	DWC	12 28 06.72	12 21 42.0	0.03	13.4	24.5	1.9	5.6	28.8	21.1	-10.1
16-21 (8.6)	Bg Sc	12 28 07.84	12 24 08.3	0.21	36	24.2	2.4	9.8	30.0	20.3	-10.9
16-23 (8.3)		12 28 05.94	12 50 14.5	0.15	-9	23.0	2.4	12	28.5	19.1	—
16-25 (8.5)	SW2 lsb31	12 27 54.16	12 43 45.7	0.24	16	22.6	2.1	12	29.3	19.0	-12.2
16-31 (8.12)		12 27 34.22	12 48 19.1	0.1	80	25.0	7.8	26	30.4	18.6	-12.6
16-37 (8.14)		12 27 02.35	12 34 50.1	0.2	70	24.9	16.6	34	27.0	16.8	-14.4
16-41 (8.13)		12 26 48.89	12 31 35.3	0.2	-60	25.3	11.3	26	27.8	18.0	-13.2
16-43 (8.11)		12 26 26.23	12 39 09.7	0.2	-60	24.2	5.8	13	26.7	18.4	-12.8
16-45 (8.15)		12 26 20.10	12 34 29.2	0.1	10	24.8	9.5	31	29.4	17.9	-13.3
16-46 (8.11)		12 26 10.17	12 31 19.9	0.1	45	24.5	6.7	16	26.8	18.3	-12.8
22-1 (8.12)	L N N lsb10	12 28 14.32	13 43 42.0	0.35	-49	24.3	7.3	31	29.3	18.0	-13.2
22-2 (8.11)		12 28 56.23	13 26 39.4	0.3	41	24.3	6.4	28	28.7	18.3	-12.9
22-3 (8.12)		12 28 20.18	13 21 35.9	0.06	-20	25.6	—	26	29.7	—	—
22-4 (8.13)		12 27 57.25	13 55 51.6	0.05	51	23.9	9.1	26	26.9	17.1	-14.1
22-5 (8.2)		12 27 28.46	13 33 04.3	0.66	30	25.2	213	396	27.4	11.6	—
22-6 (8.12)		12 27 15.46	13 24 43.9	0.2	61	24.6	7.1	26	28.7	18.4	-12.8
22-7 (8.13)		12 27 15.80	13 26 58.8	0.2	-80	25.3	12.9	34	28.7	17.8	-13.4
22-8 (8.15)		12 26 48.34	13 21 24.0	0.3	-80	25.9	13.8	31	27.6	18.2	-13.0
22-10 (8.12)		12 26 14.53	13 51 10.5	0.2	70	25.1	7.8	31	29.5	18.7	-12.5
23-1 (8.12)		12 25 47.74	13 19 09.4	0.2	-10	25.0	7.4	26	31.1	18.7	-12.5
23-3 (8.11)		12 25 23.41	13 24 46.0	0.12	42	24.6	5.2	21	29.1	19.0	-12.2
23-6 (8.14)		12 24 41.35	13 30 54.7	0.1	10	25.7	41	66	27.5	15.6	-15.6
23-9 (8.9)		12 24 42.44	13 55 39.4	0.1	-4	24.7	4.4	14	28.5	19.5	-11.7
23-14 (8.14)		12 23 47.17	13 36 13.6	0.1	-10	25.5	15.4	50	29.1	17.5	-13.7
23-21 (8.13)		12 22 47.79	13 21 10.3	0.2	-80	25.3	13.8	45	28.7	17.6	-13.7
23-22 (8.14)		12 24 02.40	13 51 59.0	0.1	10	26.3	59	66	27.7	15.5	-15.7
24-2 (8.3)	Bg E/S0	12 22 36.16	13 16 38.1	0.36	51	24.4	1.5	5.0	28.6	21.5	—
24-3 (8.3)	Bg E/S0	12 22 35.18	13 16 20.9	0.2	10	24.8	1.8	5.0	28.5	21.5	—
24-4 (8.3)	Bg	12 22 34.15	13 19 11.5	0.36	72	24.8	2.2	5.5	27.8	21.0	—
24-5 (8.4)	Bg L S	12 22 30.14	13 25 37.1	0.46	-5	21.8	3.4	21	28.6	17.2	—
24-6 (8.3)	Bg	12 22 34.40	13 25 10.4	0.68	36	24.9	3.8	11	28.9	20.1	—
24-7 (8.4)	Bg L E/S0	12 22 31.78	13 32 48.6	0.5	46	21.9	2.7	14	27.5	17.7	—
24-8 (8.3)	Bg E/S0	12 22 30.74	13 33 42.2	0.43	48	23.4	1.4	7.4	29.4	20.6	—
24-9 (8.3)	Bg Sc	12 22 25.46	13 41 30.2	0.34	32	20.4	5.7	50	29.1	14.6	—
24-10 (8.4)	Bg Br E	12 22 31.68	13 39 55.6	0.24	-25	20.8	3.2	23	29.3	16.3	—
24-11 (8.4)	Bg Br E	12 22 32.87	13 40 7.46	0.39	81	21.3	2.2	16	29.2	17.6	—
24-12 (8.4)	Bg Br E	12 22 36.51	13 41 21.0	0.16	57	20.5	2.9	21	28.3	16.2	—
24-16 (8.3)	Bg	12 22 18.55	13 25 10.3	0.4	-89	24.2	2.8	12	30.3	19.9	—
24-18 (8.8)	Bg S	12 21 52.96	13 48 32.4	0.124	8.7	24.1	3.2	13	29.4	19.5	-11.7
24-19 (8.4)		12 21 49.38	13 35 48.9	0.5	-46	24.7	5.2	21	29.3	19.1	—
24-20 (8.7)		12 21 48.12	13 34 56.1	0.168	64	24.4	2.7	9	28.6	20.2	-11.0
24-23 (8.11)		12 21 22.68	13 36 07.4	0.3	10	25.1	6.1	16	29.1	19.2	-12.0
24-24 (8.10)		12 21 23.41	13 34 59.4	0.13	-83	24.5	4.7	17	28.7	19.2	-12.1
24-25 (8.13)		12 21 14.19	13 40 33.0	0.486	0.8	24.2	8.3	37	29.6	17.7	-13.6
24-26 (8.6)		12 21 04.36	13 42 33.5	0.297	17	23.8	2.4	7	28.0	19.9	-11.3
24-27 (8.13)		12 21 08.84	13 35 25.8	0.177	-27	24.2	13.3	41	27.0	16.6	-14.6
24-28 (8.13)		12 21 08.69	13 34 26.0	0.1	5	25.3	9.1	28	28.3	18.5	-12.8
24-29 (8.6)		12 20 52.44	13 49 21.5	0.2	50	23.9	2.3	11	29.4	20.1	-11.1
24-31 (8.8)		12 20 42.42	13 55 50.6	0.124	25	24.3	3.4	16	30.0	19.6	-11.6

*continued on next page*

Tab. 8.2: *continued*

(1) ID (Fig.)	(2) Class.	(3) RA	(4) Dec	(5) $e$	(6) $pa$	(7) $\mu_0$	(8) $a$	(9) $r_{max}$	(10) $OR_{max}$	(11) $OR$	(12) $M_{OR}$
24-33 (8.5)	Bg E/S0	12 20 34.98	13 10 58.8	0.141	58	23.0	1.9	13	30.9	19.6	-11.6
24-34 (8.12)		12 20 37.12	13 19 11.1	0.3	-23	24.6	7.3	28	28.7	18.3	-12.9
24-35 (8.8)		12 20 20.10	13 39 50.3	0.2	17	25.0	3.5	13	30.0	20.3	-11.0
24-37 (8.10)		12 20 17.87	13 16 46.9	0.178	-4	24.0	4.5	23	29.3	18.7	-12.5
24-38 (8.9)		12 20 06.38	13 17 58.4	0.594	-84	24.1	4.1	16	28.3	19.1	-12.1
24-39 (8.3)		12 19 53.38	13 10 03.2	0.447	-73	23.3	2.0	12	30.0	19.7	—
24-40 (8.11)		12 19 45.78	13 42 07.7	0.35	-69	24.9	5.5	21	29.7	19.2	-12.0
28-2 (8.8)	L	12 29 24.75	14 23 44.1	0.5	-20	25.0	3.9	10	28.8	20.1	-11.1
28-3 (8.5)		12 29 23.21	14 27 15.7	0.05	5	24.5	2.0	7	28.5	21.1	-10.1
28-5 (8.6)		12 29 19.50	14 27 21.4	0.23	-42	23.6	2.4	9	27.7	19.7	-11.5
28-6 (8.7)		12 29 18.16	14 25 39.1	0.213	-56	24.6	2.9	9	28.7	20.2	-11.0
28-7 (8.7)		12 29 15.13	14 23 21.5	0.387	-38	24.1	2.8	11	28.8	19.8	-11.3
28-8 (8.12)		12 29 09.92	14 13 39.5	0.2	-80	25.0	7.5	21	28.7	18.7	-12.5
28-11 (8.5)		12 29 08.76	14 39 44.1	0.086	-40	23.1	1.8	7	28.0	19.9	-11.3
28-12 (8.8)		12 29 03.28	14 40 15.2	0.47	50	23.6	3.2	13	28.6	19.1	-12.1
28-14 (8.8)		12 29 06.84	14 44 29.2	0.5	-45	25.2	3.8	14	29.4	20.3	-10.9
28-15 (8.7)		12 29 06.40	14 45 47.6	0.051	-5	25.2	2.9	10	29.3	20.8	-10.4
28-17 (8.7)		12 28 51.00	14 13 52.9	0.1	5	25.5	—	6	28.5	—	—
28-18 (8.6)		12 28 57.85	14 42 56.4	0.1	5	24.9	2.2	7	28.7	21.2	-10.0
28-19 (8.9)		12 28 51.10	14 37 06.7	0.3	80	25.1	4.0	14	29.2	20.1	-11.1
28-21 (8.11)		12 28 54.47	14 30 36.8	0.339	-75	25.7	5.7	14	29.2	19.9	-11.3
28-22 (8.10)		12 28 59.46	14 25 34.3	0.1	45	25.5	4.7	10	28.4	20.1	-11.1
28-25 (8.6)		12 28 51.16	14 17 34.2	0.174	87	24.8	2.2	7	28.7	21.1	-10.1
28-26 (8.6)		12 28 51.36	14 02 42.7	0.5	45	24.1	2.4	9	28.6	20.3	-11.0
28-28 (8.7)		12 28 44.10	14 16 59.1	0.5	-45	24.6	2.9	11	28.7	20.3	-10.9
28-31 (8.13)		12 28 44.84	14 29 36.8	0.143	-71	24.7	9.7	31	27.8	17.8	-13.4
28-33 (8.5)		12 28 46.24	14 44 24.7	0.072	-66	24.0	1.8	6	28.4	20.7	-10.5
28-34 (8.5)		12 28 42.33	14 47 13.6	0.2	50	23.7	1.7	6	28.1	20.6	-10.6
28-36 (8.9)		12 28 34.83	14 36 25.7	0.05	5	25.2	4.2	13	29.2	20.1	-11.1
28-37 (8.6)		12 28 33.88	14 36 34.1	0.24	-5.6	21.8	2.4	19	30.5	17.9	-13.3
28-38 (8.11)		12 28 32.94	14 11 25.7	0.1	-45	24.8	6.2	14	27.5	18.9	-12.3
28-39 (8.6)		12 28 29.50	14 40 12.0	0.4	-10	23.7	2.2	11	30.9	20.0	-11.2
28-40 (8.11)		12 28 18.97	14 08 14.5	0.09	-3	24.3	5.4	16	28.1	18.6	-12.6
28-42 (8.10)		12 28 01.83	14 16 59.8	0.15	220	24.9	4.8	17	29.1	19.5	-11.7
28-44 (8.5)		12 27 54.47	14 42 14.2	0.2	-10	24.0	1.5	7	30.6	21.1	-10.1
28-45 (8.9)		12 27 55.24	14 37 17.4	0.251	8	21.6	4.0	34	29.3	16.6	-14.6
28-48 (8.8)		12 27 46.13	14 06 42.3	0.05	40	24.7	3.2	12	28.2	20.2	-11.1
28-50 (8.9)		12 27 31.28	14 04 42.0	0.284	22	24.0	4.3	16	28.1	18.9	-12.3
28-51 (8.10)		12 27 19.49	14 17 24.5	0.224	4	24.6	4.8	16	28.7	19.2	-12.0
28-52 (8.11)		12 27 12.20	14 00 51.3	0.192	25	24.4	5.4	19	27.9	18.7	-12.5
28-53 (8.10)		12 27 07.14	14 42 45.6	0.085	42	24.0	4.6	21	29.0	18.7	-12.5
28-54 (8.14)		12 26 56.98	14 47 45.6	0.3	62	25.8	23.2	66	29.0	17.0	-14.2
28-56 (8.12)		12 26 34.54	14 13 32.3	0.631	11	24.3	6.7	26	28.7	18.2	-13.1
28-57 (8.6)		12 26 21.19	14 41 26.4	0.318	69	23.8	2.6	11	30.2	19.7	-11.5

## 8.5 Galaxy Images and Radial Profiles

Galaxy images and profiles are placed on odd-numbered pages in this section. Even-numbered pages are left blank intentionally so as not to degrade the image quality. Image sizes are specified in the figure captions. Galaxy scale length ( $a$ ), in arcseconds, is specified below each image. Central surface brightness (in  $OR\mu$ ) is the number that appears in the upper right corner of each radial profile plot ( $y$ -intercept in the trendline equation). All plots have radius in arcseconds on the  $x$ -axis (indicating the angular extent of the galaxy) and  $OR$  surface brightness in magnitudes per arcsec<sup>2</sup> on the  $y$ -axis.

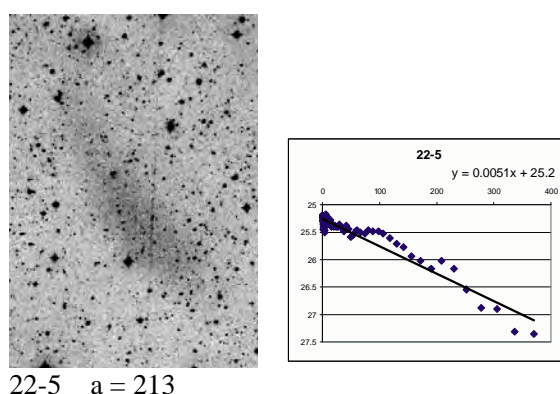


Fig. 8.2: Presumed Foreground Object: Bryn's Mystery Object

*Image size is  $19 \times 16.75$  arcminutes. This object is extraordinarily large. Its profile may be traced for 396 arcseconds from end to end. It is referred to in this project as Bryn's Mystery Object and is presumed to be a foreground object. Refer Section 6.3 for further discussion.*



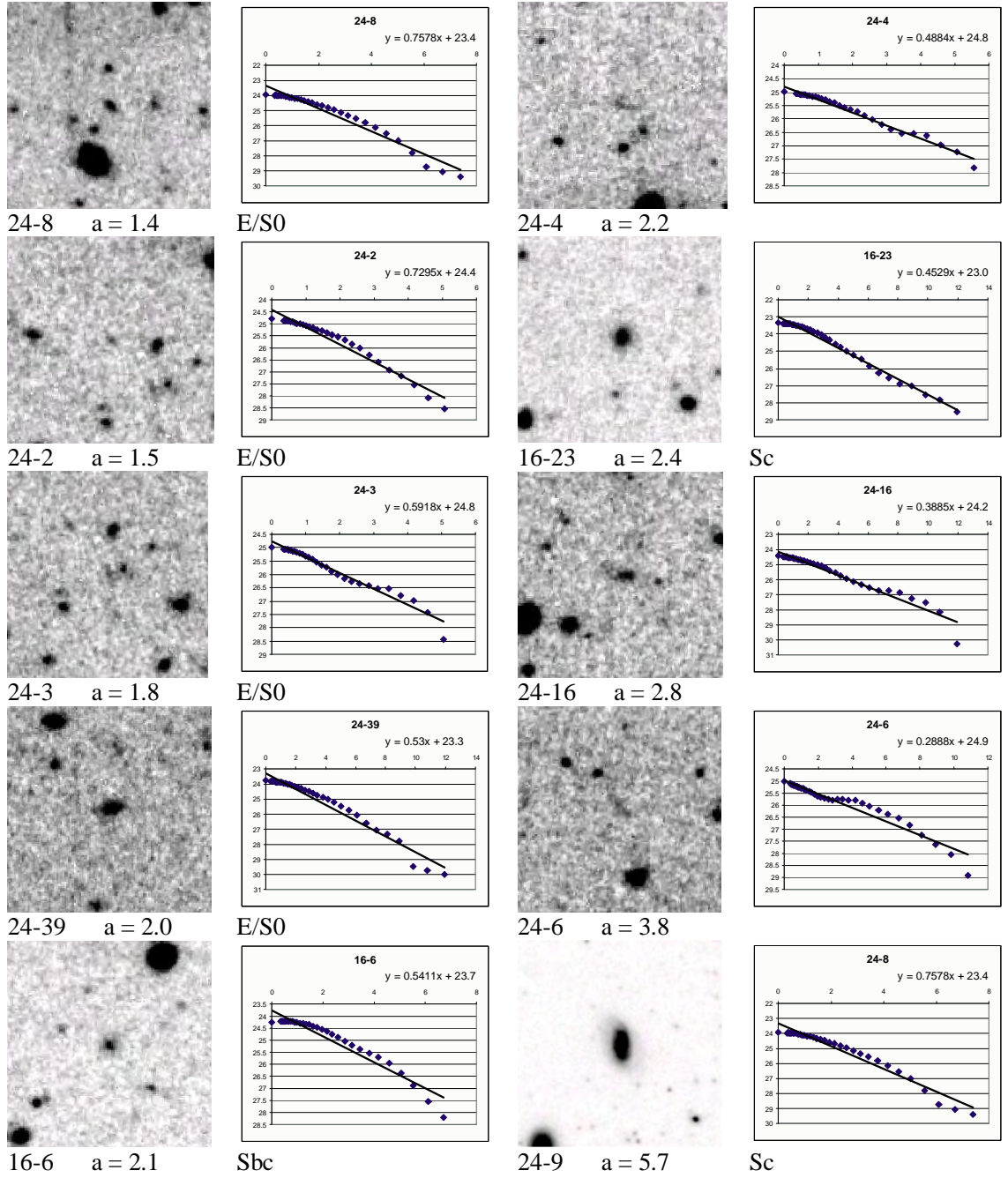


Fig. 8.3: Presumed Background Galaxies I

Images measure approximately  $67 \times 67$  arcseconds. Angular sizes are less than  $\sim 12$  arcsec. Classification, based on scale length and morphology, is specified under the corresponding plot. The contrast level of galaxy 24-9 has been adjusted to reveal the spiral arms. All are VLSB galaxies.





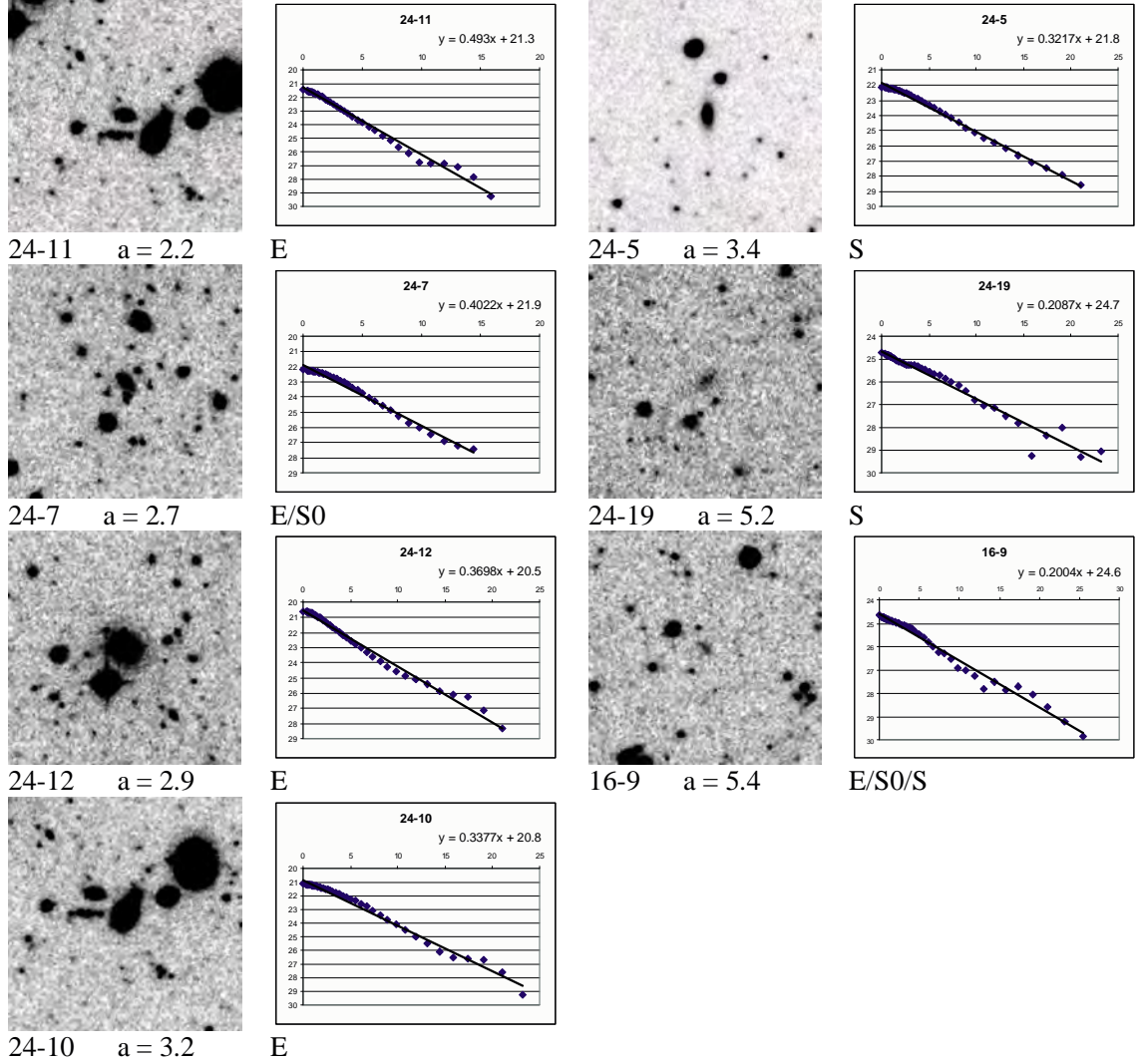


Fig. 8.4: Presumed Background Galaxies II

Images measure approximately  $134 \times 134$  arcseconds. Angular sizes are greater than 12 arcsec. Classification, based on scale length and morphology, is specified under the corresponding plot. The contrast level of galaxy 24-5 has been adjusted to reveal the spiral arms. Galaxies 24-19 and 16-9 are VLSB galaxies; 24-5 and 24-7 are LSB; 24-10, 24-11 and 24-12 are brighter.



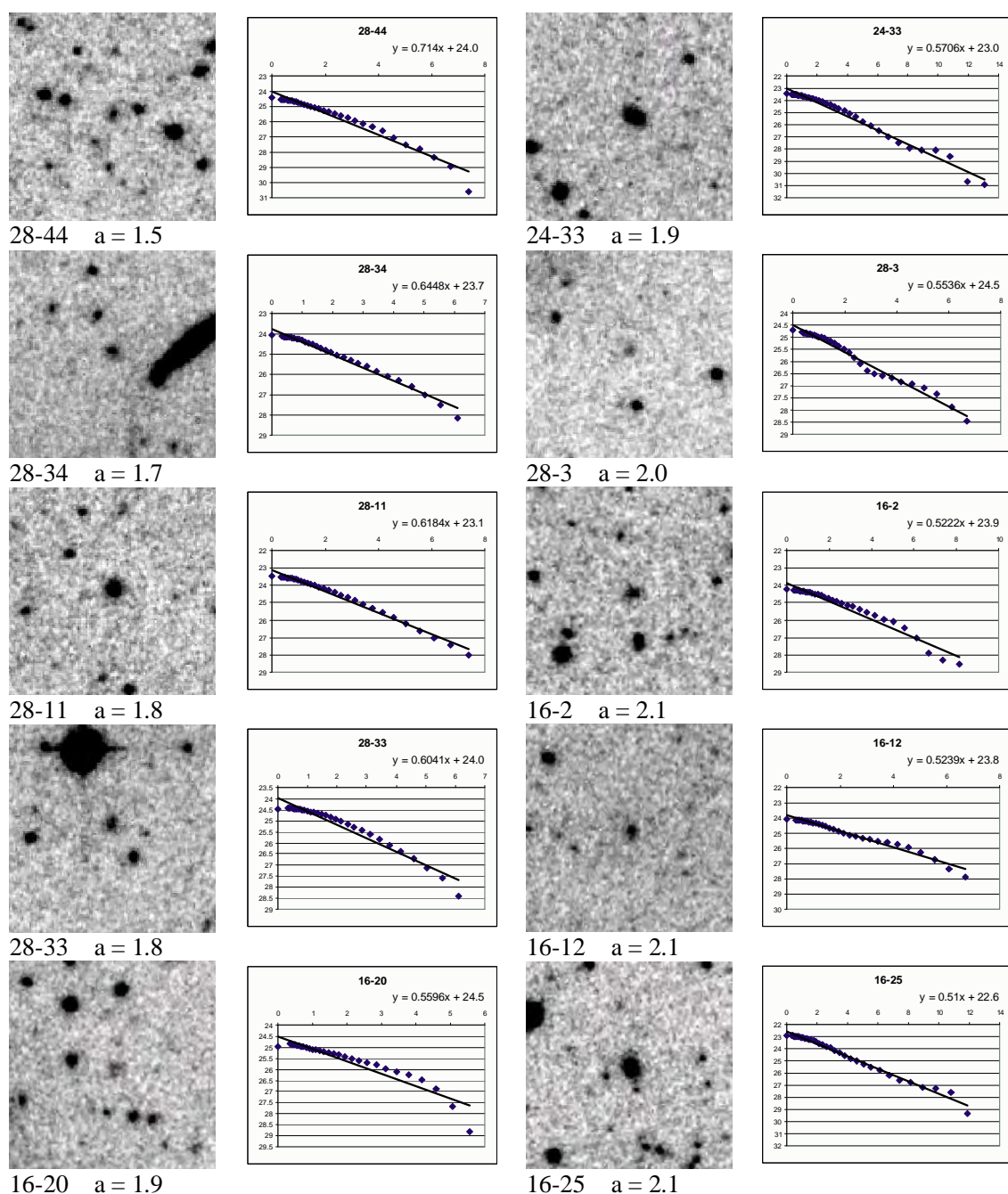


Fig. 8.5: Possible Cluster Members I

*Images measure approximately  $67 \times 67$  arcseconds. All are VLSB galaxies. Scale lengths range from 1.5 to 2.1 arcseconds. Dwarf galaxies of the Local Group would have comparable scale lengths to these galaxies if placed at 15 Mpc (refer Table 4.3 p.69).*



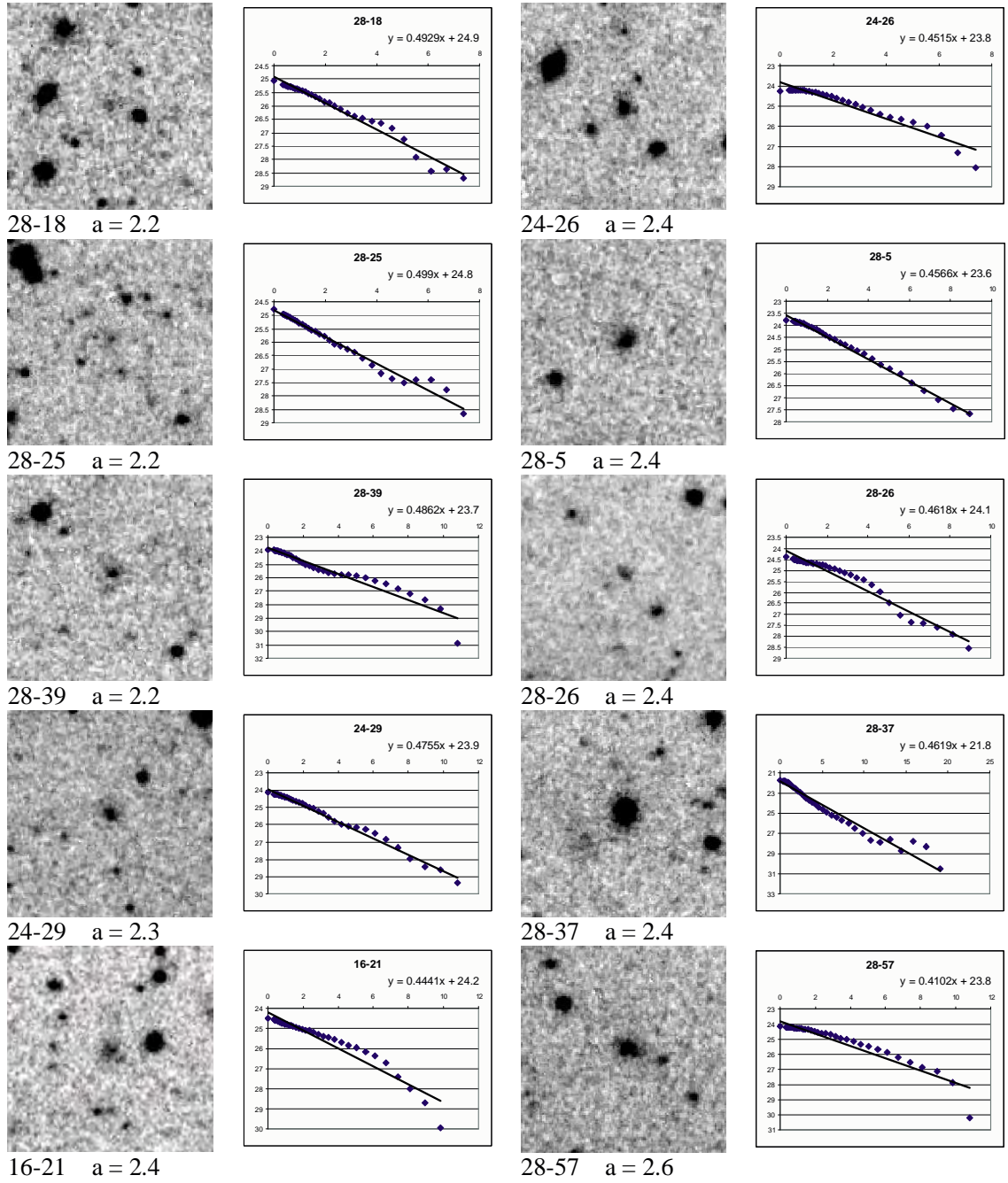


Fig. 8.6: Possible Cluster Members II

*Images measure approximately  $67 \times 67$  arcseconds. All are VLSB galaxies.  
Scale lengths range from 2.2 to 2.6 arcseconds.*



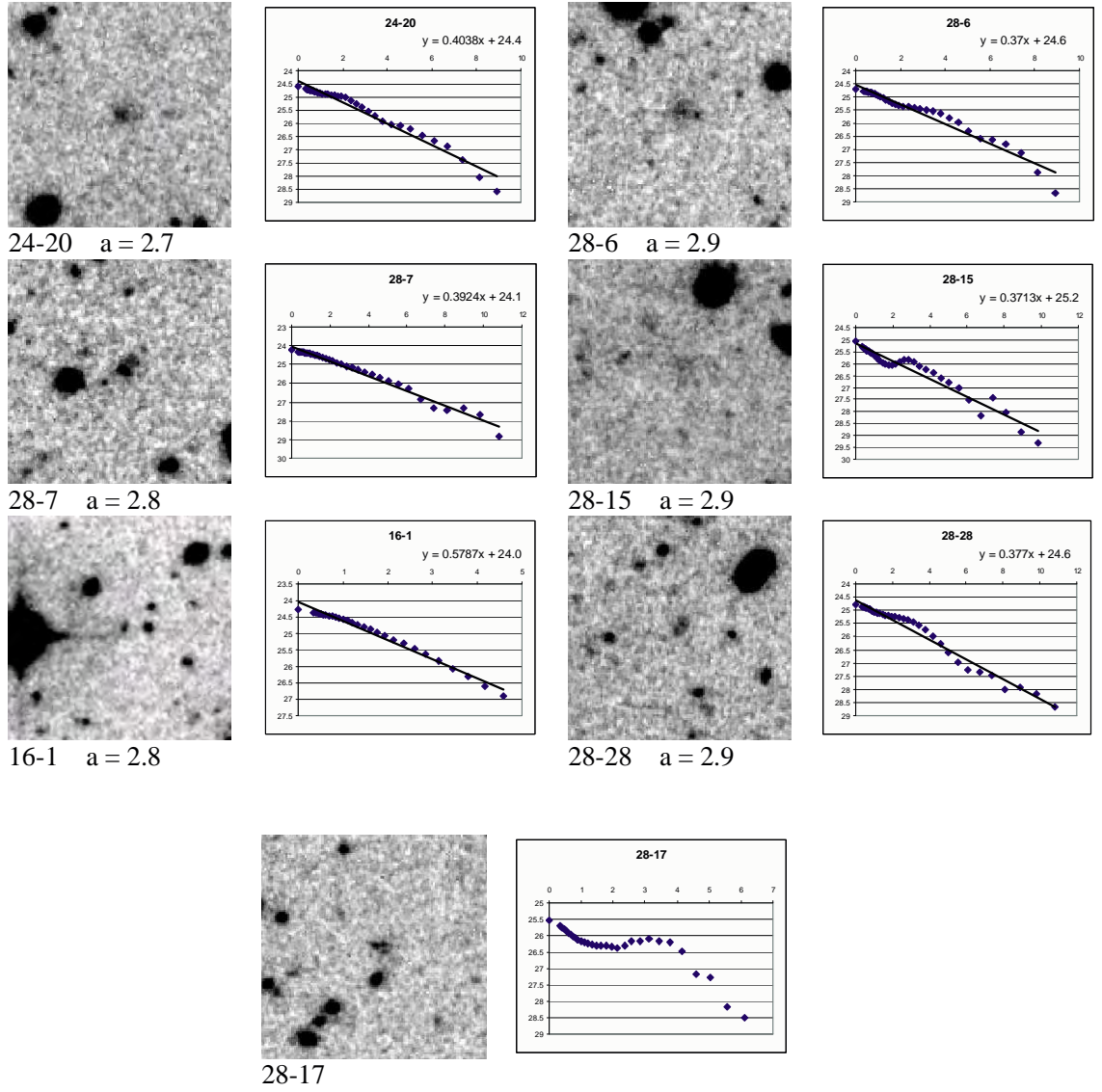


Fig. 8.7: Possible Cluster Members III

*Images measure approximately  $67 \times 67$  arcseconds. All are VLSB galaxies. Scale lengths range from 2.7 to 2.9 arcseconds. Properties of galaxy 28-17 could not be measured by the means used for the rest of the galaxies due to its irregular profile, but it is deemed to be similar to galaxies in this category.*





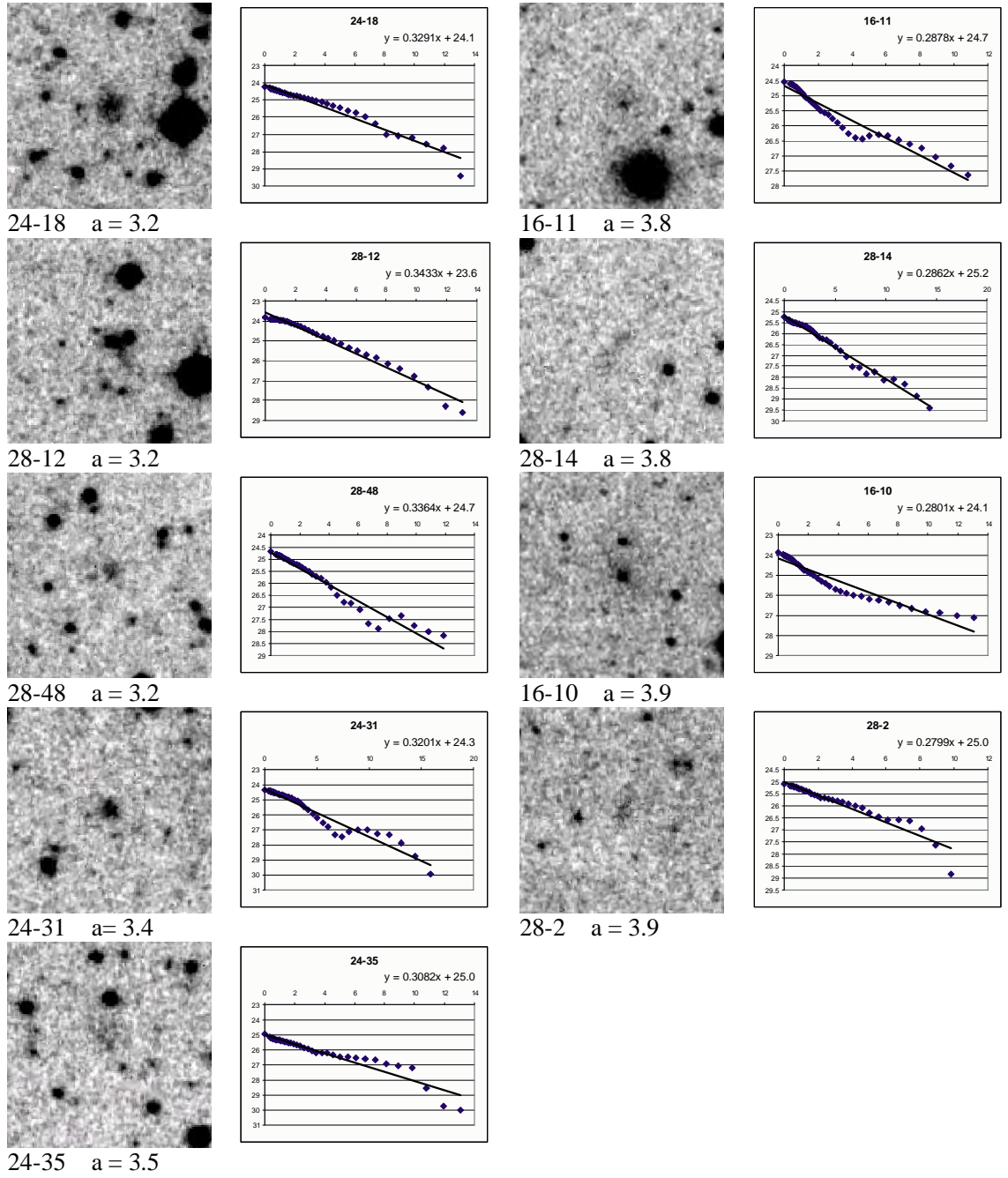


Fig. 8.8: Probable Cluster Members I

*Images measure approximately  $67 \times 67$  arcseconds. All are VLSB galaxies. Scale lengths range from 3.2 to 3.9 arcseconds. Scale length  $> 3$  arcseconds is a commonly-used criterion to infer cluster membership.*



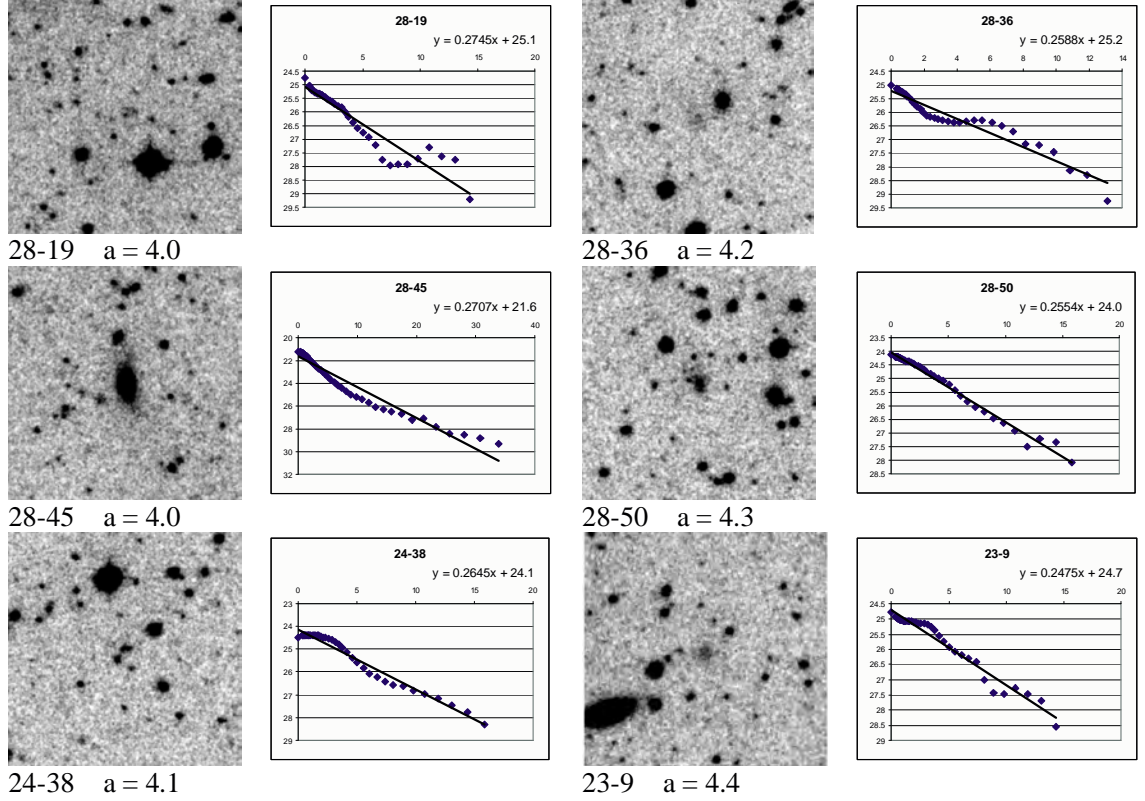


Fig. 8.9: Probable Cluster Members II

Images measure approximately  $134 \times 134$  arcseconds. Scale lengths range from 4.0 to 4.4 arcseconds. The profile of galaxy 28-19 is irregular due to off-centre clumps in the galaxy. Galaxy 28-45 is an LSB galaxy. All the others are VLSB galaxies.



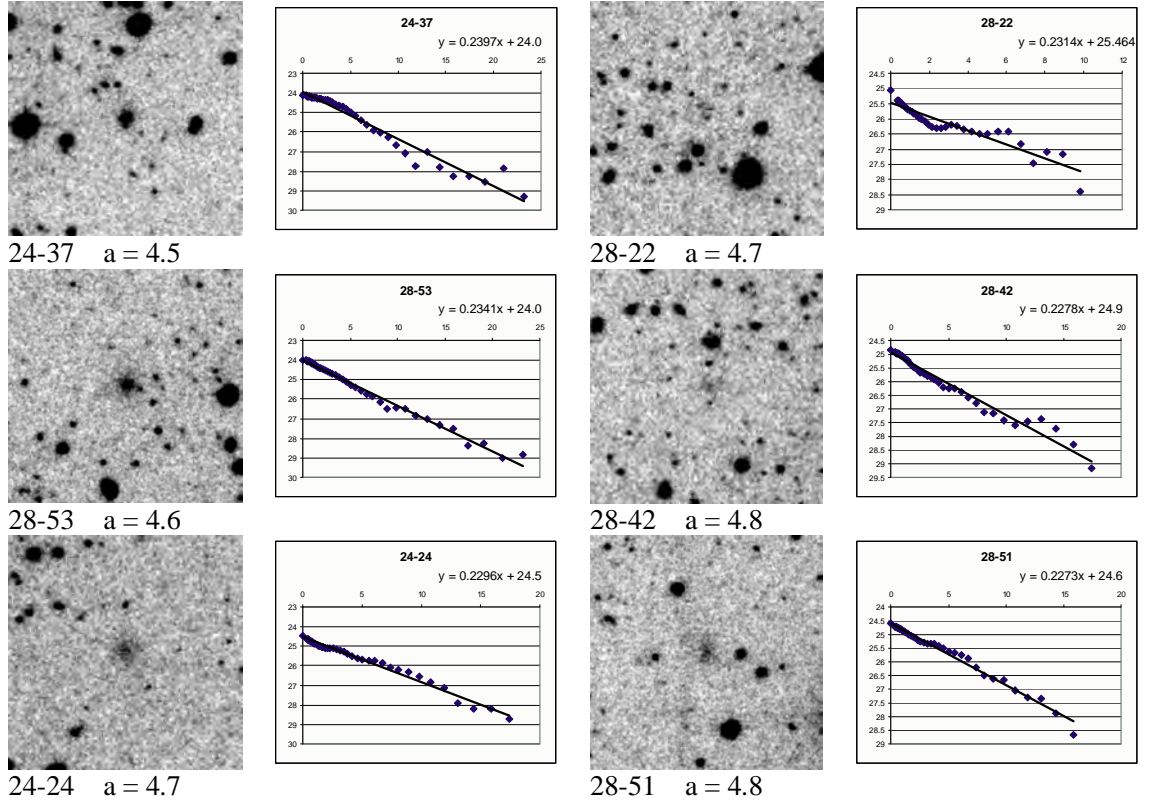


Fig. 8.10: Probable Cluster Members III

*Images measure approximately  $134 \times 134$  arcseconds. Scale lengths range from 4.5 to 4.8 arcseconds. All are VLSB galaxies.*



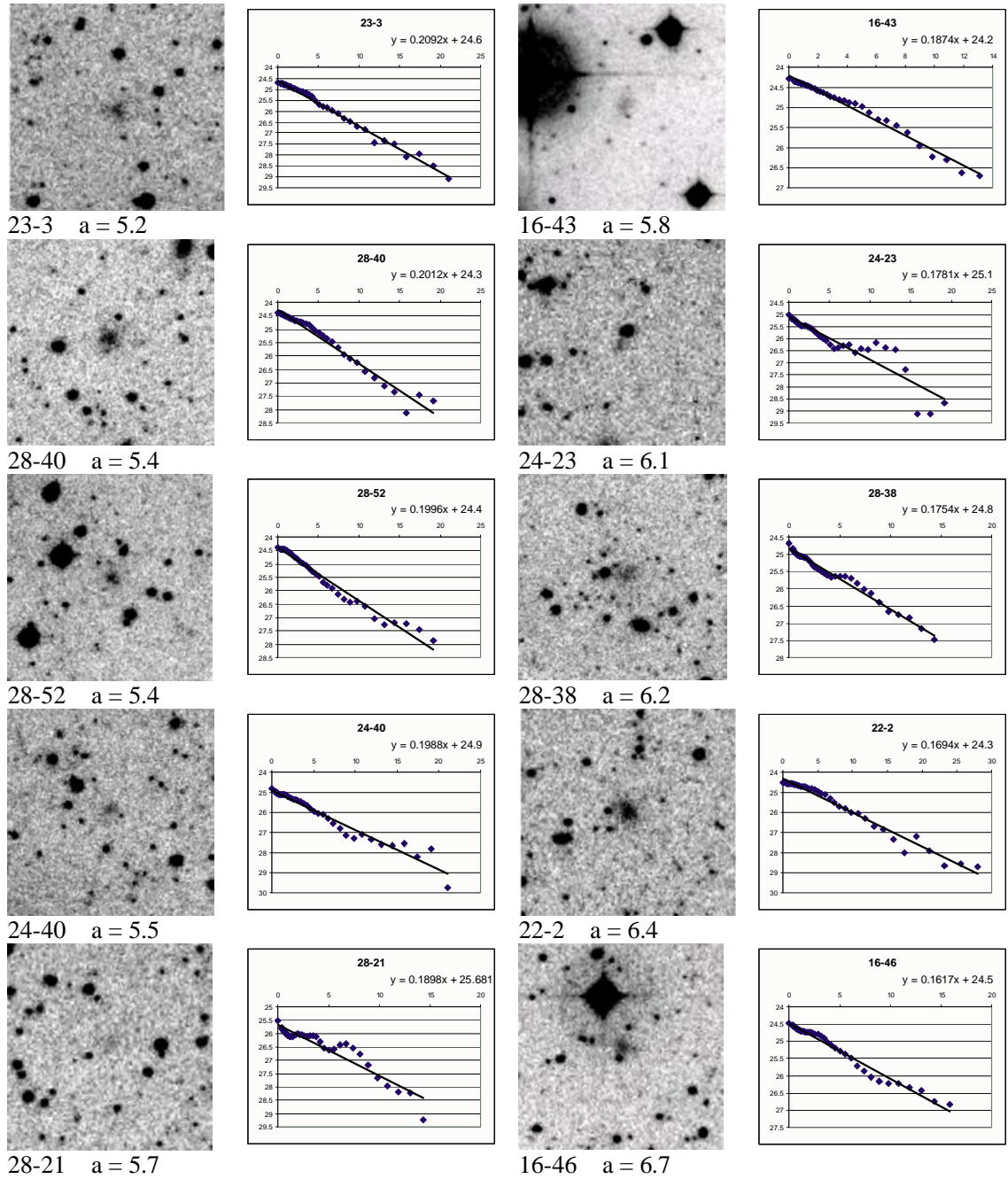


Fig. 8.11: Presumed Cluster Members I

Images measure approximately  $134 \times 134$  arcseconds. Scale lengths range from 5.2 to 6.7 arcseconds. The contrast level of galaxy 24-43 has been adjusted to distinguish the galaxy from the diffraction halo of the bright star in the image. All are VLSB galaxies. The profiles of galaxies 28-21 and 24-23 show the irregularity that is typical of very diffuse VLSB galaxies. Note that these two galaxies have fainter central surface brightness than the other galaxies in this figure.





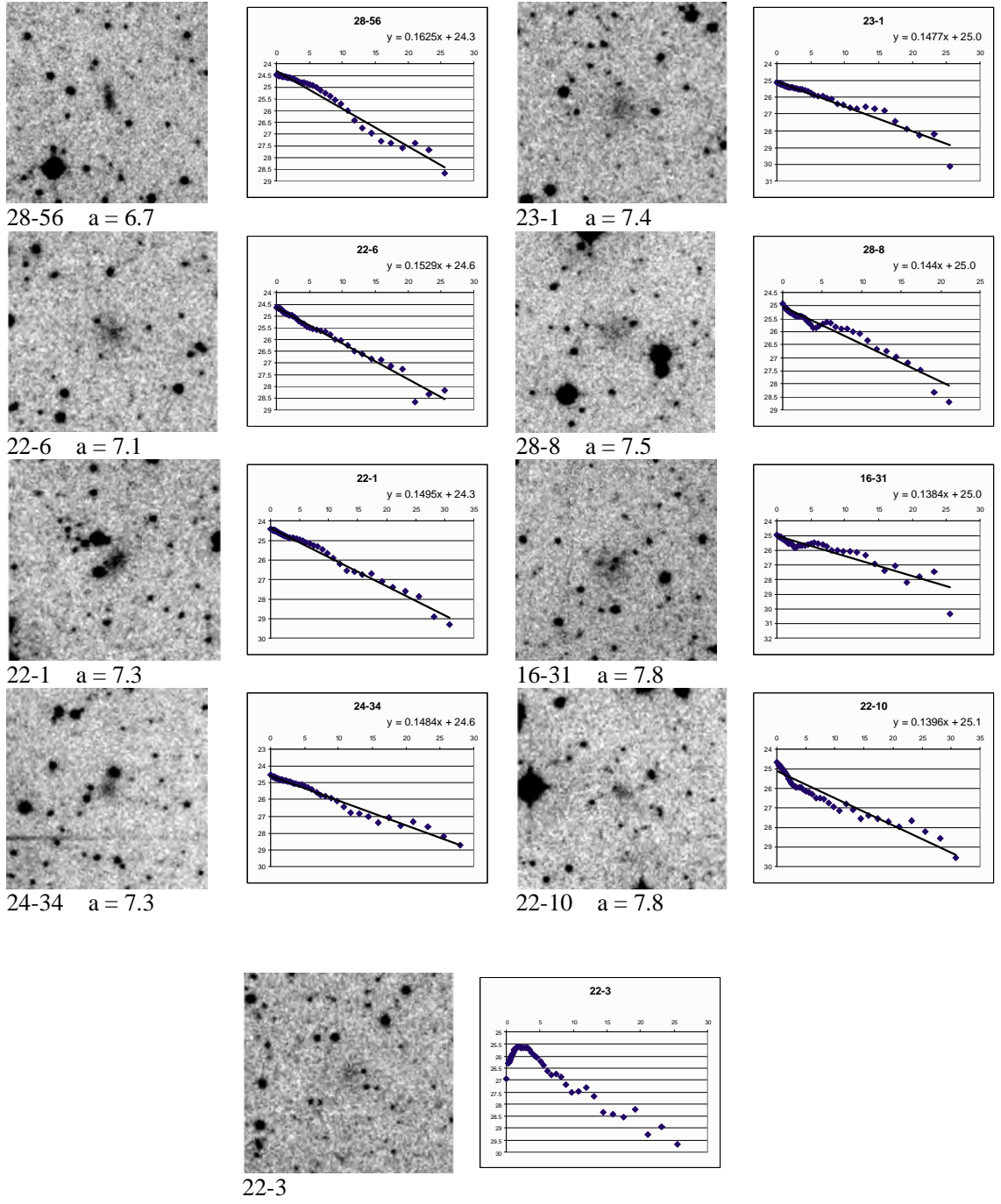


Fig. 8.12: Presumed Cluster Members II

Images measure approximately  $134 \times 134$  arcseconds. Scale lengths range from 6.7 to 7.8 arcseconds. All are VLSB galaxies. Properties of galaxy 22-3 could not be measured by the means used for the rest of the galaxies due to its irregular profile, but it is deemed to be similar to galaxies in this category.



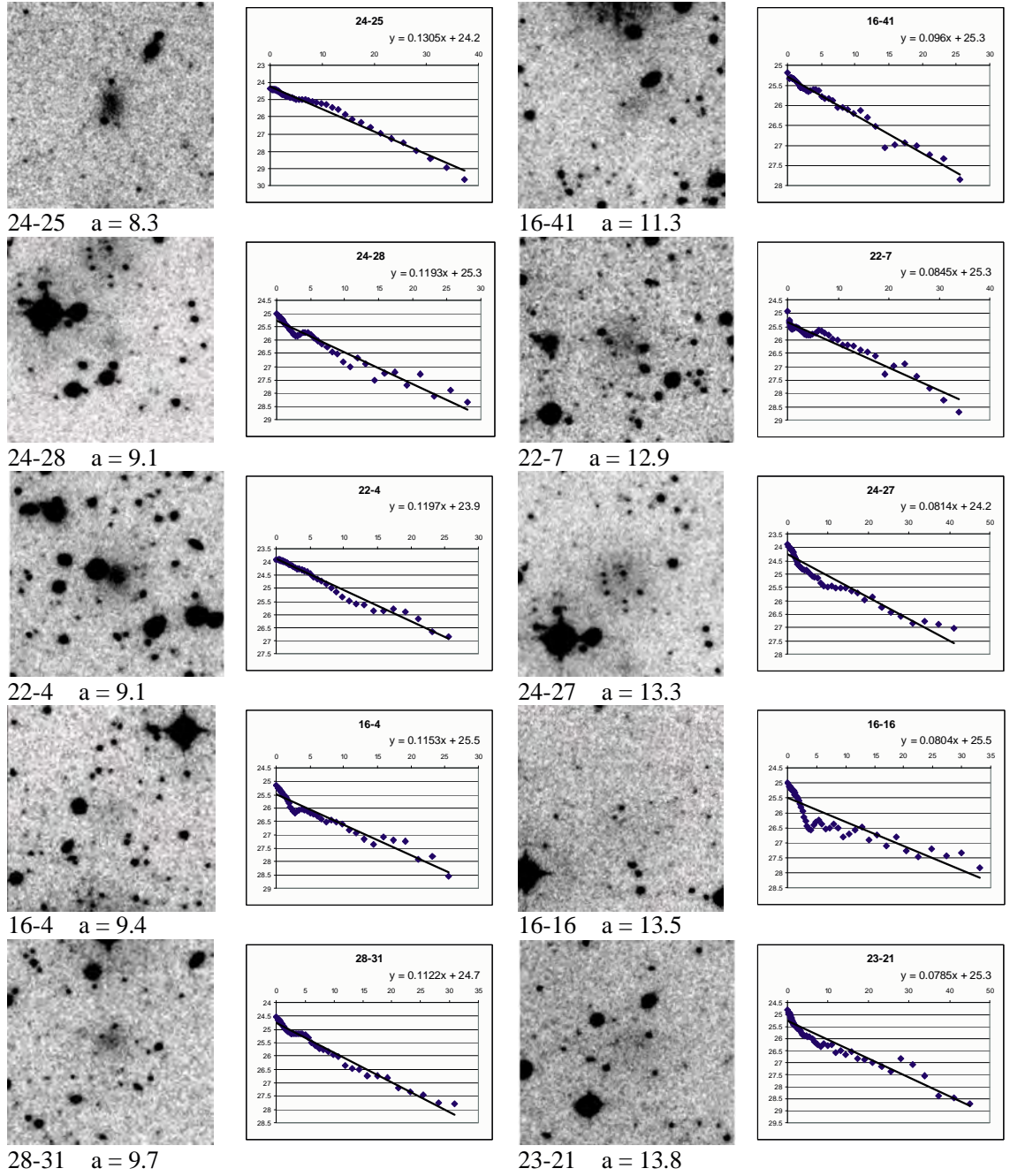
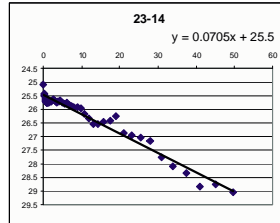
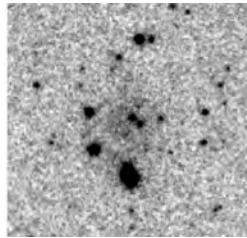


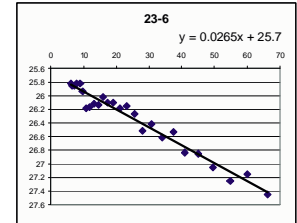
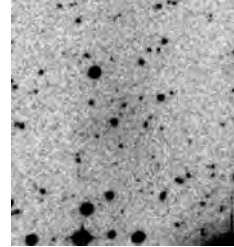
Fig. 8.13: Presumed Cluster Members III

Images measure approximately  $134 \times 134$  arcseconds. Scale lengths range from 8.3 to 13.8 arcseconds. Galaxy 22-4 is an LSB galaxy. All the others are VLSB galaxies. With galaxies of this angular size, masking of foreground stars in the surface photometry process becomes crucially important. It may be seen again that the galaxies with the faintest central surface brightness have more irregular profiles.

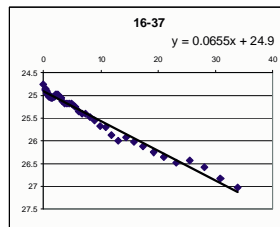
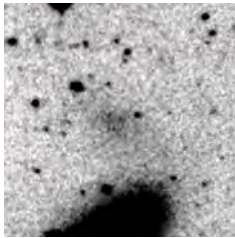




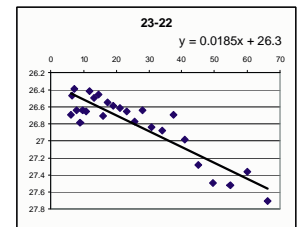
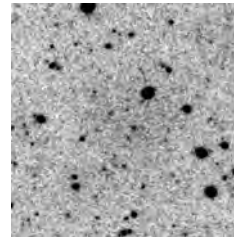
23-14  $a = 15.4$   
Image size is 134 x 134 arcsec



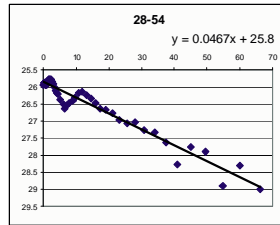
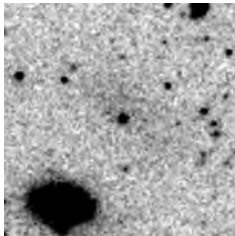
23-6  $a = 41$   
Image size 216 x 232 arcsec



16-37  $a = 16.6$   
Image size is 134 x 134 arcsec



23-22  $a = 59$   
Image size 200 x 200 arcsec



28-54  $a = 23.2$   
Image size is 134 x 134 arcsec

Fig. 8.14: Presumed Cluster Members IV

*These are the most diffuse galaxies detected in this project. Image sizes vary and are quoted below the images. All are VLSB galaxies.*



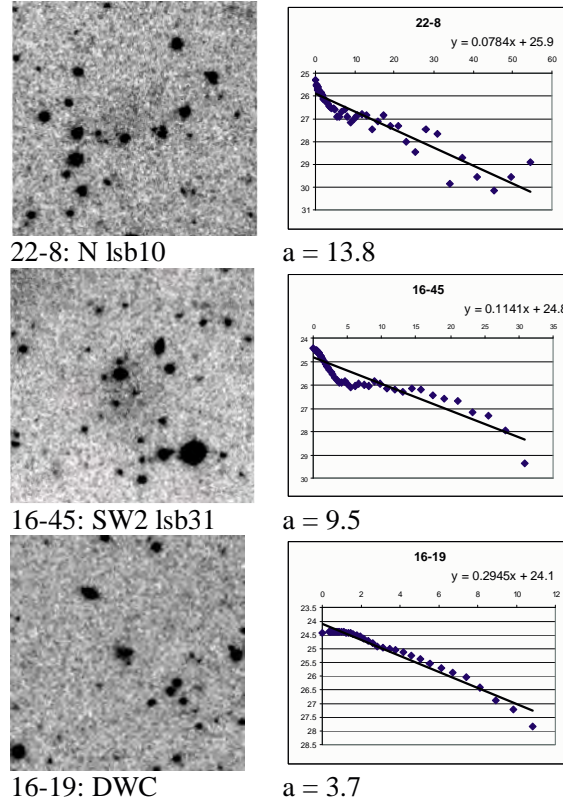


Fig. 8.15: Verified Cluster Members

Three galaxies identified as part of this project have been independently studied and verified as cluster members. Images measure approximately  $134 \times 134$  arcseconds. All are VLSB galaxies.

Galaxies 22-8 and 16-45 were observed by Caldwell (2005), but no radial profiles were obtained. TRGB measurements place these galaxies in the Virgo Cluster.

HST observations of galaxy 16-19 (DWC) by Durrell et al. (2007) resolved the stellar population, for which a colour-magnitude diagram was constructed. Those data verify that this galaxy is a cluster member. The radial profile indicates that the galaxy has a scale length of 3.7 arcseconds. Galaxies of similar scale length, identified as part of this project, are classified as 'probable cluster members'.





## 9. DISCUSSION, CONCLUSIONS AND FUTURE WORK

The following sections (9.1 and 9.2) contain discussion of the catalogue of newly-identified galaxies presented in Chapter 8. Aspects that are considered are the validity of the membership classifications, using comparisons with other methods, and the potential impact of the new discoveries on the luminosity function of the Virgo Cluster. Conclusions are summarised in Section 9.3. These conclusions point to the importance of valid distance information to confirm cluster membership. To that end, follow-up observations with the Gemini North Telescope to obtain spectroscopic data were planned. Two observing proposals were successful, but poor weather prevented any observations being completed. The observing process is described and the observing proposals are included in Appendix F. Section 9.4 details other follow-up work that could be performed using the Virgo Deep Stack.

### *9.1 Cluster Membership of the New Galaxies*

Most galaxies in this catalogue have been classified as members or non-members of the Virgo Cluster based on the commonly-used criteria of morphology and scale length (refer Section 8.3) after Phillipps et al. (1998), Sabatini et al. (2003) and Roberts et al. (2007). Different methods of membership classification were used by Trentham and Tully (2002) and Trentham and Hodgkin (2002). For comparison, a subset of the current catalogue was evaluated using one of these methods.

The concentration parameters described by Trentham and Tully (2002) and summarised in Section 4.5.3 were applied to a selection of galaxies covering the complete range of scale lengths in the catalogue. Aperture photometry was performed in **GAIA**

on isolated targets so that no stars or neighbouring objects would influence the measurements. The results of these measurements appear in Table 9.1.

ID	OR(4.4)	OR(2.2)	ICP	OR(12)	OR(6)	OCP	a	Classification
24-2	22.683	23.261	-0.578	22.424	22.442	-0.018	1.5	Morph Bg
16-9	21.644	22.935	-1.291	20.949	21.246	-0.297	5.4	Morph Bg
28-34	21.405	22.351	-0.946	21.006	21.163	-0.157	1.7	Possible Mem
28-3	21.914	22.964	-1.05	21.305	21.837	-0.532	2.0	Possible Mem
28-39	21.425	22.258	-0.833	20.729	21.155	-0.426	2.2	Possible Mem
28-5	20.922	21.968	-1.046	20.095	20.57	-0.475	2.4	Possible Mem
24-20	21.525	22.754	-1.229	20.717	21.228	-0.511	2.7	Possible Mem
24-31	21.183	22.537	-1.354	20.32	20.84	-0.52	3.4	Probable Mem
23-9	21.709	23.145	-1.436	20.498	21.091	-0.593	4.4	Probable Mem
24-24	21.443	22.78	-1.337	19.955	20.952	-0.997	4.7	Probable Mem
28-21	22.472	23.828	-1.356	21.095	21.964	-0.869	5.7	Presumed Mem
23-1	21.993	23.305	-1.312	20.241	21.36	-1.119	7.4	Presumed Mem
28-31	21.719	23.021	-1.302	19.697	20.927	-1.23	9.7	Presumed Mem
16-37	21.872	23.226	-1.354	19.785	21.002	-1.217	16.6	Presumed Mem
22-8	22.811	24.381	-1.57	21.258	22.38	-1.122	13.8	Confirmed Mem
16-19	20.876	21.998	-1.122	19.78	20.472	-0.692	3.7	Confirmed Mem

Tab. 9.1: Concentration Parameters for Catalogue Galaxies

*Aperture magnitudes (OR) and concentration parameters (ICP and OCP), as described by Trentham and Tully (2002) and reproduced in Section 8.3 (p.164), were measured for a sample of catalogue galaxies. Scale length and membership classifications assigned in this project are listed in the table. Membership classifications that would result from the Trentham and Tully (2002) criteria are discussed in the text.*

Trentham and Tully (2002) selected Virgo Cluster dwarfs based on two criteria. The first criterion requires  $R(6 \text{ arcsec}) < 20$ ,  $ICP < -0.7$  and  $OCP < -0.4$ . All galaxies in Table 9.1 are fainter than this, so the second criterion must be applied, i.e. for  $20 < R(6 \text{ arcsec}) < 23$ , the authors specify  $ICP < -0.4$ . Every galaxy in the table also satisfies this criterion, even those with morphology and scale length in the range where they would be excluded as members according to commonly-used scale-length criteria. Of the galaxies that satisfied the concentration parameter

criteria, Trentham and Tully (2002) then excluded grand-design luminous spirals, merging galaxies, smooth edge-on galaxies and possible tidal debris from nearby giant galaxies. Of the galaxies evaluated in Table 9.1, only the first two appear to be smooth edge-on galaxies and have thus been classified as background. This still leaves five galaxies with scale length smaller than 3 arcseconds in this data subset.

The possibility was considered that the  $ICP < -0.4$  is a typographical error that should read  $ICP < -0.7$  (as for the first criterion). Because the Trentham and Tully (2002) paper evaluates galaxies in several galaxy groups and the Ursa Major and Virgo Clusters, it would be reasonable to use various different ICP values because the groups and clusters lie at different distances. Evidence for this reasoning comes from another publication, Trentham et al. (2001), where the same process was used for the Ursa Major Cluster (which is only about 1.6 Mpc farther than the Virgo Cluster) and  $ICP < -1.1$  is specified. However, entries 70 and 99 in Table 2 of Trentham and Tully (2002) both fall within the  $20 < R(6 \text{ arcsec}) < 23$  criterion and have ICP values of  $-0.56$  and  $-0.52$  respectively. Hence, the parameters used for the Virgo Cluster appear to have been correctly stated.

Therefore, it appears probable that many galaxies with scale lengths as small as 1.5 arcsec, that would be excluded as members based on scale length criteria, would have been included as cluster members by Trentham and Tully (2002). The impact of this finding on the luminosity function is discussed in Section 9.2.

The cluster membership assessment of Trentham and Hodgkin (2002) has not been evaluated because it relies on a probability formula that uses the concentration parameters of the entire data set of galaxies. Such a comprehensive comparison is beyond the scope of this project.

Nevertheless, for further evaluation of the membership criteria used for this catalogue, the Rines-Geller threshold (discussed in Section 4.5.5) is extrapolated, based on the assumption that no correction is required for the shift from  $r$ - to  $OR$ -band, and plotted against the catalogue data (refer Figure 9.1). Most of these new data lie beyond the magnitude limit of the SDSS data, presented by Rines and Geller (2008), which cuts off at  $\mu_{0r} = 24$  and  $R_T = 18$ .

As discussed in Section 4.5.5, the Rines-Geller threshold approximates the 3-arcsec locus. The new data lie at the faint-apparent-magnitude end of the range and the few ‘possible member’ galaxies that lie above the threshold in Figure 9.1 (galaxies 28-6, 28-15 and 28-18) have scale lengths of 2.9 arcsec. Two that lie right on the threshold (galaxies 28-7 and 16-1) have scale lengths of 2.8 arcsec.

The amount of scatter in the original Rines-Geller plot (refer Figure 4.6 p.75) warns against using this as a definitive membership-classification method. Independent distance data are still required for a firm determination of cluster membership. However, the comparison between Figure 9.1 and the Trentham and Tully (2002) method of evaluating cluster membership does raise questions about the validity of both the scale-length and concentration-parameter methods of inferring cluster membership.

## 9.2 Impact on the Luminosity Function

Figure 8.1 (p.165) illustrates that the number of newly-detected galaxies is small compared with the overall number previously known. The region most densely populated with previously-known galaxies is the upper portion of sub-frame 16, surveyed by Trentham and Tully (2002). Section 6.2.1 described the depth of the Virgo Deep Stack data and detailed the discovery of only two new likely-cluster-member dwarfs in this region. The failure to detect many new objects in this region attests to the completeness of the Trentham and Tully (2002) survey. However, the findings from Section 9.1 suggest that the Trentham and Tully (2002) data may be contaminated with background objects. The concentration-parameter criterion, when applied to Virgo Deep Stack data, included many galaxies with very small scale lengths as cluster members, whereas other analyses would exclude these as background galaxies.

Background contamination should make for a steep faint-end slope in the luminosity function, as is likely the case with the Phillipps et al. (1998) data, where the count of faint galaxies with small scale length continues to increase with decreasing galaxy

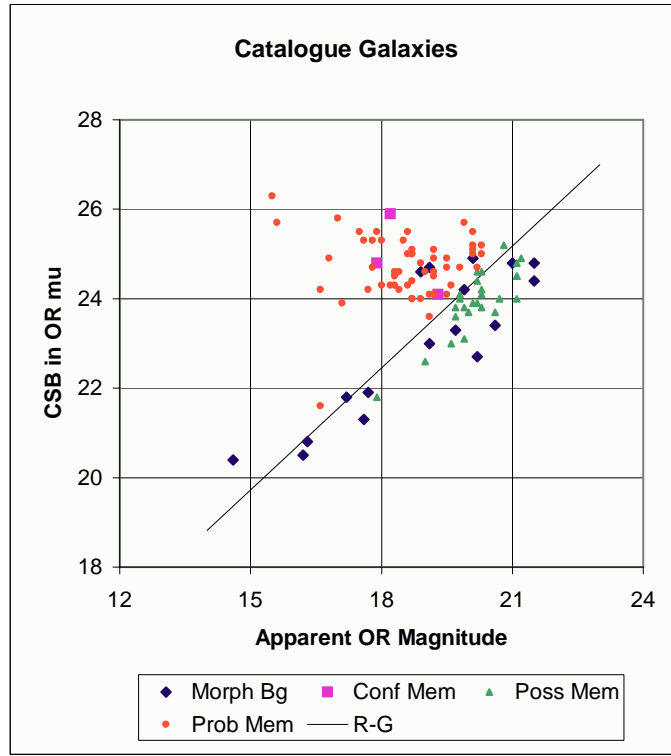


Fig. 9.1: Cluster Membership of Newly-Identified Galaxies

All data from this catalogue are plotted using central surface brightness versus apparent magnitude. Data sets are: morphologically assigned background galaxies (blue diamonds), confirmed cluster members (pink squares), possible cluster members (scale length  $< 3$  arcsec, green triangles) and probable & presumed cluster members (scale length  $> 3$  arcsec, red dots). The threshold between probable cluster members and probable background galaxies (R-G) is extrapolated from Rines and Geller (2008) without any conversion between the  $r$  and OR passbands.

luminosity. This does not explain why the Trentham and Tully (2002) luminosity function has a shallower slope than every other survey listed in Table 4.5 (p.87).

A possible explanation for this shallow slope may lie in the other result from Section 6.2.1, which is summarised in Table 6.1 (p.130), i.e. that inaccuracies in measured apparent magnitudes may contribute significantly to the shape of the luminosity function. If the galaxy magnitudes are measured fainter than their true values,

this would shift those galaxies into fainter magnitude bins. Rather than increasing the total counts in the faint bins, this would have the overall effect of distributing some constant number of galaxies over more magnitude bins, extending to fainter magnitudes than would otherwise be the case, effectively decreasing the slope of the luminosity function. Recalling that the Trentham and Tully (2002) magnitudes were fainter than Virgo Deep Stack measurements for the same galaxies, it may be that the shallow slope of the Trentham and Tully (2002) luminosity function is due to this effect.

It is difficult to make comparisons between the Virgo Deep Stack data and other luminosity functions listed in Table 4.5 (p.87). It appears that the galaxy database used by Phillipps et al. (1998) is neither available online nor listed in the paper (or other related publications). However, including galaxies with small scale lengths ( $< 3$  arcsec) would increase the number of galaxies in several faint magnitude bins, steepening the faint end of the luminosity function. Possible members of the Virgo Deep Stack catalogue in this scale-length bracket range in total apparent  $OR$  magnitude from 19.0 to 21.2, with one outlier at a magnitude of 17.9.

The data of Sabatini et al. (2003) (possibly overlapping part of sub-frame 16) and Roberts et al. (2007) (overlapping sub-frames 23 and 24) are in  $B$ -band and, although an approximate conversion of  $B - R = 1.5$  magnitudes is a useful guide when considering an overall population, the precise conversions for individual galaxies are not known and would affect final magnitudes and the binning of galaxies into the luminosity distribution. The other complications are that Roberts et al. (2007) solely use the DGR, rather than the luminosity function, and that the full data set relating to this paper is not yet available online.

One factor that may be compared and which has a clear effect on the luminosity function is the space distribution of galaxies and the prevalence of dwarf galaxies. All surveys that have produced luminosity functions for the Virgo Cluster have covered different regions of the cluster. Area coverage has ranged from very large (Sandage et al. (1985) covered the whole VCC) to very small (the compact Trentham and Tully (2002) coverage). The uneven distribution of both bright and faint galaxies

is evident in the low-contrast images of the cluster (refer Figure 1.1p.3) and plots of the positions of all likely cluster members (refer Figures 3.3 p.33 and 6.2 p.125). Positions of the newly-discovered galaxies also show an uneven distribution (refer Figure 8.1 p.165).

However, specific detection limits were not used consistently over the five sub-frames during inspection of the Virgo Deep Stack. Due to time constraints, galaxies of very small angular size were sampled only in some areas, notably the eastern portion of sub-frame 28, where the area density of galaxies appears higher than in adjacent regions, and the eastern portion of sub-frame 24, which includes a concentration of probable background galaxies.

It should also be stated that, by using only optical detection, some galaxies within the surface brightness limit of the Virgo Deep Stack may have been missed in this survey. Nevertheless, the sample does indicate that there are regions that are virtually devoid of LSB galaxies within the cluster. Hence, different results for the luminosity function based on surveys of different regions may all be accurate, despite yielding different values for the faint-end slope, as is suggested by the diversity of results found when comparing the cluster core with the periphery or the E-W and N-S strips of the INT Wide Field data (refer Table 4.5 p.87).

Whilst a complete survey covering the entire Virgo Deep Stack is beyond the scope of this project, the richness of the eastern region of sub-frame 28 is comparable with the Trentham and Tully (2002) survey demonstrating that many more dwarf galaxies await discovery. Any impact on the luminosity function would depend on the overall number density of new dwarf galaxies found, as this number density is normally extrapolated from small-area surveys to evaluate the luminosity function for the entire cluster. However, small areas may not be representative of the cluster as a whole.

### 9.3 Conclusions

Time constraints prevented the conduct of a fully comprehensive survey of LSB galaxies in the Virgo Deep Stack. Indeed, even within the sub-frames covered, galaxies within the detection limits of the data and not seen in other surveys may have been missed due to the simple optical detection method applied, or omitted simply due to very small angular size. In regions not heavily surveyed by other authors (e.g. sub-frame 28) cluster members of intermediate brightness, i.e. fainter than those detected in the VCC but brighter than the LSB galaxies targeted in this project, may also exist but still be missing from the catalogues.

Nevertheless, this project has comprehensively detailed the optical surveys of the Virgo Cluster. Comparisons with data from other surveys have demonstrated the depth and quality of the Virgo Deep Stack image. The limiting surface brightness is approximately 29 magnitudes per square arcsecond in the *OR*-band, allowing visual detection of galaxies with central surface brightness fainter than  $26\ OR\mu$ . The data reach an equivalent depth or deeper than any published deep CCD surveys to date. One hundred newly-identified galaxies have been catalogued, including 55 presumed and probable cluster members and 27 that are classified as possible cluster members based on scale length. Most of these are VLSB galaxies. With only a small percentage of the Virgo Deep Stack having been examined thus far, the potential remains for detecting hundreds more LSB and VLSB galaxies.

In other studies from this project, the value of the Virgo Deep Stack for examining intra-cluster light and the outer margins of giant galaxies has been demonstrated. A virtually complete outer shell has been revealed around the galaxy M89 and new data on Malin 1 have helped to refine the knowledge of this galaxy's inclination and visible extent, now seen to match closely with the HI disk. The Virgo Deep Stack has also been used to examine real and apparent tidal features and identify areas of probable intra-cluster light.

One comparison in particular has highlighted discrepancies in LSB galaxy magnitudes. These are attributed to different methods of calculating total magnitudes



from measured parameters of observational data. This project has highlighted that discrepancies in magnitude measurements, lack of crucial distance information to determine cluster membership and coverage of different survey areas all have demonstrated effects on the parameters of the Virgo Cluster luminosity function. Further observations to obtain distance information, either through spectroscopic velocity measurements or through TRGB techniques, would be necessary to overcome the ambiguity in cluster membership of individual galaxies.

Meanwhile, a homogeneous wide-area survey using the deepest possible data, i.e. the Virgo Deep Stack, could help resolve the disagreement between luminosity functions based on various small-area surveys. This unique resource should be further exploited in the future.

## 9.4 Future Work

A number of follow-up investigations may be pursued in reference to the data presented here and the Virgo Deep Stack source image. These include:

### 1. Refined Calibration of the Virgo Deep Stack

The value of the plate constant could be refined by measuring additional stars with aperture photometry and comparing with magnitudes quoted in the literature. This would also provide an improved value of the correction to be applied when converting from *OR*-band to Cousins *R*-band.

### 2. Extended LSB Galaxy Survey

The Virgo Deep Stack is an invaluable data set with its large area coverage and proven depth and quality. Further studies using this image could yield a fully comprehensive *OR*-band survey including galaxies of very small angular size and faint surface brightness. This would provide a more complete understanding of the galaxy population and provide many more targets for further studies at other wavelengths.

### 3. Additional Galaxy Surface Brightness Comparisons

Surface photometry of galaxies in the Virgo Deep Stack could be compared with other literature data on the same galaxies in the same or different passbands. Data in the same passbands enhances the understanding of possible sources of error and data in different passbands could be used to derived colour information for individual galaxies.

### 4. Analysis of Luminosity Functions for the Virgo Cluster

Because of the large area coverage of the Virgo Deep Stack, and the availability of data on most of the source galaxies in online databases, it would be possible to re-evaluate the properties of the galaxies included in published luminosity functions. This would yield a standard data set over a large area, from which a full-cluster luminosity function could be better approximated. This may also highlight discrepancies in data analysis methods, such as the large differences in magnitude found between the Virgo Deep Stack data and the Trentham and Tully (2002) data. Unfortunately, due to the saturation problem for brighter galaxies, some literature magnitudes would have to be used. Nevertheless, a homogeneous data set covering a large area over a range of fainter magnitudes would be extremely valuable.

### 5. Distance Determinations

Distance information, particularly in the borderline region for likely cluster membership (i.e. where galaxy scale length is between 2 and 5 arcseconds) is crucial in obtaining a meaningful luminosity function for the Virgo Cluster. Distances may be inferred from spectroscopic observations that measure redshifts to derive radial velocities. This type of investigation may be performed using long-slit or IFU spectroscopy. The alternative is to use high-resolution optical observations that resolve individual stars and provide data that may be used for TRGB measurements (e.g. Caldwell (2006) and Durrell et al. (2007)).

### 6. Intra-Cluster Light

The wide-field coverage of the Virgo Deep Stack provides a valuable baseline data set for follow-up studies of intra-cluster light.

## 7. Studies of Well-Known Galaxies

Outer haloes of bright galaxies may be further investigated to unprecedented depth, as demonstrated by the discovery of a near-complete shell around galaxy M89. Many other bright galaxies, contained within the field of the Virgo Deep Stack, may be re-examined to develop a better understanding of their extent and to potentially discover new evidence of tidal interactions.

## 8. Bryn's Mystery Object

This object appears especially worthy of follow-up study. This could take the form of spectroscopy using a telescope-instrument combination with reasonable area coverage and high through-put, e.g. the  $80 \times 80$ -arcsec field-of-view Sparsepak IFU on the WIYN 3.5-m telescope at Kitt Peak National Observatory, Arizona, the PPAK 1-arcminute field-of-view IFU used with the 3.5-m Telescope at Calar Alto Observatory, Spain or the  $22 \times 11$ -arcsec field-of-view SPIRAL IFU on the Anglo-Australian Telescope. The other option is to obtain observations with a high-resolution instrument such as the HST to resolve the stellar population.



## Appendices



## A. SCALE LENGTH AND SLOPE OF THE FITTING FUNCTION

One scale length  $a$  is where the intensity of light  $I$  falls to  $1/e$  from its peak  $I_0$ , i.e.  $I_a = I_0/e$ . In terms of surface brightness  $\mu$  and the plate constant  $Z$ , the difference between the peak surface brightness and the surface brightness at one scale length is derived as follows:

$$\begin{aligned}
 \mu_0 &= Z - 2.5 \log(I_0) \\
 \mu_a &= Z - 2.5 \log\left(\frac{I_0}{e}\right) \\
 &= Z - 2.5 \log(I_0) + 2.5 \log(e) \\
 &= \mu_0 + 2.5 \log(e) \\
 \mu_a - \mu_0 &= 2.5 \log(e)
 \end{aligned}$$

This last term may also be expressed in the form of a natural logarithm by using change of base where:

$$\begin{aligned}
 2.5 \log(e) &= \frac{1}{\log(100^{1/5})} \log(e) \\
 &= \frac{1}{\ln(100^{1/5})},
 \end{aligned}$$

i.e. both terms are equivalent and equal  $\sim 1.08573$ .

Then from the equation of a straight line ( $y = mx+b$ ) in terms of a magnitude-radius plot, using  $s$  for slope and taking the values at one scale length  $a$ :

$$\begin{aligned}\mu_a &= sa + \mu_0 \\ a &= \frac{\mu_a - \mu_0}{s} \\ &= \frac{2.5 \log(e)}{s}\end{aligned}$$

or, using natural logarithms:

$$a = \frac{\frac{1}{\ln(100^{1/5})}}{s}.$$



## B. LUMINOSITY-TO-MAGNITUDE CONVERSION OF THE SCHECHTER FUNCTION

Schechter's original formulation of the luminosity function is:

$$\phi(L)dL = \phi_*(L/L_*)^\alpha \exp(-L/L_*)d(L/L_*). \quad (\text{B.1})$$

The relationship between magnitude and luminosity is:

$$M - M_* = -2.5 \log(L/L_*) \quad (\text{B.2})$$

Several relations are derived using change of base, absolute value of  $dM$ , and some rearrangements:

$$\begin{aligned} M &= M_* - 2.5 \frac{\ln(L/L_*)}{\ln(10)} \\ dM &= \frac{2.5}{\ln(10)} \frac{L_*}{L} \frac{dL}{L_*} \\ dL &= 0.4 \ln(10) L dM \end{aligned} \quad (\text{B.3})$$

$$\begin{aligned} M_* - M &= 2.5 \log(L/L_*) \\ \frac{M_* - M}{2.5} &= \log\left(\frac{L}{L_*}\right) \\ \frac{L}{L_*} &= 10^{0.4(M_* - M)} \end{aligned} \quad (\text{B.4})$$

$$1/L_* = 10^{0.4(M_* - M)} (1/L) \quad (\text{B.5})$$

The terms B.4, B.3 and B.5 are then substituted into the fundamental equality of the two functions:

$$\begin{aligned}
\phi(M)dM &= \phi(L)dL & (B.6) \\
&= \phi_*(L/L_*)^\alpha \exp(-L/L_*)dL \, 1/L_* \\
&= \phi_* \, 10^{0.4(M_*-M)\alpha} \exp(-10^{0.4(M_*-M)})(0.4 \ln(10) \, L \, dM) \, 10^{0.4(M_*-M)}(1/L)
\end{aligned}$$

The ‘L’s cancel and terms are collected and rearranged:

$$\phi(M)dM = 0.4 \ln(10) \, \phi_* 10^{0.4(\alpha+1)(M_*-M)} \exp(-10^{0.4(M_*-M)})dM \quad (B.7)$$

## C. ABSOLUTE MAGNITUDE AND THE HUBBLE PARAMETER

Absolute magnitude in some given passband  $X$  is sometimes shown as an expression of the form:

$$M_X - 5 \log h. \quad (\text{C.1})$$

This expression allows for the fact that the Hubble Constant  $H_0$  is not known with certainty. The magnitude may be recalculated using a preferred value of  $h$  where  $H_0 = hH$ ,  $H = 100 \text{ km s}^{-1} \text{ Mpc}^{-1}$  and thus:

$$H_0 = 100 h \text{ km s}^{-1} \text{ Mpc}^{-1} \quad (\text{C.2})$$

This overcomes problems encountered when comparing some of the earlier literature where specific values for  $H_0$  are used (e.g. Sabatini et al. (2003) used  $H_0 = 75 \text{ km s}^{-1} \text{ Mpc}^{-1}$  but Dalcanton et al. (1997) used  $H_0 = 50 \text{ km s}^{-1} \text{ Mpc}^{-1}$ ).

The origin of expression C.1 is in the distance modulus  $DM$ , used to convert apparent magnitude  $m_X$  to absolute magnitude  $M_X$  (i.e. the magnitude an object would have if at 10 pc distance) based on distance  $d$  where:

$$DM = m_X - M_X = -5 + 5 \log_{10}(d). \quad (\text{C.3})$$

This may be rewritten as:

$$DM = 5 \log \left( \frac{d}{10} \right) \quad (\text{C.4})$$

and

$$M_X = m_X - DM. \quad (\text{C.5})$$

To find the distance modulus the steps are to measure redshift  $z$ , calculate a recession velocity ( $v = cz$ ) and determine distance based on an assumed Hubble Constant

$H_0 = hH$  (using  $d = v/H_0$ ). Terms are substituted into the distance modulus equation with a factor to convert Mpc (in the Hubble Constant) to parsecs (for the  $DM$  formula). Terms are then separated to isolate  $h$ :

$$\begin{aligned} DM &= 5 \log \left( \frac{cz \text{ km s}^{-1}}{10 hH \text{ km s}^{-1} \text{Mpc}^{-1}} \right) \\ &= 5 \log \left( \frac{cz \times 10^6 \text{ pc}}{10 H} \right) - 5 \log h. \end{aligned}$$

Magnitudes calculated from Equation C.5 thus represent:

$$M_X = m_X - 5 \log \left( \frac{cz \times 10^6}{10 H} \right) + 5 \log h. \quad (\text{C.6})$$

Therefore the true absolute magnitude  $M_{true_X}$  is:

$$M_{true_X} = M_X - 5 \log h. \quad (\text{C.7})$$

If  $h = 1$ , the magnitude is unchanged. If  $h < 1$  the object is closer and the absolute magnitude is larger (fainter) than  $M_X$  for a given apparent magnitude. Current best estimates of the Hubble Constant imply  $h \sim 0.7$ .

## D. IMAGE AND DATA FILES SUPPLIED BY ROYAL OBSERVATORY, EDINBURGH

The data files and related processing files for the Virgo Deep Stack that were provided by ROE are listed below. Mapping mode files, produced by the scanning/digitisation process, begin with `mm`. Image analysis mode files, that are produced when the scan is run through image detection and parameterisation software, begin with `IAM`. Files with extension `.sdf` are in Starlink format and may be inspected using `hdstrace`. Position information for objects detected in `IAM` mode is available in the `iam.srtrd` file, from which data may be accessed using `Fortran`. Refer Hambly (1998a) and Hambly (1998b) for further details.

In addition to the files listed below, there were 28 separate `mm` data files supplied, one for each scanning lane in the Virgo Deep Stack.

Data File	Description
<code>batch.log</code>	Object statistics, quality control data
<code>hkfile.lis</code>	‘Housekeeping’ file with exposure information
<code>iam.srtrd</code>	32 image parameters for every object detected in <code>IAM</code> mode
<code>mmdata.fits</code>	The final image - the Virgo Deep Stack
<code>RASUMMARY</code>	Details of stars used in coordinate fitting

Other files supplied: `hkfile.sdf`; `iam.fits`; `residual.corrns`; `skymap.sdf`; `sky.sdf`; `T\_to\_I.old`; `T\_to\_I.sdf`; `xyreport.lis`; `yoptdist.corrns`.



## E. VIRGO DEEP STACK CALIBRATION STARS

Table E.1 (overleaf) contains details of stars used in the calibration of the Virgo Deep Stack described in Section 5.4 (p.102). Object IDs,  $i$  and  $r$  data and colour corrections are from the SDSS. Blank data cells were outliers or outside the range for colour correction. Refer text for full details.

ID	RA (hh mm ss.ss)	Dec (dd mm ss.s)	$r$	$i$	$R$	$I$	$R - I$	$OR$	Sky	Signal	2.5 log(sig)	$OR + sig$	Residual
588017703470170000	12 26 25.39	12 27 01.5	20.4	18.9	19.9	18.2	1.6	19.8	6515	40418	11.52	31.28	-0.246
588017703470170000	12 26 26.78	12 24 03.5	20.0	19.1	19.6	18.5	1.1	19.6	6493	53049	11.81	31.38	-0.146
588017566564221000	12 26 29.24	12 35 19.8	20.1	20.0	19.9	19.6	0.3	19.9	6734	49780	11.74	31.61	0.090
588017703470170000	12 26 29.46	12 25 47.2	19.8	19.7	19.6	19.3	0.4	19.6	6478	64202	12.02	31.62	0.099
588017566564221000	12 26 31.34	12 34 07.0	18.8	18.5	18.5	18.1	0.5	18.5	6572	154046	12.97	31.48	-0.042
588017566564221000	12 26 31.44	12 31 40.5	19.8	19.6	19.6	19.1	0.5	19.6	6508	61778	11.98	31.55	0.032
588017566564221000	12 26 33.01	12 35 32.8	20.0	19.8	19.8	19.4	0.4	19.8	6886	45483	11.64	31.43	-0.096
588017703470235000	12 26 36.35	12 24 26.7	19.1	18.9	18.9	18.5	0.4	18.9	6519	109631	12.60	31.49	-0.034
588017566564221000	12 26 37.53	12 35 54.8	20.2	19.2	19.8	18.5	1.2	19.7	6723	49603	11.74	31.42	-0.101
588017566564221000	12 26 38.70	12 33 31.7	18.5	18.3	18.3	17.9	0.4	18.3	6526	191347	13.20	31.48	-0.045
588017566564286000	12 26 42.43	12 32 07.8	20.3	19.5	19.9	18.9	1.0	19.9	6534	48830	11.72	31.58	0.058
588017566564286000	12 26 45.43	12 35 52.8	19.1	19.0	18.9	18.6	0.3	18.9	6597	114910	12.65	31.56	0.040
588017566564286000	12 26 46.18	12 30 42.8	20.4	19.6	20.0	19.0	1.1	20.0	6539	36386	11.40	31.37	-0.150
588017703470235000	12 26 48.20	12 25 46.2	20.4	19.6	20.0	19.0	1.0	20.0	6541	45567	11.65	31.61	0.090
588017703470235000	12 26 49.27	12 28 49.6	19.6	19.4	19.4	19.0	0.4	19.4	6546	47003			
588017566564286000	12 26 49.82	12 30 30.5	20.1	19.9	19.9	19.5	0.4	19.9	6519	51489	11.78	31.64	0.119
588017566564286000	12 26 52.97	12 31 29.0	19.6	19.5	19.5	19.1	0.4	19.4	6526	78536	12.24	31.67	0.151
588017703470235000	12 26 55.84	12 28 13.4	19.5	18.0	18.9	17.2	1.7	18.8	6529	93900			
588017566564286000	12 26 56.04	12 35 32.1	19.5	19.4	19.3	18.9	0.4	19.3	6555	85138	12.33	31.63	0.105
588017703470235000	12 26 57.69	12 27 19.4	19.4	19.1	19.2	18.6	0.5	19.1	6508	96707	12.46	31.59	0.067
588017566564286000	12 26 59.65	12 31 49.0	19.7	18.0	19.0	17.2	1.9	18.9	6567	102526			

Tab. E.1: Calibration Stars

*Details of stars used to derive the plate constant for the Virgo Deep Stack.*



## F. GEMINI OBSERVING PROPOSALS

Despite difficulties of obtaining redshifts outlined in Section 4.5.1 (p.64), observing time was sought on three telescopes with large aperture and the spectroscopic capability to observe selected VLSB galaxies found in the Virgo Deep Stack. Applications were submitted to use the 3.5-metre telescope at Calar Alto in Spain, the WIYN 3.5-metre telescope on Kitt Peak in Arizona and the 8-metre Gemini North telescope in Hawaii. Each of these telescopes supports an IFU.

Two nights of classical mode observing time were granted on Gemini North in Semester 1, 2006, but poor weather on the allocated nights prevented any observations being made. The application for time in 2007 was awarded 10 hours of time in Band 2 of queue-mode observing. Again, poor weather during the semester meant that the targets were never observed. Nevertheless, the awarding of time in two observing rounds indicates that the proposed observations have scientific merit and that future applications would likely be viewed with similar favour.

### *F.1 Observing Procedure*

The successful observing proposals requested the use of the GMOS (Gemini Multi-Object Spectrograph) IFU. Targets were selected based on criteria of size and surface brightness at the ‘half-radius’ of the IFU. The concept was that the area covered by the galaxy would overfill the area covered by the IFU, and all spectra obtained would be co-added to improve the signal to noise. The IFU covers an area of 5 x 7 arcseconds, so the galaxy surface brightness at 2 arcsec radius was used as a mean over the instrument field of view.

These targets are extremely faint and even with this co-addition method, observations of up to 50 minutes per galaxy are required for those with 2-arcsec surface brightness of  $\sim 25 R\mu$ . There is also inherent difficulty in acquiring each target as these galaxies are too faint to be seen in an acquisition image. Therefore offsets from nearby stars are required where the reference stars need to be brighter than 19th magnitude in  $R$  band. A bright guide star is required for each observing target, must be close enough to be acquired by the instrument, and must be between magnitude 9.5 and 16 in  $V$  band. The IFU allows for sky data to be collected from a smaller fibre bundle located off-target. Therefore, a background region at a distance set by the instrument needs to be available. For the GMOS IFU the object field and the sky field are separated by one arcminute.

All the specified requirements were checked and observational data were loaded into the Gemini ‘Observing Tool’ software along with reference `.fits` images from the Virgo Deep Stack. In the Observing Tool, the observing target may be displayed, overlaid with the instrument fields and other information. A typical prepared observation is displayed in Figure F.1. The two successful observing proposals are included in Section F.2.

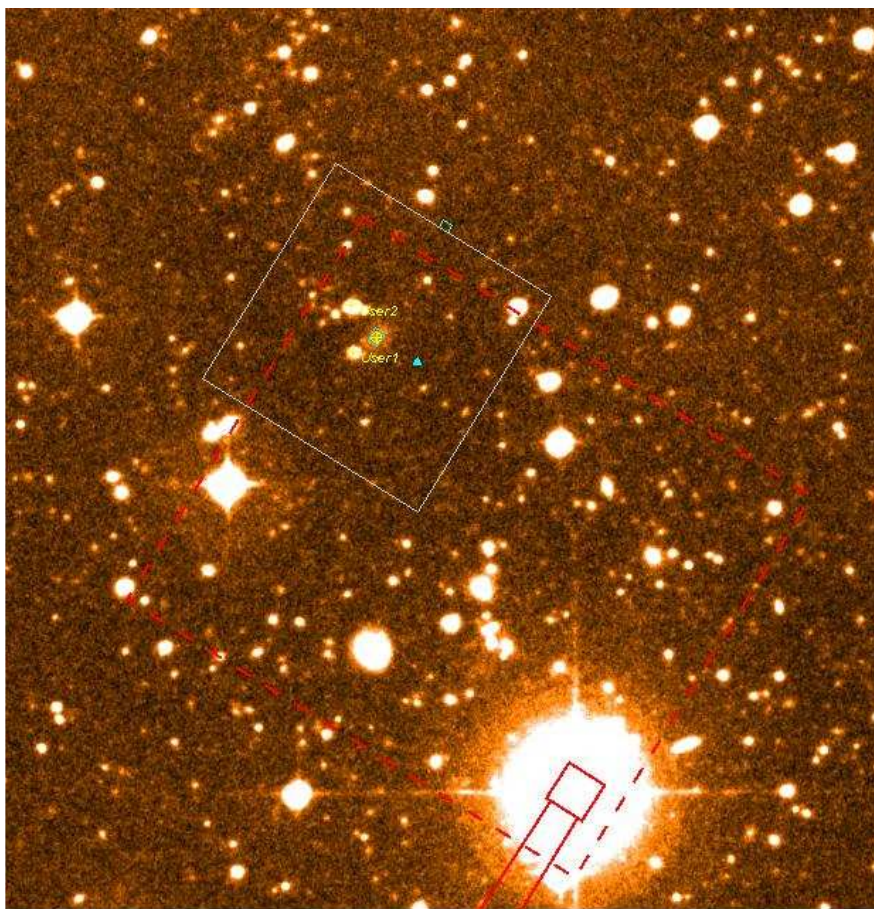


Fig. F.1: Sample Display: Gemini Observing Tool

*This display shows the  $2 \times 2$ -arcmin field of the acquisition camera (white square, upper left) and ‘User 1’ and ‘User 2’ reference stars, each around 19th magnitude, for blind offsets to the target galaxy, which is in the centre of acquisition field. The IFU target fibres cover  $5 \times 7$  arcsecs. Sky fibres are located 1 arcminute from the target in the tiny green rectangle at the centre of the top right side of the acquisition camera field, and cover  $5 \times 3.5$  arcsecs. The small red square at lower right indicates the centre of the bright 12th magnitude guide star. The red dotted line outlines the guide star field. Different orientations are possible to acquire guide stars within the effective field radius. The target galaxy is catalogued 22-1 and has an OR-band surface brightness of  $24.5\mu$  at a 2-arcsec radius. The base image is from the Virgo Deep Stack. North is at the top and east is to the left.*

## F.2 Observing Proposals

Phase 1 Proposal

Page 1 of 6

### GEMINI OBSERVATORY

*observing time request (HTML summary)*

**Semester:** 2006A    **Observing Mode:** classical    **Partner Lead Scientist:**  
 Quentin Parker  
 Anglo-Australian Observatory / Macquarie University

**Instruments:** GMOS North    **Gemini Reference:** Not Available    **Partner:**  
 Australia

**Time Awarded:**  
 Not Available

**Title:** A Pilot Study of newly-identified Low Surface Brightness Galaxies in Virgo

**Partner Lead Scientist:** Quentin Parker  
 Anglo-Australian Observatory / Macquarie University

**Principal Investigator:** Quentin Parker

**PI institution:** Anglo-Australian Observatory / Macquarie University, P.O. Box 296 (167 Vimiera Road), Epping, NSW 2121, Australia

**PI status:** PhD/Doctorate

**PI phone / fax / e-mail:** +61 2 9850 8910 / +61 2 9850 8115 / qap@ics.mq.edu.au

**Co-investigators:** Lesa Moore: Macquarie University, starrylady@hotmail.com  
 Simon Driver: Mount Stromlo Observatory, spd@mso.anu.edu.au

#### Partner Submission Details (multiple entries for joint proposals)

Partner	Partner Lead Scientist	Time Requested	Minimum Time Requested	Reference number	NTAC		Rank
					Recommended time	Minimum Recommended Time	
Australia	Parker	3.0 nights	1.0 nights	Not Available	0.0 hours	0.0 hours	
	Total Time	3.0 nights					

**Abstract:** The advent of powerful IFU systems on large telescopes permit realistic spectroscopy of extended low surface brightness sources. Here we plan to obtain redshifts, for the first time, for a carefully selected sample of newly-identified small-scale ( $< 10$  arcsecond diameter) very low surface brightness galaxies (LSBGs) in Virgo. These will allow us to unequivocally distinguish true cluster members from the background population. Previously, cluster membership for LSBGs has had to rely on aspects of galaxy morphology, or statistical or modelled estimates. Our redshifts will establish what proportion of LSBGs are true cluster members and significantly improve the determination of the faint-end slope of the Virgo Cluster luminosity function. This will have implications for total cluster luminosity, mass and evolution.

#### Science Justification

Scientific Background:

Contributions of different galaxy populations (normal Hubble types, low surface brightness galaxies (LSBGs), etc.) to the overall cluster population is of extreme significance in understanding the composition of galaxy clusters in

terms of galaxy number and mass. LSBGs are shown to comprise an important fraction of the cluster population (Phillipps et al., 1998) contributing substantially to: the cluster luminosity function (LF); total cluster luminosity; total cluster mass; and galaxy evolution within the cluster.

Since the Impey, Bothun, Malin (1988) study of the Virgo dwarf population, work on ultra-compact dwarfs (Drinkwater et al., 2005), the Millennium Galaxy Catalogue of faint galaxies (Driver, 2004), dwarf spheroidal galaxies in Virgo (Phillipps et al., 1998 and Parker et al., 1999) and LSBGs (Sabatini et al., 2003) has revealed the dependence on environment of the LF of different galaxy populations. Variations in the LF challenge hierarchical clustering models (Sabatini et al., 2003) and are inconsistent with cold dark matter theory (Trentham & Hodgkin, 2002). For LSBGs in the Virgo Cluster, Sabatini et al. (2003) and Trentham & Hodgkin (2002) find a faint-end slope of -1.6 whilst Phillipps et al. (1998) find a value of -2.26 (refer Figure 1). The steeper slope, remarkably, implies an infinite luminosity density. The different values are based on alternative methods of assessing cluster membership and looking at different cluster regions.

Ideally, cluster membership can be found from redshift, but whilst obtaining redshifts for Hubble-type galaxies is straightforward, it is far more difficult for LSBGs. In the radio regime, the beam is too wide and in the optical, large light-gathering grasp is needed to get adequate S/N. Methods of inferring cluster membership for LSBGs in the absence of redshift data have been based on: specific galaxy morphological characteristics (Binggeli et al., 1985); statistical sampling of cluster and field galaxy numbers (Jones et al., 1999); or using numerical simulations to find selection criteria that minimize background contamination (Sabatini et al., 2003). This is difficult to do properly. The only way to unequivocally determine cluster membership and resolve the faint-end slope debate is with our proposed spectroscopic confirmation.

Redshift measurements are vital if we want to understand cluster evolution, possible LSBG sub-structure, the true level of background contamination and overall cluster mass. For instance, how does the LSBG distribution vary with proximity to large elliptical galaxies (Sabatini et al., 2003) and through the cluster as a whole? Why does the dwarf to giant ratio not progress towards the field value in the outskirts of the Virgo cluster (Sabatini et al., 2003)? Do LSBGs provide enough mass to cluster systems to close or significantly narrow the "missing" dark matter gap (Jarrett, 1998)?

#### Current Observations:

We now have a unique, ultra-deep, R-band UKST 63-exposure stack which provides us with detections of significant numbers of new, small to large scale LSBGs (refer Figure 3). With redshift data for a statistically significant sample of these galaxies, we will be able to address these important questions. The digital stack yields detections to  $>27.5$  R mag per square arcsec. This is 2.25 magnitudes fainter than a single deep R-band exposure and is directly competitive with deep, but small area, CCD surveys (Sabatini et al., 2003). This stack gives us uniform and complete coverage to a deeper threshold than previous work over the entire central 25 square degrees of the Virgo Cluster area (refer Figure 2). In this pilot study we aim to obtain integrated IFU spectra with S/N of  $>5$  for a carefully selected, representative sample of small-scale ( $<10$  arcsecond scale length) newly-identified LSBGs in Virgo from which reliable redshifts can be determined for the first time.

A complementary program for larger scale ( $<100$  arcseconds) LSBGs is proposed for large-format IFUs on 3 - 4 metre telescopes where similar S/N to Gemini may be obtained. However, the smaller scale LSBGs dominate the population so it is important to estimate their contaminant fraction. For these we require the larger aperture of Gemini.

ONLY redshifts can reveal which are true cluster members and which are background galaxies. We can then directly estimate the true fraction of LSBGs as a function of scale length actually belonging to the Virgo Cluster and properly evaluate their contribution to the faint end slope of the cluster LF.

Our preliminary sample contains 20 targets, the minimum that is likely to lead to a publication. A smaller allocation is still useful to demonstrate viability, but will of course delay the project and eventual publication. Our ultimate aim, for statistical rigour, is to obtain redshifts of at least 100 LSBGs over a range of scale lengths and distances between the centre and the edge of the Virgo cluster. Gemini N will target the smaller scale length galaxies, with angular sizes appropriate to the field of view of the GMOS IFU.

Phase 1 Proposal

Page 3 of 6

## References:

Binggeli, Sandage, Tammann, 1985, AJ, 90, 1681.

Drinkwater, Gregg, Couch, et al., 2005, PASA, 21, 375.

Driver, Liske, Cross, et al., 2005, MNRAS, 360, 81.

Impey, Bothun, Malin, 1988, ApJ, 330, 634.

Jarrett, 1998, The Impact of Near-Infrared Sky Surveys on Galactic and Extragalactic Astronomy: Proceedings of the 3rd Euroconference on Near-Infrared Surveys held at Meudon Observatory (France) on June 19-20, 1997. Edited by N. Epchtein. Dordrecht; Boston, Mass.: Kluwer Academic Pub., 1998. (Astrophysics and space science library) 230, 239.

Jones, Phillipps, Schwartzberg, Parker, 1999, Astronomical Society of the Pacific Conference Series, 84.

Parker, Phillipps, 1999, Looking Deep in the Southern Sky, Proceedings of the ESO/Australia Workshop held at Sydney, Australia, 10-12 December 1997. Edited by Faffaella Morganti and Warrick J. Couch. Berlin: Springer-Verlag, 1999, p83.

Phillipps, Parker, Schwartzberg, Jones, 1998, ApJ, 493, L59.

Sabatini, Davies, Scaramella, et al., 2003, MNRAS, 341, 981.

Trentham & Hodgkin, 2002, MNRAS, 333, 423.

## Attachments:

Name	Source	Type
Figure 1: The luminosity function of Phillipps et al. (1998) for a sample of LSBGs in the outer part of the Virgo cluster. They find a faint-end slope of -2.26. The solid line is the LSBG field count.	SchPlot600.jpg	JPEG
Figure 2: Dots represent locations of the 2096 Virgo Cluster Catalogue galaxies (Binggeli et al. 1985). Small boxes are the 113 CCD fields observed by Trentham & Hodgkin (2002). The large box is the full 6x6-degree field of our deep UKST stacked image; the uniform unvignetted area is the central 5x5 degrees. (Image from Trentham & Hodgkin, 2002.)	th600.jpg	JPEG
Figure 3: Images of six of our newly-discovered LSBGs in Virgo corresponding to (left to right, top) 22-6,-7,-9 and (left to right, bottom) 22-1,-2,-4 in our Targets list.	siximages.jpg	JPEG

## Technical Justification

It has been difficult to obtain redshifts for LSBGs using slit spectroscopy due to the long observing times needed to obtain sufficient S/N for these objects. This is coupled with the need to obtain redshifts for a large enough number of galaxies to get meaningful statistics. The advent of powerful wide-area IFUs enables us to tackle this problem realistically for the first time by being able to sample much of the galaxy and co-add spectra from all on-target fibres whilst retaining optimum spectral resolution. The GMOS IFU is well suited to observe a representative sample of small-scale LSBGs in Virgo. Their redshifts will be used to determine cluster membership. Statistical or probabilistic methods of estimating cluster membership can then be directly compared with real redshift data.

Gemini North is preferred because our targets are at +10 to +16 Dec. Depending on the success of our application, and the observing time granted, we hope to obtain redshifts of 20 small-scale galaxies in various regions of the Virgo



## Phase 1 Proposal

Page 4 of 6

cluster (from the core to the edge). Whilst we have not requested long-term status, we may apply for future time depending on the outcome of the current proposal.

## Instrumentation details:

Gemini N telescope with GMOS IFU: our targets are at +13 Dec. with mean surface brightness down to 24.5 in R.

R150\_G5306 grating: spectral coverage 400 to 900 nm (central 700nm); grating resolution = 632 at slit width 0.5" yields spectral resolution for the IFU (with effective slit width 0.31") of 0.59nm at 600nm, giving us velocities accurate to ~300 km/s.

With spatial and spectral binning x 4, pixel size will be 0.288 arcsec (spatial) and 0.6972nm (spectral).

S/N for a single IFU element (using any image quality, 50%-ile cloud, any water vapour, 50%-ile sky background) for a 3000s exposure is around 0.18 for an elliptical sample spectrum. By co-adding all 1000 spectra from the IFU, this increases by  $\sqrt{1000}$  to 5.7, sufficient for obtaining redshifts.

The wavelength range will cover MgB, NaD (absorption), H-beta, OIII and H-alpha (emission) over the expected redshift range for cluster and background galaxies.

## Observations:

For each target we will use a single exposure of 3000s. Allowing readout time of 55s, acquisition of 1200s and arc exposure & read of 120s, this adds to 4375s per target (73 minutes). To observe 20 targets will require 24.3 hours of GMOS-North time, though for some brighter sources, exposure times may be reduced. We have requested Classical mode observing as times may also be reduced in ideal observing conditions.

We will observe 6-7 targets per night (total 18-21) if the granted time is in the optimum date range. Our target galaxies are low surface brightness extended objects with central surface brightness < 24.5 R mag/sq arcsec. Scale sizes are typically 10 arcseconds in diameter, and will completely fill the GMOS IFU. Observing 18 or more targets would give us a meaningful sample for our survey, thus we have requested 3 nights of Gemini North time. Dark time is needed for all but our brightest targets due to their low surface brightness; "darkest" would be preferred, but our S/N calculations are based on "dark" conditions. A minimum useful requirement would be 1 night.

## Targets:

A sample of 6 targets appears in the Observations section of this application. We are currently in the process of assessing the priority of remaining targets based on their extent and central surface brightness. We will have a full list of targets in the coming weeks. All targets will be in the range 12h15m to 12h50m, +10 to +16 degrees.

## Observation Details

Observation	RA	Dec	Brightness	Total Time (including overheads)
<b>22-1</b>	12:28:14.32	13:43:42.0	R 24.25	73.0 minutes
<b>GSC0088000626</b> (oiwfs)	12:28:07.98	13:40:08.04	11.21 mag	separation 3.88
<a href="#">observing conditions</a> : Global Default		<a href="#">resources</a> : GMOS North		
<b>22-2</b>	12:28:56.9	13:26:39.4	R 24.25	73.0 minutes
<b>GSC0088000618</b> (oiwfs)	12:28:47.23	13:22:49.51	12.69 mag	separation 4.5
<a href="#">observing conditions</a> : Global Default		<a href="#">resources</a> : GMOS North		

Phase 1 Proposal

Page 5 of 6

<b>22-4</b>	12:27:57.21	13:55:51.3	R 23.7	73.0 minutes
<b>GSC0088000428</b> (oiwfs)	12:28:11.626	13:57:50.62	12.47 mag	separation 4.02
<a href="#">observing conditions</a> : Global Default		<a href="#">resources</a> : GMOS North		
<b>22-6</b>	12:27:15.46	13:24:43.9	R 24.5	73.0 minutes
<b>GSC0088000685</b> (oiwfs)	12:27:02.527	13:25:14.81	14.34 mag	separation 3.19
<a href="#">observing conditions</a> : Global Default		<a href="#">resources</a> : GMOS North		
<b>22-9</b>	12:26:46.53	13:16:1.2	R 24.2	73.0 minutes
<b>GSC0088000515</b> (oiwfs)	12:26:40.502	13:18:37.26	10.74 mag	separation 2.99
<a href="#">observing conditions</a> : Global Default		<a href="#">resources</a> : GMOS North		
<b>22-7</b>	12:27:15.57	13:26:59.8	R 25.3	73.0 minutes
<b>GSC0088000685</b> (oiwfs)	12:27:02.527	13:25:14.81	14.34 mag	separation 3.62
<a href="#">observing conditions</a> : Global Default		<a href="#">resources</a> : GMOS North		

**Resources**

- Gemini North
  - GMOS North
    - Focal Plane Unit
      - IFU w/ 2 slits
    - Disperser
      - R150\_G5306
    - Filter
      - GG455\_G0305

**Observing Conditions**

Name	Image Quality	Sky Background	Water Vapor	Cloud Cover
Global Default	Any	50%	Any	50%

**Scheduling Information:****Synchronous dates:****Optimal dates:** 2006/2/27-2006/3/5, 2006/3/23-2006/4/1, 2006/4/22-2006/5/1**Reason:** Longest time on target with airmass less than 2 and no Moon**Impossible dates:****Allocation Committee Comments****Additional Information****Keyword Category:** Extra Galactic**Keywords:** Distances and redshifts, Dwarf galaxies, Low surface brightness galaxies, Survey



Phase 1 Proposal

Page 6 of 6

**Publications:**

- Driver S.P., (2004), "Beyond the galaxy luminosity function", PASA, 21, 344.

**Allocations:**

Reference	Time	% Useful	Status of previous data
GS-2005A-C-12	3.0 nights	90	(Parker) AGB halos surrounding Planetary Nebulae in the Large Magellanic Cloud. Progressive reduction near completion with paper in prep.
GS-2005B-Q-61	1.0 nights		(Parker) Not yet observed
GN-2004A-Q-38	17.5 hours	22	(Driver) GMOS spectroscopy of Millennium Galaxy Catalog extreme-LSB galaxies. Successful observations of 4 galaxies, remaining category 2 time lost to weather. Forms a part of 3 publications and 2 submitted papers.

**Related proposal Information:**

Proposal to Calar Alto, Spain: Requesting 5 nights to observe 35-40 larger scale-size LSBGs using PPak IFU on 3.5m telescope. Proposal to NOAO: Requesting 5 nights to observe 35-40 larger scale-size LSBGs using DensePak IFU on WIYN 3.5m telescope. Proposals can be scheduled over a three-month range.

**Proposal Contents**[Summary](#)[Investigators](#)[Partner Submission Details](#)[Abstract](#)[Science Justification](#)[Technical Justification](#)[Observation Details](#)[Allocation Committee Comments](#)[Additional Information](#)

## GEMINI OBSERVATORY

*observing time request (HTML summary)*

**Semester:** 2007A**Observing Mode:** queue**Partner Lead Scientist:**Quentin Parker  
Macquarie University**Instruments:**  
GMOS North**Gemini Reference:**  
Not Available**Partner:**  
Australia**Time Awarded:**  
Not Available**Title:** A Pilot Study of newly-identified Low Surface Brightness Galaxies in Virgo**Partner Lead Scientist:** Quentin Parker  
Macquarie University**Principal Investigator:** Quentin Parker**PI institution:** Macquarie University, North Ryde, NSW 2109, Australia**PI status:** PhD/Doctorate**PI phone / fax / e-mail:** +61 29850891- / +61 298508115 / qap@ics.mq.edu.au**Co-investigators:** Lesa Moore: Macquarie University, starrylady@hotmail.com  
Steve Phillipps: University of Bristol, S.Phillipps@bristol.ac.uk  
Simon Driver: University of St. Andrews, spd3@st-andrews.ac.uk  
Bryn Jones: Queen Mary University of London, Bryn.Jones@qmul.ac.uk**Partner Submission Details** (*multiple entries for joint proposals*)

Partner	Partner Lead Scientist	Time Requested	Minimum Time Requested	Reference number	NTAC		Rank
					Recommended time	Minimum Recommended Time	
Australia	Parker	24.3 hours	5.0 hours	Not Available	0.0 hours	0.0 hours	
	Total Time	24.3 hours					

**Abstract:** Powerful IFU systems on large telescopes now permit spectroscopy of extended low surface brightness sources. We will obtain redshifts, for the first time, for a carefully selected sample of newly-identified small-scale (<10 arcsecond diameter) very low surface brightness galaxies (LSBGs) in Virgo from our unique ultra-deep map. These will allow us to unequivocally distinguish true cluster members from the background population. Previously, cluster membership for LSBGs has had to rely on aspects of galaxy morphology, or statistical or modelled estimates. Our redshifts will establish what proportion of LSBGs are true cluster members and significantly improve the determination of the faint-end slope of the Virgo Cluster luminosity function. This will have implications for total cluster luminosity, mass and evolution.

**Science Justification**

Contributions of different galaxy populations (normal Hubble types, low surface brightness galaxies (LSBGs), etc.) to the overall cluster population is of extreme significance in understanding the composition of galaxy clusters in terms of galaxy number and mass. LSBGs are shown to comprise an important fraction of the cluster population (Phillipps et al., 1998) contributing substantially to: the cluster luminosity function (LF); total cluster luminosity; total cluster mass; and galaxy evolution within the cluster.

Since the Impey, Bothun, Malin (1988) study of the Virgo dwarf population, work on ultra-compact dwarfs (Drinkwater et al., 2005), the Millennium Galaxy Catalogue of faint galaxies (Driver, 2004), dwarf spheroidal galaxies in Virgo (Phillipps et al., 1998 and Parker et al., 1999) and LSBGs (Sabatini et al., 2003) has revealed the dependence on environment of the LF of different galaxy populations. Variations in the LF challenge hierarchical clustering models (Sabatini et al., 2003) and are inconsistent with basic cold dark matter theory (Trentham & Hodgkin, 2002). For LSBGs in the Virgo Cluster, values of the faint-end slope of the LF have included -1.35 (Sandage, Binggeli, Tammann, 1985), -1.6 (Sabatini et al., 2003 and Trentham & Hodgkin, 2002) and steeper values to -1.8 (Phillipps, private communication). Figure 1 compares two of these LFs. The different values are based on detection capability, surveys of different cluster regions and, most significantly, various methods of assessing cluster membership.

Ideally, cluster membership can be found from redshift, but whilst obtaining redshifts for Hubble-type galaxies is straightforward, it is far more difficult for LSBGs. In the radio regime, the beam is too wide and in the optical, large light-gathering grasp is needed to get adequate S/N. Methods of inferring cluster membership for LSBGs in the absence of redshift data have been based on: specific galaxy morphological characteristics (Binggeli et al., 1985); statistical sampling of cluster and field galaxy numbers (Jones et al., 1999); or using numerical simulations to find selection criteria that minimize background contamination (Sabatini et al., 2003). This is difficult to do properly. The only way to unequivocally determine cluster membership and resolve the faint-end slope debate is with our proposed spectroscopic confirmation.

Redshift measurements are vital if we want to understand cluster evolution, possible LSBG sub-structure, the true level of background contamination and overall cluster mass. For instance, how does the LSBG distribution vary with proximity to large elliptical galaxies (Sabatini et al., 2003) and through the cluster as a whole? Why does the dwarf to giant ratio not progress towards the field value in the outskirts of the Virgo cluster (Sabatini et al., 2003)? Do LSBGs provide enough mass to cluster systems to close or significantly narrow the "missing" dark matter gap (Jarrett, 1998)?

#### Current Observations:

We now have a unique, ultra-deep, R-band UKST 63-exposure stack which provides us with detections of significant numbers of new, small to large scale LSBGs (refer Figure 3). With redshift data for a statistically significant sample of these galaxies, we will be able to address these important questions. The digital stack yields detections to  $>27.5$  R mag per square arcsec. This is 2.25 magnitudes fainter than a single deep R-band exposure and is directly competitive with deep, but small area, CCD surveys (Sabatini et al., 2003). This stack gives us uniform and complete coverage to a deeper threshold than previous work over the entire central 25 square degrees of the Virgo Cluster area (refer Figure 2). In this pilot study we aim to obtain integrated IFU spectra with S/N of  $>5$  for a carefully selected, representative sample of small-scale ( $<10$  arcsecond scale length) newly-identified LSBGs in Virgo from which reliable redshifts can be determined for the first time.

A complementary program for larger scale ( $<100$  arcseconds) LSBGs is proposed for large-format IFUs on 3 - 4 metre telescopes where similar S/N to Gemini may be obtained. However, the smaller scale LSBGs dominate the population so it is important to estimate their contaminant fraction. For these we require the larger aperture of Gemini.

ONLY redshifts can reveal which are true cluster members and which are background galaxies. We can then directly estimate the real fraction of LSBGs as a function of scale length actually belonging to the Virgo Cluster and properly evaluate their contribution to the faint end slope of the cluster LF.

Our preliminary sample contains 20 targets, the minimum that is likely to lead to a publication. A smaller allocation is still useful to demonstrate viability, but will of course delay the project and eventual publication (and the student's thesis). Our ultimate aim, for statistical rigour, is to obtain redshifts of at least 100 LSBGs over a range of scale lengths and distances between the centre and the edge of the Virgo cluster. Gemini N will target the smaller scale length galaxies, with angular sizes appropriate to the field of view of the GMOS IFU.

#### References:

Phase 1 Proposal

Page 3 of 7

Binggeli, Sandage, Tammann, 1985, AJ, 90, 1681.

Drinkwater, Gregg, Couch, et al., 2005, PASA, 21, 375.

Driver, Liske, Cross, et al., 2005, MNRAS, 360, 81.

Impey, Bothun, Malin, 1988, ApJ, 330, 634.

Jarrett, 1998, The Impact of Near-Infrared Sky Surveys on Galactic and Extragalactic Astronomy: Proceedings of the 3rd Euroconference on Near-Infrared Surveys held at Meudon Observatory (France) on June 19-20, 1997. Edited by N. Epchtein. Dordrecht; Boston, Mass.: Kluwer Academic Pub., 1998. (Astrophysics and space science library) 230, 239.

Jones, Phillipps, Schwartzberg, Parker, 1999, Astronomical Society of the Pacific Conference Series, 84.

Parker, Phillipps, 1999, Looking Deep in the Southern Sky, Proceedings of the ESO/Australia Workshop held at Sydney, Australia, 10-12 December 1997. Edited by Faffaella Morganti and Warrick J. Couch. Berlin: Springer-Verlag, 1999, p83.

Phillipps, Parker, Schwartzberg, Jones, 1998, ApJ, 493, L59.

Sandage, Binggeli, Tammann, 1985, AJ, 90, 1759.

Sabatini, Davies, Scaramella, et al., 2003, MNRAS, 341, 981.

Trentham & Hodgkin, 2002, MNRAS, 333, 423.

#### Attachments:

Name	Source	Type
Figure 2: Dots represent locations of the 2096 Virgo Cluster Catalogue galaxies (Binggeli et al. 1985). Small boxes are the 113 CCD fields observed by Trentham & Hodgkin (2002). The large box is the full 6x6-degree field of our deep UKST stacked image; the uniform unvignetted area is the central 5x5 degrees. (Image from Trentham & Hodgkin, 2002.)	th600.jpg	JPEG
Figure 3: Images of 4 of our newly-discovered LSBGs in Virgo corresponding to (left to right, top) 28-53,24-19 and (left to right, bottom) 28-40,24-40 in our Targets list.	fourimages.jpg	JPEG
Figure 1: Sabatini et al. (2003) compare their faint end of the LF in Virgo (circles, slope -1.6) with that of Sandage, Binggeli and Tamman (1985) (squares, slope -1.35).	LF.jpg	JPEG

#### Technical Justification

It has previously been extremely difficult to obtain redshifts for LSBGs using slit spectroscopy due to the long observing times needed to obtain sufficient S/N for these objects. This is coupled with the need to obtain redshifts for a large enough number of galaxies to get meaningful statistics when looking at populations within rich clusters such as Virgo. The advent of powerful wide-area IFUs enables us to tackle this problem realistically for the first time by being able to sample much of the galaxy and co-add spectra from all on-target fibres whilst retaining optimum spectral resolution. The GMOS IFU is well suited to observe a representative sample of small-scale LSBGs in Virgo. Their redshifts will be used to determine cluster membership. Statistical or probabilistic methods of estimating cluster membership can then be directly compared with real redshift data. Gemini North is the preferred option because our targets are at +10 to +16 Dec but Gemini South can also access the field for much of the Semester although at a generally larger airmass. Depending on the success of our application, and the observing time granted, we hope to obtain redshifts of 20 small-scale galaxies in various regions of the Virgo cluster (from the core to the edge). Whilst

## Phase 1 Proposal

Page 4 of 7

we have not requested long-term status, we may apply for future time depending on the outcome of the current proposal. This number is sufficient for preliminary stastical evaluation.

## Instrumentation details:

Gemini N/S telescope(s) with GMOS IFU: our targets are generally at +13 Dec (range 10-16), most with mean surface brightness down to 24.5 in R and just two fainter targets.

R150\_G5306 grating: spectral coverage 400 to 900 nm (central 700nm); grating resolution = 632 at slit width 0.5" yields spectral resolution for the IFU (with effective slit width 0.31") of 0.59nm at 600nm, giving us velocities accurate to ~300 km/s.

With spatial and spectral binning x 4, pixel size will be 0.288 arcsec (spatial) and 0.6972nm (spectral).

S/N for a single IFU element (using any image quality, 50%-ile cloud, any water vapour, 50%-ile sky background) for a 3000s exposure is around 0.18 for an elliptical sample spectrum. By co-adding all 1000 spectra from the IFU, this increases by  $\sqrt{1000}$  to 5.7, sufficient for obtaining redshifts.

The wavelength range will cover MgB, NaD (absorption), H-beta, OIII and H-alpha (emission) over the expected redshift range for cluster and background galaxies.

## Observations:

For each target we will use a single exposure of 3000s. Allowing readout time of 55s, acquisition of 1200s and arc exposure & read of 120s, this adds to 4375s per target (73 minutes). To observe 20 targets will require 24.3 hours of GMOS-North or South time, though for some brighter sources, exposure times may be reduced. We have requested Queue mode observing and modest observing conditions.

We could observe ~8 targets per full night if the granted time is in the optimum date range and executed concurrently. Our target galaxies are low surface brightness extended objects with central surface brightness <24.5 R mag/sq arcsec. Scale sizes are typically 10 arcseconds in diameter, and will completely fill the GMOS IFU. Observing 20 or more targets would give us a meaningful sample for our survey, thus we have requested the equivalent of 2.5 nights of Gemini time. Dark time is needed for all but our brightest targets due to their low surface brightness; "darkest" would be preferred, but our S/N calculations are based on "dark" conditions. A minimum useful requirement would be the equivalent of 0.5 night or 5 hours to obtain 4 targets as proof of concept.

## Targets:

All 20 proposed targets are entered in the Observations section of this application. All targets are in the range 12h20m to 12h30m, +13d16m to +14d 48m.

## Observation Details

Observation	RA	Dec	Brightness	Total Time (including overheads)
<b>22-1</b>	12:28:14.32	13:43:42.0	R 24.25	73.0 minutes
<b>U0975_06966946</b> (oiwfs)	12:28:07.997	13:40:08.0	11.2 mag	separation 3.88
<a href="#">observing conditions</a> : Global Default		<a href="#">resources</a> : GMOS North		
<b>22-2</b>	12:28:56.9	13:26:39.4	R 24.25	73.0 minutes
<b>U0975_06969159</b> (oiwfs)	12:28:47.237	13:22:48.58	11.8 mag	separation 4.51
<a href="#">observing conditions</a> : Global Default		<a href="#">resources</a> : GMOS North		

<b>22-4</b>	12:27:57.21	13:55:51.3	R 23.7	73.0 minutes
<b>U0975_06967157</b> (oiwfs)	12:28:11.594	13:57:50.98	11.6 mag	separation 4.02
<a href="#">observing conditions</a> : Global Default		<a href="#">resources</a> : GMOS North		
<b>22-6</b>	12:27:15.46	13:24:43.9	R 24.5	73.0 minutes
<b>U0975_06963179</b> (oiwfs)	12:27:02.546	13:25:15.02	12.6 mag	separation 3.18
<a href="#">observing conditions</a> : Global Default		<a href="#">resources</a> : GMOS North		
<b>22-7</b>	12:27:15.57	13:26:59.8	R 25.3	73.0 minutes
<b>U0975_06963179</b> (oiwfs)	12:27:02.546	13:25:15.02	12.6 mag	separation 3.62
<a href="#">observing conditions</a> : Global Default		<a href="#">resources</a> : GMOS North		
<b>22-9</b>	12:26:46.53	13:16:1.2	R 24.2	73.0 minutes
<b>U0975_06961880</b> (oiwfs)	12:26:40.502	13:18:37.51	11.3 mag	separation 2.99
<a href="#">observing conditions</a> : Global Default		<a href="#">resources</a> : GMOS North		
<b>28-53</b>	12:28:42.33	14:47:13.6	R 24.3	73.0 minutes
<b>U0975_06968862</b> (oiwfs)	12:28:41.899	14:45:49.79	11.5 mag	separation 1.4
<a href="#">observing conditions</a> : Global Default		<a href="#">resources</a> : GMOS North		
<b>24-19</b>	12:21:49.38	13:35:48.9	R 24.49	73.0 minutes
<b>U0975_06945930</b> (oiwfs)	12:21:48.353	13:33:45.36	14.4 mag	separation 2.07
<a href="#">observing conditions</a> : Global Default		<a href="#">resources</a> : GMOS North		
<b>28-40</b>	12:28:51.1	14:37:6.7	R 24.4	73.0 minutes
<b>U0975_06969331</b> (oiwfs)	12:28:50.638	14:33:14.04	11.5 mag	separation 3.88
<a href="#">observing conditions</a> : Global Default		<a href="#">resources</a> : GMOS North		
<b>24-40</b>	12:19:45.78	13:42:7.7	R 24.8	73.0 minutes
<b>U0975_06939549</b> (oiwfs)	12:19:53.669	13:39:14.65	9.9 mag	separation 3.46
<a href="#">observing conditions</a> : Global Default		<a href="#">resources</a> : GMOS North		
<b>23-19</b>	12:25:23.41	13:24:46.0	R 24.49	73.0 minutes
<b>U0975_06957108</b> (oiwfs)	12:25:12.355	13:20:51.79	11.1 mag	separation 4.74
<a href="#">observing conditions</a> : Global Default		<a href="#">resources</a> : GMOS North		
<b>24-16</b>	12:22:18.55	13:24:10.3	R24.22	73.0 minutes
<b>U0975_06948202</b> (oiwfs)	12:22:28.838	13:23:29.0	13.7 mag	separation 2.59
<a href="#">observing conditions</a> : Global Default		<a href="#">resources</a> : GMOS North		
<b>24-17</b>	12:21:54.25	13:27:41.8	R24.4	73.0 minutes
<b>U0975_06946911</b> (oiwfs)	12:22:05.431	13:30:00.83	11.8 mag	separation 3.57
<a href="#">observing conditions</a> : Global Default		<a href="#">resources</a> : GMOS North		
<b>24-18</b>	12:21:52.96	13:48:32.4	R23.98	73.0 minutes
<b>U0975_06945780</b> (oiwfs)	12:21:46.022	13:51:16.45	11.6 mag	separation 3.21
<a href="#">observing conditions</a> : Global Default		<a href="#">resources</a> : GMOS North		
<b>24-19</b>	12:21:49.38	13:35:48.9	R24.49	73.0 minutes
<b>U0975_06945930</b> (oiwfs)	12:21:48.353	13:33:45.36	14.4 mag	separation 2.07
<a href="#">observing conditions</a> : Global Default		<a href="#">resources</a> : GMOS North		
<b>24-24</b>	12:21:23.41	13:34:59.4	R24.37	73.0 minutes
<b>U0975_06945233</b> (oiwfs)	12:21:35.645	13:31:41.05	12.0 mag	separation 4.45

Phase 1 Proposal

Page 6 of 7

<a href="#">observing conditions:</a> Global Default		<a href="#">resources:</a> GMOS North		
<b>24-31</b>	12:20:42.42	13:55:50.6	R24.2	73.0 minutes
<b>U0975_06942804</b> (oiwfs)	12:20:50.539	13:56:36.89	12.0 mag	separation 2.12
<a href="#">observing conditions:</a> Global Default		<a href="#">resources:</a> GMOS North		
<b>24-37</b>	12:20:17.87	13:16:46.9	R23.7	73.0 minutes
<b>U0975_06942060</b> (oiwfs)	12:20:36.01	13:16:30.72	13.7 mag	separation 4.42
<a href="#">observing conditions:</a> Global Default		<a href="#">resources:</a> GMOS North		
<b>24-42</b>	12:21:50.64	13:27:27.0	R21.7	73.0 minutes
<b>U1125_06500551</b> (oiwfs)	12:22:08.986	27:25:39.68	11.7 mag	separation 838.22
<a href="#">observing conditions:</a> Global Default		<a href="#">resources:</a> GMOS North		
<b>28-2</b>	12:27:7.14	14:42:45.6	R23.8	73.0 minutes
<b>U0975_06963655</b> (oiwfs)	12:27:11.045	14:40:41.95	14.8 mag	separation 2.27
<a href="#">observing conditions:</a> Global Default		<a href="#">resources:</a> GMOS North		

**Resources**

- Gemini North
  - GMOS North
    - Focal Plane Unit
      - IFU w/ 2 slits
    - Disperser
      - R150\_G5306
    - Filter
      - GG455\_G0305

**Observing Conditions**

Name	Image Quality	Sky Background	Water Vapor	Cloud Cover
Global Default	Any	50%	Any	Any

**Scheduling Information:****Synchronous dates:****Optimal dates:** 2007/4/9-2007/4/20**Reason:** April is the optimum lunation but in Queue Schedule mode our field can be observed with both Gemini North and South for part nights from February to mid July so long as bright of moon is avoided**Impossible dates:** 2007/2/1-2007/2/8, 2007/2/23-2007/3/9, 2007/4/1-2007/4/5, 2007/5/1-2007/5/9, 2007/5/24-2007/6/7, 2007/6/21-2007/6/30**Reason:** Need to avoid Bright of Moon due to low surface brightness of targets**Allocation Committee Comments****Additional Information**

Phase 1 Proposal

Page 7 of 7

**Keyword Category:** Extra Galactic**Keywords:** Distances and redshifts, Dwarf galaxies, Galaxy cluster substructure, Galaxy clusters, Low surface brightness galaxies, Survey**Publications:****Allocations:**

Reference	Time	% Useful	Status of previous data
GN-2006A-C-8	2.0 nights	0	Previous allocation for this project completely wiped out by bad weather - no data obtained- hence move to queue mode
GS-2005A-C-12	3.0 nights	80	Data has now been reduced after considerable problems with the GMOS IFU pipeline - paper(s) are now in preparation plus Shaw, Reid and Parker, 2006, PASP, submitted.
GS-2006A-Q-63	12.0 hours	40	Data still being acquired

## Proposal Contents

[Summary](#)[Investigators](#)[Partner Submission Details](#)[Abstract](#)[Science Justification](#)[Technical Justification](#)[Observation Details](#)[Allocation Committee Comments](#)[Additional Information](#)



## G. GLOSSARY

### *G.1 Abbreviations*

**$\Lambda$ CDM** cold dark matter (theory) including a cosmological constant

**2dF** two-degree field instrument on the Anglo-Australian Telescope

**2dFGRS** 2dF Galaxy Redshift Survey

**IIIa-J, IIIa-F** glass photographic plates used at UKST prior to introduction of Tech Pan film

**3D** three-dimensional

**ACS** Advanced Camera for Surveys (instrument on the Hubble Space Telescope)

**APM** Automated Plate Measuring (machine) at Cambridge

**BCD** blue compact dwarf galaxy

**BCG** brightest cluster galaxy (also cD)

**CCD** ‘charge-coupled device’, electronic optical or infrared detector

**cD** brightest cluster galaxy (also BCG)

**CDM** cold dark matter

**COSMOS** automated plate measuring machine at Royal Observatory, Edinburgh, acronym stands for ‘CoOrdinates, Sizes, Magnitudes, Orientation and Shape’

***dE; dS0; dE,N; dI; dSph*** classifications of dwarf galaxies: elliptical; S0; elliptical (nucleated); irregular; spheroidal

***DGR*** dwarf-to-giant ratio

***DR6*** Data Release 6

***DS9*** image display software named after the mythological Deep Space 9 spacecraft

***DWC*** Durrell, Williams, Ciardullo et al. (Durrell et al. 2007)

***E, E0 - E7*** classifications of elliptical galaxies

***ESO*** European Southern Observatory

***FITS*** Flexible Image Transport System

***FP*** fundamental plane (distance indicator based on relationship between surface brightness, velocity dispersion and effective radius of elliptical galaxies)

***GAIA*** Graphical Astronomy and Image Analysis

***Gb*** gigabytes

***gE*** giant elliptical galaxy

***GMOS*** Gemini Multi-Object Spectrograph

***Gyr*** gigayears = billion ( $10^9$ ) years

***HI*** neutral (atomic) hydrogen

***HIPASS*** HI Parkes All-Sky Survey

***HSB*** high surface brightness

***HST*** Hubble Space Telescope

***IAM*** image analysis mode (of SuperCOSMOS)

***IBM*** Impey, Bothun, Malin (Impey et al. 1988)

**IC** Index Catalogue (extension of the NGC)

**ICM** intra-cluster medium

**ICP** inner concentration parameter

**ID** identifier

**IFU** integral field unit

**INT** Isaac Newton Telescope

**Irr, Im** classifications of irregular galaxies

**kpc** kiloparsec

**KPNO** Kitt Peak National Observatory

**LF** luminosity function

**LG** Local Group of galaxies, includes the Milky Way

**LSB** low surface brightness

**MGC or MGS** Millennium Galaxy Catalogue / Millennium Galaxy Survey /  
Millennium Galaxy Strip

**mm** mapping mode (of SuperCOSMOS)

**Mpc** megaparsec, one million parsecs

**NED** NASA Extragalactic Database

**NGC** New General Catalogue

**nm** nanometres

**OCP** outer concentration parameter

**pc** parsec

**POSSII** Palomar Oschin Schmidt Survey II

**RGB** red giant branch (stars)

**ROE** Royal Observatory, Edinburgh

**S/N** signal-to-noise (ratio)

**S0, SB0, Sa, Sb, Sc, SBa, SBb, SBc** classifications of spiral galaxies

**SAO** Smithsonian Astrophysical Observatory

**SDSS** Sloan Digital Sky Survey

**SDV** Sabatini, Davies, van Driel et al. (Sabatini et al. 2005)

**SSS** SuperCOSMOS Sky Survey

**TF** Tully-Fisher (distance indicator based on relationship between luminosity and velocity width of spiral galaxies)

**TRGB** tip red giant branch (stars)

**UCD** ultra-compact dwarf galaxy

**UKST** UK Schmidt Telescope

**VCC** Virgo Cluster Catalogue

**VDS** Virgo Deep Stack

**VLSB** very low surface brightness

**VPC** Virgo Photometry Catalogue

**WCS** world coordinate system (a system of coordinates applied to an image, usually RA and Dec)

**WFS** Wide Field Survey

**WMAP** Wilkinson Microwave Anisotropy Probe

---

G.2 Symbols

$\alpha$  faint-end slope of the luminosity function

$\chi^2$  measure of goodness of fit of function with multiple fitting parameters

$\gamma$  contrast, or slope of characteristic curve of a photographic process

$\Lambda_0$  cosmological constant

$\mu(r)$  surface brightness in units of magnitudes per square arcsecond as a function of radius

$\mu_{lim}$  limiting surface brightness

$\mu_0$  central surface brightness in units of magnitudes per square arcsecond

$\mu$  magnitudes per square arcsecond (a measure of surface brightness)

$\Omega_0$  mean mass density of the universe

$\Omega_b$  mean baryonic density of the universe

$\phi_*$  number of galaxies per unit volume at the characteristic luminosity of the luminosity function

$\pi$  pi, the ratio of the circumference to the diameter of a circle

$^h$  hours of RA

$^m$  minutes of RA

$^s$  seconds of RA

$^\circ$  degrees of Dec

$'$  minutes of Dec

$''$  seconds of Dec

$\text{\AA}$  angstrom

$a$  scale length of a galaxy radial profile, where intensity drops to  $1/e$  of its value at the galaxy centre

$A_R$   $R$ -band Galactic extinction values

$b/a$  ratio of minor and major diameters of an ellipse

$b$  galactic latitude (in degrees from 0 to  $\pm 90$ )

$c$  the speed of light,  $c \approx 300,000 \text{ km s}^{-1}$

$C$  data counts per pixel

$d$  distance

$D$  density (of grains in photographic emulsion)

$DM$  distance modulus

$e$  ellipticity

$h$  variable Hubble parameter used in expression of the Hubble constant ( $H_0 = 100 h \text{ km s}^{-1} \text{ Mpc}^{-1}$ ) when a value of  $H_0$  is not quoted

$H_0$  Hubble constant in units of  $\text{km s}^{-1} \text{ Mpc}^{-1}$

$i$  inclination

$I(r)$  surface brightness in units of intensity as a function of radius

$I_0$  central surface brightness in units of intensity

$l$  galactic longitude (in degrees from 0 to 360)

$L$  luminosity

$L_*$  characteristic luminosity where luminosity function changes shape

$L_\odot$  solar luminosity

$m$  apparent magnitude when passband is not specified

$m_p$  apparent photographic magnitude when passband is not specified

$m-M$  distance modulus related to distance by:  $m - M = -5 + 5 \log(d)$

$M_*$  characteristic magnitude where luminosity function changes shape

$M$  mass or absolute magnitude - refer context

$M_\odot$  solar mass

$M_g$  gas mass of disk

$M_h$  dark matter mass of halo

$M_{HI}/L$  ratio of mass of neutral hydrogen to luminosity (in units of solar mass to solar luminosity  $(M/L)_\odot$ )

$M_x$  absolute magnitude, subscript denotes passband

**OR** passband specified by Tech Pan film with OG590 filter, used for Virgo Deep Stack

$p$  ratio of smallest to largest axis of a spheroid

$pa$  position angle

$r^{1/4}$  de Vaucouleurs law governing radial profile of elliptical galaxies

$r_x$  radius, or semi-major axis in pixels

$r$  radius, or semi-major axis (in arcseconds unless otherwise specified)

$s$  slope of linear fit to radial profile

$T$  transmission (of light through photographic plate/film)

$U, B, V, R, I, u', g', r', i', z'$  apparent magnitude or passband, upper case are standard Johnson-Morgan or Cousins (also  $R_C, I_C$ ), lower case (sometimes primed) are Sloan passbands

$\mathbf{v}_{helio}$  heliocentric radial velocity

$\mathbf{v}$  velocity

$\mathbf{x}$  plate scale from scanning process, 0.6714 arcseconds per pixel for the Virgo Deep Stack

$\mathbf{z}$  redshift

$\mathbf{Z}$  plate constant, 31.5 magnitudes for the Virgo Deep Stack

### G.3 Definitions

$\mathbf{D}_n - \sigma$  distance indicator based on relationship between surface-brightness-limited diameter and velocity dispersion of elliptical galaxies

***K-correction*** correction for broadband photometric shifts in wavelength due to recession

***R(x arcsec)***  $R$  magnitude based on light contained within radius  $x$

***R-band*** broad red passband, usually refers to standard Cousins  $R$  ( $R_C$ )

***21cm*** wavelength at which neutral hydrogen may be observed

***Cepheid*** variable star referred to as a ‘standard candle’ and used as a distance indicator

***distance modulus*** a measure of distance - the difference between apparent and absolute magnitude ( $m - M$ )

***gas surface density*** vertical integral of the volume density through the disk, i.e. the amount of gas that would be measured in the disk if viewed face-on, derived from the measured HI (or other tracer) brightness distribution as a function of sky coordinates  $x$  and  $y$  after corrections for inclination and position angle and assuming an axially symmetric distribution, units are  $g\ cm^{-2}$  or  $M_{\odot}\ pc^{-2}$



**luminosity function** analytic function fitted to a luminosity or magnitude histogram

**mass function** analytic function fitted to a mass histogram

**metal** all elements heavier than helium on the periodic table

**scale length** distance from the core of a galaxy where intensity drops to  $1/e$  of its central value expressed in arcseconds or kiloparsecs

**surface brightness** a measure of magnitudes per square arcsecond, i.e. assuming light from an object of given magnitude is distributed evenly over one arcsecond then every point within that arcsecond of area has a surface brightness equal to the given magnitude

**T number** unique project identifier for series of images taken with the UKST

**Tech Pan** Kodak Technical Pan film with fine grain and high sensitivity, available from 1977 to 2004, used at UKST

**velocity function** analytic function fitted to a velocity histogram

**vignetting** reduced light transmission due to physical obstruction or properties of the optical system



## BIBLIOGRAPHY

- ARNABOLDI, M., AGUERRI, J. A. L., NAPOLITANO, N. R., GERHARD, O., FREEMAN, K. C., FELDMEIER, J., CAPACCIOLI, M., KUDRITZKI, R. P. AND MÉNDEZ, R. H. (2002) *Intracluster Planetary Nebulae in Virgo: Photometric Selection, Spectroscopic Validation, and Cluster Depth*, AJ **123** pp. 760–771.
- ARP, H. (1965) *A Very Small, Condensed Galaxy*, ApJ **142** pp. 402–406.
- AULD, R., DE BLOK, W. J. G., BELL, E. AND DAVIES, J. I. (2006) *Morphology and star formation in nearby low surface brightness galaxies*, MNRAS **366** pp. 1475–1492.
- BARAI, P., BRITO, W. AND MARTEL, H. (2007) *The Fate of Dwarf Galaxies in Clusters and the Origin of Intracluster Stars. I. Isolated Clusters*, ArXiv e-prints **707**, 0707.1533.
- BARAZZA, F. D., BINGGELI, B. AND JERJEN, H. (2003) *VLT surface photometry and isophotal analysis of early-type dwarf galaxies in the Virgo cluster*, A&A **407** pp. 121–135.
- BARTH, A. J. (2007) *A Normal Stellar Disk in the Galaxy Malin 1*, AJ **133** pp. 1085–1091.
- BEKKI, K., COUCH, W. J. AND DRINKWATER, M. J. (2001) *Galaxy Threshing and the Formation of Ultracompact Dwarf Galaxies*, ApJL **552** pp. L105–L108.
- BELL, E. F. (2002) *Exponential Stellar Disks in Low Surface Brightness Galaxies: A Critical Test of Viscous Evolution*, ApJ **581** pp. 1013–1018.

- BELOKUROV, V., ZUCKER, D. B., EVANS, N. W., KLEYNA, J. T., KOPOSOV, S., HODGKIN, S. T., IRWIN, M. J., GILMORE, G., WILKINSON, M. I., FELLHAUER, M., BRAMICH, D. M., HEWETT, P. C., VIDRIH, S., DE JONG, J. T. A., SMITH, J. A., RIX, H.-W., BELL, E. F., WYSE, R. F. G., NEWBERG, H. J., MAYEUR, P. A., YANNY, B., ROCKOSI, C. M., GNEDIN, O. Y., SCHNEIDER, D. P., BEERS, T. C., BARENTINE, J. C., BREWINGTON, H., BRINKMANN, J., HARVANEK, M., KLEINMAN, S. J., KRZESINSKI, J., LONG, D., NITTA, A. AND SNEDDEN, S. A. (2007) *Cats and Dogs, Hair and a Hero: A Quintet of New Milky Way Companions*, ApJ **654** pp. 897–906.
- BESSELL, M. S. (1986) *VRI photometry III - Photographic and CCD R and I bands and the Kron-Cousins RI system*, PASP **98** pp. 1303–1311.
- BINGGELI, B., SANDAGE, A. AND TAMMANN, G. A. (1985) *Studies of the Virgo Cluster. II - A catalog of 2096 galaxies in the Virgo Cluster area*, AJ **90** pp. 1681–1759.
- BINGGELI, B., SANDAGE, A. AND TAMMANN, G. A. (1988) *The luminosity function of galaxies*, ARA&A **26** pp. 509–560.
- BLAND-HAWTHORN, J., SHOPBELL, P. L. AND MALIN, D. F. (1993) *Deep sky surveys: A motivation for stacking digitized photographic plates*, AJ **106** pp. 2154–2160.
- BLANTON, M. R., HOGG, D. W., BAHCALL, N. A., BRINKMANN, J., BRITTON, M., CONNOLLY, A. J., CSABAI, I., FUKUGITA, M., LOVEDAY, J., MEIKSIN, A., MUNN, J. A., NICHOL, R. C., OKAMURA, S., QUINN, T., SCHNEIDER, D. P., SHIMASAKU, K., STRAUSS, M. A., TEGMARK, M., VOGLEY, M. S. AND WEINBERG, D. H. (2003) *The Galaxy Luminosity Function and Luminosity Density at Redshift  $z = 0.1$* , ApJ **592** pp. 819–838.
- BOSELLI, A., BOISSIER, S., CORTESE, L. AND GAVAZZI, G. (2008) *The Origin of Dwarf Ellipticals in the Virgo Cluster*, ApJ **674** pp. 742–767.

- BOTHUN, G., IMPEY, C. AND MCGAUGH, S. (1997) *Low-Surface-Brightness Galaxies: Hidden Galaxies Revealed*, PASP **109** pp. 745–758.
- BOUÉ, G., ADAMI, C., DURRET, F., MAMON, G. A. AND CAYATTE, V. (2008) *The galaxy luminosity function of the Abell 496 cluster and its spatial variations*, A&A **479** pp. 335–346.
- BULLOCK, J. S., KRAVTSOV, A. V. AND WEINBERG, D. H. (2000) *Reionization and the Abundance of Galactic Satellites*, ApJ **539** pp. 517–521.
- CALDWELL, N. (2005) *Low luminosity and ultra low surface brightness galaxies in the Virgo cluster*, IAU Colloq. 198: *Near-fields cosmology with dwarf elliptical galaxies*, pp. 285–289.
- CALDWELL, N. (2006) *Color-Magnitude Diagrams of Resolved Stars in Virgo Cluster Dwarf Galaxies*, ApJ **651** pp. 822–834.
- CHIBOUCAS, K. AND MATEO, M. (1999) *Low Surface Brightness Dwarf Galaxies in Nearby Clusters*, J. I. Davies, C. Impey and S. Phillips, eds., *The Low Surface Brightness Universe, Astronomical Society of the Pacific Conference Series*, vol. 170, *Astronomical Society of the Pacific Conference Series*, vol. 170, pp. 157–159.
- CHIBOUCAS, K. AND MATEO, M. (2006) *The Luminosity Function of Nearby Galaxy Clusters. II. Redshifts and Luminosity Function for Galaxies in the Region of the Centaurus Cluster*, AJ **132** pp. 347–359.
- CIARDULLO, R., JACOBY, G. H., FELDMEIER, J. J. AND BARTLETT, R. E. (1998) *The Planetary Nebula Luminosity Function of M87 and the Intracluster Stars of Virgo*, ApJ **492** pp. 62–73.
- COLE, S., LACEY, C. G., BAUGH, C. M. AND FRENK, C. S. (2000) *Hierarchical galaxy formation*, MNRAS **319** pp. 168–204.
- CONSELICE, C. J., O’NEIL, K., GALLAGHER, J. S. AND WYSE, R. F. G. (2003) *Galaxy Populations and Evolution in Clusters. IV. Deep H I Observations of Dwarf Elliptical Galaxies in the Virgo Cluster*, ApJ **591** pp. 167–184.

- CÔTÉ, P., BLAKESLEE, J. P., FERRARESE, L., JORDÁN, A., MEI, S., MERRITT, D., MILOSAVLJEVIĆ, M., PENG, E. W., TONRY, J. L. AND WEST, M. J. (2004) *The ACS Virgo Cluster Survey. I. Introduction to the Survey*, ApJS **153** pp. 223–242.
- DALCANTON, J. J., SPERGEL, D. N., GUNN, J. E., SCHMIDT, M. AND SCHNEIDER, D. P. (1997) *The Number Density of Low-Surface Brightness Galaxies with  $23 < \mu_0 < 25$  V Mag/arcsec<sup>2</sup>*, AJ **114** pp. 635–654.
- DAVIES, J. I., SABATINI, S. AND ROBERTS, S. (2004) *Low Luminosity Galaxies*, PASA **21** pp. 360–365.
- DE BLOK, E. (1997) *The Properties and Evolution of Low Surface Brightness Galaxies*, Rijkuniversiteit Groningen.
- DE BLOK, E., WALTER, F. AND BELL, E. (1999) *The Morphology of Nearby Low Surface Brightness Galaxies*, Astrophys. Space Science **269** pp. 101–108.
- DE VAUCOULEURS, G. AND DE VAUCOULEURS, A. (1964) *Reference catalogue of bright galaxies*, University of Texas Monographs in Astronomy, Austin: University of Texas Press, —c1964.
- DJORGOVSKI, S. AND DAVIS, M. (1986) *An improved distance indicator for elliptical galaxies*, B. F. Madore and R. B. Tully, eds., *NATO ASIC Proc. 180: Galaxy Distances and Deviations from Universal Expansion*, pp. 135–138.
- DRINKWATER, M. J., CURRIE, M. J., YOUNG, C. K., HARDY, E. AND YEARSLEY, J. M. (1996) *Blue compact dwarf galaxies and new velocities in Virgo*, MNRAS **279** pp. 595–614.
- DRINKWATER, M. J., GREGG, M. D., COUCH, W. J., FERGUSON, H. C., HILKER, M., JONES, J. B., KARICK, A. AND PHILLIPPS, S. (2004) *Ultra-Compact Dwarf Galaxies in Galaxy Clusters*, PASA **21** pp. 375–378.
- DRINKWATER, M. J., PHILLIPPS, S., JONES, J. B., GREGG, M. D., PARKER, Q. A., SMITH, R. M., DAVIES, J. I. AND SADLER, E. M. (1999) *Found:*

- High Surface Brightness compact galaxies*, J. I. Davies, C. Impey and S. Phillips, eds., *The Low Surface Brightness Universe, Astronomical Society of the Pacific Conference Series*, vol. 170, *Astronomical Society of the Pacific Conference Series*, vol. 170, pp. 128–130.
- DRIVER, S. (2004) *Beyond the Galaxy Luminosity Function*, PASA **21** pp. 344–351.
- DRIVER, S. P., LISKE, J., CROSS, N. J. G., DE PROPRIIS, R. AND ALLEN, P. D. (2005) *The Millennium Galaxy Catalogue: the space density and surface-brightness distribution(s) of galaxies*, MNRAS **360** pp. 81–103.
- DUBINSKI, J. (1998) *The Origin of the Brightest Cluster Galaxies*, ApJ **502** pp. 141–149.
- DUC, P.-A., BRAINE, J., LISENFELD, U., BRINKS, E. AND BOQUIEN, M. (2007) *VCC 2062: an old tidal dwarf galaxy in the Virgo cluster?*, A&A **475** pp. 187–197.
- DURRELL, P. R., WILLIAMS, B. F., CIARDULLO, R., FELDMEIER, J. J., VON HIPPEL, T., SIGURDSSON, S., JACOBY, G. H., FERGUSON, H. C., TANVIR, N. R., ARNABOLDI, M., GERHARD, O., AGUERRI, J. A. L., FREEMAN, K. AND VINCIGUERRA, M. (2007) *The Resolved Stellar Populations of a Dwarf Spheroidal Galaxy in the Virgo Cluster*, ApJ **656** pp. 746–755.
- FELDMEIER, J. J. (2006) *Intracuster Planetary Nebulae*, M. J. Barlow and R. H. Méndez, eds., *Planetary Nebulae in our Galaxy and Beyond, IAU Symposium*, vol. 234, *IAU Symposium*, vol. 234, pp. 33–40.
- FELDMEIER, J. J., CIARDULLO, R., JACOBY, G. H. AND DURRELL, P. R. (2004) *Intracuster Planetary Nebulae in the Virgo Cluster. III. Luminosity of the Intracuster Light and Tests of the Spatial Distribution*, ApJ **615** pp. 196–208.
- FERRARESE, L., FREEDMAN, W. L., HILL, R. J., SAHA, A., MADORE, B. F., KENNICUTT, R. C., STETSON, P. B., FORD, H. C., GRAHAM, J. A., HOESSEL, J. G., HAN, M., HUCHRA, J., HUGHES, S. M., ILLINGWORTH, G. D., KELSON, D., MOULD, J. R., PHELPS, R., SILBERMANN, N. A., SAKAI, S.,

- TURNER, A., HARDING, P. AND BRESOLIN, F. (1996) *The Extragalactic Distance Scale Key Project. IV. The Discovery of Cepheids and a New Distance to M100 Using the Hubble Space Telescope*, ApJ **464** pp. 568–599.
- FONTANOT, F., MONACO, P., SILVA, L. AND GRAZIAN, A. (2007) *Reproducing the assembly of massive galaxies within the hierarchical cosmogony*, MNRAS **382** pp. 903–914.
- FREEMAN, K. C. (1970) *On the Disks of Spiral and so Galaxies*, ApJ **160** pp. 811–830.
- GALLAGHER, J. S. AND WYSE, R. F. G. (1994) *Dwarf spheroidal galaxies: Key-stones of galaxy evolution*, PASP **106** pp. 1225–1238.
- GAVAZZI, G., BOSELLI, A., SCODEGGIO, M., PIERINI, D. AND BELSOLE, E. (1999) *The 3D structure of the Virgo cluster from H-band Fundamental Plane and Tully-Fisher distance determinations*, MNRAS **304** pp. 595–610.
- GAVAZZI, G., BOSELLI, A., VAN DRIEL, W. AND O’NEIL, K. (2005a) *Completing H I observations of galaxies in the Virgo cluster*, A&A **429** pp. 439–447.
- GAVAZZI, G., DONATI, A., CUCCIATI, O., SABATINI, S., BOSELLI, A., DAVIES, J. AND ZIBETTI, S. (2005b) *The structure of elliptical galaxies in the Virgo cluster. Results from the INT Wide Field Survey*, A&A **430** pp. 411–419.
- GONZALEZ, A. H., WILLIAMS, K. A., BULLOCK, J. S., KOLATT, T. S. AND PRIMACK, J. R. (2000a) *The Velocity Function of Galaxies*, ApJ **528** pp. 145–155.
- GONZALEZ, A. H., ZABLUDOFF, A. I., ZARITSKY, D. AND DALCANTON, J. J. (2000b) *Measuring the Diffuse Optical Light in Abell 1651*, ApJ **536** pp. 561–570.
- GOOCH, R. (1996) *Karma: a Visualization Test-Bed*, G. H. Jacoby and J. Barnes, eds., *Astronomical Data Analysis Software and Systems V*, *Astronomical Society of the Pacific Conference Series*, vol. 101, *Astronomical Society of the Pacific Conference Series*, vol. 101, pp. 80–83.



- GOVERNATO, F., MAYER, L., WADSLEY, J., GARDNER, J. P., WILLMAN, B., HAYASHI, E., QUINN, T., STADEL, J. AND LAKE, G. (2004) *The Formation of a Realistic Disk Galaxy in  $\Lambda$ -dominated Cosmologies*, ApJ **607** pp. 688–696.
- HAMBLY, N. C. (1998a) *Beginner's Guide to SuperCOSMOS data*, [http://www.roe.ac.uk/ifa/wfau/cosmos/begin\\_guide.html](http://www.roe.ac.uk/ifa/wfau/cosmos/begin_guide.html).
- HAMBLY, N. C. (1998b) *The SuperCOSMOS data processing guides: Introduction; Photometry*, [http://www.roe.ac.uk/ifa/wfau/cosmos/data\\_guide.html](http://www.roe.ac.uk/ifa/wfau/cosmos/data_guide.html).
- HAMBLY, N. C., MACGILLIVRAY, H. T., READ, M. A., TRITTON, S. B., THOMSON, E. B., KELLY, B. D., MORGAN, D. H., SMITH, R. E., DRIVER, S. P., WILLIAMSON, J., PARKER, Q. A., HAWKINS, M. R. S., WILLIAMS, P. M. AND LAWRENCE, A. (2001) *The SuperCOSMOS Sky Survey - I. Introduction and description*, MNRAS **326** pp. 1279–1294.
- HAYNES, M. P., GIOVANELLI, R. AND KENT, B. R. (2007) *NGC 4254: An Act of Harassment Uncovered by the Arecibo Legacy Fast ALFA Survey*, ApJL **665** pp. L19–L22.
- HOGG, D. W., BALDRY, I. K., BLANTON, M. R. AND EISENSTEIN, D. J. (2002) *The K correction*, ArXiv Astrophysics e-prints astro-ph/0210394.
- HOLMBERG, E. (1958) *A photographic photometry of extragalactic nebulae.*, Meddelanden fran Lunds Astronomiska Observatorium Serie II **136**.
- HUBBLE, E. P. (1936) *Realm of the Nebulae*, Yale University Press.
- IMPEY, C., BOTHUN, G. AND MALIN, D. (1988) *Virgo dwarfs - New light on faint galaxies*, ApJ **330** pp. 634–660.
- JACOBY, G. H., BRANCH, D., CIARDULLO, R., DAVIES, R. L., HARRIS, W. E., PIERCE, M. J., PRITCHET, C. J., TONRY, J. L. AND WELCH, D. L. (1992) *A critical review of selected techniques for measuring extragalactic distances*, PASP **104** pp. 599–662.

- JARRETT, T. (1998) *Detection of Low Surface Brightness Galaxies in 2MASS, ASSL Vol. 230: The Impact of Near-Infrared Sky Surveys on Galactic and Extragalactic Astronomy*, pp. 239–243.
- JEDRZEJEWSKI, R. I. (1987) *CCD surface photometry of elliptical galaxies. I - Observations, reduction and results*, MNRAS **226** pp. 747–768.
- JERJEN, H., BINGGELI, B. AND BARAZZA, F. D. (2004a) *Distances, Metallicities, and Ages of Dwarf Elliptical Galaxies in the Virgo Cluster from Surface Brightness Fluctuations*, AJ **127** pp. 771–788.
- JERJEN, H., TULLY, B. AND TRENTAM, N. (2004b) *Securing the Faint End of the Galaxy Luminosity Function*, PASA **21** pp. 356–359.
- JONES, J. B., DRINKWATER, M. J., JUREK, R., PHILLIPPS, S., GREGG, M. D., BEKKI, K., COUCH, W. J., KARICK, A., PARKER, Q. A. AND SMITH, R. M. (2006) *Discovery of Ultracompact Dwarf Galaxies in the Virgo Cluster*, AJ **131** pp. 312–324.
- KARACHENTSEV, I. D., KARACHENTSEVA, V. E., HUCHTMEIER, W. K. AND MAKAROV, D. I. (2004) *A Catalog of Neighboring Galaxies*, AJ **127** pp. 2031–2068.
- KARICK, A. M., DRINKWATER, M. J., WEST, M. J., GREGG, M. D. AND HILKER, M. (2004) *Galaxy Disruption Caught in the Act*, IAU Symposium, pp. 83–84.
- KATSIYANNIS, A. C., KEMP, S. N., BERRY, D. S. AND MEABURN, J. (1998) *Results of the digital co-addition of thirteen Schmidt films of the Virgo cluster of galaxies*, A&AS **132** pp. 387–399.
- KAUFFMANN, G. AND CHARLOT, S. (1998) *The K-band luminosity function at  $z=1$ : a powerful constraint on galaxy formation theory*, MNRAS **297** pp. L23–L28.

- KENNICUTT, R. C., JR. (1989) *The star formation law in galactic disks*, ApJ **344** pp. 685–703.
- KIBBLEWHITE, E. J., BRIDGELAND, M. T., BUNCLARK, P. S. AND IRWIN, M. J. (1984) *The Automated Photographic Measuring Facility at Cambridge*, D. A. Klinglesmith, ed., *Astronomical Microdensitometry Conference*, pp. 277–288.
- KLYPIN, A., KRAVTSOV, A. V., VALENZUELA, O. AND PRADA, F. (1999) *Where Are the Missing Galactic Satellites?*, ApJ **522** pp. 82–92.
- KNOX, R. A., HAMBLBY, N. C., HAWKINS, M. R. S. AND MACGILLIVRAY, H. T. (1998) *Digital stacking of photographic plates with SuperCOSMOS*, MNRAS **297** pp. 839–848.
- KROUPA, P., THEIS, C. AND BOILY, C. M. (2005) *The great disk of Milky-Way satellites and cosmological sub-structures*, A&A **431** pp. 517–521.
- LEMSON, G. AND KAUFFMANN, G. (1999) *Environmental influences on dark matter haloes and consequences for the galaxies within them*, MNRAS **302** pp. 111–117.
- LISKE, J., LEMON, D. J., DRIVER, S. P., CROSS, N. J. G. AND COUCH, W. J. (2003) *The Millennium Galaxy Catalogue:  $16 \leq B_{MGC} < 24$  galaxy counts and the calibration of the local galaxy luminosity function*, MNRAS **344** pp. 307–324.
- LUPTON, R. (2005) *Transformations Between SDSS Magnitudes and  $UBVR_CI_C$*   
<http://www.sdss.org/dr4/algorithms/sdssUBVRITransform.html>.
- MAC LOW, M.-M. AND FERRARA, A. (1999) *Starburst-driven Mass Loss from Dwarf Galaxies: Efficiency and Metal Ejection*, ApJ **513** pp. 142–155.
- MACGILLIVRAY, H. T. AND STOBIE, R. S. (1984) *New results with the COSMOS machine*, Vistas in Astronomy **27** pp. 433–475.
- MADDOX, S. J., EFSTATHIOU, G., SUTHERLAND, W. J. AND LOVEDAY, J. (1990) *The APM galaxy survey. I - APM measurements and star-galaxy separation*, MNRAS **243** pp. 692–712.

- MALIN, D. F. (1979) *A jet associated with M89*, *Nature* **277** pp. 279–280.
- MALIN, D. F. AND CARTER, D. (1983) *A catalog of elliptical galaxies with shells*, *ApJ* **274** pp. 534–540.
- MAPELLI, M., MOORE, B., RIPAMONTI, E., MAYER, L., COLPI, M. AND GIOR-DANO, L. (2008) *Are ring galaxies the ancestors of giant low surface brightness galaxies?*, *MNRAS* **383** pp. 1223–1231.
- MASTROPIETRO, C., MOORE, B., DIEMAND, J., MAYER, L. AND STADEL, J. (2004) *Morphological evolution of cluster galaxies, IAU Colloq. 195: Outskirts of Galaxy Clusters: Intense Life in the Suburbs*, pp. 519–523.
- MEI, S., BLAKESLEE, J. P., CÔTÉ, P., TONRY, J. L., WEST, M. J., FERRARESE, L., JORDÁN, A., PENG, E. W., ANTHONY, A. AND MERRITT, D. (2007) *The ACS Virgo Cluster Survey. XIII. SBF Distance Catalog and the Three-dimensional Structure of the Virgo Cluster*, *ApJ* **655** pp. 144–162.
- MIHOS, J. C., HARDING, P., FELDMEIER, J. AND MORRISON, H. (2005) *Diffuse Light in the Virgo Cluster*, *ApJL* **631** pp. L41–L44.
- MILLER, L. (1995) *The SuperCOSMOS Scanning System*,  
<http://www.roe.ac.uk/ifa/wfau/cosmos/scansystem/node1.html>.
- MINCHIN, R., DAVIES, J., DISNEY, M., BOYCE, P., GARCIA, D., JORDAN, C., KILBORN, V., LANG, R., ROBERTS, S., SABATINI, S. AND VAN DRIEL, W. (2005) *A Dark Hydrogen Cloud in the Virgo Cluster*, *ApJ* **622** pp. L21–L24.
- MOORE, B., GHIGNA, S., GOVERNATO, F., LAKE, G., QUINN, T., STADEL, J. AND TOZZI, P. (1999a) *Dark Matter Substructure within Galactic Halos*, *ApJL* **524** pp. L19–L22.
- MOORE, B., LAKE, G. AND KATZ, N. (1998) *Morphological Transformation from Galaxy Harassment*, *ApJ* **495** pp. 139–151.

- MOORE, B., LAKE, G., STADEL, J. AND QUINN, T. (1999b) *The fate of Low Surface Brightness galaxies in clusters and the origin of the diffuse intra-cluster light*, *ASP Conf. Ser. 170: The Low Surface Brightness Universe*, pp. 229–236.
- MOORE, L. AND PARKER, Q. A. (2006) *Malin 1: A Deeper Look*, *PASA* **23** pp. 165–169.
- MORGAN, D. H. AND PARKER, Q. A. (2005) *Colour equations for UK Schmidt Telescope Tech-Pan film exposures*, *MNRAS* **360** pp. 360–363.
- MORGAN, W. W. (1958) *A Preliminary Classification of the Forms of Galaxies According to Their Stellar Population*, *PASP* **70** pp. 364–391.
- MORSHIDI, Z., DAVIES, J. I. AND SMITH, R. (1997) *The Distribution of Low-Surface-Brightness Galaxies in the Local Universe*, *ASP Conf. Ser. 117: Dark and Visible Matter in Galaxies and Cosmological Implications*, pp. 510–516.
- NEISTEIN, E., VAN DEN BOSCH, F. C. AND DEKEL, A. (2006) *Natural downsizing in hierarchical galaxy formation*, *MNRAS* **372** pp. 933–948.
- NELAN, J. E., SMITH, R. J., HUDSON, M. J., WEGNER, G. A., LUCEY, J. R., MOORE, S. A. W., QUINNEY, S. J. AND SUNTZEFF, N. B. (2005) *NOAO Fundamental Plane Survey. II. Age and Metallicity along the Red Sequence from Line-Strength Data*, *ApJ* **632** pp. 137–156.
- NORBERG, P., COLE, S., BAUGH, C. M., FRENK, C. S., BALDRY, I., BLAND-HAWTHORN, J., BRIDGES, T., CANNON, R., COLLESS, M., COLLINS, C., COUCH, W., CROSS, N. J. G., DALTON, G., DE PROPRIS, R., DRIVER, S. P., EFSTATHIOU, G., ELLIS, R. S., GLAZEBROOK, K., JACKSON, C., LAHAV, O., LEWIS, I., LUMSDEN, S., MADDOX, S., MADGWICK, D., PEACOCK, J. A., PETERSON, B. A., SUTHERLAND, W. AND TAYLOR, K. (2002) *The 2dF Galaxy Redshift Survey: the  $b_J$ -band galaxy luminosity function and survey selection function*, *MNRAS* **336** pp. 907–931.
- OKE, J. B. AND SANDAGE, A. (1968) *Energy Distributions,  $K$  Corrections, and the Stebbins-Whitford Effect for Giant Elliptical Galaxies*, *ApJ* **154** pp. 21–32.

- PARKER, Q. A. AND MALIN, D. (1999) *The introduction of Tech Pan film at the UK Schmidt Telescope*, PASA **16** pp. 288–98.
- PARKER, Q. A. AND PHILLIPPS, S. (1999) *A Deep Tech Pan Survey of Dwarf Spheroidal Galaxies in Virgo, Looking Deep in the Southern Sky*, pp. 83–88.
- PELETIER, R. F., DAVIES, R. L., ILLINGWORTH, G. D., DAVIS, L. E. AND CAWSON, M. (1990) *CCD surface photometry of galaxies with dynamical data. II - UBR photometry of 39 elliptical galaxies*, AJ **100** pp. 1091–1142.
- PHILLIPPS, S. (2005) *The Structure & Evolution of Galaxies*, John Wiley & Sons, Ltd.
- PHILLIPPS, S., JONES, J. B., SMITH, R. M., COUCH, W. J. AND DRIVER, S. P. (1999) *Environmental effects on the faint end of the luminosity function*, ASP Conf. Ser. 170: *The Low Surface Brightness Universe*, pp. 183–190.
- PHILLIPPS, S. AND PARKER, Q. A. (1993) *Galaxy Surface Photometry with Kodak Technical Pan Film*, MNRAS **265** pp. 385–394.
- PHILLIPPS, S., PARKER, Q. A., SCHWARTZENBERG, J. M. AND JONES, J. B. (1998) *Dwarf Spheroidal Galaxies in the Virgo Cluster*, ApJ **493** pp. L59–L62.
- PHOOKUN, B., VOGEL, S. N. AND MUNDY, L. G. (1993) *NGC 4254: A Spiral Galaxy with an  $M = 1$  Mode and Infalling Gas*, ApJ **418** pp. 113–122.
- PICARD, A. (1991) *Inhomogeneities in the universe on scales of  $(125/h \text{ Mpc})^3$* , AJ **102** pp. 445–453.
- PICKERING, T. E., IMPEY, C. D., VAN GORKOM, J. H. AND BOTHUN, G. D. (1997) *Neutral Hydrogen Distributions and Kinematics of Giant Low Surface=20 Brightness Disk Galaxies*, AJ **114** pp. 1858–1882.
- PIERCE, M. J., WELCH, D. L., MCCLURE, R. D., VAN DEN BERGH, S., RACINE, R. AND STETSON, P. B. (1994) *The Hubble Constant and Virgo Cluster Distance from Observations of Cepheid Variables*, Nature **371** pp. 385–389.

- POPESSO, P., BIVIANO, A., BÖHRINGER, H. AND ROMANIELLO, M. (2006) *RASS-SDSS Galaxy cluster survey. IV. A ubiquitous dwarf galaxy population in clusters*, A&A **445** pp. 29–42.
- RAHMAN, N., HOWELL, J. H., HELOU, G., MAZZARELLA, J. M. AND BUCKALEW, B. (2007) *Exploring Infrared Properties of Giant Low Surface Brightness Galaxies*, ApJ **663** pp. 908–923.
- RINES, K. AND GELLER, M. J. (2008) *Spectroscopic Determination of the Luminosity Function in the Galaxy Clusters A2199 and Virgo*, AJ **135** pp. 1837–1848.
- ROBERTS, S., DAVIES, J., SABATINI, S., AULD, R. AND SMITH, R. (2007) *The dwarf low surface brightness galaxy population of the Virgo cluster - III. Comparisons with different environments*, MNRAS **379** pp. 1053–1066.
- ROBERTS, S., DAVIES, J., SABATINI, S., VAN DRIEL, W., O’NEIL, K., BAES, M., LINDER, S., SMITH, R. AND EVANS, R. (2004) *A search for low surface brightness dwarf galaxies in different environments*, MNRAS **352** pp. 478–492.
- RUDICK, C. S., MIHOS, J. C. AND MCBRIDE, C. (2006) *The Formation and Evolution of Intracluster Light*, ApJ **648** pp. 936–946.
- RYDEN, B. S., TERNDROP, D. M., POGGE, R. W. AND LAUER, T. R. (1997) *Dwarf Elliptical and Dwarf SO Galaxies in the Virgo Cluster*, M. Arnaboldi, G. S. Da Costa and P. Saha, eds., *ASP Conf. Ser. 116: The Nature of Elliptical Galaxies; 2nd Stromlo Symposium*, pp. 283–286.
- SABATINI, S., DAVIES, J., SCARAMELLA, R., SMITH, R., BAES, M., LINDER, S. M., ROBERTS, S. AND TESTA, V. (2003) *The dwarf LSB galaxy population of the Virgo cluster - I. The faint-end slope of the luminosity function*, MNRAS **341** pp. 981–992.
- SABATINI, S., DAVIES, J., VAN DRIEL, W., BAES, M., ROBERTS, S., SMITH, R., LINDER, S. AND O’NEIL, K. (2005) *The dwarf low surface brightness galaxy population of the Virgo Cluster - II. Colours and HI line observations*, MNRAS **357** pp. 819–833.

- SAHA, A., SANDAGE, A., LABHARDT, L., TAMMANN, G. A., MACCHETTO, F. D. AND PANAGIA, N. (1997) *Cepheid Calibration of the Peak Brightness of Type IA Supernovae. VIII. SN 1990N in NGC 4639*, ApJ **486** pp. 1–20.
- SAHA, A., THIM, F., TAMMANN, G. A., REINDL, B. AND SANDAGE, A. (2006) *Cepheid Distances to SNe Ia Host Galaxies Based on a Revised Photometric Zero Point of the HST WFPC2 and New PL Relations and Metallicity Corrections*, ApJS **165** pp. 108–137.
- SANCISI, R. AND FRATERNALI, F. (2007) *The Bright and the Dark Side of Malin 1*, ArXiv e-prints **707**, 0707.2377.
- SANDAGE, A. (2005) *The Classification of Galaxies: Early History and Ongoing Developments*, Annu. Rev. Astron. Astrophys. **43** pp. 581–624.
- SANDAGE, A. AND BINGGELI, B. (1984) *Studies of the Virgo cluster. III - A classification system and an illustrated atlas of Virgo cluster dwarf galaxies*, AJ **89** pp. 919–931.
- SANDAGE, A., BINGGELI, B. AND TAMMANN, G. A. (1985) *Studies of the Virgo Cluster - Part Five - Luminosity Functions of Virgo Cluster Galaxies*, AJ **90** pp. 1759–1771.
- SCHECHTER, P. (1976) *An analytic expression for the luminosity function for galaxies*, ApJ **203** pp. 297–306.
- SCHLEGEL, D. J., FINKBEINER, D. P. AND DAVIS, M. (1998) *Maps of Dust Infrared Emission for Use in Estimation of Reddening and Cosmic Microwave Background Radiation Foregrounds*, ApJ **500** pp. 525–553.
- SCHOMBERT, J. M., MCGAUGH, S. S. AND EDER, J. A. (2001) *Gas Mass Fractions and the Evolution of Low Surface Brightness Dwarf Galaxies*, AJ **121** pp. 2420–2430.
- SCHWARTZENBERG, J. M. (1996) *Field and Cluster Surveys for Low Surface Brightness Galaxies*, PhD Thesis, University of Bristol.



- SCHWARTZENBERG, J.-M., PHILLIPPS, S. AND PARKER, Q. (1996) *Digital stacking of Tech Pan films and the photometry of faint galaxies*, A&AS **117** pp. 179–187.
- SCHWARTZENBERG, J. M., PHILLIPPS, S., SMITH, R. M., COUCH, W. J. AND BOYLE, B. J. (1995) *A deep field survey for low surface brightness galaxies*, MNRAS **275** pp. 121–128.
- STRAUSS, M. A., WEINBERG, D. H., LUPTON, R. H., NARAYANAN, V. K., ANNIS, J., BERNARDI, M., BLANTON, M., BURLES, S., CONNOLLY, A. J., DALCANTON, J., DOI, M., EISENSTEIN, D., FRIEMAN, J. A., FUKUGITA, M., GUNN, J. E., IVEZIĆ, Ž., KENT, S., KIM, R. S. J., KNAPP, G. R., KRON, R. G., MUNN, J. A., NEWBERG, H. J., NICHOL, R. C., OKAMURA, S., QUINN, T. R., RICHMOND, M. W., SCHLEGEL, D. J., SHIMASAKU, K., SUBBARAO, M., SZALAY, A. S., VANDEN BERK, D., VOGLEY, M. S., YANNY, B., YASUDA, N., YORK, D. G. AND ZEHAVI, I. (2002) *Spectroscopic Target Selection in the Sloan Digital Sky Survey: The Main Galaxy Sample*, AJ **124** pp. 1810–1824.
- TADROS, H., WARREN, S. AND HEWETT, P. (1998) *How to find MACHOs in the Virgo cluster*, New Astronomy Review **42** pp. 115–119.
- TAMMANN, G. A., SANDAGE, A. AND REINDL, B. (2000) *The distance of the Virgo cluster*, Nuclear Physics B Proceedings Supplements **80** pp. C1311–1323.
- TONRY, J. L., DRESSLER, A., BLAKESLEE, J. P., AJHAR, E. A., FLETCHER, A. B., LUPPINO, G. A., METZGER, M. R. AND MOORE, C. B. (2001) *The SBF Survey of Galaxy Distances. IV. SBF Magnitudes, Colors, and Distances*, ApJ **546** pp. 681–693.
- TRACHTERNACH, C., BOMANS, D. J., HABERZETTL, L. AND DETTMAR, R.-J. (2006) *An optical search for low surface brightness galaxies in the Arecibo HI Strip Survey*, A&A **458** pp. 341–348.

- TRENTHAM, N. AND HODGKIN, S. (2002) *The luminosity function of the Virgo Cluster from  $M_B = -22$  to  $-11$* , MNRAS **333** pp. 423–442.
- TRENTHAM, N., SAMPSON, L. AND BANERJI, M. (2005) *The galaxy luminosity function from  $M_R = -25$  to  $M_R = -9$* , MNRAS **357** pp. 783–792.
- TRENTHAM, N. AND TULLY, R. B. (2002) *The faint end of the galaxy luminosity function*, MNRAS **335** pp. 712–732.
- TRENTHAM, N., TULLY, R. B. AND VERHEIJEN, M. A. W. (2001) *The Ursa Major cluster of galaxies - III. Optical observations of dwarf galaxies and the luminosity function down to  $M_R = -11$* , MNRAS **325** pp. 385–404.
- TULLY, R. B. AND FISHER, J. R. (1977) *A new method of determining distances to galaxies*, A&A **54** pp. 661–673.
- UKSTU (1983) *UK Schmidt Telescope Unit Handbook*, Royal Observatory, Edinburgh.
- VAN DEN BERGH, S. (1960) *A Preliminary Luminosity Classification of Late-Type Galaxies*, ApJ **131** pp. 215–226.
- VAN DEN BERGH, S. (1992) *The luminosity function of the Local Group*, A&A **264** pp. 75–76.
- VOLLMER, B., BRAINE, J., COMBES, F. AND SOFUE, Y. (2005) *New CO observations and simulations of the NGC 4438/NGC 4435 system. Interaction diagnostics of the Virgo cluster galaxy NGC 4438*, A&A **441** pp. 473–489.
- VOLLMER, B., CAYATTE, V., BALKOWSKI, C. AND DUSCHL, W. J. (2001) *Ram Pressure Stripping and Galaxy Orbits: The Case of the Virgo Cluster*, ApJ **561** pp. 708–726.
- VOLLMER, B., SOIDA, M., CHUNG, A., VAN GORKOM, J. H., OTMIANOWSKA-MAZUR, K., BECK, R., URBANIK, M. AND KENNEY, J. D. P. (2008) *Pre-peak ram pressure stripping in the Virgo cluster spiral galaxy NGC 4501*, ArXiv e-prints **801**, 0801.4874.

- VOLLMER, B., SOIDA, M., OTMIANOWSKA-MAZUR, K., KENNEY, J. D. P., VAN GORKOM, J. H. AND BECK, R. (2006) *A dynamical model for the heavily ram pressure stripped Virgo spiral galaxy NGC 4522*, A&A **453** pp. 883–893.
- WHITE, S. D. M. AND FRENK, C. S. (1991) *Galaxy formation through hierarchical clustering*, ApJ **379** pp. 52–79.
- WILLIAMS, B. F., CIARDULLO, R., DURRELL, P. R., FELDMEIER, J. J., SIGURDSSON, S., VINCIGUERRA, M., JACOBY, G. H., VON HIPPEL, T., FERGUSON, H. C., TANVIR, N. R., ARNABOLDI, M., GERHARD, O., AGUERRI, J. A. L. AND FREEMAN, K. C. (2007) *Virgo’s Intracuster Globular Clusters as Seen by the Advanced Camera for Surveys*, ApJ **654** pp. 835–843.
- WINDHORST, R. A., SCHMIDTKE, P. C., PASCARELLE, S. M., GORDON, J. M., GRIFFITIS, R. E., RATNATUNGA, K. U., NEUSCHAEFER, L. W., ELLIS, R. S., GILMORE, G., GLAZEBROOK, K., GREEN, R. F., HUCHRA, J. P., ILLINGWORTH, G. D., KOO, D. C. AND TYSON, J. A. (1994) *Hubble Space Telescope Medium Deep Survey. 2: Deconvolution of Wide Field Camera field galaxy images in the 13 hour + 43 deg field*, AJ **107** pp. 930–945.
- YOUNG, A. J., WILSON, A. S. AND MUNDELL, C. G. (2002) *Chandra Imaging of the X-Ray Core of the Virgo Cluster*, ApJ **579** pp. 560–570.
- YOUNG, C. K. AND CURRIE, M. J. (1998) *The “Virgo photometry catalogue”; a catalogue of 1180 galaxies in the direction of the Virgo Cluster’s core*, A&AS **127** pp. 367–395.
- ZUCCA, E., ZAMORANI, G., VETTOLANI, G., CAPPI, A., MERIGHI, R., MIGNOLI, M., STIRPE, G. M., MACGILLIVRAY, H., COLLINS, C., BALKOWSKI, C., CAYATTE, V., MAUROGORDATO, S., PROUST, D., CHINCARINI, G., GUZZO, L., MACCAGNI, D., SCARAMELLA, R., BLANCHARD, A. AND RAMELLA, M. (1997) *The ESO Slice Project (ESP) galaxy redshift survey. II. The luminosity function and mean galaxy density*, A&A **326** pp. 477–488.

ZUCKER, D. B., BELOKUROV, V., EVANS, N. W., KLEYNA, J. T., IRWIN, M. J., WILKINSON, M. I., FELLHAUER, M., BRAMICH, D. M., GILMORE, G., NEWBERG, H. J., YANNY, B., SMITH, J. A., HEWETT, P. C., BELL, E. F., RIX, H.-W., GNEDIN, O. Y., VIDRIH, S., WYSE, R. F. G., WILLMAN, B., GREBEL, E. K., SCHNEIDER, D. P., BEERS, T. C., KNIAZEV, A. Y., BARENTINE, J. C., BREWINGTON, H., BRINKMANN, J., HARVANEK, M., KLEINMAN, S. J., KRZESINSKI, J., LONG, D., NITTA, A. AND SNEDDEN, S. A. (2006a) *A Curious Milky Way Satellite in Ursa Major*, ApJL **650** pp. L41–L44.

ZUCKER, D. B., BELOKUROV, V., EVANS, N. W., WILKINSON, M. I., IRWIN, M. J., SIVARANI, T., HODGKIN, S., BRAMICH, D. M., IRWIN, J. M., GILMORE, G., WILLMAN, B., VIDRIH, S., FELLHAUER, M., HEWETT, P. C., BEERS, T. C., BELL, E. F., GREBEL, E. K., SCHNEIDER, D. P., NEWBERG, H. J., WYSE, R. F. G., ROCKOSI, C. M., YANNY, B., LUPTON, R., SMITH, J. A., BARENTINE, J. C., BREWINGTON, H., BRINKMANN, J., HARVANEK, M., KLEINMAN, S. J., KRZESINSKI, J., LONG, D., NITTA, A. AND SNEDDEN, S. A. (2006b) *A New Milky Way Dwarf Satellite in Canes Venatici*, ApJL **643** pp. L103–L106.

ZWICKY, F., HERZOG, E. AND WILD, P. (1961-1963) *Catalogue of galaxies and of clusters of galaxies, Vols. I and II*, Pasadena: California Institute of Technology.

This research project has made use of NASA's Astrophysics Data System Bibliographic Services.